 ANL-5719 (Addendum)

ARGONNE NATIONAL LABORATORY

ADDENDUM TO HAZARD SUMMARY REPORT EXPERIMENTAL BREEDER REACTOR II (EBR-II)

by

L. J. Koch, W. B. Loewenstein
and H. O. Monson

Argonne National Laboratory, with facilities in the states of Illinois and Idaho, is owned by the United States government, and operated by The University of Chicago under the provisions of a contract with the Department of Energy.

DISCLAIMER

This report was prepared as an account of work sponsored by an agency of the United States Government. Neither the United States Government nor any agency thereof, nor any of their employees, makes any warranty, expressed or implied, or assumes any legal liability or responsibility for the accuracy, completeness, or usefulness of any information, apparatus, product, or process disclosed, or represents that its use would not infringe privately owned rights. Reference herein to any specific commercial product, process, or service by trade name, trademark, manufacturer, or otherwise, does not necessarily constitute or imply its endorsement, recommendation, or favoring by the United States Government or any agency thereof. The views and opinions of authors expressed herein do not necessarily state or reflect those of the United States Government or any agency thereof.

Printed in the United States of America
Available from
U. S. Department of Energy
Technical Information Center
P. O. Box 62
Oak Ridge, Tennessee 37830
Price: Printed Copy $16.00

ANL-5719 (Addendum)
Reactor Technology
(TID-4500, 17th Ed.)
AEC Research and
Development Report

ARGONNE NATIONAL LABORATORY
9700 South Cass Avenue
Argonne, Illinois

ADDENDUM TO HAZARD SUMMARY REPORT EXPERIMENTAL BREEDER REACTOR-II (EBR-II)

by

L. J. Koch, W. B. Loewenstein and H. O. Monson

Major Contributors

T. R. Bump
H. H. Hooker
E. Hutter
C. A. Pesce
R. L. Ramp
R. W. Seidensticker
O. S. Seim
W. R. Simmons
F. Verber

June 1962

Operated by The University of Chicago
under
Contract W-31-109-eng-38

PREFACE

The initial "Hazard Summary Report - Experimental Breeder Reactor-II (EBR-II)" was published as ANL-5719 in May, 1957. At the time of preparation of ANL-5719 (early 1957), the design of the EBR-II Facility was in progress - construction had not started. This Addendum is limited, for the most part, to changes which have been made in the EBR-II Facility, and to supporting experimental data developed, since the publication of ANL-5719.

The normal detailed design modifications which occur as the construction design develops are not reported unless they relate to reactor and plant safety. However, where the design bases or criteria have been changed, they are described and the reasons for the changes are given. These too are limited to areas related to reactor and plant safety, except in a few instances, where additional information improves the understanding of plant functions.

Minor revisions in the reactor system were also effected as a result of the Dry Critical Experimental Program. The nature of this program and the experimental results are described in ANL-6299[1] and ANL-6462,[2] respectively. Dry criticality was achieved on September 30, 1961. Information pertinent to proposed "wet" critical experiments or power operation has been extracted from these reports and reproduced in this Addendum.

Emphasis is given to the first loading of the "wet" reactor, as contrasted to the normal or subsequent loadings, particularly with respect to uncertainties relating to critical mass and reactor size. The early operational plans as well as the normal power operations are discussed briefly.

This Addendum follows the outline and format of ANL-5719 to the maximum extent possible. Information contained in ANL-5719 is not repeated except where required to maintain continuity and for purposes of clarity and emphasis. Section headings are reproduced and followed by a simple statement of "no change" where appropriate to provide correlation between both reports. Changes or additions to the text published in ANL-5719 are implied, rather than stated, to avoid repeated reference to that report. In some instances where specific references are made to text descriptions, figures, and tables in ANL-5719, these references are enclosed in brackets; for example: [Section III.A.1.a.]; [Page 165]; [Fig. 12, p. 126]; [Table XI, p. 89]. References to other than ANL-5719 are indicated by superscript numerals in the text. These numerals correspond to publications listed in the Bibliography.

ACKNOWLEDGMENTS

Acknowledgment is made of the contributions and advice by the following people:

B. C. Cerutti	A. E. McArthy
J. D. Geier	M. Novick
H. H. Hummel	D. Okrent
A. R. Jamrog	J. A. Pardini
V. Z. Jankus	V. Rutkauskas
W. J. Kann	A. B. Shuck
J. H. Kittel	M. R. Sims
K. D. Kuczen	T. E. Sullivan
W. C. Lipinski	F. J. Tebo
A. Lovoff	G. K. Whitham

TABLE OF CONTENTS

	Page
I. INTRODUCTION	1
II. SUMMARY	4
III. DESCRIPTION OF EBR-II FACILITY	15
A. The Primary System	16
1. Reactor	17
a. Reactor Arrangement	17
b. Subassemblies (General)	18
c. Core Subassembly	18
d. Inner Blanket Subassembly	19
e. Outer Blanket Subassembly	19
f. Control Subassembly	19
g. Safety Subassembly	20
h. Reactor Vessel Assembly	20
2. Primary Cooling System	21
3. Shutdown Cooling System	22
4. Neutron Shield	23
a. Radial Shield	23
b. Bottom Shield	23
c. Top Shield	23
d. Fabrication of Canned Graphite Shielding	23
5. Counters, Chambers, and Instrument Thimbles	25
a. Counters and Chambers	25
b. Instrument Thimbles	25
c. Instrument Thimble Cooling System	25
6. Control and Safety Drive Systems	26
7. Fuel Handling and Unloading Systems	26
a. Fuel-Handling System	27
b. Fuel-Unloading System	30
8. Primary Tank and Biological Shield	31
a. Primary Tank	31
b. Primary Tank Support Structure	31
c. Blast Shield	32
d. Biological Shield and Shield Cooling System	32

TABLE OF CONTENTS

Page

A. The Primary System (Cont'd.)

9. Interbuilding Fuel Transfer System 32

10. Primary Sodium Purification System 33

11. Argon Blanket Gas System 34

B. Secondary System 34

1. Steam Generator 35

2. Sodium Relief System 36

C. Steam System 36

D. Fuel Process System 36

IV. PLANT OPERATION AND PERFORMANCE 38

A. Control and Instrumentation 38

1. General 38

2. Nuclear System 42

a. Control Rod Characteristics 42
b. Safety Rod Characteristics 42
c. Description of Nuclear Instrumentation 42
d. Neutron Source 45
e. Reactor Scram Circuit 45
f. Control of Flux-Flow Relationship 45
g. Automatic Flux Level Control System 46

3. Primary System 48

4. Secondary System 49

5. Steam System 49

6. Electric Power System 50

7. Building Isolation System 50

B. Normal Steady-State Operation 51

1. Flux Distributions 51

a. Neutron Flux 51
b. Gamma Flux 53
c. Secondary System Sodium Activation 54

TABLE OF CONTENTS

Page

B. Normal Steady-State Operation (Cont'd.)

2. Reactor Heat Generation Distributions 54

3. Reactor Temperature Distributions 55

4. Power Cycle Operating Conditions 63

a . Primary System 63
b . Secondary System 65
c . Steam System 65

C. Steady-State Operation at Three-Fourths Power 65

1. Flux Distributions 66

2. Reactor Heat Generation Distributions 66

3. Reactor Temperature Distributions 66

D. Pre-Operational Testing and Experiments 68

1. Mechanical, Hydraulic, and Miscellaneous Testing 68

a . Control Rod Drives 68
b . Safety Rod Drive 69
c . Instrumentation and Circuitry 69
d . Fuel-Handling System 70
e . Fuel Unloading and Interbuilding Transfer Systems . 71
f . Subassembly Basin 72
g . Primary Tank Cover Deflection 72
h . Primary Tank Leakage 73
i . Sodium Cleanup System 73
j . Argon Purification System 73
k . Primary and Auxiliary Sodium Pumps 73
l . Shutdown Coolers 74
m. Shield and Instrument Thimble Cooling Systems . . . 74
n . Primary System Heat Balance 74
o . Building Isolation System 74
p . Power Systems 75

2. Wet Critical Experiments 75

a . Neutron Source and Subcritical Instrument Response 77
b . Approach to Critical 78
c . Reactivity Measurements 78
d . Preliminary Power Calibration and Neutron Flux Distributions 80

TABLE OF CONTENTS

Page

D. Pre-Operational Testing and Experiments (Cont'd.)

3. Approach to Power 80

E. Normal Startup 83

F. Normal Shutdown 83

G. Fast Shutdown (Scram) 83

1. Primary Pumps Operative 83

2. Only Auxiliary Pump Operative 84

H. Shutdown Cooling 84

I. Reactivity Coefficients and Nuclear Performance 84

1. Isothermal Temperature Coefficient of Reactivity 84

2. Power Coefficient of Reactivity 86

3. Critical Configuration 88

4. Plutonium Production 89

5. Predicted Kinetic Characteristics 91

J. Fuel Handling, Unloading, and Interbuilding Transfer 93

1. General 93

2. Fuel-Handling Center 93

3. Numerically-Controlled Positioning System 95

4. Fuel-Unloading Machine 95

5. Manual Operations 96

a. Transfer Arm 96

b. Port Plugs 96

c. Locking Pins (Fuel-Unloading Machine) 96

6. Interbuilding Coffin 96

V. SUMMARY OF HAZARDS CONSIDERATIONS 98

TABLE OF CONTENTS

Page

APPENDICES

APPENDIX A: Properties of Fissile and Fertile Material 169

1. Fuel and Fuel Element Fabrication 169
2. Thermal Cycling of EBR-II Fuel Alloy 170
3. Irradiation Stability of EBR-II Fuel Alloy 170
4. Phase Characteristics of EBR-II Fuel Alloy 172
5. Blanket Uranium 172
6. Enrichment of EBR-II Fuel Alloy - Analysis after Fabrication 173

APPENDIX B: Component Tests 175

1. Mechanical Stability and Integrity of Core Subassemblies 175
   a. Hydrodynamic Tests in Water 175
   b. Hydrodynamic Tests in Sodium 175
   c. Mechanical Strength of Core Subassemblies . . 176
   d. Mechanical Strength of Fuel Elements 176
2. Control Rod and Safety Rod Drive Mechanisms . . . 177
   a. Control Rod Drive Mechanisms 177
   b. Safety Rod Drive Mechanism 179
3. Fuel-Handling System Components 179
   a. Packing Gland 179
   b. Rotating Plug Freeze Seals 180
   c. Gripper Mechanism Load Limit Tests 182
   d. Gripper Tests in Sodium 183
4. Fuel-Unloading System Components 183
   a. Fuel-Transfer Port Tests 183
   b. Fuel-Unloading Machine Tests 185

TABLE OF CONTENTS

		Page
APPENDIX B:	Component Tests (Cont'd.)	
5.	Sodium Pumps	187
	a. Primary System Mechanical Centrifugal Pumps	187
	b. Primary System d-c Electromagnetic Auxiliary Pump	188
	c. Secondary System a-c Linear Electromagnetic Pump	189
APPENDIX C:	Reactor Coolant Flow Distribution	201
1.	General	201
2.	Preliminary Tests	201
3.	Proof Tests	201
4.	Special Tests	205
APPENDIX D:	Stability Studies on EBR-I, Mark III Core	214
APPENDIX E:	Critical Experiments on ZPR-III	218
1.	Critical Mass and Reactivity Effects	218
2.	Power Distribution	220
3.	Neutron Source and Instrument Thimble Experiments	220
4.	Other Experiments	222
APPENDIX F:	Effects of Operational Abnormalities	225
1.	Nuclear Accidents	225
2.	Failure of All Primary System Pumps	229
3.	Bowing	230
4.	Fuel Element Failure	232
APPENDIX G:	Maximum Credible Nuclear Accidents	254
1.	Predicted Consequences of Core Meltdown	254
2.	In-Pile Tests on Single EBR-II Fuel Elements	259

TABLE OF CONTENTS

		Page
APPENDIX H:	Containment of a Possible Accident	262
APPENDIX I:	Experimental Equipment	277
1.	Reactivity Generator	277
2.	Fuel Element Failure Detector	277
APPENDIX J:	Operation with 61- to 73-Subassembly Core	282
APPENDIX K:	System Abnormalities Causing Alarm	285
APPENDIX L:	The Dry Critical Experiments	297
1.	Neutron Source and Instrument Response	298
2.	The Critical Approach and the Dry Critical Configuration	300
3.	Neutron Flux and Power Distributions	301
a.	Foil Subassembly in 7-C-4	301
b.	Foil Subassembly in 7-D-1	301
c.	Foil Subassembly in 7-F-5	302
d.	Foil Subassembly in 6-C-4	302
4.	Reactivity Effects	302
BIBLIOGRAPHY		305

LIST OF TABLES

No.	Title	Page
I	Summary of EBR-II Design and Operating Data	12-14
II	Subassembly Composition	18
III	System Abnormalities Causing Scram and Alarm	39-41
IV	Summary of Period and Level Trips for Normal Reactor Operation and for Fuel Handling	44
V	Neutron Flux and Fission Densities at Center of Core	53
VI	Gamma and Fission Heat Generation	53
VII	Regional Distribution of Power Generation	54
VIII	Illustration of Uncertainty Factor Application Method	58
IX	Uncertainty Factors for Thermal Analysis of Fuel and Blanket Elements	59
X	Summary of Thermal Analyses Results for Maximum Temperature Region of Core and Behavior (No Uncertainty Factors Included)	61
XI	Summary of Thermal Analyses Results for Maximum Temperature Region of Core and Blankets (Including Uncertainty Factors)	61
XII	Summary of Primary Coolant Flow Rates	64
XIII	Summary of Thermal Analyses Results for Maximum Temperature Region of Core and Blankets (No Uncertainty Factors Included)	67
XIV	Summary of Thermal Analyses Results for Maximum Temperature Region of Core and Blankets (Including Uncertainty Factors)	67
XV	Stability Investigations During Approach to Power	81
XVI	Isothermal Temperature Coefficients of Reactivity	85
XVII	Average Reactor Temperatures at Full Power with Full Flow	86
XVIII	Power-Induced Reactivity Changes and Power Coefficients of Reactivity (Without Bowing)	87
XIX	Possible Influence of Bowing on the Power Coefficient of Reactivity	88
XX	Bred Plutonium Reactivity Effect in the Radial Blanket with 1.0 at-% Pu^{239} Content	90

LIST OF TABLES

No.	Title	Page
XXI	Bred Plutonium Perturbation of Core Midplane Fission Densities in Depleted Uranium	91
XXII	Explosive Energy Yield as a Function of Reactivity Insertion Rate	102
A-1	Average Fuel Pin Data	169
A-2	Thermal Cycling of EBR-II Fuel Alloy between 370°C and 670°C	170
A-3	Irradiation Effects on EBR-II Fuel Alloy	171
A-4	Irradiation Effects on EBR-II Fuel Elements (Dimensional Changes of Fuel Tubes)	171
A-5	Uranium Content and Uranium Enrichment of the 5-wt-% Fissium Alloy	174
A-6	Fissium Alloy, Uranium, and U^{235} Content of Typical Core Subassemblies	174
E-1	Reactivity Worths of Core and Blanket Subassemblies as a Function of Position	218
E-2	Regional Material Replacement Experiments	219
E-3	Material Replacement Experiments	219
E-4	Instrument Thimble Fission Counter Response	221
E-5	Subcritical Count Rates in J-1 Thimble	222
F-1	Normal Rates of Reactivity Insertion	226
F-2	Reactivity Effects of Changes in Material Density	227
F-3	Summary of Six Hypothetical Accidents	228
G-1	Maximum Reactivity Attained and Maximum Energy Developed for Various Reactivity Insertion Rates in the EBR-II	257
G-2	Total Possible Reactivity Addition by Compacting EBR-II Fuel Alloy Near Core Midplane	261
H-1	Mechanical Penetrations in Containment Vessel	263
H-2	Electrical Penetrations in Containment Vessel	264
K-1	System Abnormalities Causing Alarm	285-296
L-1	Low-Power Instrument Response	298

LIST OF TABLES

No.	Title	Page
L-2	Counting Rates with Instruments Disposed as for Wet Critical Experiments	300
L-3	Reactivity Worth of Control Rods, Safety Rods, and Fuel Subassemblies	303

LIST OF FIGURES

No.	Title	Page
1	EBR-II Facility	105
2	EBR-II Plant Arrangement	106
3	Simplified Flow Diagram	107
4	Primary System	108
5	Reactor Plant - Operating Floor and Balcony Equipment Layout	109
6	Reactor Arrangement	110
7	Core Subassembly	111
8	Core Subassembly Elements	112
9	Inner Blanket and Outer Blanket Subassemblies	113
10	Inner Blanket and Outer Blanket Subassembly Cross Sections	114
11	Control Subassembly	115
12	Safety Subassembly	116
13	Reactor Vessel Assembly	117
14	Pictorial of Reactor Vessel Grid Assembly	118
15	Section of Reactor Grid Plenum	119
16	Location of Thermocouples in Upper Plenum for Measuring Sodium Coolant Outlet Temperatures	120
17	Primary System Mechanical Sodium Pump	121
18	Location of Nuclear Instrument Thimbles	122
19	Control Rod Drive Mechanism	123
20	Principal Components of Fuel Handling and Unloading Systems	124
21	Subassembly Basin	125
22	Fuel-Unloading Machine	126
23	Primary Tank Support Structure	127
24	Blast Shield and Typical Column Detail for Primary Tank Support Structure	128
25	Argon Blanket Gas System	129
26	Heat Exchanger	130
27	Steam Generator	131

LIST OF FIGURES

No.	Title	Page
28	Superheater and Evaporator Assemblies	132
29	Superheater and Evaporator Details	133
30	Major System Temperatures and Flow Rates as Functions of Reactor Power	134
31	Control Rod Displacement vs Time after Start of Rod Movement (Maximum Acceleration of 1.5 g)	135
32	Fraction of Total Control Rod Worth Effective vs Time after Start of Rod Movement (Maximum Rod Acceleration of 1.5 g)	136
33	Nuclear Instrument Range Chart	137
34	Nuclear Instrumentation Block Diagram	138
35	Reactor Scram Circuit	139
36	Simplified Instrument Flow Sheet	140
37	Single-Line Diagram of EBR-II Electric Power Distribution	141
38	High-Energy (>1.35 Mev) Neutron Flux at Core Midplane, 62.5 Mw	142
39	Low-Energy (<1.35 Mev) Neutron Flux at Core Midplane, 62.5 Mw	143
40	High (>1.35 Mev) and Low (<1.35 Mev) Energy Neutron Flux at Core Midplane	144
41	Radial Power Density Distribution at Center Plane of "Clean" Reactor (Z = 0)	145
42	Axial Power Density Distributions in "Clean" Reactor	146
43	Radial Temperature Distribution through the Fuel Element at Point of Maximum Fuel Temperature	147
44	Axial Temperature Distributions in Hottest Channel of Core and Upper Blanket (4th Row, R = 13.9 cm)	148
45	Axial Temperature Distributions in Hottest Channel of Inner Blanket (6th Row, R = 23.2 cm)	149
46	Axial Temperature Distributions in Hottest Channel of Outer Blanket (8th Row, R = 33.3 cm)	150
47	Power Output per Subassembly for "Clean" Reactor	151
48	Coolant Flow Distribution in "Clean" Reactor	152

LIST OF FIGURES

No.	Title	Page
49	Mixed Mean Coolant Temperature through Each Subassembly for "Clean" Reactor	153
50	Radial Temperature Distributions through Fuel Element at Point of Maximum Fuel Temperature	154
51	Axial Temperature Distributions in Hottest Channel of Core and Upper Blanket (4th Row, R = 13.9 cm)	155
52	Axial Temperature Distributions in Hottest Channel of Inner Blanket (6th Row, R = 23.2 cm)	156
53	Axial Temperature Distributions in Hottest Channel of Outer Blanket (8th Row, R = 33.3 cm)	157
54	Subassembly Locating Diagram	158
55	Various Reactor Temperatures during Scram vs Time after Scram Signal Reaches Control Rods (All Pumps Remain in Operation)	159
56	Various Reactor Temperatures during Scram vs Time after Failure of Both Main Pumps (Auxiliary Pump Continues in Operation)	160
57	Various Reactor Temperatures during Scram vs Time after Failure of Both Main Pumps (Auxiliary Pump Continues in Operation)	161
58	Approximate Reactor Conditions during the Long-Term (Natural Convection) Cooling Process	162
59	Amplitude of EBR-II Closed-Loop Transfer Function	163
60	Phase of EBR-II Closed-Loop Transfer Function	164
61	Fuel-Handling Console	165
62	Fuel-Handling Console Operating Panel	166
63	Fuel-Unloading Machine Control Panel	167
B-1	Core Subassembly (91 Fuel Elements) Exposed for 732 hr in Sodium at 500°F - 960°F and 3fps - 26.2 fps	191
B-2	Typical Appearance of Fuel Elements Removed from Core Subassembly (Fig. B-1)	192
B-3	Displacement vs. Time for Control Rods during Scram	193

LIST OF FIGURES

No.	Title	Page
B-4	Displacement vs. Time for Safety Rods during Scram	194
B-5	Shaft Seal Packing Gland Assembly	195
B-6	Experimental Model of Rotating Plug Freeze Seal (Test Head Open)	196
B-7	Experimental Model of Rotating Plug Freeze Seal (Test Head Closed)	197
B-8	Fuel-Transfer Port	198
B-9	Operating Characteristics of Primary Pump with Sodium at 700°F	199
B-10	Auxiliary Pump Flow on Battery Power	200
C-1	Reactor Test Model Grid	208
C-2	Installing Model Subassemblies in Reactor Test Model	209
C-3	Six-Tenths Scale Reactor	210
C-4	EBR-II Control Rod Flow Variation with Insertion	211
C-5	Model Subassembly Components	212
C-6	Model Subassembly Probes and Supports	213
E-1	Radial Fission Distributions at Core Midplane	223
E-2	Axial Fission Distributions at Three Radial Positions	224
F-1	Primary System Coolant Flow Rate vs. Time after Cessation of All Pumping Power (Based on 100% Initial Reactor Power and Coolant Flow Rate)	238
F-2	Various Reactor Temperatures during Scram vs. Time after Cessation of All Pumping Power	239
F-3	Various Reactor Temperatures during Scram vs. Time after Cessation of All Pumping Power	240
F-4	Various Reactor Temperatures during Scram vs. Time after Cessation of All Pumping Power	241
F-5	Various Reactor Temperatures during Scram vs. Time after Cessation of All Pumping Power	242
F-6	Approximate Maximum Core Fuel Temperature Occurring during Transient vs. Time Delay between Start of Scram and Cessation of all Pumping Power	243

LIST OF FIGURES

No.	Title	Page
F-7	Various Reactor Temperatures vs. Time after Cessation of All Pumping Power Subsequent to Scram.	244
F-8	Various Reactor Temperatures vs. Time after Cessation of All Pumping Power Subsequent to Scram.	245
F-9	Reactor Temperatures vs. Time after Loss of All Pumping Power (Without Scram)	246
F-10	Foreign Particle Accumulation (Case 1).	247
F-11	Foreign Particle Accumulations (Case 2) and Their Effects on EBR-II Core Temperatures	248
F-12	Foreign Particle Accumulation (Case 3).	249
F-13	Foreign Particle Accumulations (Case 4) and Their Effects on EBR-II Core Temperatures	250
F-14	Foreign Particle Accumulations (Case 5) and Their Effects on EBR-II Core Temperatures	251
F-15	Exterior View of Four Test Subassemblies after Extreme Temperature Excursions in TREAT.	252
F-16	Interior View of Four Test Subassemblies after Extreme Temperature Excursions in TREAT.	253
H-1	Electrical Penetration Nos. 1 through 16	270
H-2	Cannon Type "TBF" Connector	271
H-3	Electrical Penetration Nos. 20,22, and 23	272
H-4	Mechanical Penetration No. 13L	273
H-5	Mechanical Penetration No. 6	274
H-6	Mechanical Penetration Nos. 22 and 23	275
H-7	Holddown Arrangement for Rotating Plugs	276
I-1	Reactivity Generator Assembly.	280
I-2	Schematic of Experimental Loop Arrangement.	281
J-1	Maximum Temperatures in Each Subassembly Row and the Effect of Core Size upon Certain of Them (For Reactor Power of 62.5 Mw)	283
J-2	Maximum Temperatures in Each Subassembly Row and the Effect of Core Size upon Certain of Them (For Reactor Power of 45.0 Mw)	284

I. INTRODUCTION

The Experimental Breeder Reactor-II (EBR-II) is an experimental fast power reactor under construction at the National Reactor Testing Station in Idaho. The Laboratory proposes to begin placing this plant into operation during 1962, approximately on the schedule indicated at the end of this section. The Laboratory also proposes to perform extensive pre-operational tests and experiments (see Section IV.D.1. and 2.), and to place the plant into operation in accordance with a comprehensive startup program (see Section IV.D.3.).

The EBR-II complex (Fig. 1) comprises an unmoderated, heterogeneous, sodium-cooled reactor and power plant with a power output of 62.5 megawatts (Mw) of heat. The power produced in the reactor is converted to 20 Mw of electricity through a conventional steam cycle. The reactor is fueled with U^{235} or plutonium, and the plant includes an integral, remote-controlled, fuel-processing facility where the irradiated fuel elements are reprocessed, re-enriched, refabricated, and reassembled for return to the reactor.

The EBR-II is primarily an engineering facility to determine the feasibility of this type of reactor for central station power plant application. Major emphasis has been placed on achieving high thermal performance at high temperatures, and high fuel burnup with a fast and economical fuel-processing system. The thermal performance of the reactor and the size of the system components are amenable to direct extrapolation to central station application. The plant has been designed to permit a maximum of experimental operational flexibility by separation of the plant systems, and yet permit extrapolation to a commercial plant which would not require the same degree of separation.

The EBR-II is a high-performance reactor with a maximum power density in the core in excess of 1200 kw/liter of core volume. Associated with this high thermal performance are high heat fluxes and coolant temperatures, and coolant velocities as high as approximately 24 fps. The determination of reactor performance at these operating conditions, and the investigation of the effects of operating variables, are a significant part of the experimental program.

The separations process employed results in the buildup of certain fission products; operation of the EBR-II Facility will determine the effect of buildup of these fission products within the fuel alloy as well as the buildup of the higher isotopes of uranium and plutonium.

Although provisions are being made for subsequent loading of the reactor with uranium-plutonium fuel, the descriptions and analyses presented in this report pertain only to an enriched uranium loading. The

uranium-plutonium alloy fuel element development program will continue, including the probable use of EBR-II as an irradiation facility and for engineering-scale, fuel processing and fabrication experiments. Systems and kinetics analyses will be made similar to those presented in this report for the enriched uranium-fueled reactor. It is planned to publish these data in a supplement to this report prior to operation of the reactor with a uranium-plutonium fuel loading.

Argonne National Laboratory has been responsible for all aspects of the design and development of the plant. Design, development, and construction have been carried out concurrently, and it is expected that some phases of operation and construction also will be performed concurrently. The following chronology describes pertinent engineering, construction, and operational events as they have occurred (or are expected to occur):

November, 1956	Award of A-E Contract - Start Title I Engineering
April, 1957	Title I Engineering Completed
May, 1957	Hazard Summary Report (ANL-5719) Completed
May, 1957	Start Title II Engineering
November, 1957	Start Construction of Containment Vessel
April, 1958	Start Construction of Laboratory and Service Building, and Site Development
July, 1958	Start Construction of Power Plant and Reactor Plant
April, 1959	Start Construction of Sodium-Boiler Plant and Fuel Cycle Facility
April, 1960	Start Fabrication of Initial Fuel Loading
April, 1960	Award Contract for Component Installation
August, 1960	Laboratory and Service Building Accepted
September, 1960	Start Component Installation in Power Plant and Reactor Plant
November, 1960	Construction of Power Plant and Reactor Plant Completed
February, 1961	Hazard Summary Report for Dry Critical Experimental Program (ANL-6299) Completed
April, 1961	Fabrication of Initial Fuel Loading Completed
May, 1961	Component Installation in Reactor Plant Completed
May, 1961	Start Preparations for Dry Critical Experiments

June, 1961	Start Component Installation in Sodium-Boiler Plant
September, 1961	Dry Criticality Achieved
November, 1961	Dry Critical Experiments Completed
December, 1961	Component Installation in Power Plant Completed
March, 1962	Start Component Installation in Fuel Cycle Facility
April, 1962	Elevated Temperature Test of Primary System Completed
June, 1962	Addendum to Hazard Summary Report (ANL-5719) Completed
July, 1962	Start Filling Primary Tank with Sodium
July, 1962	Construction of Sodium-Boiler Plant Completed
July, 1962	Fill Secondary System Storage Tank with Sodium
August, 1962	Construction of Fuel Cycle Facility Completed
October, 1962	Begin Approach to Critical and Wet Critical Experiments
December, 1962	Begin Approach to Power
February, 1963	Component Installation in Fuel Cycle Facility Completed
July, 1963	Start "Hot Operation" of Fuel Cycle Facility

II. SUMMARY

All major features of the EBR-II concept as described in ANL-5719 have been incorporated in the plant as constructed. Minor changes occurred as the construction design developed and a few rearrangements were made to improve the design or plant operation. The basic features relating to plant reliability and safety were retained or enhanced, including:

(1) The "submerged concept" for the reactor primary system.

The reactor and primary coolant system, including pumps, heat exchanger, piping, etc., as well as the fuel-handling system components, are contained in the large primary tank and operate submerged in sodium. The design of the primary tank was improved by modifying the beam structure arrangement in the tank bottom, and by installing roller-type rather than pin-type hangers.

(2) Fission product decay heat removal under all conditions.

Natural circulation of sodium through the reactor removes the decay heat and transfers it to the secondary system if it is operational; if not operational, the heat is delivered to the bulk sodium in the primary tank from which it is removed by the shutdown coolers. The two shutdown coolers operate by natural convection and dissipate the heat to the atmosphere (no power is required). Natural circulation is augmented by a d-c electromagnetic auxiliary pump which is provided with a parallel (floating) battery power supply. As a result, fission product decay cooling is provided in the event of a complete and total power failure (including emergency power).

(3) Reactor and primary system containment.

The Containment Vessel provided to contain a nuclear incident, should it occur, has successfully passed two pressure tests and two leak-rate tests. The measured leak rate was substantially lower than that specified.

Changes were made in the design which enhance reliablity of operation. These include:

(1) Improved coolant flow control.

Rate-of-change control was added to the primary pumps to limit the rate of change of pumping rate. Also, mechanical-centrifugal pumps were used in place of d-c electromagnetic pumps because they have proven to be more reliable (at least in large sizes).

(2) Additional method of reactor shutdown.

The safety rod control has been revised to include a "manual scram" control during reactor operation. This is in addition to the automatic and manual scram control during fuel handling.

(3) Increased reactor core size.

To preclude the possibility of the reactor becoming critical with less than the basic 61 subassemblies (including control and safety rods), a nominal core size of 67 subassemblies was established for the first loading. The enrichment was established on the basis of this loading with an estimated maximum variation of ± 6 subassemblies (61 to 73 subassemblies).

Reactor operation was reanalyzed on the basis of the 67-subassembly nominal loading (as well as variations from the nominal loading). The result is a decrease in the maximum power density and an increase in total coolant flow.

(4) Reduction in subassembly and control rod bowing.

The total coolant flow through the reactor was increased, resulting in smaller temperature differences available to cause bowing. This further decreases the anticipated bowing effect which was believed to be acceptably small due to the mechanical design and arrangement of the subassemblies. The effect of bowing on control rod operation was reduced by the addition of a "flow twister" in the rods. The "flow twister" effectively rotates the coolant from the hot side to the cold side of the rods.

(5) Separation of reactor operation and fuel cycle operations.

The Disassembly Cell was removed from the Reactor Plant and incorporated in the Fuel Cycle Facility. This provides essentially independent operation of the two facilities, and reduces the number and complexity of fuel-handling operations to be performed in the Reactor Plant. It confines all fuel manufacturing and disassembly operations to the Fuel Cycle Facility.

(6) Improved administrative control.

Key switches have been added for control of significant reactor and fuel-handling operations which enhance administrative control of the Plant.

Operation of certain plant systems and the completion of plant and equipment has provided the opportunity to obtain the appropriate experience and/or data to verify or improve predictions. These include:

(1) System neutronics.

The performance of the Dry Critical Experiments has verified the predicted nuclear characteristics of the reactor. These include critical mass, control, flux distributions, reactivity worths of the various subassemblies in different locations and the control and safety rods.

(2) Instrumentation and control.

The Dry Critical Experiments also provided a check of the instrument response and safety circuits. In addition, the low-level sensitivity was determined and the instrumentation arrangement established for initial plant startup.

(3) Operation of control and fuel-handling systems.

System check-outs and the Dry Critical Experiments provided an opportunity (as well as the necessity) to operate and test the various components comprising these systems as integrated systems. This entailed operation under many of the conditions of reactor operation and enforced administrative procedures.

(4) Primary pump test results.

Both primary pumps have been tested with water. The actual pump performance curves and pump control characteristics are known.

(5) Fuel composition and variations.

The first loading for the reactor has been fabricated. The actual enrichment and alloy composition are known.

(6) Sodium composition.

The sodium for the primary and secondary systems has been manufactured (stored on site) and the composition analyzed.

The operational testing and system check-outs have provided verification of the reliability of some of the more important components and systems. Difficulties have been encountered, of course, and corrections and improvements have been made.

The major systems remaining to be tested and operated are: the primary sodium system, the shutdown cooling system, the secondary sodium system, and the steam system. Other test-operations will include the control and fuel-handling systems in sodium, and the sodium and argon purification and circulation systems. These will be tested and operated after sodium filling and prior to reactor loading. Sufficient electrical heating capacity is available to make these systems operational. (The turbine-generator, feed water, and condensate systems have been operated on 175-psi plant heating steam including synchronizing the generator with the 138-kv NRTS distribution loop and delivery of approximately 800 kw to the loop.)

All of the test operations are being performed by the EBR-II Operating Staff and are an essential part of their training.

Additional data were obtained on fuel and fuel element performance which indicate that the operational objectives of 1% to 2% burnup probably can be achieved at the anticipated EBR-II operating conditions (see Appendix A). The most difficult variables to assess involve the relationship between fuel temperature and irradiation damage. It is well established that irradiation damage increases as the temperature increases (for a given burnup); however, it is difficult to obtain reliable quantitative data because of the difficulty in controlling and measuring these variables in experimental irradiations. It is quite clear that there is no "threshold" temperature and, therefore, there is no specific operational temperature "limit" for the EBR-II fuel alloy, uranium-fissium (as is generally assumed for unalloyed uranium - approximately 1200°F). There could be a "practical temperature limit" within the EBR-II operating range whereupon irradiation damage will limit the fuel to impractically low burnup levels (below about 1% burnup).

The EBR-II will be utilized to determine the correlation between temperature and irradiation damage to provide a basis for optimizing operating conditions. Analyses have been made of reactor operation at three-fourths power (see Section IV.C.). The reactor will be operated at this power level (see Section IV.D.3.) to permit assessment of fuel element performance prior to operation at full power. These analyses (as well as those at full power) have been made with a smaller net application of uncertainty factors (see Section IV.B.3.) which reflect lower estimated temperatures. For a given operating condition, this results in a smaller estimated temperature range (with and without uncertainty factors) to be applied in evaluating irradiation damage.

The revisions and additions to the EBR-II are treated in detail in this Addendum. The hazards considerations are summarized in Section V and are essentially unchanged from ANL-5719. The following conclusions are drawn in summary of these evaluations:

(1) Intrinsic protection of the reactor system from a meltdown accident resulting either from loss of sodium or from loss of heat removal capability is provided by the reliability of sodium containment afforded by the primary tank, and by natural circulation of sodium through the reactor (augmented by the auxiliary pump) together with natural convection heat dissipation by the shutdown coolers.

(2) Intrinsic protection of the reactor system from a loading accident is provided by loading the reactor by substitution (minimum void in the reactor), speed control and check points in the fuel-handling sequence, and safety rods which are operational during fuel handling.

(3) A large number of errors and malfunctions in combination must occur to cause a serious accident. Although these requirements make such an accident extremely improbable, it cannot be considered impossible.

(4) Such an accident would be contained unless the energy release is considerably larger than predicted on the basis of very pessimistic assumptions, and the safety factors employed in the design of the structural and containment systems fail to provide the expected capability.

(5) If the containment vessel is breached, the consequences would be primarily local because of the isolated location of the plant. The general public would not be seriously endangered.

The design, evaluation, and plant operation of the EBR-II reflects the experimental nature and experimental objectives of this facility. Various conditions of operation have been evaluated in this report to provide a thorough description of the anticipated operating characteristics and performance of this reactor and power system. The planned operational program is designed to verify these predictions. The Laboratory proposes to operate the reactor at full power (62.5 Mwt), preceded by the pre-operational testing, the initial operational experiments, and the approach-to-power procedures as specified herein. Operation at full power is dependent upon experience obtained from the plant during these initial periods of operation and confirmation of operational reliability. The planned approach-to-power sequence may require considerable operating time and several months may elapse between initial loading to critical and full-power operation. Power-level-trip settings ranging from 104% to 110% of the desired power level will be operational at all power levels (above 1% power level).

The period- and power-level-trip settings for reactor operation are incorporated in two-out-of-three coincidence circuits to ensure continuity of operation without sacrificing reliability or safety. If a single circuit becomes inoperative, operation will be continued while corrective measures are taken. This will result in a one-out-of-two trip condition until the

defective unit is restored. If a single channel gives evidence of malfunction (but without initiating a trip signal - alarm) it will be disconnected from the system for checking and correction as necessary. This also will result in a one-out-of-two trip condition until the malfunctioning unit is corrected (or replaced) and restored to the system.

The experimental character of the EBR-II is most evident with respect to fuel element and assembly irradiation. Normal operation of the Plant includes operation with recycled fuel in which certain fission products and higher isotopes of the fissionable and fertile elements build up during each cycle. One of the primary objectives of the EBR-II is to investigate reactor operation with fuel recycled in this manner as well as to evaluate fuel performance. The EBR-II will be an invaluable irradiation facility also for experimental fuels, both for possible future EBR-II loadings and for other reactor systems. In the design of the EBR-II reactor, particular attention was given to the arrangement of the inner blanket to permit experimental irradiations in this region of the reactor. Maximum coolant flow can be provided in this region of relatively low statistical worth.

A second major area of experimental investigation involves the determination of reactor operating characteristics. This includes the kinetics characteristics such as determined by oscillator measurements, and static characteristics such as flux distributions and breeding measurements. An oscillator rod containing B^{10} has been designed to replace one of the twelve standard control rods and drives. A static calibration of the rod was made during the Dry Critical Experiments. The determination of flux distributions and breeding characteristics will require the irradiation and subsequent measurement of foils, wires, samples, etc. These will be inserted in subassemblies and handled in the conventional manner, subject to all of the fuel-handling controls, etc. (The EBR-II is not designed to accommodate the insertion and removal of small individual samples or devices. The subassembly is the smallest unit which can be inserted or removed from the reactor.) After the breeding data have been obtained, sections of the blanket may be replaced with reflector material (such as stainless steel) since the EBR-II blanket was made intentionally thick to obtain plutonium production distributions, but is too thick for optimum economy of operation. The upper and lower blanket and the outer regions of the outer blanket are the most probable regions for replacement.

Another general area of investigation involves the EBR-II nonnuclear performance characteristics. These may be generally defined as the system operational characteristics under normal and abnormal conditions. To determine this information may require the intentional temporary removal of specific operational features; for example, the determination of the thermal convection characteristics of the reactor without forced convection from the main primary pumps and the auxiliary pump. The system is designed to continue operation of the main pumps and auxiliary pump in the

event of a reactor scram, and the auxiliary pump in the event of complete power failure (including emergency power). To determine the characteristics of the system upon shutdown will require electrical disconnect of the auxiliary pump (which is normally interlocked to prevent reactor startup) and to administratively permit shutoff of the main primary pumps simultaneous with reactor scram. This type of investigation must be performed under strict administrative control in order that system performance can be determined under these conditions and can be assessed with respect to possible unintentional failure of these devices. This type of investigation will, of course, be conducted in steps beginning at operating conditions where the results can be predicted with confidence and where the consequences are completely acceptable.

The operational management of the EBR-II also reflects the character and operational objectives of this facility. The operating organization will consist of three functional levels of organization: Managerial, Supervisory, and Operational. The Operations Manager will be responsible for the program and the safe operation of the reactor and associated systems. He will have complete authority and responsibility within the limits established by the Hazards Summary Report and Addendum, the Operating Manual, and other applicable documents. He will be appointed by and directly responsible to the Division Director. In the absence of the Operations Manager, an Acting Operations Manager may be appointed by the Division Director (or in his absence, by the Acting Division Director).

An Assistant Operations Manager will act for the Operations Manager when specifically instructed by the latter. He may not assume the responsibilities of the Operations Manager without authorization of the Division Director.

The Supervisory level for each shift will consist of one Shift Supervisor and one Foreman. The Shift Supervisor will have direct responsibility for the safe operation of the reactor and associated systems for his shift. He will direct the operation of the facility for his shift. He will comply with standard operating procedures and may not deviate from them of his own volition except to take the necessary action to safeguard the facility in an emergency. The Shift Supervisor will be responsible to the Operations Manager.

The Foreman will have the responsibility for performing routine supervision of the shift personnel and to assure that procedures are properly followed for each shift. He will supervise routine operation of the reactor but will not be permitted to start up the reactor or to perform any functions not regarded as routine. He will perform other duties as delegated by the Shift Supervisor and will be responsible to the Shift Supervisor.

The Operational level will consist of qualified and authorized operators. Only authorized reactor operators will perform actual operation of the reactor controls. Operators in training who may be required to perform such operations will do so under the direct supervision of an authorized operator and with the approval of the Operations Manager. Only operators previously qualified will be assigned the responsibility of operating other plant systems. Qualification of reactor operators and supervisors will be by the Operations Manager and authorization will be by the Division Director. A member of the operating organization of higher level of responsibility and who is also an authorized operator may act in this capacity.

The Operating Organization for this reactor has been planned for a three-shift operation, seven days a week. Instructions may be forwarded from Shift Supervisor to Shift Supervisor within prescribed limits authorized by the Operations Manager or the Acting Operations Manager.

Any departure from standard operating procedures for special experiments will be reviewed in advance by the Operations Manager and approved by the Division Director. The proposal for experiments will contain complete details of the experiment and a discussion of any hazards that might be involved. The Operations Manager will review the proposal and, if he deems it safe and feasible, will endorse the request and submit it to the Division Director for approval.

During reactor operation, at least two authorized reactor operators will be stationed in the control room. In an emergency, one may leave the control room for a short time to investigate the abnormality.

A single set of operational keys will be available to the Shift Supervisors. These will be transferred from shift to shift in the prescribed manner; control of these keys will be the responsibility of the Shift Supervisor on duty.

Special operations, such as those permitted by the use of special keys, will be under the control of the Operations Manager and will be performed in accordance with his specific operating instructions.

For convenient reference, the major design and operating features of the EBR-II plant are summarized in Table I. Where changes have occurred, the earlier data are shown in brackets. (Many of the changes result from the use of a 67- rather than a 61-subassembly core as the basis for the first loading.)

Table I

SUMMARY OF EBR-II DESIGN AND OPERATING DATA

General		
Heat Output, Mw	62.5	
Gross Electrical Output, Mw	20	
Primary Sodium Temperature, to reactor, °F	700	
Primary Sodium Temperature, from reactor, °F	883	[900]
Primary Sodium Flow Rate, through reactor, gpm	9,000	[8,200]
Primary Sodium Maximum Velocity, in core, fps	23.8	[26]
Primary System Sodium Capacity, gal	89,000	[86,000]
Secondary Sodium Temperature, to heat exchanger, °F	588	[610]
Secondary Sodium Temperature, from heat exchanger, °F	866	[880]
Secondary Sodium Flow Rate, gpm	5,890	[6,050]
Steam Generator		
Output, lb/hr	250,000	[248,000]
Steam Temperature, °F	837	[850]
Steam Pressure, psig	1,300	[1,250]
Feed-water Temperature, °F	550	
Turbine Throttle Conditions		
Steam Flow, lb/hr	195,300	[198,000]
Steam Temperature, °F	837	[850]
Steam Pressure, psig	1,250	
Reactor Data (67-Subassembly Core)		
Core Dimensions		
Equivalent Diameter, in.	19.94	[19.04]
Height, in.	14.22	
Total Volume, liter	72.79	[66.3]
Upper and Lower Blanket Dimensions		
Equivalent Diameter, in.	19.94	[19.04]
Length (each end), in.	18.0	
Inner Blanket Dimensions		
Equivalent O.D., in.	27.46	
Length, in.	55.0	
Radial Thickness, in.	3.76	[4.21]
Outer Blanket Dimensions		
Equivalent O.D., in.	61.5	
Length, in.	55.0	
Radial Thickness, in.	17.02	
Core Composition		
Fuel Alloy, vol-%	31.8	
Stainless Steel (Type 304), vol-%	19.5	
Sodium, vol-%	48.7	
Control and Safety Rod Composition (Fuel Section)		
Fuel Alloy, vol-%	21.3	
Stainless Steel (Type 304), vol-%	21.5	[20.8]
Sodium, vol-%	57.2	[57.9]
Upper and Lower Blanket Composition		
Uranium (depleted), vol-%	30.3	[32]
Stainless Steel (Type 304), vol-%	18.5	[20.4]
Sodium, vol-%	51.2	[47.6]
Inner Blanket Composition		
Uranium, vol-%	60.0	
Stainless Steel (Type 304), vol-%	19.6	[17.6]
Sodium, vol-%	20.4	[22.4]
Outer Blanket Composition		
Uranium (depleted), vol-%	60.0	
Stainless Steel (Type 304), vol-%	20.9	[17.6]
Sodium, vol-%	19.1	[22.4]

Table I (Cont'd.)

SUMMARY OF EBR-II DESIGN AND OPERATING DATA

Reactor Data (cont'd.)		
Subassemblies		
Core	53	[47]
Control (Rod and Thimble)	12	
Safety (Rod and Thimble)	2	
Inner Blanket	60	[66]
Outer Blanket	510	
Total	637	
Configuration	Hexagonal	
Dimension Across Flats, in.	2.290	
Hexagonal Tube Thickness, in.	0.040	
Structural Material	304 SST	
Lattice Spacing (Pitch), in.	2.320	
Clearance Between Subassemblies, in.	0.030	
Fuel Elements (Pin-Type, Sodium Bonded)		
Fuel Pin Diameter, in.	0.144	
Fuel Pin Length, in.	14.22	
Fuel Tube O.D., in.	0.174	
Fuel Tube Wall Thickness, in.	0.009	
Thickness Sodium Bond Annulus, in.	0.006	
Elements per Subassembly	91	
Upper and Lower Blanket Elements (Pin-Type, Sodium Bonded)		
Blanket Pin Diameter, in.	0.3165	
Blanket Pin Length (total), in.	18.0	
Blanket Tube, O.D., in.	0.376	
Blanket Tube Wall Thickness, in.	0.022	
Thickness Sodium Bond Annulus, in.	0.008	
Blanket Elements per Subassembly (each end)	18	[19]
Control and Safety Rods		
Configuration	Hexagonal	
Dimension Across Flats, in.	1.908	
Fuel Elements	Same as Core Subassembly	
Fuel Elements per Rod	61	
Inner and Outer Blanket Elements (Pin-Type, Sodium Bonded)		
Blanket Pin Diameter, in.	0.433	
Blanket Pin Length (total), in.	55.0	
Blanket Tube O.D., in.	0.493	
Blanket Tube Wall Thickness, in.	0.018	
Thickness Sodium Bond Annulus, in.	0.012	
Blanket Elements per Subassembly	19	
Fuel Alloy (Enriched Uranium-Fissium)		
Total Core Loading, kg	385	[363]
U^{235} Enrichment, at-%	48.4	[49]
Critical Mass - U^{235} (clean, full power), kg	172	[170]
Total Mass of U^{235} in core, kg	176	
Fuel Alloy Composition (Fissium)		
Uranium, wt-%	95.0	
Zirconium, wt-%	0.06	[0.2]
Molybdenum, wt-%	2.48	[2.5]
Ruthenium, wt-%	1.97	[1.5]
Rhodium, wt-%	0.29	[0.3]
Palladium, wt-%	0.19	[0.5]
Niobium, wt-%	0.01	[Not given]
Fertile Blanket Material (depleted uranium)		
Total Blanket Loading, kg	28,100	

Table I (Cont'd.)

SUMMARY OF EBR-II DESIGN AND OPERATING DATA

Nuclear Data		
Total Fissions per cc/sec at Center of Core	3.7×10^{13}	[4.4×10^{13}]
Neutron Energy Distribution at Center of Core		
Flux above 1.35 Mev, n/(cm²)(sec)	0.69×10^{15}	[0.8×10^{15}]
Flux below 1.35 Mev, n/(cm²)(sec)	2.86×10^{15}	[2.9×10^{15}]
Total Neutron Flux, n/(cm²)(sec)	3.55×10^{15}	[3.7×10^{15}]
Prompt Neutron Lifetime, sec	8×10^{-8}	
Reactor Control		
Full-Flow Power Coefficients		
0-62.5 Mw (no bowing), (Δk/k)/Mw	-3.5×10^{-5}	[See page 8 for original ranges and values.]
0-25 Mw (with bowing), (Δk/k)/Mw	-3.5×10^{-5}	
25-34 Mw (with bowing), (Δk/k)/Mw	$+1.0 \times 10^{-5}$	
34-62.5 Mw (with bowing), (Δk/k)/Mw	-4.0×10^{-5}	
Doppler Effect - Average, (Δk/k)/°C	$< +0.04 \times 10^{-5}$	[$+0.04 \times 10^{-5}$]
Isothermal Temperature Coefficient, (Δk/k)/°C	-3.6×10^{-5}	
Total Reactivity Worth		
12 Normal Control Rods, Δk/k	0.048	[0.06]
2 Safety Rods, Δk/k	0.013	[0.015-0.020]
Control Rod		
Total	12	
Operating Drive (each rod)	Rack and pinion	
Velocity, in./min	5	
Total Movement, in.	14.0	
Scram Drive	Pneumatic	
Safety Rod		
Total	2	
Operating Drive	Rack and pinion	
Velocity, in./min	2.0	
Total Movement, in.	14.0	
Scram Drive	Gravity	
Long-term Reactivity Effects (from Clean to 2% Burnup)		
Burnup of U^{235} in Core, Δk/k	-0.02	
Buildup of Plutonium in Core, Δk/k	+0.002	
Buildup of Plutonium in Blanket, Δk/k	+0.0072	
Buildup of Fission Products, Δk/k	-0.002	
Irradiation Growth of Fuel (4% growth), Δk/k	-0.011	
Heat Transfer		
Heat Generation in Reactor		
Core, Control, and Safety Subassemblies, Mw	53.5	[53.3]
Upper and Lower Blanket, Mw	1.5	[1.2]
Inner Blanket, Mw	6.1	[5.2]
Outer Blanket, Mw	1.4	[2.6]
Neutron Shield, Mw	0.03	[0.2]
Heat Generation in Core		
Radial Maximum-to-Average Power Density at Reactor Center Plane	1.46	[1.33]
Axial Maximum-to-Average Power Density at Reactor Centerline	1.15	[1.17]
Power Density, Average, Mw/liter	0.735	[0.89]
Power Density, Maximum, Mw/liter	1.23	[1.37]
Power Density, Maximum to Average	1.67	[1.53]
Specific Power, Mw/kg	0.311	[0.314]
Fuel Elements, Surface Area, ft²	260	[231]
Control Elements, Surface Area (in active zone), ft²	32.4	
Safety Elements, Surface Area, ft²	6.6	
Total Surface Area, ft²	299	[270]
Maximum Heat Flux, Btu/(hr)(ft²)	929,000	[1,030,000]
Average Heat Flux, Btu/(hr)(ft²)	619,000	[680,000]

III. DESCRIPTION OF EBR-II FACILITY

The EBR-II Facility as described in ANL-5719 featured four basic systems housed in five plants, and miscellaneous supporting facilities:

(1) The Primary System: the reactor and associated equipment, and the primary sodium cooling system.

(2) The Secondary System: the intermediate sodium heat transfer system.

(3) The Steam System: the steam-electric system.

(4) The Fuel Process System: the system for disassembly, decontamination, fabrication, and assembly of fuel elements and subassemblies.

These same systems are now housed in four plants and miscellaneous supporting facilities as shown in Fig. 2. The reduction in the number of plants was effected by combining the Sodium Plant and the Boiler Plant into a single facility identified as the Sodium-Boiler Plant. This rearrangement has simplified design and control of the secondary and steam systems.

The arrangement of systems and components within the respective plants is as follows:

The Reactor Plant houses the reactor system, the primary sodium cooling system, and supporting facilities for these systems. The Disassembly Cell has been removed from the Reactor Plant and incorporated into the Fuel Cycle Facility. The building is a cylindrical gastight shell constructed of steel plate (1 in. thick), and designed to withstand an internal pressure of 24 psi. Air locks and service connections also meet this rating.

The Power Plant houses the turbine-generator and associated equipment, the control room for the reactor and power system, and personnel facilities for the reactor and power system operating staff. The building is of conventional construction.

The Sodium-Boiler Plant contains the entire secondary sodium system (including the steam generator), except for the piping to the Reactor Plant and the sodium-to-sodium heat exchanger which is installed in the primary tank. It also houses a receiving station for sodium. (The sodium is delivered to the site in tank cars.) The building is comprised of two wings - the sodium wing and the boiler wing - separated by a reinforced concrete wall (18 in. thick). The openings in the wall are limited to penetrations for piping and electrical interconnections between the components in the respective wings.

The sodium wing contains the pumping, purification, and storage facilities for the secondary system sodium, and includes the sodium receiving station. The sodium wing is a single-story structure of fireproof construction.

The boiler wing contains the 6,500-gpm, a-c linear induction electromagnetic sodium pump; the sodium surge tank; the steam generator (evaporators, superheaters, and steam drum); and associated steam and feed-water piping. The boiler wing is a multi-story, reinforced-concrete structure with no windows in the wall facing the Reactor Plant, and a corrugated plastic "blow-out panel" in a wall facing away from the Reactor Plant. The "blow-out panel" is designed to release at a pressure of 30 lb/ft^2 inside the building. The concrete building walls have been designed for an internal pressure of 40 lb/ft^2. Considering the normal safety factors used in the design of reinforced concrete structures, the rupture strength of the building is many times greater than the "blow-out panel" release pressure.

The Sodium-Boiler Plant is somewhat isolated, with sodium lines linking it to the Reactor Plant (75 ft distant from the nearest point of the Sodium-Boiler Plant), and steam and condensate lines linking it with the Power Plant (~200 ft distant). The building contains only the minimum facilities for operation and, normally, will not be occupied continuously by operating personnel.

The Fuel Cycle Facility (formerly designated the Process Plant) contains two shielded cells for disassembly, processing, fabrication, and assembly of fuel elements and subassemblies, and supporting facilities for these operations. It also contains the inert-gas storage facilities, the sodium equipment cleanup cell, and exhaust ventilation system and stack for the exhaust from the Fuel Cycle Facility, Reactor Plant, and Laboratory and Service Building. The building is of conventional construction.

The EBR-II power system is comprised of the primary, secondary, and steam systems. The heat produced in the reactor is removed and transferred by the primary system to the secondary system in the heat exchanger. From the secondary system, the heat is transferred in the steam generator to produce superheated steam which is delivered to a conventional condensing turbine. The flow diagram of the power system [Fig. 1] has been revised slightly and is shown in Fig. 3.

A. The Primary System

The Primary System (Fig. 4) is housed in the Reactor Plant (Fig. 5), and includes the following:

Reactor
Primary Cooling System
Shutdown Cooling System
Neutron Shield
Counters, Chambers, and Instrument Thimbles
Control and Safety Drive Systems
Fuel-Handling System
Primary Tank and Biological Shield
Fuel Unloading and Interbuilding Transfer
Primary Sodium Purification System
Argon Blanket Gas System

The Disassembly Cell has been removed from the Reactor Plant and incorporated in the Fuel Cycle Facility. Other modifications and improvements in the primary system are described in the following subsections.

1. Reactor

a. Reactor Arrangement

The nominal core size has been increased by adding six core-type subassemblies in the sixth row (one near the center of each flat). This has been done to preclude criticality with a core of smaller size than initially contemplated [Section III.A.1.a.], should the critical mass prove to have been overestimated.. Fuel enrichment for the first loading has been based upon the new nominal core size and is expected to produce criticality at this size, ±6 subassemblies. The sixth row, core-type subassemblies will be loaded into the reactor in the sequence indicated in Fig. 6 (to promote symmetry and to minimize inner blanket temperatures).

Numerical distribution of the various types of subassemblies within the reactor is shown below, with the original configuration included for comparison.

Subassembly Type	[Section III.A.1.a.]	Nominal Loading	First Loading
Core	47	53	53 ± 6
Safety	2	2	2
Control	12	12	12
Inner Blanket	*66	*60	*60 ∓ 6
Outer Blanket	510	510	510
Total	637	637	637

*Includes one neutron source subassembly.

Unless otherwise noted, all analytical results described herein are based upon the nominal loading. The term "67-subassembly core" is frequently

used to refer to this loading (meaning 53 core, 2 safety, and 12 control-type subassemblies in the core).

a. Subassemblies (General)

The most significant dimensions of the various subassembly types have not changed. Minor modifications to certain types (described later) have resulted in minor changes in their compositions. The composition of each type of subassembly is listed in Table II. Values which differ from those originally reported [Table II, p. 15] are identified with an asterisk.

Table II

SUBASSEMBLY COMPOSITION
(in vol-%)

Subassembly Type	Fuel Alloy	Uranium	Steel	Sodium
Core - Fuel Section	31.8	0	19.5	48.7
Core - Blanket Sections	0	*30.3	*18.5	*51.2
Control and Safety - Fuel Section	21.3	0	*21.5	*57.2
Inner Blanket	0	60.0	*19.6	*20.4
Outer Blanket	0	60.0	*20.9	*19.1

c. Core Subassembly

Each core subassembly (Fig. 7) is comprised of three "active" sections: upper blanket, core, and lower blanket. The core section contains ninety-one (91) fuel elements. The blanket sections each contain eighteen (18) blanket elements.

The fuel elements (Fig. 8) are unchanged except for the design of the cap. The slotted tube design has been replaced by a column design which is more easily fabricated and provides adequate column strength. The gap between the end of the fuel and the end of the cap remains unchanged.

The upper and lower blanket sections previously contained a cluster of nineteen (19) blanket elements. The central element has been removed and replaced with a steel tie rod that interconnects the upper and lower blanket support grids (see insert, Fig. 7). This method of connecting the support grids in the blanket sections: (1) eliminates the contemplated flat plate strips at the corners of the hexagonal cluster; (2) provides a sturdier structure; and (3) is more amenable to disassembly. The reduction in breeding gain (due to the small reduction in fertile material) is insignificant.

The lower adapter of the core subassembly (Fig. 7) has been revised to employ a series of holes, rather than slots, through which the

coolant enters the subassembly from the high-pressure inlet coolant plenum. The hole arrangement provides a more simple, flexible, and reproducible coolant orificing system. The flow system and orificing arrangement are described later.

d. Inner Blanket Subassembly

This subassembly (Fig. 9) has been altered in two ways. First, holes are used instead of slots in the lower adapter. As in the case of the core subassembly, the holes provide an improved and more flexible flow orificing system. Second, flow distribution strips have been inserted into the twelve, comparatively large, peripheral coolant flow channels to improve flow distribution within the subassembly (see Fig. 10).

e. Outer Blanket Subassembly

This subassembly (Fig. 9) also has been altered in two ways; i.e., the coolant flow orificing arrangement in the lower adapter was modified and flow distribution strips were inserted in the twelve peripheral flow channels (see Fig. 10).

Because these flow strips are relatively large, the associated flow channels are smaller than those in the interior of the subassembly and may increase the possibility of plugging during operation. Due to the low power densities in the outer blanket, however, extensive plugging could be tolerated without damage to the blanket elements.

f. Control Subassembly

The detailed design of the control subassembly was developed as described [Section III.A.1.f., p. 17]. Coolant inlet holes, instead of slots, are used in the lower adapter of the control rods to effect improved flow control (Fig. 11). The hole sizes and location are based primarily on maximum flow requirements. The flow variation with control rod position was determined experimentally. The results (Appendix C) indicate a flow reduction of approximately 35% with the control rod down (out of the core).

A "flow twister" has been installed in the void section immediately above the core section of each control subassembly (Fig. 11). The purpose of this device is to reduce the temperature differentials in the control rod hexagonal can and, therefore, to minimize bowing of the control rod within its thimble. Upon leaving the core section, the hotter coolant flowing along the inside surface of the control rod (the surface facing the center of the reactor) will be "rotated" approximately 180° to the opposite surface. Thus, exposure of the opposite surface to the higher-temperature sodium will tend to reverse any bowing of the rod. The "flow twister" does not introduce any significant pressure drop in the coolant flow.

g. Safety Subassembly

The safety subassembly (Fig. 12) is unchanged except for the use of coolant flow orifice holes, instead of slots, in the lower adapter. The "flow twister" is not used because of the very small temperature gradient across these rods.

h. Reactor Vessel Assembly

The reactor vessel assembly (Fig. 13) consists of the reactor vessel, the grid plenum assembly, and the top cover.

(1) Reactor Vessel

The reactor vessel has been enlarged to a constant diameter extending from upper plenum to the grid assembly. This change has eliminated discontinuities in the vicinity of the coolant outlet plenum [Fig. 15]. These discontinuities gave rise to stress concentrations and complicated the design of thermal baffles and other thermal protective devices.

The increase in vessel diameter resulted in an increase in the width of annulus between the outer blanket and the vessel wall. This annulus has been filled with graphite-containing shielding cans (inner radial neutron shield), and a second liner (retaining shell) to separate these cans from the outer blanket. In a portion of the annulus, the shielding cans are filled with sodium, instead of graphite, to aid nuclear instrument response.

Minor revisions have been made in the detailed design of the thermal baffling system and the thermal insulation system. These are also indicated in Fig. 13.

(2) Grid-Plenum Assembly

A pictorial of the reactor vessel grid plenum assembly is shown in Fig. 14. Certain detail dimensions have been finalized and modified slightly as indicated in Fig. 15. The arrangement of subassembly engagement diameters in the grid (largest in the core, intermediate in the inner blanket, and smallest in the outer blanket) is retained, as is the stepped lower plate for flow orificing. As stated earlier, coolant inlet holes, instead of slots, are now provided in the subassembly adapters.

The arrangement of the holes in the subassembly lower adapters provides positive variable orificing from row to row in the core and inner blanket. The proportional flow in each hole can be altered

in the future by revising the hole diameters in the appropriate rows of holes. The orificing, therefore, can be altered even though the stepped lower plate is a permanent installation.

(3) Reactor Vessel Cover

The reactor vessel cover is unchanged except for construction details; i.e., final configuration of the thermal baffles, etc. In addition, the locations of the thermocouples which measure coolant outlet temperature from selected subassemblies have been established (Fig. 16).

2. Primary Cooling System

The arrangement of the primary coolant system components is essentially unchanged. The d-c electromagnetic primary coolant pumps [Fig. 17] have been replaced with vertical-mounted, single-stage, centrifugal-type mechanical pumps (Fig. 17).

Although reliability is a prime requisite for the EBR-II pumps, some of the other major requirements are: (1) the pump motor and top shield plug flange assembly must be completely gastight to prevent leakage of the primary system blanket inert gas; (2) a six and one-half foot (overall length) radiation shield plug must exist between the pump and the drive motor to conform to the top biological shield of the primary system; (3) the pump shaft must extend through the shielding and inert-gas blanket areas, and into the sodium for proper impeller submergence; (4) the sodium "hydraulic" bearing must not require any external sodium source or auxiliary external equipment; and (5) the pump speed should be controllable from about 20% to 100% speed with specified rates of acceleration and deceleration.

These pumps are driven by variable-speed motors powered by a motor-generator set providing variable voltage and frequency. The direct-coupled pump drives are special, totally enclosed, gastight, 480-volt, a-c motors. Labyrinth-type shaft seals are employed to minimize diffusion of sodium vapor into the motor enclosure.

The maximum capacity of each pump is 5,000 gpm at 85 psig; the EBR-II flow requirement per pump at full power is approximately 4,670 gpm at 54 psig.

The radiation shielding installed in the shield plug structure consists of field-placed carbon steel balls 33 in. in depth, followed by 8 in. of insulation, and 34 in. of field-placed high-density concrete. The center portion of this shield plug and the pump shaft are stepped to reduce radiation streaming along the vertical shaft.

The pump shaft in the 350-hp pump motor has a maximum diameter of 5.5 in. and is hollow to accommodate the draw bolt for the coupling immediately below the motor. The center distance between the upper ball thrust and radial bearing and the lower radial roller bearing is 4 ft - 2.5 in. The pump shaft connects at the top of the shield plug to the motor shaft, projects downward through the shield plug, then through the spacing baffle assembly, and into the pump case, where it is located radially by a hydrostatic bearing. The pump impeller is overhung on the shaft immediately below this bearing. The center distance between bearings on the pump shaft portion is 10 ft - 8.75 in. and the maximum shaft diameter is 9.5 in. This large diameter was selected to insure that no vibrational instabilities will occur. The pump shafts were precisely balanced. Sodium is fed to the bearing from the impeller discharge. The hydrostatic pressures in the bearing shell act to center the bearing journal within the bearing clearance provided. Pads within the hydrostatic bearing pockets provide an additional hydraulic centering action; this is desirable at startup when the available pressures are insufficient for good hydrostatic bearing action. The bearing surfaces are hard faced with Colmonoy to minimize wear and galling.

The centrifugal-type pump was selected in preference to the d-c electromagnetic pump because of the very favorable performance of the 5,000-gpm centrifugal pump during long-term loop tests (Appendix B). The success of the centrifugal pump can be attributed largely to the development of the hydraulic bearing which resolved the most difficult problem peculiar to rotating-type pumps for sodium.

In contrast with the successful development of the centrifugal pump, considerable difficulty has been encountered with large d-c electromagnetic pumps. Extrapolation from experience with 500-gpm to 1,000-gpm units, to larger sizes, introduced new and difficult problems. The power source is more complicated because of the extremely high currents and low voltages.

At the present time, large-sized centrifugal pumps are more reliable, more efficient, and more economical than d-c electromagnetic pumps. However, the EBR-II primary system has been arranged to facilitate experimentation with electromagnetic pumps at a later date.

Other features of the primary cooling system remain unchanged.

3. Shutdown Cooling System

The shutdown cooling system is unchanged.

4. Neutron Shield

The basic composition of the neutron shield remains unchanged; however, revisions have been made in the shield configuration. These revisions are described below. The shield was mocked-up on ZPR-III, and experimental results are included in Appendix E.

a. Radial Shield

As described earlier (Section III.A.1.h.), part of the radial shield cans are now positioned within the reactor vessel. As shown in Figs. 6 and 13, retainers and liners have been added which provide positive positioning of the shield cans and enhance the natural convection cooling of the shield. In addition to the special cans surrounding the coolant inlet and outlet pipes, specially shaped cans are installed around the "J" instrument thimbles(which now terminate in the neutron shield).

b. Bottom Shield

The canned borated graphite shield originally contemplated for use below the reactor vessel has been deleted. Detailed analyses indicated that the heat generation in the structure below the reactor was not critical and that a less elaborate shielding arrangement could be used.

Borated stainless steel plates are now located between the vertical webs of the beams on the bottom of the primary tank. This arrangement provides adequate shielding and significant simplification of the structure below the reactor vessel. It also removes the moderator (graphite) from below the reactor vessel, which could be of significance in the very unlikely event of a major meltdown with fuel reaching this zone.

c. Top Shield

The neutron shielding in the reactor vessel cover is basically unchanged.

d. Fabrication of Canned Graphite Shielding

The neutron shield is comprised of both non-borated and borated graphite sealed in stainless steel cans. The non-borated graphite consists of reactor-grade graphite from the dismantled CP-2 reactor. The borated graphite was produced to AGSR specifications with 3 wt-% B_4C added. All graphite pieces were machined to size prior to loading into the cans. Two canning procedures were employed: one for the standard cans (4 in. square cross section of various lengths), and the other for special cans (the various odd-shaped cans to fit the odd geometries created by instrument thimbles, pipes, etc., penetrating the neutron shield).

The cans were designed for internal pressure of 50 psig. Accordingly, the standard cans feature a wall thickness of 0.109 in. (12 ga.), and end plates 0.5 in. thick. Pressure tests of fabricated cans revealed that at 50 psig internal pressure the stresses were lower than the allowable stress - by strain gauge measurement, and at an internal pressure of 300 psig the cans bulged but did not burst. A side wall thickness of 0.25 in. was established for the large special cans. A maximum unsupported span of about 9 in. was achieved by tack-welding 12 ga. thick partitions, where necessary, to limit bending stresses to the allowable value. The top and bottom heads of these cans were also fabricated of 0.5 in. thick plate.

The standard cans were filled as follows:

(1) Outgas graphite in vacuum furnace at 1300°F and 400 micron pressure for 1 hr; cool to about 200°F in 4 hr (under vacuum).

(2) Break furnace vacuum with argon.

(3) Remove graphite and load directly into can (maximum exposure to air: 0.5 hr).

(4) Close can and make final weld (leaving vent tube open); evacuate can to 400 microns and hold for 1 hr.

(5) Pressurize can with helium to 5 psig; make temporary seal weld at end of vent tube.

(6) Helium leak test can.

(7) Heat can assembly to 1000°F and hold for 8 hr.

(8) Helium leak test can, assuming helium pressure was not lost during Step (7).

(9) Cut off temporary vent tube seal, checking for outward flow of helium by sound and feel to assure that helium pressure was not lost during Step (7).

(10) Evacuate can to 150-200 mm Hg (helium).

(11) Make two permanent seal welds on vent tube; helium leak test each weld.

The special cans were loaded and welded prior to outgassing. They were outgassed by manifolding their open vent tubes to a vacuum pump and holding in a furnace at 1000°F and 400-micron pressure for at least 8 hr (normally 16 hr overnight). After cooling, the cans were pressurized to 5 psig with helium and leak tested. Subsequently, the special cans were evacuated and sealed as in Steps (10) and (11).

5. Counters, Chambers, and Instrument Thimbles

a. Counters and Chambers

(1) General

Three fission counters and eight compensated ion chambers comprise the detectors for the nuclear instrument channels. For reliable operation, the temperatures of counters and chambers are maintained below 140°F.

A description of the nuclear instrument channels is given in Section IV.A.2.c.

(2) Counters

Three U^{235}-enriched fission counters are employed to detect neutrons in the startup range of operation instead of the two counters originally contemplated. The counters are positioned in "J" thimbles located in the radial neutron shield (Fig. 18).

(3) Chambers

All eight compensated ion chambers are now located adjacent to (or in) the radial neutron shield. The two chambers originally located in the biological shield cooling annulus are now located in "O" thimbles (Fig. 18).

The gamma shielding originally contemplated around the detectors (to increase effective chamber neutron sensitivities), has been determined to be unnecessary and has been eliminated.

b. Instrument Thimbles

The general arrangement of the nuclear instrument thimbles and their associated fission counters and ion chambers is shown in Fig. 18. Eight thimbles are provided (the three thimbles originally located in the biological shield cooling annulus have been eliminated). Four "J" thimbles are now imbedded in the radial graphite neutron shield outside of the reactor vessel, and four "O" thimbles are located immediately adjacent to the neutron shield.

c. Instrument Thimble Cooling System

Thimble cooling is accomplished by drawing room air through the thimbles. The air-cooling system was chosen in preference to the original closed, helium-cooling system because it: (1) reduced the

complexity of the system; (2) increased its reliability; and (3) minimized leak-integrity requirements. The system is non-recirculating; the exhaust air is combined with the biological shield cooling air and discharged through the 200-foot stack.

Two full-capacity blowers are available; one is on standby. A dual exhaust manifold is provided: one branch services thimbles J-2, J-3, O-1, and O-2, designated Bank (A); and the other branch services thimbles J-1, J-2, O-3, and O-4, designated Bank (B). A thermocouple is located on each neutron detector mounting. Any two thermocouple trips (temperature above 125°F) in either bank of four thimbles will scram the reactor.

For maximum reliability, the standby blower system is provided with automatic switch-over and a 100-kw auxiliary diesel generator power supply. This is in addition to the 400-kw plant auxiliary diesel generator. The reactor is scrammed, of course, in the event of thimble cooling failure, but these additional precautionary measures are designed to protect the nuclear detectors and preamplifiers from thermal damage.

6. Control and Safety Drive Systems

The detailed design of the control drive system was developed in accordance with the previous basic schematic diagram [Fig. 25]. Refinements were incorporated to effect the various detailed requirements as they developed, and to meet the stringent space requirements as indicated in Fig. 19.

The safety drive system [Fig. 27] is essentially unchanged except for the lower beam structure arrangement as indicated in Fig. 13.

Extensive testing of prototpye and production units (including tests at simulated operating conditions) has affirmed the performance and reliability of these units. Performance curves and operational data are included in Appendix B.

7. Fuel-Handling and Unloading Systems

The fuel-handling system involves the movement of fuel and blanket subassemblies between the reactor and storage rack. These operations are performed within the primary tank with the subassemblies completely submerged in sodium. The fuel-unloading system involves the movement of subassemblies into and out of the primary tank, between the storage rack and the interbuilding coffin (within the Reactor Plant). The interbuilding fuel transfer system (described in Section III.A.9.) effects transfer of subassemblies between the Reactor Plant and the Fuel Cycle Facility.

a. Fuel-Handling System

The fuel-handling system includes the gripper and holddown mechanisms for removing (and installing) the subassemblies from the reactor; the transfer arm for transferring subassemblies between the gripper mechanism and storage rack; and the storage rack. It also includes operation of the rotating plugs and their "freeze seals," and certain operations of the control rod drives and safety rod drives.

The freeze seals for the two rotating plugs have been revised to provide a combination molten-frozen seal, rather than a completely frozen seal as originally contemplated. The completely frozen experimental seal leaked in an unpredictable and non-reproducible manner. To resolve this problem, the trough and dip ring arrangement were revised to permit freezing the upper portion of the seal while retaining the lower region in a molten state. The frozen upper region prevents seal metal loss in the event of a large pressure differential across the seal, while the molten lower region prevents leakage. The entire seal is melted, of course, to permit rotation of the plugs. The operation of this seal arrangement has been demonstrated successfully in a series of mock-up tests described in Appendix B.

(1) Mechanical Components

The mechanical components of the fuel-handling system (Fig. 20) have remained essentially as described. Each unit in the system has been assembled and tested extensively prior to shipment to the field (see Appendix B). The following descriptions are made with reference to Fig. 20.

The gripper mechanism is an electro-mechanical device used to insert or to extract subassemblies from the reactor vessel. It is mounted on the small rotating shield plug and extends into the sodium in the primary tank. The gripper mechanism grips the upper adapter of the subassembly and moves it vertically into or out of the reactor vessel. By rotation of the large and small shield plugs, the gripper mechanism is brought to the location ("transfer point") where it transfers the subassembly to or from the transfer arm.

The holddown mechanism is an electro-mechanical device which works in conjunction with the gripper mechanism. It is also mounted on the small rotating shield plug and extends into the sodium in the primary tank. During the removal of a subassembly from the reactor vessel, the holddown mechanism prevents inadvertent extraction or movement of adjacent subassemblies. The holddown mechanism also acts as a guide funnel for the subassembly during the loading sequence.

The transfer arm mechanism, a manually operated and electrically controlled device, transports subassemblies between various points in the fuel-handling and unloading systems. The transfer arm swings in a horizontal arc between the transfer point, storage rack, and transfer port location.

The storage rack mechanism, an electromechanical device, provides temporary storage of new and spent fuel (and blanket) subassemblies. The rack is suspended from the primary tank cover, and is fully submerged in the tank sodium at all times to permit natural convection cooling of spent subassemblies within it. The rack is cylindrical, with a capacity of 75 subassemblies. The associated drive mechanism imparts vertical and rotational movement of the rack to permit either insertion or removal of a subassembly from the rack by the transfer arm.

Although the gripper and transfer arm and the related control circuits are designed to prevent accidental release of a subassembly, provisions have been made for recovery. A "subassembly basin" (Fig. 21), consisting of a funnel-shaped trough, traverses the area under much of the transfer arm path (the arc between the reactor, storage rack, and transfer port). All sides of the "funnel" slope toward a depression located directly below an access nozzle in the primary tank cover. If a subassembly were accidentally released from the transfer arm at any point along its travel (other than over the reactor, the radial neutron shield, or the storage rack), it would drop into the basin and slide to the retrieving position, standing in a vertical attitude. In this position, the subassembly may be grappled through the access nozzle. Natural convection cooling of this subassembly will occur in the same fashion as for subassemblies located in the storage rack. Should the subassembly become wedged in the basin without sliding into the retrieving position, cooling by the bulk sodium would limit the maximum fuel temperature to less than 1100°F (even in the horizontal position, one hour after shutdown from full-power operation).

The basin was thoroughly tested after installation by repeated, deliberate dropping of a dummy subassembly from the transfer arm.

(2) Fuel-Handling System Control

Fuel handling is accomplished semi-automatically. The operator must supply the intelligence by initiating instructions relating to the sequence of operations to be performed. Interlock circuits provide information to the operator indicating the next operation to perform, but the operator must initiate the operation. Preventive control is provided to preclude the operator from initiating the wrong operation (the system will only respond to the correct instructions).

The fuel-handling center is the primary control point for fuel-handling operations. With the exception of the transfer arm, all mechanisms constituting the fuel-handling system are controlled and supervised by an operator at the fuel-handling center. The transfer arm is manually operated; however, its operation is limited to the appropriate motions in the fuel-transfer cycle by electro-mechanical interlocks. The position of the transfer arm is transmitted to the fuel-handling center.

The circuitry for fuel-handling operations is interlocked with the reactor control system to prevent fuel-handling operations unless the reactor is shut down and the reactor control system is locked out. Conversely, reactor operation is prevented unless the fuel-handling control system is shut down and locked out. (This is accomplished by appropriate key switches as described in Section IV.J.)

The fuel-handling center is comprised of: (1) main operating panel; (2) punched card reader; (3) card punch; (4) alarm lights; (5) log count rate recorder; (6) scaler and scaler timer; and (7) miscellaneous controls and indicators.

The fuel-handling control system performs two distinct functions: (1) control operation of the various components in the system, and (2) prepare a record of certain operations performed (data gathering).

(3) Control of Component Operation

Repetitive, identical motions for a given operating sequence are controlled by conventional circuits utilizing limit switches, push buttons, etc. Motions which are a function of the point of origin or destination of a subassembly are performed in response to a numerically-controlled positioning system; for example: plug rotation, gripper rotation, storage rack rotation and vertical positioning, etc.

Prior to the transfer operations, the following information is supplied to the system on "input" punched cards: (1) type of operation (reactor to storage tank, etc.); (2) card serial number; (3) subassembly identification; (4) core location: row, sector, and number; and (5) storage rack, rotating plug, and gripper angular coordinates. The approximate accuracy and resolution of the numerical positioning system are summarized below.

Mechanism	Positioning Accuracy	System Resolution
Large rotating plug	$\pm 4 \times 10^{-5}$ rev.	1.0×10^{-5} rev.
Small rotating plug	$\pm 5 \times 10^{-5}$ rev.	1.0×10^{-5} rev.
Gripper (angular position)	$\pm 1 \times 10^{-3}$ rev.	5×10^{-4} rev.

The storage rack elevation and rotation drives are controlled in an "on-off" fashion to effect indexing at certain discrete points, the accuracy of which is determined by limit switch settings and other mechanical considerations. The transfer arm positions over the storage rack are supervised but are not controlled by the system.

The numerically-controlled positioning system utilizes digital position data throughout with one exception: conversion to analog data is made in the circuits controlling drive motor speed.

Several measures are taken to enhance reliability and eliminate errors. Coordinate information is punched in duplicate on the input cards. The two sets of data are automatically checked for agreement before the system takes action. Parity checking and redundancy checking techniques are employed where appropriate in the position transducer data handling circuits. And finally, each input card is punched with a serial number which is automatically checked for proper sequence.

(4) Data Gathering

A permanent record of operations regulated by the numerically-controlled positioning system is made on punched output cards. The output cards are automatically punched as the mechanisms are indexed in response to the input cards. The information punched corresponds to that on the input cards except that the coordinate data are derived from actual mechanism positions. The output cards are also punched to record the date and time. Thus a permanent record of actual performance is available and may be checked against the input cards at any time.

b. Fuel-Unloading System

The fuel-unloading system effects transfer of subassemblies between the primary tank and the interbuilding coffin. The mechanical components include the storage rack, transfer arm, transfer port, and fuel-unloading machine (see Fig. 20). The transfer of fuel between the Reactor Plant and Fuel Cycle Facility is described in Section III.A.9. The operations involved in fuel unloading (and interbuilding transfer) may be performed during reactor operation.

The transfer port provides access to the inside of the primary tank through the transfer arm nozzle. It forms the link between the transfer arm inside the primary tank and the fuel-unloading machine which operates on the main floor. The transfer port is basically a large, manually operated valve, normally closed, which is opened for fuel unloading. It has provisions for argon gas purging during the operations.

The fuel-unloading machine (Fig. 22) is an electromechanical device which transfers fuel subassemblies from the transfer arm inside the primary tank to the interbuilding coffin outside the primary tank. The machine is basically a shielded container-carriage assembly mounted on a set of tracks. The internal mechanisms include a gripping device, an argon gas-circulating system, and a drive unit which moves the machine between the transfer port and the interbuilding coffin location.

Briefly, the sequence of fuel unloading is as follows. An irradiated subassembly is removed from the storage rack by the transfer arm and aligned directly under the transfer port. The fuel-unloading machine is positioned over and sealed to the transfer port. The gripping device is lowered through the transfer port to the level of the transfer arm to engage the subassembly. The subassembly is lifted into the shielded container, transported to and lowered into the interbuilding coffin. The reverse procedure is employed to load a new subassembly into the primary tank.

The argon gas-circulating system is used to remove excess sodium from the subassembly, to cool the spent fuel during the transfer, and to preheat a new subassembly before insertion into the sodium.

8. Primary Tank and Biological Shield

The primary tank, primary tank support structure, blast shield, biological shield, and shield cooling system comprise an integrated system. The basic design requirements and design bases described in ANL-5719 were followed in developing the construction design.

a. Primary Tank

Minor revisions were made in the design of the primary tank as a result of more detailed structural analyses. The configuration of the beam structure in the bottom of both the inner and outer vessel was changed from a radial beam arrangement to several parallel beam stiffeners. The thickness of the outer tank cylindrical shell was reduced from 0.50 in. to 0.25 in. and stiffener rings placed on the outside of this vessel to prevent distortion. The six support hangers were revised from the pin type originally contemplated [Fig. 7], to a simple roller type. This eliminates the possibility of secondary stresses in the primary tank cover due to horizontal loads developed in the hanger links, and increases the reliability of symmetrical, unrestricted radial thermal expansion of the tank.

b. Primary Tank Support Structure

The primary tank support structure (Fig. 23) remains essentially unchanged except for a revision of the bottom beam arrangement tying the columns together and a reduction in depth of the circular beam

in the top structure. The radial beam arrangement [Fig. 32] was replaced with a box-like structure which ties the bottom end of the columns together with channels. The channels, in turn, are anchored to the concrete by a basket-shaped reinforcing bar arrangement hooked over the channels and imbedded in the concrete. This arrangement increased the utilization of the mass of concrete in the bottom structure, is more amenable to analysis, and is less expensive.

c. Blast Shield

The radial blast shield (Fig. 24) surrounding the primary tank was retained but its composition was revised. Ideally, each lamination of the blast shield attenuates the incident energy (and pressure) to a level for which the next lamination will exhibit maximum efficiency in further attenuating the energy and pressure. The efficiency of any one lamination depends principally on its thickness, density, dynamic crushing strength, and ability to absorb large amounts of energy (through crushing deformation). The material, thickness, and relative position of each lamination within the shield was selected to reduce the maximum credible accident pressure on the biological shield to a few psi above normal in the most efficient and practicable manner. Three laminations of nominal thickness shown in Fig. 24 are now provided, each separated by a steel shell (0.375 in. thick), with a steel shell (0.50 in. thick) forming the inside diameter of the blast shield. The outer layer contains "Celotex," the intermediate layer contains aerated concrete (16.5 lb/ft^3 density), and the inner layer contains vermiculite concrete (22 lb/ft^3 density). As shown in Fig. 24, the 0.25-inch steel liner shell on the inner face of the concrete biological shield was replaced by narrow steel strips placed in front of each T-1 column. The blast shield below the primary tank [Fig. E-1] has been eliminated; detailed analysis showed it to be unnecessary.

d. Biological Shield and Shield Cooling System

The biological shield and the shield cooling system remain unchanged.

9. Interbuilding Fuel Transfer System

The removal of the Disassembly Cell from the Reactor Plant to the Fuel Cycle Facility reflected revisions in the methods of transferring fuel subassemblies unloaded from the primary tank. The operations involved in transferring a subassembly from the primary tank to the interbuilding coffin are described in Section III.A.7.b. The transporting of a subassembly between the Reactor Building and the Fuel Cycle Facility involves the interbuilding coffin, and the equipment air lock.

The interbuilding coffin is a portable, sealed, shielded vessel with an integral argon gas-cooling system. The blower units on the coffin are battery powered to insure continuous operation in the event of transport difficulties or power failure during transit to the Fuel Cycle Facility. The interbuilding coffin also has provisions for removing the sodium adhering to the subassemblies by means of steam and/or water in the Fuel Cycle Facility. The effluent from the cleaning operation is piped directly to the sodium disposal unit in the Fuel Cycle Facility.

The fuel-unloading machine inserts a subassembly into the interbuilding coffin. The coffin is then lifted by the rotary bridge crane and placed onto a dolly inside the equipment air lock. After passing through the air lock, the coffin is placed on an interbuilding coffin cart and wheeled into the Fuel Cycle Facility where the subassembly is cleaned and then transferred to the Disassembly Cell.

The same equipment is employed to transfer a subassembly from the Fuel Cycle Facility to the primary tank. Sufficient fission product heat is generated in the reprocessed fuel subassembly to require forced convection cooling during its return to the reactor. This requirement indicated the advisability of a single system which would accomplish fuel subassembly transfer in both directions.

10. Primary Sodium Purification System

The primary sodium purification system is essentially unchanged. The surge tank and analytical devices have been relocated to improve system reliability and versatility.

Plugging indicators are located on the sodium inlet and outlet sides of the cold trap. They will be used to check the efficiency of the cold-trapping operations and to provide sampling points for chemical and radiological analysis of the sodium before and after the purification cycle.

One vacuum cup sampler is employed, with sampling points provided on each of the plugging-indicator loops.

Contact leak detector probes are now installed in the pump housing and on the floor of the Sodium Purification Cell (which is lined with steel plate). In addition, a leak-monitoring device has been included in the Sodium Purification Cell ventilation system. Any one of these devices will cause an immediate shutdown of the purification system should a leak occur anywhere in the system. An alarm indicating shutdown of the system is located in the control room.

Reactor-grade sodium has been supplied to the following specifications for both the primary and secondary sodium systems:

Element	Specified (Maximum)	Actual Analysis*
Calcium	10 ppm	<10.0 ppm
Carbon	50 ppm	17.0 ppm
Chlorides	30 ppm	23.0 ppm
Sulphur	10 ppm	5.0 ppm
Boron	5 ppm	<3.0 ppm
Lithium	20 ppm	<0.5 ppm
Silver	20 ppm	<3.0 ppm
Cadmium	20 ppm	<0.3 ppm
Gold	30 ppm	<13.0 ppm
Indium	30 ppm	<0.3 ppm
Potassium	1,000 ppm	<250.0 ppm
Sodium (including Potassium)	99.97% (min.)	99.98%

*Average of measurements made on samples taken during filling of railroad tank cars prior to delivery to EBR-II Site.

Subsequent analysis for uranium and thorium indicated average values of <0.5 ppm and <2.0 ppm, respectively.

11. Argon Blanket Gas System

The argon blanket gas system is essentially unchanged except for deletion of provisions for servicing the Disassembly Cell in the Reactor Plant. The removal of the Disassembly Cell decreased considerably the volume of the system and simplified the system requirements as shown in Fig. 25. This system maintains a static argon gas blanket over the primary sodium with provision for dynamic operation when necessary.

A floating head tank is used to control the argon blanket pressure to within ±1 in. H_2O pressure differential with respect to building atmospheric pressure under normal static operating conditions.

B. Secondary System

The coolant flow rate, temperatures, and pressure differences vary slightly from those originally contemplated. In general, these changes reflect only the estimated performance of the "as-built" equipment and additional information developed since the original report.

The secondary sodium flow rate is 2.5×10^6 lb/hr (approximately 5,900 gpm). Approximate inlet temperature to the heat exchanger is 588°F; the outlet temperature is 866°F (also the inlet temperature to the steam generator). The heat exchanger and steam generator are shown in Figs. 26 and 27, respectively.

Circulation is maintained by an a-c linear induction electromagnetic pump with a capacity of 6,500 gpm at about 53 psi. Flow control down to near zero flow is achieved by a generator voltage regulator which uses an amplidyne motor-generator set for very accurate voltage control of the main generator output to the pump.

1. Steam Generator

The steam generator (Fig. 27) consists of a natural circulation evaporating section, a conventional steam drum, and a once-through superheating section. The evaporating section comprises eight, identical, shell-and-tube heat exchangers connected in parallel on the tube side to a horizontal, overhead steam drum with conventional moisture separation internals. Dry and saturated steam leaves the top of the steam drum and flows downward through four, identical, vertical shell-and-tube superheaters and into the turbine-generator unit.

The design of the evaporators and superheaters is shown in Figs. 28 and 29. They are constructed entirely of $2\frac{1}{4}$% Cr-1% Mo material and utilize double-walled tubes. Each duplex tube consists of two, single length, seamless tubes which have been individually inspected as single-wall tubes and again inspected as a duplex tube. Four evaporators have mechanically-bonded duplex tubes, and four evaporators have metallurgically-bonded tubes. The units have double-tube sheets at each end; the outer tube is welded to the sodium tube sheet and the inner tube is welded to the steam tube sheet. The space between the tube sheets communicates directly with the atmosphere. No weld exists in these units with sodium on one side and water and/or steam on the other side. As a result, the only path between the sodium and the water and/or steam is across two seamless tubes which have been individually and jointly non-destructively inspected.

Difficulty has been encountered in fabricating the superheater units; more specifically, the outer tube-to-sodium tube sheet welds (see inset, Fig. 29). Many sound and reliable welds have been made, but not consistently. This welding problem did not prevail during fabrication of the larger tube evaporators. The smaller tube diameter and thinner wall of the superheater tube appear beyond the scope of the present welding techniques to produce consistently reliable welds. The effort to develop a satisfactory welding procedure for the superheater tubes is continuing; however, an alternate method of superheating has been selected pending solution of this welding problem.

Two additional evaporators modified as superheaters will be used temporarily. The evaporator design is similar to the superheater design, and analyses indicate that reasonable superheater performance can be obtained with a slightly modified evaporator. The modification

consists of coring the evaporator tubes with a 0.812 in. O.D. tube which provides increased steam velocity in the 0.125-inch steam annulus (see inset, Fig. 29).

The use of two modified evaporators as substitute superheaters will produce a steam temperature of about 820°F at 45 Mwt. The moisture content in the final stage of the turbine will increase slightly. Sufficient information is not available to determine the precise effect of increased moisture content on turbine life; however, the slight moisture increase expected should not seriously affect the useful life of the machine for this application.

Owing to the external similarity between the evaporators and superheaters, only minor modifications to the building, supporting structure, and piping were required to effect use of the modified evaporators.

2. Sodium Relief System

The secondary sodium system includes a sodium relief system to accommodate a pressure surge in the event of a sodium-water reaction. This system consists of two duplex, 10-inch blow-out diaphragms. One diaphragm is connected to each 10-inch sodium header which interconnects the superheaters and the evaporators. Each duplex diaphragm (two individual diaphragms in series) is designed to rupture at 100 psi. Rupture of the two diaphragms allows the sodium to flow from the header into a 1,200-gallon relief tank. The tank, in turn, communicates with the atmosphere via two 12-inch lines. Each of these lines is sealed with a rupture diaphragm set for 25 psi. The normal sodium pressure in the superheater-evaporator headers is about 10 psig.

C. Steam System

The steam system is shown schematically in Fig. 3. It is essentially as originally contemplated except for the addition of initial pressure regulation to the turbine-generator steam control. Accordingly, the turbine steam admission valves are controlled as a function of the pressure in the steam system to maintain a constant steam pressure. Thus, the turbine generator takes only that steam required to maintain a constant 1,250 psig in the steam headers. Normally, this is approximately equivalent to the heat generated in the reactor. In this manner, the electrical energy generated is a direct function of the reactor power and is independent of electrical demand.

D. Fuel Process System

The structural arrangement of the Fuel Cycle Facility has been altered considerably to improve the various operations involved in the

fuel cycle. These alterations do not affect the functions of the facility as they apply to the reactor or plant operation.

The first loading of the reactor fuel charge has been fabricated from 48.4% enriched uranium-"fissium" alloy using prototype equipment to be employed in the Fuel Cycle Facility. The methods of fabrication and the composition of the fabricated fuel materials are described in Appendix A.

IV. PLANT OPERATION AND PERFORMANCE

A. Control and Instrumentation

1. General

Minor modifications have been made to the control and instrumentation [Section IV.A.1.].

Throttle steam temperature during steady-state operation will not be maintained constant at 850°F irrespective of power level, but will deviate from this temperature at very low and very high power levels. A minimum primary coolant flow rate of approximately 23% (of full flow) is now stipulated; consequently, reactor coolant outlet temperatures at very low powers (below 20% of full power) are reduced from those required to generate 850°F steam, and the steam temperature decreases progressively with decreasing power in this range. Final thermal analyses have reflected higher reactor coolant flow rates with resulting lower outlet temperatures, and reduced performance of steam generation equipment. As a result, steam temperatures at all powers above 73% also will be lowered. These and associated major system temperatures and flow rates are shown in Fig. 30, which supersedes [Fig.47]. It should be noted that, while these values represent the normal operating conditions to be employed, the reactor will be operated occasionally with higher coolant flow rates and with corresponding secondary flow rates, steam temperatures, etc. The revised simplified flow diagram for the major systems shown in Fig. 3 supersedes [Fig. 1].

The number of nuclear instrument channels employed has been increased from ten to eleven; their detailed functions are described in Section IV.A.2.c. The number of thimbles housing the nuclear detectors has been reduced from ten to eight. All thimbles are now located inside the primary tank, as shown in Fig. 18.

General alarm and scram provisions are unchanged except that the "pre-scram warning alarm" has been eliminated. The list of specific system abnormalities causing scram and/or alarm [Table VII] has been extensively revised, principally by additions. The abnormalities which now cause scram are listed in Table III. System abnormalities causing alarm (only) are listed in Table K-1, Appendix K.

Table III

SYSTEM ABNORMALITIES CAUSING SCRAM AND ALARM

	Abnormality	During Reactor Operation	During Fuel Handling
1. Channel 1:	Source Flux Level	x(1)	x(2)
2. Channel 2:	Source Flux Level	x(1)	x(2)
3. Channel 3:	Source Flux Level	x(1)	x(2)
4. Channel 1:	Log Count Rate Level		x
5. Channel 2:	Log Count Rate Level		x
6. Channel 3:	Log Count Rate Level		x
7. Channel 1:	Period	x(3)(4)	x
8. Channel 2:	Period		x
9. Channel 3:	Period		x
10. Channel 1:	Fission Counter High-Voltage Supply	x(4)	x
11. Channel 2:	Fission Counter High-Voltage Supply	x(4)	x
12. Channel 3:	Fission Counter High-Voltage Supply	x(4)	x
13. Channel 4:	a) Period or b) Ion Chamber High-Voltage Supply	x(5)	x(5)
14. Channel 5:	a) Period or b) Ion Chamber High-Voltage Supply		
15. Channel 6:	a) Period or b) Ion Chamber High-Voltage Supply		
16. Channel 7:	Linear Level	x(6)	x
17. Channel 7:	Ion Chamber High-Voltage Supply	x(6)	x
18. Channel 7:	Linear Level Range Setting Interlock		x(7)
19. Channel 8:	Automatic Flux Control Rod Down	x(8)	

(1) Effective only prior to reactor operation; bypassed when control power is made available.
(2) Can be bypassed by keyswitch for replacing neutron source.
(3) Any two out of three will cause scram and alarm; any one out of three will cause alarm.
(4) Bypassed when neutron flux level exceeds prescribed power level (approximately 4×10^2 watt).
(5) Any two out of three channels will cause scram and alarm; any one out of three will cause alarm.
(6) Normally bypassed by a keyswitch during reactor operation; normally used only for experimental operations.
(7) Channel 7 amplifier must be on correct (low) range setting.
(8) Bypassed when on manual reactor control.

Table III (Cont'd.)

SYSTEM ABNORMALITIES CAUSING SCRAM AND ALARM

Abnormality	During Reactor Operation	During Fuel Handling
20. Channel 9: a) High-Flux Level (Manual)(9) or b) High-Flux Level (Automatic)(10) or c) Ion Chamber High-Voltage Supply		
21. Channel 10: a) High-Flux Level (Manual)(9) or b) High-Flux Level (Automatic)(10) or c) Ion Chamber High-Voltage Supply	x(5)	
22. Channel 11: a) High-Flux Level (Manual)(9) or b) High-Flux Level (Automatic)(10) or c) Ion Chamber High-Voltage Supply		
23. Instrument Thimble Detector Mounting, Bank (A) Temp. High	x(11)	x(11)
24. Instrument Thimble Detector Mounting, Bank (B) Temp. High	x(11)	x(11)
25. Any Control Rod Unlatched	x	
26. Any Control Rod Not In "Full Down" Position	x(1)	x(12)
27. Control Rod Scram Assist Air Pressure Low	x	
28. Safety Rods Not in "Full Up" Position	x	x(13)
29. Safety Rod "Hand Operated" Drive Interlock		x(13)
30. Reactor Inlet Coolant (high pressure) No. 1 Flow Low	x	
31. Reactor Inlet Coolant (low pressure) No. 1 Flow Low	x	
32. Reactor Inlet Coolant (high pressure) No. 1 Flow Rate-of-Change High	x	
33. Reactor Inlet Coolant (high pressure) No. 2 Flow Low	x	
34. Reactor Inlet Coolant (low pressure) No. 2 Flow Low	x	
35. Reactor Inlet Coolant (high pressure) No. 2 Flow Rate-of-Change High	x	
36. Reactor Outlet Coolant Flow Low	x	
37. Reactor Outlet Coolant Temperature High	x	
38. Core Subassembly Outlet Coolant Temperature High	x(11)	

(9) Trip is manually set at the channel amplifier prior to reactor startup.
(10) Trip is automatically set by Flux and Flow Trip Setter on Console.
(11) Four thermocouples are used: high temperature sensed by any two out of four causes scram and alarm.
(12) Bypassed when reactor vessel cover is not completely down.
(13) Can be bypassed by a keyswitch on the Console to permit Fuel Handling of the Safety Rods only after these rods have been raised mechanically (by hand-operated drive) to the "remove" position.

Table III (Cont'd.)

SYSTEM ABNORMALITIES CAUSING SCRAM AND ALARM

Abnormality	During Reactor Operation	During Fuel Handling
39. Bulk Sodium Temperature High	x(11)	
40. Bulk Sodium Level High	x	
41. Bulk Sodium Level Low	x	
42. Reactor Outlet Plenum Pressure High	x	
43. Primary Pump No. 1: Motor Power Off	x	
44. Primary Pump No. 1: Motor Winding Temperature High	x	
45. Primary Pump No. 1: Power to MG Off	x	
46. Primary Pump No. 1: Power to MG On		x
47. Primary Pump No. 1: MG Clutch Reference Voltage Low	x	
48. Primary Pump No. 1: MG Cooling Water Pressure Low	x	
49. Primary Pump No. 2: Motor Power Off	x	
50. Primary Pump No. 2: Motor Winding Temperature High	x	
51. Primary Pump No. 2: Power to MG Off	x	
52. Primary Pump No. 2: Power to MG On		x
53. Primary Pump No. 2: MG Clutch Reference Voltage Low	x	
54. Primary Pump No. 2: MG Cooling Water Pressure Low	x	
55. Auxiliary Pump Rectifier Output Voltage Low	x(1)	
56. Auxiliary Pump Input Current Low	x(1)	
57. Auxiliary Pump Battery Not Fully Charged (Charge Current High)	x(1)	
58. Auxiliary Pump Battery Discharge Current High	x(1)	
59. Argon Blanket Temperature High	x	x
60. Argon Blanket Pressure High	x	x
61. Fuel-Handling Operation Incomplete	x	
62. Reactor Vessel Cover Not Completely Down	x	
63. Reactor Vessel Cover: Any Lock Not in "Locked" Position	x	
64. Reactor Vessel Cover: Any Lock Holddown Force Low	x	
65. Reactor Building Isolation System	x	x
66. Reactor Building Gamma Radiation Level High	x	x
67. Reactor Building Air Temperature High	x	x
68. Reactor Building Air Differential Pressure High	x	x
69. Earthquake Detection System	x	x

2. Nuclear System

a. Control Rod Characteristics

Measurements obtained during Dry Critical Experiments have permitted an improved estimate of control rod worth. The expected worth of each rod is 0.004 $\Delta k/k$, and of all twelve rods approximately 0.048 $\Delta k/k$. With rod drive speed mechanically limited to 5 in./min, the maximum possible rate of reactivity addition by two rods moving simultaneously is less than 0.00008 $(\Delta k/k)$/sec. However, the automatic flux control system is designed to preclude the simultaneous movement of two rods in the same direction (see Section IV.A.2.g.).

The time elapsed between receipt of scram signal at the rod drive and start of rod movement has been determined experimentally (on the actual mechanisms, after final installation) to be less than 0.020 sec.

Maximum control rod acceleration during scram has been revised from approximately 2g to 1.5g (by lowering the scram assist pressure). The resulting curve(Fig. 31) of rod displacement versus time after start of rod movement during scram supersedes [Fig. 41]. The corresponding curve (Fig. 32) of fraction of total rod worth effective versus time after start of rod movement supersedes [Fig. 42].

b. Safety Rod Characteristics

Measurements obtained during Dry Critical Experiments have permitted an improved estimate of safety rod worth. The expected total worth of the two safety rods is approximately 0.013 $\Delta k/k$, slightly less than previously estimated.

c. Description of Nuclear Instrumentation

The instruments for measuring neutron flux and reactor period have been rearranged and increased to eleven channels. The reactor power range covered by each channel is indicated in Fig. 33 and described below.

(1) Three Log Count Rate-Period Channels (1, 2, and 3) measure log count rate and period from source level to about 500 w.

(2) Three Log N-Period Channels (4, 5, and 6) measure Log N and period from about 100 w to 100 Mw.

(3) One Linear Level Channel (7) measures flux level from about 300 w to 150 Mw.

(4) One Automatic Flux Control Channel (8) regulates neutron flux level from about 6 Mw to 60 Mw.

(5) Three High-Flux Level Channels (9, 10, and 11) measure flux level from about 1200 w to 250 Mw.

Figure 34 shows the connections and locations of the detector, amplifier, and readout equipment for each channel.

The Log Count Rate Range is covered by three fission counter channels (1, 2, and 3) which indicate reactor period and record log count rate. These channels provide a startup level interlock which withholds control power for reactor operation, or for fuel handling, unless the neutron flux level exceeds a preset level (300 cpm). For reactor operation, the period trips are connected in coincidence, with two out of three channel trips causing reactor scram. This arrangement decreases the probability of reactor scram due to faulty equipment or spurious signals. In addition, scram will result from loss of high voltage to any counter. These scrams are bypassed when the flux level reaches a preset level setting in channels 4, 5, and 6 (approximately 400 w). For fuel-handling operation, the period trips, the log count rate trips, and the counter high-voltage trips are connected in series; any one of these trips will scram the safety rods.

The Log N-Period Range is covered by three compensated ion chamber channels (4, 5, and 6) which indicate reactor period and record log N. During reactor operation or fuel-handling operation, tripping of two out of three channels causes scram. A channel trip can be caused by either an abnormally short period or a loss of high voltage to the ion chamber.

The Linear Level Range is covered by one compensated ion chamber channel (7) which records reactor power level. Linear indication of reactor power level is given on an expanded scale, obtained by manual range switching. Linear level trip is provided with automatic adjustment of trip level setting integral with the range switching. A trip is also provided for the loss of high voltage to the compensated ion chamber. Normally, these trips will be bypassed by a keyswitch on the Console, and will be employed only for experimental operations. They will be effective throughout fuel-handling operations; in addition, an interlock requires that the range switch be set at the correct (low) range.

The function of the Automatic Flux Control Channel (8) is described in Section IV.A.2.g.

The high-flux-level range is covered by three compensated ion chamber channels (9, 10, and 11) which record reactor power level. The high-flux level trips will be preset at approximately 104%, 108%, and 110% of the power level at which the reactor is to be operated. In addition, a second high-flux level trip for each channel is provided and is set automatically by the Flux-Flow Trip Setter on the Console (see Section IV.A.2.f.). Each channel has a trip for the loss of high voltage to the ion chamber. Each of the foregoing trips causes a channel trip. The channel trips are connected in coincidence, with trip of two out of three channels causing scram.

A summary of the period and level trips provided for reactor operation and for fuel handling is given in Table IV.

Table IV

SUMMARY OF PERIOD AND LEVEL TRIPS FOR NORMAL REACTOR OPERATION AND FOR FUEL-HANDLING

Channel No. and Range	Reactor Operation				Fuel Handling			
	Period Trip	Approx. Setting	Level Trip	Approx. Setting	Period Trip	Approx. Setting	Level Trip	Approx. Setting
Source Flux Level (Startup)* (Channels 1, 2, and 3)			1 of 3	300 cpm			1 of 3	300 cpm
Log Count Rate-Period (Channels 1, 2, and 3) Source to 500 w	2 of 3	20 sec			1 of 3	20 sec	1 of 3	500 w
Log N - Period (Channels 4, 5, and 6) 100 w to 100 Mw	2 of 3	20 sec			2 of 3	20 sec		
Linear Level (Channel 7) 300 w to 150 Mw			Available for Experimental Operation				1	1,000 w
High Flux Level (Channels 9, 10, and 11) 1,200 w to 250 Mw			2 of 3	104% to 110% of Operating Power Level				
Flux-Flow Trip Setter (Channels 9, 10, and 11) 1% Power to 100% Power			2 of 3	105% of Operating Power Level				

*Withholds control power for reactor operation or fuel-handling operations unless neutron flux level exceeds 300 cpm.

Regulated a-c power is supplied to the nuclear instrument channels from the Nuclear Continuous Power Supply through three separate electronic regulator circuits. Channels 1, 4, 7, and 9 are connected to one regulator; Channels 2, 5, and 10 are connected to the second; and Channels 3, 6, 8, and 11 are connected to the third. In addition to furnishing well-regulated power for the instrumentation, this method of supplying power to the nuclear channels accomplishes the following:

(1) During normal operation, failure of one regulator will not cause reactor shutdown since only one channel in each of the startup, intermediate, and power ranges will trip. Two trips in the same range will cause shutdown.

(2) In the remote event of two regulator failures, the reactor will scram but one complete chain of nuclear instrumentation will continue to monitor the neutron flux after shutdown.

(3) In the event of primary power failure, the electrical load can be reduced to conserve auxiliary (battery) power on the Nuclear Continuous Power System. One or two regulator supplies can be turned off, retaining one channel in each range operative.

d. Neutron Source

The neutron source is unchanged; however, the neutron source strength requirements have been determined experimentally (Appendices E and L).

e. Reactor Scram Circuit

The reactor period and flux level trips which scram automatically the twelve control rods during reactor operation, or the two safety rods during fuel-handling operations, are summarized on the reactor scram circuit diagram, Fig. 35. Also shown are abnormalities other than nuclear trips which cause scram, interlocks which permit transfer of control power to either reactor operation or fuel-handling operations, and conditions prerequisite to reactor startup.

f. Control of Flux-Flow Relationship

The reactor and the power system are designed to operate through the power range with a proper balance between the various thermal systems as indicated in Fig. 30. Trip points are set automatically for neutron flux and primary sodium coolant flow for any preset power level.

The trip points are set to alarm (only) at conditions where the reactor is "overcooled," and to alarm scram at conditions where the reactor is "under cooled." This is accomplished by the Flux-Flow Trip Setter (calibrated in per cent of full power), on the Console. Interconnected on a single shaft are a series of adjustable potentiometers. The potentiometers establish the desired voltage in appropriate bucking circuits to match the signal voltage from Channels 9, 10, and 11, and the electromagnetic flow meters which measure the coolant flow from each pump and from the reactor. These signals are supplied to four deviation meters, located on the Console, which measure per cent deviation from the desired value of: sodium flow from Primary Pump No. 1 to high-pressure plenum; sodium flow from Primary Pump No. 2 to high-pressure plenum; sodium flow from reactor; and neutron flux level. The deviation meter for the neutron flux level is supplied with a three-position selector switch to Channel 9, 10, or 11.

The deviation meters are of the "zero-center" type and each circuit features independent, adjustable high and low trips that can be set to any value between 0% and ±50% deviation. The trips will be set at about ±5% deviation for normal reactor operation. The trip settings are arranged to alarm (only) at coolant flow "too high," and to alarm and scram at coolant flow "too low" (on any one of the three deviation circuits) and neutron flux "too high" (in a 2 out of 3 coincidence trip circuit).

The control voltages for flow are established by specially wound potentiometers which conform to the relationship between reactor power level and primary coolant flow shown in Fig. 30. The desired flux setting is simultaneously established.

The flow-deviation system includes a "rate of change of flow" measurement device with trips that can be set at any value between 0 and 10% (of existing flow)/sec. These trips will be set at approximately 1% (of existing flow)/sec for normal reactor operations. (This system is somewhat analogous to the period trips actuated by rate of change of neutron flux.)

g. Automatic Flux Level Control System

An automatic flux level control system has been developed for future application on the EBR-II. The system is designed to maintain reactor power at ±1% of a preselected power level after equilibrium operation at that level has been established manually by the operator.

The automatic flux controller consists of a comparator circuit and amplifier with a relay output. The current from an ionization chamber is compared to a reference current. The reference current is adjustable from the Console and is called a power demand setting. Deviations of ±1% in ionization chamber current result in relay closure for rod up or down motion, depending on whether the ionization chamber current is less than or greater than the reference current. The relay contacts energize the control rod drive mechanisms. The system is designed to provide automatic flux level control, using only one rod at a time. Any one of the twelve control rods may be selected for this purpose.

Several design features are incorporated into the automatic control system to ensure safe operation. Prior to placing the selected rod into the automatic mode, the rod must be located within narrow limits at a designated position, i.e., within ±0.5 in. of the 7.0 in. position (interlock enforced), and the actual reactor power must match the demanded power within ±1% (interlock enforced). After the control rod position and power requirements have been met, the operator can transfer the selected rod to automatic operation. After the rod has been placed under automatic control, the power demand setting control is inoperative. To change reactor power,

the control rod must be returned to manual operation, the power demand setting changed to the desired power level, and the rod position and power matching procedure must be repeated.

While in the automatic mode, the range of rod motion is monitored by limit switches. If the movement into the core (up) exceeds a predetermined rod position (11.0 in.) in response to a downward drift of reactor power, an audible and visual alarm on the Console is energized. These alarms will not cease until manual shim rod action is taken to restore the rod to its normal operating range. At 14 in. of rod travel, a second limit switch will energize another audible alarm, de-energize the automatic control circuit, and restore manual control. If the reactor power drift is upward, the automatic circuit will drive the control rod out of the core (down). If manual corrective shim rod action is not taken by the operator and control rod travel exceeds a predetermined rod position (3.0 in.), a limit switch will operate an audible and visual alarm on the Console. If rod movement (downward) continues, a second limit switch (0 in.) will de-energize the automatic control circuit and initiate reactor shutdown automatically (scram).

Another safety feature of the automatic control system involves timing of rod motion. In the event the automatic control unit suffers an internal failure which results in a continuous demand to raise or lower the control rod, a timer circuit which measures the duration of motor starter closure will transfer the system to manual control when the preset time limit is exceeded. The limit will be determined experimentally on the operating reactor by timing the magnitude of control rod required to change reactor power by 3% at full power with the rod in its most effective position. The magnitude of rod motion may be estimated by assuming a power coefficient of reactivity of 3.5×10^{-5} $(\Delta k/k)/Mw$, and a maximum rod worth of 4.9×10^{-4} $(\Delta k/k)/in.$ Since 3% of full power is 1.88 Mw, the assumed power coefficient gives a reactivity change of 6.58×10^{-5} $\Delta k/k$ and a corresponding rod motion of 0.134 in. This example is based on analysis; the final value of timer setting will be determined from actual reactor operating data.

Timing is accomplished by measuring the voltage across a capacitor, which is charged exponentially through a resistor. This voltage trips a relay on a preset value. The capacitor is charged positive for rod raise, and charged negative for rod lower. The capacitor discharges with a time constant identical to the charge time constant, and, in a sense, has a memory. This insures that application of a sequence of rod motions, each slightly less in duration than the set trip time, will not allow the rod to be driven to an end limit as would be the case if the capacitor were instantaneously discharged after each increment of rod motion.

The following abnormal conditions will automatically transfer the system to manual control:

(1) Reactor scram.
(2) Automatic control rod at 14 in.
(3) Automatic control rod at 0 in. (also causes scram).
(4) Loss of automatic control system ionization chamber high voltage.
(5) Loss of positive and negative voltages in automatic control unit.
(6) Filament failure of relay driver in automatic control unit.
(7) Time of rod movement exceeded.

The system is interlocked to give the "rod-lower" control relay preference over the "rod-raise" control relay. If several control system failures occur simultaneously, such that the "raise" and "lower" relays both call for control rod motion and the protective interlocks fail to transfer the system from automatic mode to manual operation, the control rod will be driven to its "full down" position, automatically scramming the reactor. Another interlock will prevent automatic control rod motion in the "up" direction if manual shimming is being performed in the "up" direction.

The performance of the automatic control system has been experimentally evaluated. The final control system hardware, including control amplifier and three-phase motor, has been incorporated in a closed loop control system. An analog computer has been used to simulate the reactor transfer function. Prior to using the automatic control system on the reactor, the reactor transfer function and control rod worth will be experimentally measured at several power levels. The measurements will be compared to the theoretical parameters used in the control system design to determine that the system will perform satisfactorily on the operating reactor. The automatic control system will not be connected into the operating system until extensive experience is gained with the reactor at several power levels and its kinetic behavior is understood.

3. Primary System

The control and instrumentation for the primary system is essentially unchanged. Minor modifications have been made in scram and alarm provisions, as shown in Table III and Table K-1 (Appendix K). The principal monitoring points [Fig. 18] have been revised as indicated on Fig. 36. Revision of the auxiliary pump flow decay curve when on battery power supply [Fig. 48] is described in Appendix B.

4. Secondary System

The instrumentation and control of the secondary system is essentially unchanged. (A complete list of alarm indications is included in Appendix K.)

5. Steam System

The principal change in the steam system control and instrumentation is the addition of the initial pressure regulation feature to the turbine-generator steam control. Steam pressure is controlled by the initial pressure regulator when the turbine-generator is in service, and by the automatic controller in the steam bypass line when the turbine-generator is not in service.

To provide the desired degree of reliability, the steam system is arranged to isolate the reactor from turbine-generator load variations. The turbine-generator normally will be in parallel (electrically) with the NRTS 138-kv loop; consequently, electrical load variation will be minimized. Two modes of operation are available:

(1) Bypass a small quantity of steam around the turbine at all times to provide available steam to absorb minor load variations. The amount of bypass steam required to absorb the maximum load variations must be determined by actual operational experience, but the bypass system is capable of handling up to 100% of the steam generated. (For purposes of establishing a heat balance for this mode of operation, a bypass flow of 5,000 lb/hr is assumed at full load.)

(2) Operate the turbine under the control of the initial pressure regulator. Bypassed steam is not required.

In addition to the above change, the pressure reducing-desuperheating stations have been removed. Consequently, at low load on the turbine, steam is supplied to Heater No. 1 from the low-pressure flash tank and the exhaust from condensate pump turbine driver, and to Heater No. 3 from a PRV station and the low-pressure flash tank. This system provides a reasonable cycle efficiency under normal turbine operation, essentially constant feed-water temperature at all loads irrespective of turbine operation, and adequate pressure head for draining the heaters during operation without the turbine in service.

All other instrumentation and control are essentially unchanged.

6. Electric Power System

Numerous revisions and additions were made to the electrical power system as the final plant design evolved. The single-line diagram shown in Fig. 37, supersedes [Fig. 49]. The most significant effect of these changes has been to increase the reliability and/or continuity of power supply for the more critical systems. The principal revisions include:

(1) Three, automatic starting, diesel-generator sets (400-kw, 200-kw, and 100-kw), are provided, instead of one. The 400-kw unit supplies emergency power for all areas of the EBR-II except the Fuel Cycle Facility; the latter is serviced by the 200-kw unit. The 100-kw unit provides backup emergency power for the instrument thimble cooling system, the shield cooling system, and the Reactor Plant emergency instrument air compressor in the event the 400-kw unit should fail to operate.

(2) The ARBOR feeders [Page 70] have been deleted.

(3) The rectifier unit for the primary system auxiliary pump is now manually applied to the emergency power supply system. The pump flow characteristics on the parallel (floating) battery power supply [Fig. 48] have been revised (see Appendix B, and Fig. B-10).

7. Building Isolation System

The containment design of EBR-II as previously described [Appendix E] and as described in Appendix H, includes the "primary containment system" and the "building containment system." The latter system consists primarily of a steel shell enclosing the complete Reactor Plant. Penetrations are provided for access of personnel, equipment, freight, air ducts, and piping. To assure gastight integrity of the shell, immediately subsequent to a maximum credible nuclear excursion, it is necessary to render each of these penetrations leakproof. Many are designed to be continuously leaktight; however, eighteen of the total of twenty-seven ducts or pipes penetrating the shell must be mechanically (automatically) closed. For this purpose, nineteen fast-acting isolation valves are incorporated in these lines (two valves on the double-branched ventilating air inlet duct, one on each of the others). A complete listing of these valves is included in Appendix H.

The building "isolation system" includes the isolation valves, nuclear-incident detection devices, and the system circuitry which controls the position of the valves. All valves are air-to-open, spring-to-close, with electrical (solenoid) pilot valve control. They close automatically upon loss of either instrument air pressure or electrical power.

The detection devices include:

(1) Two radiation detectors to sense radioactivity level inside the building.

(2) One pressure detector to sense building air pressure relative to atmospheric pressure.

(3) Four thermocouples to sense reactor coolant temperature at outlet from subassemblies.

(4) One thermocouple to sense building air temperature.

(5) Two resistance thermometers (long time constant) to sense building air temperature.

Each detector circuit is provided with an adjustable trip. The four thermocouples sensing reactor coolant temperature are connected in a two-out-of-four trip arrangement. This latter trip is effective only during reactor operation or standby, since fuel-handling operations require the reactor cover (carrying the thermocouples) to be raised to the top of the primary tank.

In the remote event of a significant nuclear incident or primary system sodium fire, trip initiated by one or more of the above detectors will interrupt electrical power to the isolation valves and all valves will close immediately. Trip of the isolation system will also scram the reactor.

B. Normal Steady-State Operation

This section describes the numerous minor revisions in operating conditions of the power system at full power (62.5 Mw). In general, these revisions stem from the change in nominal core configuration (from 61 to 67 subassemblies), design detail changes in the reactor and heat transfer systems, and refinements in neutronic and thermal analyses. For clarity, portions of the section [Section IV.B.] are rewritten in their entirety.

1. Flux Distributions

a. Neutron Flux

The expected neutron flux distributions do not differ greatly from those presented in ANL-5719. However, refinements in analysis and availability of pertinent experimental data have resulted in greater confidence and precision in the predicted distributions. Differences between the present analysis and the earlier analysis include the following (in addition to the change in core configuration):

(1) The assumed fuel alloy density is 17.95 gm/cc, instead of 18.7 gm/cc. (Actual density of the fabricated first loading is approximately 17.8 gm/cc.)

(2) The assumed fuel alloy constitution is that of the fabricated first loading (including actual fissium content), instead of pure uranium.

(3) Minor changes in composition and dimensions of axial and radial blankets have been taken into account.

(4) Multigroup results are based on 3- and 11-energy groups. Previous results were based on 2- and 10-energy groups.

(5) Multigroup analyses are based on two-dimensional models. Previously, only the two-group calculations were based on two-dimensional models..

Since the present neutron flux distributions are quite similar to those reported previously, only typical comparative results are presented here. High-energy (>1.35 Mev) neutron flux as a function of radius at the core midplane is shown in Fig. 38 for the core and inner blanket regions. Low-energy (<1.35 Mev) flux for the same regions is shown in Fig. 39. Both high and low energy neutron flux distributions for the outer blanket are shown in Fig. 40. The three curves in each figure represent the following (two-dimensional) cases: (1) an 11-group analysis for the 67-subassembly core; (2) a 3-group analysis for the 67-subassembly core; and (3) the previous 2-group analysis for a 61-subassembly core. All curves are normalized to 62.5 Mw. Comparisons of the analytical results with experimental data have shown the 11-group analysis is the more accurate method.

The results indicate that both high-energy and low-energy neutron fluxes near the center of the core are lower than previously predicted; therefore, the expected power densities are lower. In most of the inner blanket, however, both high-energy and low-energy fluxes are several per cent higher than previously predicted; consequently, the expected power densities are higher. (The high-energy flux produces more than 90% of the fission power in this region.) The high-energy flux level in the outer blanket is substantially higher than reported earlier; however, fission power is derived primarily from the high-energy flux only in the innermost regions.

Table V summarizes the predicted maximum neutron fluxes, fission density, and power density, together with corresponding values reported previously.

Table V

NEUTRON FLUX AND FISSION DENSITIES AT CENTER OF CORE

(Power = 62.5 Mw)

	Previously Reported [Page 77]	Present Analysis
Neutron Flux, n/(cm²)(sec)		
Total	3.7×10^{15}	3.55×10^{15}
Below 1.35 Mev	2.9×10^{15}	2.86×10^{15}
Above 1.35 Mev	0.8×10^{15}	0.69×10^{15}
Fission Density, F/(cc)(sec)	4.4×10^{13}	3.7×10^{13}
Power Density, Mw/liter	1.37	1.23

b. Gamma Flux

The gamma-ray flux distributions [Section IV.B.1.b.] still prevail except in two areas. The change in reactor vessel configuration and corresponding changes in the radial neutron shield (see Section III.A.1.h.), have reflected a decrease (~20% - 50%) in the gamma-ray flux in and around the reactor vessel wall. The corresponding maximum internal heat generation in the vessel wall is: 0.02 w/cc for the area with, and 0.01 w/cc for the area without graphite between the wall and the outer blanket.

Table VI lists the revised estimates of gamma and fission heat generation within the blanket regions at locations where such heating is of greatest significance.

Table VI

GAMMA AND FISSION HEAT GENERATION

(in kw/liter of reactor volume)

Location	Gamma	Fission
*Inner blanket, Row 6, R = 23.2 cm, Z = 0	62	170
*Inner blanket, Row 7, R = 28.5 cm, Z = 0	32	95
*Outer blanket, Row 8, R = 33.3 cm, Z = 0	11	29
Outer blanket, Row 15, R = 73 cm, Z = 0	0.1	0.2
Bottom end of upper blanket, R = 0	29	31

*Near core-type subassemblies in sixth row.

c. Secondary System Sodium Activation

Multigroup neutron flux calculations have been performed to estimate the number of neutrons captured by the secondary system sodium in passing through the heat exchanger within the primary tank. Based on the total neutron capture rate and the sodium gamma activity, the radiation level at the surface of insulation surrounding a 12-inch pipe (main secondary system piping) is estimated not to exceed approximately 5 mr/hr. This value is subject to considerable calculational uncertainty, but it is clear that shielding requirements, if any, will be minimal.

2. Reactor Heat Generation Distributions

The heat generation distributions described pertain to the nominal (67 subassembly) core loading. Loadings of 61 to 73 subassemblies will alter these distributions, particularly within inner and outer blanket regions immediately adjacent to, or near core-type subassemblies in the sixth row.

Table VII shows the approximate distribution of power generation in various regions of the "clean" reactor.

Table VII

REGIONAL DISTRIBUTION OF POWER GENERATION

Region	Power, Mw	% of Total
Core	53.5	85.6
Upper plus lower blanket	1.5	2.4
Inner blanket	6.1	9.8
Outer blanket	1.4	2.2
	62.5	100.0

The radial maximum power density distribution (including gamma-absorption contributions) at the center plane of the reactor is shown in Fig. 41. This distribution is based on 82% insertion of each of the twelve control rods, and 100% insertion of the two safety rods. The power densities at given radii vary somewhat with angular orientation and significantly within the inner blanket and innermost portion of the outer blanket.

The radial maximum-to-average power density ratio of the core at the reactor center plane is 1.46; the effective radial maximum-to-average ratio over the entire height of the core (assuming the control rods to be fully inserted) is 1.44.

Figure 42 shows the axial power density distributions at the core centerline and at the hottest channels: within the core (R = 13.9 cm), within the inner blanket (R = 23.2 cm), and within the outer blanket (R = 33.3 cm). The "hottest channel" in a given reactor zone is that fuel or blanket element, with its associated coolant channel(s), within which occurs the highest uranium temperature.

The axial maximum-to-average power density ratio at the core centerline is 1.15. The effective axial maximum-to-average ratio over the entire radius of the core (assuming the control rods to be fully inserted) is 1.14. The axial maximum-to-average ratio for the hottest channels are: 1.14 within the core; 3.60 within the inner blanket; and 3.60 within the outer blanket.

Maximum power density in the core, with control rods 82% inserted, is 1.23 Mw/liter (of core volume). Average power density in the core is 0.735 Mw/liter. The ratio of maximum-to-average power density in the core is 1.67.

These power densities and distributions are based on the "clean" reactor. Analysis indicates that sensible changes in heat generation distribution are incurred slowly during operation as a result of core burnup and plutonium formation. The most rapid changes (of practical significance) occur within the inner rows of the inner and outer blankets where maximum power densities increase approximately 3% and 6%, respectively, per atom per cent core burnup. The major significance of the power density increase is the increase in temperature of the blanket and its possible effect on radiation damage resistance. This change is slow enough, however, to permit adequate monitoring for radiation damage by periodic withdrawal and inspection of subassemblies on a basis of progressively increasing exposure. In addition, a large portion of the blanket is substantially "overcooled" and only a small region will experience a temperature rise which could significantly affect radiation damage resistance. Accordingly, these changes in heat generation distribution have not been included in the calculation of maximum blanket temperatures described in the following section.

3. Reactor Temperature Distributions

In a given reactor, the maximum mean reactor outlet coolant temperature achievable for specific maximum permissible fuel and blanket alloy temperatures is a function of various parameters; e.g., reactor inlet coolant temperature level, reactor power level, and coolant distribution. In general, to attain high, mean coolant outlet temperature at a practical coolant inlet temperature and high reactor power, it is necessary to orifice the coolant flow to certain subassemblies; i.e., it is necessary to establish

an optimum coolant mass flow distribution. Achievement of this distribution in the EBR-II requires orificing of all rows of subassemblies except Rows 1 and 2 (numbered radially outward from the center of the core). In most cases, the degree of orificing required will vary, since significantly different amounts of power per subassembly are generated in the various rows. The degree of orificing employed in each row is based on one or more of the following limitations (depending upon the row): maximum permissible fuel alloy or blanket uranium temperature; maximum permissible coolant temperature at subassembly outlet; and minimum acceptable orifice size.

An additional consideration affecting calculated temperature distributions within the reactor is the degree of uncertainty associated with each of the thermo-physical quantities employed in the calculations. These include uranium thermal conductivity value, heat transfer coefficient, neutron and gamma flux level, etc. The most important calculations are those which determine the temperatures occurring along the centerlines of fuel elements and blanket elements. The centerline temperature at a specified point is equal to the inlet coolant temperature plus the sum of a series of calculated temperature rises; e.g., coolant ΔT from inlet to the point of interest, rise through the coolant film, rise through the element clad, etc. If each thermo-physical quantity affecting the magnitude of the various temperature rises is analyzed separately, a degree of uncertainty can be estimated and an "uncertainty factor" assigned. The magnitude of this uncertainty factor reflects the degree of uncertainty associated with the magnitude of the particular quantity. Multiplication of a nominal calculated temperature rise by an uncertainty factor results in a larger temperature rise, the validity of which presumes the factor to have been manifested at its fullest magnitude and in the adverse direction. For example, with an uncertainty factor of 1.20 for the film heat transfer coefficient, the nominal temperature rise through the coolant film would be increased by 20%.

Application of a discrete uncertainty factor to a discrete nominal temperature rise is straight-forward in concept. Expansion of this method to include all the uncertainty factors operating upon all the nominal temperature rises which each might affect, however, results in an excessively conservative estimate of maximum temperature. Using this procedure, all uncertainty factors applicable to a given nominal temperature rise first are multiplied together to obtain a "total" factor. The nominal rise is then multiplied by this "total" factor. All the increased temperature rises so obtained are then added. This sum represents the total temperature rise (with all uncertainty factors included) from coolant inlet to point of interest on the element centerline.

The above procedure for application of uncertainty factors is unrealistic. It assumes that all factors will become manifest at the same

time, at the same location, each to its fullest magnitude, and each in the adverse direction. With respect to predicting maximum fuel temperature, it also assumes that the location of such manifestation is at or near a location of nominally highest temperature. The probability that all of these conditions will be met is virtually zero.

Because of the excessive conservatism inherent in application of the full uncertainty factors (as above) for the thermal analysis reported earlier [ANL-5719], each "total" factor was arbitrarily reduced in magnitude. A "$\frac{2}{3}$" factor was applied to each nominal temperature rise instead of the "total" factor; i.e., 1.18 instead of 1.27, 1.36 instead of 1.54, etc. By this procedure, the indicated increase in each temperature rise (including total rise from coolant inlet to point of interest on element centerline) is 67% of that which would result from application of the full uncertainty factors.

Further study and experience has led to the conclusion that a more optimistic treatment of uncertainty factors than the "$\frac{2}{3}$" factor method is justified. This has resulted, in part, from: (1) increased confidence in prediction of neutron and gamma flux distributions because of improved theoretical analyses, additional ZPR-III critical experiments, and the Dry Critical Experiments; (2) a more detailed knowledge of the reactor coolant flow distributions determined in extensive water model flow tests at Franklin Institute and at Argonne; (3) improved reliability of estimates of fuel element manufacturing deviations gained in actual fabrication of the first core loading; and (4) favorable irradiation damage data obtained at high burnups and temperatures (Appendix A).

The principal justification for more optimistic treatment, however, is based on the fact that a fuel alloy local temperature slightly in excess of the maximum calculated, while undesirable, is not destructive. Such higher temperature would merely increase the extent of local irradiation damage for a given burnup; it would not effect sudden, complete element failure. In a real sense, this incremental temperature is identical with an incremental degree of burnup in that the chief effect of each is an increment of fuel alloy (dimensional) damage. The effect of a slightly increased temperature, consequently, may be compensated by an appropriately decreased burnup, and conversely. Accordingly an increased probability of occurrence of a given high temperature can be offset by exercising increased conservatism in specifying the maximum burnup permissible.

Selection of the most suitable general method of applying uncertainty factors is a matter of judgment. One method, as described earlier, applies the full factors to the nominal temperature rises. Another method arbitrarily employs a constant "fraction" of the full factors; e.g., a "$\frac{2}{3}$" factor or "$\frac{1}{3}$" factor. More recently, statistical methods have been employed.

Le Tourneau and Grimble[3] suggested the statistical approach. Bonilla[4] described details of such an approach, and various organizations: UKAEA,[5] ORNL,[6,7] Bettis,[8,9] APDA,[10] Phillips,[11] and others,[6,12] have used or studied statistical methods. Moreover, several reactors have been designed using a statistical method; e.g., ETR, EGCR, GCRE-I, and EFFBR. The use of statistical methods in the application of uncertainty factors results in an increase in the estimated total temperature rise from coolant inlet to fuel hot spot in the range of about 25% to 50% of the temperature rise calculated with the application of full uncertainty factors.

In the present EBR-II analysis, a general statistical method is followed except that no attempt is made to correlate either the assigned uncertainty factor magnitudes or the calculated maximum fuel temperature with a precise "confidence level." Each uncertainty factor is applied to each nominal temperature rise which it might affect to obtain the increase in the rise, or deviation. All deviations stemming from a single thermo-physical quantity are then added and the sum squared. The sum of all such squares is obtained and the square root taken. This root is considered to be the total increase applicable to the nominal temperature rises, or the increase in total temperature rise from coolant inlet to point of interest on the element centerline. The method is illustrated in Table VIII for the case of maximum core fuel alloy temperature at full power (62.5 Mw). The indicated increase in total temperature rise from coolant inlet to the fuel hot spot, 58°F, is 35% of that which would result from application of full uncertainty factors.

Table VIII

ILLUSTRATION OF UNCERTAINTY FACTOR APPLICATION METHOD

(For maximum core fuel temperature at full power, 62.5 Mw)

Thermo-Physical Quantity		$\theta_{\Delta T}$ = 322°F		θ_f = 26°F		θ_c = 39°F		θ_b = 8°F		θ_l = 13°F		θ_u = 105°F		Σd	$(\Sigma d)^2$
		F	d	F	d	F	d	F	d	F	d	F	d		
Neutron and Gamma Flux		1.07	22.5	1.10	2.6	1.10	3.9	1.10	0.8	1.10	1.3	1.10	10.5	41.6	1730.6
Flow Rate Through Subassembly		1.05	16.1	-	-	-	-	-	-	-	-	-	-	16.1	259.2
Flow Profile Within Subassembly		1.05	16.1	-	-	-	-	-	-	-	-	-	-	16.1	259.2
Manufacturing Deviations From Nominal	Clad Dimens.	-	-	-	-	1.05	2.0	-	-	-	-	-	-	2.0	4.0
	Bond Dimens.	-	-	-	-	-	-	1.04	0.3	-	-	-	-	0.3	0.1
	U Dimens.	-	-	1.02	0.5	1.02	0.8	1.02	0.2	1.02	0.3	1.02	2.1	3.9	15.2
	U^{235} Conc.	1.01	3.2	1.01	0.3	1.01	0.4	1.01	0.1	1.01	0.1	1.01	1.0	5.1	26.0
Thermal Conductivity	Clad	-	-	-	-	1.10	3.9	-	-	-	-	-	-	3.9	15.2
	Bond	-	-	-	-	-	-	1.10	0.8	-	-	-	-	0.8	0.6
	Uranium	-	-	-	-	-	-	-	-	-	-	1.15	15.8	15.8	249.6
Heat Transfer Coefficient		-	-	1.20	5.2	-	-	-	-	-	-	-	-	5.2	27.0
Measurement of Power Level		1.02	6.4	1.02	0.5	1.02	0.8	1.02	0.2	1.02	0.3	1.02	2.1	10.3	106.1
Transient Overload		1.05	16.1	1.05	1.3	1.05	2.0	1.05	0.4	1.05	0.6	1.05	5.2	25.6	655.4

Note: F is the uncertainty factor; d is the temperature deviation, °F

Total $\Sigma(\Sigma d)^2$ = 3348

Square root of total = 57.9°F

Nominal maximum core fuel temperature (without uncertainty factors) = 1213°F
Increase in total temperature rise as calculated above = 58°F
Maximum core fuel temperature including uncertainty factors = 1271°F

Assigned magnitudes of the uncertainty factors are shown in Table IX. The nomenclature in parentheses at the column headings refer to pertinent temperature rises: ΔT, coolant temperature rise from inlet to point of interest; θ_f, rise through coolant (heat transfer) film; θ_c, rise through clad; θ_b, rise through sodium bond; θ_i, total rise through clad-bond and bond-uranium interfaces; and θ_u, rise through the uranium. Certain factors have been revised from their original values [Table VIII, p. 80]. The major changes are: reduction of the factors related to flux distribution and fissionable material concentration (because of greater confidence in their predictability for the reasons stated earlier); and, increase in factors related to coolant flow rate through a subassembly (principally in Rows 10-16 of the outer blanket). Although their influence is quite insignificant, for consistency the column of factors effective on the interface temperature rise has also been added.

Table IX

UNCERTAINTY FACTORS FOR THERMAL ANALYSIS OF FUEL AND BLANKET ELEMENTS

Thermo-Physical Quantity	$F(\Delta T)$	$F(\theta_f)$	$F(\theta_c)$	$F(\theta_b)$	$F(\theta_i)$	$F(\theta_u)$
Precision in Neutron and Gamma Flux Distribution	1.07	1.10	1.10	1.10	1.10	1.10
Precision in Total Coolant Flow Rate Through a Subassembly	*1.05	-	-	-	-	-
Precision in Coolant Velocity Profile Within a Subassembly	1.05	-	-	-	-	-
Manufacturing Deviations from Nominal						
Clad Dimensions	-	-	1.05	-	-	-
Bond Dimensions	-	-	-	1.04	-	-
Uranium Dimensions	-	1.02	1.02	1.02	1.02	1.02
Fissionable Material Concentration	1.01	1.01	1.01	1.01	1.01	1.01
Thermal Conductivity Values						
Clad	-	-	1.10	-	-	-
Bond	-	-	-	1.10	-	-
Uranium	-	-	-	-	-	1.15
Heat Transfer Coefficient	-	1.20	-	-	-	-
Precision of Measurement of Power Level	1.02	1.02	1.02	1.02	1.02	1.02
Possible Transient Overload	1.05	1.05	1.05	1.05	1.05	1.05

*Value is 1.25 for subassemblies of Rows 10-16 (outer blanket).

In many of the figures and tables referred to in this section, two temperatures or temperature curves for the same conditions are shown; one includes uncertainty factors (applied as above), and the other does not. The temperature distributions which include the uncertainty factors are considered conservative. The temperature distributions based on nominal calculations (without uncertainty factors) are considered more representative of the conditions expected to exist within the reactor.

Based on the above considerations, each type of fuel and blanket element is designed to cool under the most severe conditions of exposure. The most severe conditions within the various reactor zones occur at: core (and upper blanket), 4th row, R = 13.9 cm; inner blanket, 6th row, R = 23.2 cm; and outer blanket, 8th row, R = 33.3 cm. These are the "hottest channel" locations. The axial power density distributions at these locations and at the core centerline are shown in Fig. 42.

Radial temperature distribution through the "hottest channel" fuel element at the point of maximum fuel alloy temperature in the core is shown in Fig. 43. Also shown is the radial temperature distribution through a core centerline fuel element at the point of its maximum fuel temperature. For each case, the same distribution, but with uncertainty factors included, is indicated. For the latter distributions, the total temperature increase calculated by the square root of the sum-of-the-squares method has been apportioned among the individual nominal temperature rises by direct ratio. Wherever in this report individual temperature rises (with uncertainty factors included) are indicated, they have been established in this way.

Axial temperature distributions through the fuel alloy (or blanket uranium) and through the coolant of the "hottest channel" within the core and upper blanket, inner blanket, and outer blanket, are shown in Figs. 44, 45, and 46, respectively.

The power output per subassembly for the hottest and the average subassembly of each row is shown in Fig. 47. The coolant flow rate per subassembly for each row is shown in Fig. 48. This flow rate distribution has been verified by full-scale, water model tests on individual subassemblies and by six-tenths-scale, water model tests simulating the complete reactor (Appendix C). The mixed mean coolant temperature rise through the hottest and the average subassembly of each row is shown in Fig. 49.

Table X lists pertinent heat fluxes, coolant flow rates, and temperatures calculated for the hottest channel within the core, upper blanket, inner blanket, and outer blanket, without uncertainty factors. Table XI lists the corresponding data with uncertainty factors.

The information in Tables IX, X, and XI, and the power density distributions in Figs. 41 and 42 are based on fuel and blanket elements as described in Sections III.A.1.c., d., and e., and shown in Figs. 7, 8, 9, and 10.

Table X

SUMMARY OF THERMAL ANALYSES RESULTS FOR MAXIMUM TEMPERATURE REGION OF CORE AND BLANKETS

(No Uncertainty Factors Included: Reactor Power = 62.5 Mw)

	Core	Upper Blanket	Inner Blanket	Outer Blanket
Heat Flux at Element Surface, Btu/(hr)(ft^2)				
Maximum in Zone	929,000	105,000	294,000	57,400
At Point of Maximum Uranium Temperature	571,000	84,800	279,000	< 300
Coolant Flow in Hottest Subassembly				
Flow Rate, gpm (Na at 800°F)	93.7	93.7	31.0	5.9
Flow Velocity (avg.), fps	15.8	14.2	19.3	4.2
Temperatures in Hottest Channel, °F				
Uranium, Maximum	1,213	1,051	1,100	931
Coolant, at Outlet	1,037	998	906	931
Coolant, at Inlet	705	993	700	700
Coolant Temperature Rise, Inlet to Outlet	332	5	206	231
Coolant, at Point of Maximum Uranium Temperature	1,022	993	831	931
Temperature Rises in Hottest Channel at Point of Maximum Uranium Temperature, °F				
Through Uranium	105	33	186	0
Through Uranium-Sodium Interface	7	1	4	0
Through Sodium "Bond" Layer	8	2	10	0
Through Sodium-Clad Interface	6	1	4	0
Through Clad	39	15	52	0
Through Coolant Film	26	6	13	0
Total Element Temperature Difference	191	58	269	0

Note: "Uranium" here means fuel alloy or blanket uranium, as appropriate.

Table XI

SUMMARY OF THERMAL ANALYSES RESULTS FOR MAXIMUM TEMPERATURE REGION OF CORE AND BLANKETS

(Including Uncertainty Factors; Reactor Power = 62.5 Mw)

	Core	Upper Blanket	Inner Blanket	Outer Blanket
*Heat Flux at Element Surface, Btu/(hr)(ft^2)				
Maximum in Zone	929,000	105,000	294,000	57,400
At Point of Maximum Uranium Temperature	571,000	84,800	279,000	< 300
*Coolant Flow in Hottest Subassembly				
Flow Rate, gpm (Na at 800°F)	93.7	93.7	31.0	5.9
Flow Velocity (avg.), fps	15.8	14.2	19.3	4.2
Temperatures in Hottest Channel, °F				
Uranium, Maximum	1,271	1,090	1,154	958
Coolant, at Outlet	1,075	1,032	930	958
Coolant, at Inlet	705	1,027	700	700
Coolant Temperature Rise, Inlet to Outlet	370	5	230	258
Coolant, at Point of Maximum Uranium Temperature	1,058	1,027	849	958
Temperature Rises in Hottest Channel at Point of Maximum Uranium Temperature, °F				
Through Uranium	117	36	210	0
Through Uranium-Sodium Interface	8	1	5	0
Through Sodium "Bond" Layer	9	2	12	0
Through Sodium-Clad Interface	7	1	5	0
Through Clad	44	16	58	0
Through Coolant Film	28	7	15	0
Total Element Temperature Difference	213	63	305	0

*No uncertainty factors included.

Note: "Uranium" here means fuel alloy or blanket uranium, as appropriate.

The following reactor conditions, thermal property values, and heat transfer assumptions were employed:

Reactor Conditions:

(1) Nominal (67-subassembly) core.
(2) Full reactor power, 62.5 Mw.
(3) Full coolant flow through reactor, 9,000 gpm.
(4) Distributions of power and coolant flow rate per subassembly as described above.
(5) Coolant temperature at inlet to reactor, 700°F.

Thermal Properties:

(1) Thermal Conductivities (at operating temperature of hottest fuel or blanket element):

Material	Conductivity, Btu/(hr)(ft)(°F)
Fuel Alloy (5 wt-% fissium)	19.8*
Blanket Uranium	21.0*
Stainless Steel, AISI Type 304	11.5**
Bond Sodium	40.3

*From Reference 13.
**From Reference 14.

(2) Coolant (Sodium) Thermal Properties: Taken from the Liquid-Metals Handbook.[15]

Heat Transfer Assumptions:

(1) Sodium heat transfer coefficients based on the relation suggested by Monson:[16]

$$Nu = 2.3 + 0.23(Pe)^{0.5}$$

(2) All heat is generated within the fuel alloy or blanket uranium.

(3) Uniform rate of heat generation per unit volume throughout a given cross section of a fuel pin or blanket pin.

(4) No axial heat conduction.

(5) No radial heat conduction between subassemblies.

(6) Interfacial conductance between sodium bond and clad or fuel is 100,000 Btu/(hr)(ft^2)(°F).

(7) The coolant mass flow rate associated with each peripheral fuel element of a core subassembly is 1.36 times the average flow rate per element for that subassembly, and for all other elements, about 0.82 times the average (see Appendix C).

(8) Coolant temperature at inlet to the hottest channel of the upper blanket is equal to the average coolant temperature at outlet from the core section of the subassembly plus one-third of the amount by which the core section hottest channel outlet temperature exceeds the average (this is a quantitative estimate of the effectiveness of coolant mixing between exit from the core and entrance to the upper blanket).

Principal reactor temperatures for core configurations of other than 67 subassemblies are presented in Appendix J. In general, maximum temperatures in each row of the core and upper blanket increase slightly as the core is made smaller, and decrease somewhat as it is made larger. The inner and outer blanket maximum temperatures do not follow such a trend, but are of acceptable magnitude for all loadings investigated (61-73 subassemblies).

4. Power Cycle Operating Conditions

The contemplated steady-state operating temperatures and coolant flow rates in the principal heat transfer systems at full power are shown in Fig. 3, and are discussed below.

a. Primary System

The primary sodium coolant flow rate through each of the main primary pumps is approximately 4,670 gpm (based on sodium at 800°F); total flow is 9,340. The flow separates into two streams before entering the reactor lower plenums: a high-pressure stream flows to the plenum supplying the core and inner blanket, and a low-pressure stream (pressure reduction being effected by throttling valves in the inlet piping) flows to the plenum supplying the outer blanket. Flow through the reactor totals 9,000 gpm; the remaining 340 gpm represents leakage at various points back to the bulk sodium. All coolant passing through the reactor merges within a common upper plenum and then flows toward the heat exchanger. The temperatures are 883°F at the reactor outlet, and 880°F at heat exchanger inlet (reflecting heat loss to the bulk sodium). Because of additional leakage, only 8,865 gpm flows through the heat exchanger, returning to the bulk sodium with a temperature slightly different from that of the bulk sodium. This temperature difference is required to maintain the bulk sodium temperature constant at 700°F because of extraneous heat losses and gains by the bulk sodium; e.g., losses to shield cooling air, instrument thimble cooling air, and sodium purification system, and gains from the reactor outlet pipe and from leakage of high temperature coolant.

The primary system coolant flow rates are summarized in Table XII.

Table XII

SUMMARY OF PRIMARY COOLANT FLOW RATES

(in gpm; evaluated at 800° F)

From Pumps (each pump, 4,670 gpm)		9,340
Leakage at Pump Disconnects	10	
Leakage at Throttling Valves	25	
	35	
Into Reactor Lower Plenums		9,305
Leakage Past Core Subassembly Adaptors	75	
Leakage Past Control and Safety Subassembly Adaptors	125	
Leakage Past Inner Blanket Subassembly Adaptors	105	
	305	
Through Reactor		9,000
Through Core, Control and Safety, and Inner Blanket Subassemblies	7,620	
Through Outer Blanket Subassemblies	1,260	
Through Clearances Between Subassemblies	30	
Through Control and Safety Subassembly-Thimble Clearances	75	
Through Grid Structure, Vent Holes, and Neutron Shield	15	
	9,000	
Leakage Past Reactor Cover, Bearings, Flange, etc.	105	
To Heat Exchanger		8,895
Leakage at Heat Exchanger Inlet	30	
Through Heat Exchanger		8,865

The primary system coolant pressure drops are as follows:

Pump outlet to reactor inlet	2.8 psi
Reactor inlet to high pressure plenum (at Row 7)	1.4
High pressure plenum to upper plenum (at Row 7)	40.8
Upper plenum to reactor outlet nozzle	1.2
Reactor outlet nozzle to heat exchanger inlet	6.4
Heat exchanger inlet to outlet	3.4
Total for primary flow system	56.0 psi

The first three pressure drops apply only to the high-pressure stream. For the low-pressure stream, the pressure drop from pump outlet to low-pressure plenum is 39.1 psi, and from low-pressure plenum to upper plenum, 3.9 psi.

Since the pressure of the primary tank blanket gas is only a few inches of water above atmospheric and the static head of the coolant is small, the maximum pressure in the primary cooling system is less than 65 psig.

b. Secondary System

A secondary system flow rate of 5,890 gpm is provided by the main a-c linear electromagnetic pump located in the Sodium-Boiler Plant Building. The coolant flows from the pump to the tube side of the heat exchanger, entering the exchanger at 588°F and leaving at 866°F. It then flows to the superheater and, because the heat loss in the connecting piping is negligible, enters at 866°F. The coolant leaves the superheater at 794°F and, after passing through the evaporator, returns to the main pump at 588°F.

Pressure drop through the heat exchanger is 5.2 psi, and through the superheater plus evaporator, about 6.8 psi. Approximate pressure drop through all connecting piping and fittings is 34.0 psi, so that total pressure drop in this system is about 46.0 psi. Since the inlet side of the pump is maintained at a pressure of 10 psig by the argon blanket gas in the secondary system sodium expansion tank, maximum pressure in the secondary system is less than 60 psig. Pressure in the secondary side of the heat exchanger, however, is substantially greater than in the primary side; if leakage were to develop within the heat exchanger, leakage flow would be in the direction from secondary system to primary system, and radioactive sodium would not enter the secondary system.

c. Steam System

Minor revisions have been made to the steam system. The final flow diagram is shown in Fig. 3.

C. Steady-State Operation at Three-Fourths Power

The general criteria for determination of the maximum power level at which the reactor may be operated safely are unchanged [Pages 86-87]. However, additional thermal cycling and irradiation damage data on 5 wt-% fissium alloy specimens of EBR-II fuel pin diameter have been accumulated. These data (Appendix A) indicate that: 500 slow thermal cycles between 1238°F and 698°F (670-370°C) cause negligible change in diameter and less than 1.4% change in either length or density. Also, 1 at-% local burnup at temperatures up to 1166°F (630°C), with moderate thermal cycling and fission rate densities from 7 to 11 x 10^{13} F/(cc)(sec) effects a 9% (or less) change in volume. Since these test conditions approach anticipated full-power operating conditions, and because the EBR-II fuel elements incorporate a sodium bond annulus equivalent in volume to more than 16% of the fuel volume which is available for accommodation of fuel growth, it is concluded that a local burnup of at least 1 at-% can be realized safely. The calculated maximum fuel alloy-clad interface temperature at full power is now higher: 1113°F without, and 1159°F with uncertainty factors. Since the uranium-iron eutectic melting point is 1340°F, this is considered an adequate margin of safety.

However, to be conservative with respect to the above considerations, initial operation of the EBR-II will be confined to power levels of 45 Mw or less, with consequently reduced fuel element operating temperatures. Moreover, frequent removal of subassemblies for examination of fuel elements at various degrees of burnup is contemplated during initial operation. In subsequent operation, the power level will be increased gradually to permit evaluation of the effect of increased temperatures. It is thought that this testing procedure on temperature and burnup effects (and, indirectly, on degree of manifestation of uncertainty factors) will permit operation at full power.

This section describes the contemplated operating conditions of the power system at 45.0 Mw, or approximately three-fourths full power.

1. Flux Distributions

Neutron flux distributions are the same as described in Section IV.B.1. for the full-power case except that all magnitudes are reduced in the ratio of 45.0 to 62.5 Mw.

2. Reactor Heat Generation Distributions

Heat generation distributions are the same as described in Section IV.B.2. for the full-power case except that all power and power density magnitudes are reduced in the ratio of 45.0 to 62.5 Mw.

3. Reactor Temperature Distributions

The primary coolant flow rate to be used at 45.0 Mw is 6,550 gpm, as shown in Fig. 30. The reactor coolant outlet temperature is 882°F, from the same figure.

Location of the hottest channel in each reactor zone is the same as for the full-power condition (62.5 Mw).

Radial temperature distributions through the core hottest channel fuel element and through a core centerline fuel element at the point of maximum uranium temperature are shown in Fig. 50.

Axial temperature distributions of the fuel alloy (or blanket uranium) and of the coolant of the hottest channel within the core, inner blanket, and outer blanket are shown in Figs. 51, 52, and 53, respectively.

The power output per subassembly for the hottest and the average subassembly of each row is the same as indicated in Fig. 47 except reduced in magnitude in the ratio of 45.0 to 62.5 Mw. The coolant flow rate per subassembly for each row is essentially the same as shown in Fig. 48 except reduced in magnitude in the ratio of 6,550 to 9,000 gpm. The exact flow rate distribution will deviate slightly from this ratio because of differences in

flow characteristics among the several types of subassemblies in the reactor; consequently, flow rates are not reduced in precisely the same ratio. The mixed mean coolant temperature rise through the hottest and the average subassembly of each row is essentially the same as shown in Fig. 49 except altered by the ratios 45.0 Mw to 62.5 Mw, and 9,000 gpm to 6,550 gpm, or by a factor of about 0.99. The exact coolant temperature rises will differ slightly because of the flow distribution deviation described previously.

Table XIII lists pertinent heat fluxes, coolant flow rate, and temperatures, calculated for the hottest channel within the core, upper blanket, inner blanket, and outer blanket, without uncertainty factors. Table XIV gives the corresponding data with uncertainty factors.

Table XIII

SUMMARY OF THERMAL ANALYSES RESULTS FOR MAXIMUM TEMPERATURE REGION OF CORE AND BLANKETS

(No Uncertainty Factors Included; Reactor Power = 45.0 Mw)

	Core	Upper Blanket	Inner Blanket	Outer Blanket
Heat Flux at Element Surface, Btu/(hr)(ft^2)				
Maximum in Zone	669,000	75,400	212,000	41,300
At Point of Maximum Uranium Temperature	377,000	61,000	192,000	< 200
Coolant Flow in Hottest Subassembly				
Flow Rate, gpm (Na at 800°F)	68.2	68.2	22.6	4.3
Flow Velocity (avg.), fps	11.5	10.3	13.9	3.0
Temperatures in Hottest Channel, °F				
Uranium, Maximum	1,160	1,032	1,024	929
Coolant, at Outlet	1,033	995	904	929
Coolant, at Inlet	705	990	700	700
Coolant Temperature Rise, Inlet to Outlet	328	5	204	229
Coolant, at Point of Maximum Uranium Temperature	1,033	990	838	929
Temperature Rises in Hottest Channel at Point of Maximum Uranium Temperature, °F				
Through Uranium	69	24	128	0
Through Uranium-Sodium Interface	5	1	3	0
Through Sodium "Bond" Layer	5	1	7	0
Through Sodium-Clad Interface	4	1	3	0
Through Clad	26	11	35	0
Through Coolant Film	18	4	10	0
Total Element Temperature Difference	127	42	186	0

Note: "Uranium" here means fuel alloy or blanket uranium, as appropriate.

Table XIV

SUMMARY OF THERMAL ANALYSES RESULTS FOR MAXIMUM TEMPERATURE REGION OF CORE AND BLANKETS

(Including Uncertainty Factors; Reactor Power = 45.0 Mw)

	Core	Upper Blanket	Inner Blanket	Outer Blanket
*Heat Flux at Element Surface, Btu/(hr)(ft^2)				
Maximum in Zone	669,000	75,400	212,000	41,300
At Point of Maximum Uranium Temperature	377,000	61,000	192,000	< 200
*Coolant Flow in Hottest Subassembly				
Flow Rate, gpm (Na at 800°F)	68.2	68.2	22.6	4.3
Flow Velocity (avg.), fps	11.5	10.3	13.9	3.0
Temperatures in Hottest Channel, °F				
Uranium, Maximum	1,211	1,069	1,059	954
Coolant, at Outlet	1,071	1,027	927	954
Coolant, at Inlet	705	1,022	700	700
Coolant Temperature Rise, Inlet to Outlet	366	5	227	254
Coolant, at Point of Maximum Uranium Temperature	1,070	1,022	850	954
Temperature Rises in Hottest Channel at Point of Maximum Uranium Temperature, °F				
Through Uranium	76	27	144	0
Through Uranium-Sodium Interface	5	1	3	0
Through Sodium "Bond" Layer	6	1	8	0
Through Sodium-Clad Interface	5	1	3	0
Through Clad	29	12	40	0
Through Coolant Film	20	5	11	0
Total Element Temperature Difference	141	47	209	0

*No uncertainty factors included.

Note: "Uranium" here means fuel alloy or blanket uranium, as appropriate.

Principal reactor temperatures for core configurations of other than 67 subassemblies are presented in Appendix J.

D. Pre-Operational Testing and Experiments

1. Mechanical, Hydraulic, and Miscellaneous Testing

Various components in the EBR-II system have been (or will be) tested under a variety of conditions prior to power operation. Many of these pre-operational tests are related to the sequence of plant operations required prior to operation at power. The significant operational sequences relate to the reactor and primary system and include: preparations for the Dry Critical Experiments; the Dry Critical Experiments; primary tank elevated temperature test; sodium filling; sodium cleanup and system testing; preparations for Wet Critical Experiments; and Wet Critical Experiments.

The various components and systems have been (or will be) tested at one or more times during these plant operational sequences.

a. Control Rod Drives

Extensive testing was performed on a variety of experimental and prototype control rod drive units during their development. In addition, one of the fourteen actual production units was selected and extensively tested. These tests were performed in ambient air and under simulated reactor system environmental conditions (Appendix B).

Each of the twelve control rod drives installed in the EBR-II was tested at room temperature by the fabricator under Laboratory direction prior to shipment to the construction site. After final installation in EBR-II, all of the drive functions of each of the twelve control rod drives were thoroughly tested, including:

(1) Scram action (release, dashpot operation, oil pressures, accumulator tightness, check valve operation, etc.).

(2) Drive travel (direction, smoothness, limit switch actuation, position readout, etc.).

(3) Gripper operation (engage-disengage action).

(4) Gripper engage safety function (prevents accidental disengagement of the drive gripper from control rod at other than the full "down" position).

(5) Gripper sensing (provides positive indication that a control rod is actually engaged when the gripper is in the "engaged" position).

All of this testing has been conducted using the permanently installed instrumentation and control system, with most of the initiating actions performed from the control room. All of these tests were performed at room temperature prior to the Dry Critical Experiments.

During the Dry Critical Experiments, the entire control system was operated and the control rod drives were required to function many times. The latter operations included the disconnect functions prior to fuel handling and the re-engagement following fuel handling (since many fuel loading steps were required). In addition, a system check-out was performed daily; this check-out included individual operation and scram tests on each drive.

After the primary tank has been filled with sodium, the operational tests of the control drives will be repeated, both in preparation for Wet Critical Experiments and during the conduct of those experiments. These tests will include operation of the units in sodium at temperature (600°F-700°F), both with and without sodium flow through the reactor. In addition to the functional testing, time-displacement data during scram will be verified again.

b. Safety Rod Drive

The safety rod drive mechanism (with simulated safety rod loads) was completely assembled and tested at room temperature (as described in Appendix B) prior to shipment to the construction site. After final installation in the system, this testing was repeated with the actual safety rods attached and included all the drive functions, i.e., scram action (release, dashpot operation, etc.), and drive travel (direction, smoothness, limit switch actuation, position indication, etc.). This testing was conducted using the permanently installed instrumentation and control system.

The above tests were performed in preparation for the Dry Critical Experiments and, as in the case of the control rod drives, were repeated many times during the conduct of the experiments and in the daily check-out procedures.

After sodium filling, the tests will be repeated and will include verification of time-displacement characteristics in sodium. This system also will be operated extensively prior to, and during the Wet Critical Experiments.

c. Instrumentation and Circuitry

All of the circuitry including relays, interlocks, etc., associated with the various components and systems have been tested in conjunction with the system tests. In addition, each channel of the nuclear

instrumentation was tested extensively in preparation for the Dry Critical Experiments, both external to the system and after installation. The most significant tests of these channels occurred during the Dry Critical Experimental Program: all of the normal instrumentation, including trip circuits, were operated in conjunction with special in-core instrumentation. The various trip circuits were included in the daily check-out, and were, therefore, operated many times.

The various circuit components and controls will be continuously checked and tested parallel with the testing of systems and components. The nuclear instrumentation tests will be repeated after sodium filling in preparation for, and during the Wet Critical Experiments.

d. Fuel-Handling System

The fuel-handling system consists of the components involved in the movement of subassemblies between the reactor and storage rack within the primary tank. The major components of this system include: the control rod drive lifting platform (involved in the disengagement of the drives from the rods); the reactor vessel cover lock and lifting mechanisms (required to permit access to the reactor); the gripper and holddown mechanism; the large and small rotating plugs; the transfer arm, the storage rack; and the fuel-handling console. Operation of this system, as described in Sections III.A.7. and IV.J., requires accurate positioning and alignment of the various system components to assure positive and reliable mating of the components at each of the transfer and engagement points in the transfer process.

Most of the components were completely tested after assembly either at the Laboratory or at the fabricator's plant. In addition, many of the special features of the components were tested extensively in experimental systems or prototype components. These include the compression-type packing seals employed on the gripper, holddown and storage basket drive shafts, and the frozen seals employed on the two rotating plugs. These tests are described in Appendix B.

After final installation in the system, each component was tested independently, including the performance of all prescribed functions. This was accomplished initially with the use of temporary control panels which permitted independent operation of each mechanism. After each component was tested in this manner, operation of each unit was repeated both independently and as a part of the integral system, using the control system as permanently installed in the fuel transfer console and as normally required for fuel-handling operations. A number of complete transfer cycles of prototype subassemblies between the storage rack and various subassembly positions within the reactor were effected during this pre-operational check-out.

The above testing program was performed in preparation for the Dry Critical Experiments. During the conduct of the Dry Critical Experiments, including the initial loading to criticality, the fuel-handling system was used routinely in effecting reactor loading. (The storage rack was not employed during the Dry Critical Experiments; the loading and unloading operations bypassed this step in the fuel-handling cycle and subassemblies were loaded manually through the transfer port to the transfer arm.) All of the operations involved in preparing the system for fuel handling (disconnecting and raising control rod drives, raising the reactor cover, etc.), and for restoring the system to the reactor operating condition, were repeated many times during the approach to critical and during the experiments. All normal functions involved in the fuel-handling sequence were performed with the exception of melting the frozen seals on the two rotating plugs. (The seals were not filled for these experiments.)

Operation of the complete fuel-handling system was again tested (including the frozen seals on the rotating plugs) during the elevated temperature test. After sodium filling, the tests will be repeated in sodium at 600°F-700°F preparatory to the Wet Critical Experiments. During the approach to wet critical, and during the experimental program, operation of the fuel-handling system, of necessity, will be repeated many times.

e. Fuel Unloading and Interbuilding Transfer Systems

The fuel-unloading system involves the movement of subassemblies into and out of the primary tank, between the storage rack and the interbuilding coffin. The interbuilding fuel transfer system effects transfer of subassemblies between the Reactor Plant and the Fuel Cycle Facility. The major components of these systems include: the storage rack, the transfer arm, the fuel transfer port, the fuel-unloading machine (with dolly), the interbuilding coffin, and the equipment air lock (with dolly). Operation of the systems as described in Sections III.A.7., III.A.9., and IV.J., requires the accurate alignment of several of the system components, in particular, the storage rack, the transfer arm, and the fuel transfer port. It should be noted that the transfer arm is the component which interconnects the "fuel-handling" and the "fuel-unloading" systems.

In addition, these systems require the reliable operation of auxiliary systems, particularly the argon cooling systems of the transfer port, fuel-unloading machine, and interbuilding coffin (for removal of fission product decay heat from the subassemblies). It is during fuel unloading that cooling of the subassemblies is shifted from sodium to argon gas (and vice versa).

Most of the components comprising these systems have been tested extensively after assembly, either at the Laboratory or at the fabricator's plant prior to shipment to the construction site. Neither

system was utilized during the Dry Critical Experiments; a manual loader was used in place of the fuel-unloading machine. The fuel-unloading machine performs a much more complex function and has been tested extensively at the Laboratory, including simulated system environmental testing as described in Appendix B.

After sodium filling, the fuel-unloading system and the interbuilding transfer system will be tested first with dummy subassemblies and then with prototype subassemblies. All operational conditions will be simulated with the exception of internal heat generation within the fuel. Measurements of gas flow, etc., will be made to insure that adequate heat removal capability does exist for fission product decay cooling of irradiated subassemblies.

f. Subassembly Basin

Although virtually no possibility exists that a subassembly could be dropped accidentally within the primary tank during transfer operations, a "subassembly basin" has been incorporated to provide additional safety in such an event. The function of this basin (see Section III.A.7.a.) is to guide a dropped subassembly into a position in which it will be adequately cooled by natural convection until retrieved. The system has been tested by deliberately dropping a number of dummy subassemblies from various positions (within the range covered by the basin), to ensure that the subassembly comes to rest in the correct position and with the correct (vertical) attitude. Actual retrievals through the primary tank access plug directly above the subassembly position were not made, since it is not intended to devise retrieval gear unless this unanticipated accident actually occurs.

g. Primary Tank Cover Deflection

The normal operating temperature of the primary tank bulk sodium is 700°F. Under this condition, a significant heat loss occurs through the tank cover and its associated nozzles to the biological shield cooling system air. This heat loss is accompanied by production of a temperature differential across the tank cover structure of such sign as to produce downward bowing of the cover. Such bowing, in turn, tends to tilt the cover nozzles so that the lower end of mechanisms extending through them into the primary tank tend to move slightly radially outward. In the case of most nozzles, such movement is of no consequence. It is possible, however, that if the movement were sufficiently large, certain components suspended from nozzles (or from the bottom plate of the cover), might be undesirably affected either from the standpoint of alignment, or of increase in stress level. Because of the extremely complex configuration of the primary tank cover structure and its integral nozzles, the effective magnitude of the temperature differential, and therefore of the bowing deflection,

cannot be calculated accurately. Accordingly, the actual deflection exhibited with the tank at temperature (300°F-350°F) was measured during the elevated temperature test prior to sodium filling. Small electric heaters have been incorporated on the top flanges of the cover structure radial beams and are available to reduce the effective temperature differential and to minimize or eliminate excessive bowing, should they be needed. The heaters were operated during the elevated temperature test and produced the anticipated reduction in temperature differential in the structure.

h. Primary Tank Leakage

Prior to sodium filling, helium will be introduced into the primary tank and a careful inspection for leakage made at the rotating plug seals, at all primary tank nozzles, and at all other potential sources of future blanket gas (argon) leakage.

i. Sodium Cleanup System

The sodium cleanup system (cold trap) will not be tested prior to sodium filling; however, the system design is based on that used for more than six years on the EBR-II, 5,000-gallon model test sodium system. Although the design is based on an oxide capacity to meet operational requirements for an estimated ten years, a temporary cold trap system will be employed to remove the oxide contamination following initial filling. When the bulk of the initial contamination has been removed by this temporary system, operation will be shifted to the permanent cleanup system. During this period, testing of the purification system plugging meters, sodium sampling and analysis procedures, will be effected. Subsequent operation of the system will be intermittent or continuous as experience indicates to be necessary.

j. Argon Purification System

Simultaneous with the sodium cleanup process, the complete argon purification system will be tested with respect to all of its functions.

k. Primary and Auxiliary Sodium Pumps

The two primary sodium pumps and the d-c electromagnetic auxiliary pump will be tested after sodium filling. The actual system head versus flow rate characteristics will be determined. The flow decay constants exhibited upon cessation of pumping power will be obtained. The complete pump control system, including the maximum rate of change of flow rate limitation feature, will be checked out.

The primary sodium pumps were given a conventional hydraulic test with water at the fabricator's plant. Their design is based

on a 5,000-gpm prototype pump which was operated with sodium at the Laboratory for more than three years. During this period, the pump accumulated more than 16,000 hours of operation, and more than 250 starts. A prototype of the d-c auxiliary pump also was thoroughly tested at the Laboratory, including the determination of performance characteristics. These tests will be repeated on the installed unit.

l. Shutdown Coolers

Design and operation of the shutdown cooler system is relatively uncomplicated since no pumps are employed, only a minimum control system is required, and the duty requirements are not critical. Nevertheless, each shutdown cooler will be tested to determine the minimum and maximum capacity exhibited, and to assure proper functioning of the damper control system.

m. Shield and Instrument Thimble Cooling Systems

The operation of these systems, which were tested upon completion of construction, will be rechecked and readjusted to: (1) obtain optimum balancing of flow; (2) determine blast shield and biological shield (including primary tank support structure) temperature distributions; (3) check nuclear detector normal ambient temperatures; and (4) determine nuclear detector ambient temperature fluctuations occasioned by system power switch-over to the emergency generator upon failure of building power.

n. Primary System Heat Balance

With the primary tank at elevated temperature, tests will be conducted to determine the magnitudes of the major parasitic heat losses from the primary tank. This information will assist in subsequent determination of actual reactor power level by heat balance methods. The principal heat losses to be evaluated are those to the shield cooling system, the instrument thimble cooling system, the sodium purification system, the shutdown coolers, and the secondary system (via the heat exchanger).

o. Building Isolation System

The Reactor Plant Containment Vessel contains numerous penetrations to accommodate air ducts and pipes. Most of these ducts and pipes are equipped with one or more fast-acting valves which are automatically closed in the event of a nuclear incident.

Closure of the valves is initiated by a sensing of high radiation level or high pressure or temperature within the building, or of

high coolant temperature at core subassembly outlets in the reactor. With the valves in the closed position, the Containment Vessel with its penetrations constitutes an essentially leaktight envelope surrounding the entire Reactor Plant.

The complete isolation system was carefully tested prior to the start of the Dry Critical Experiments; each valve was checked to see that it was in the closed position subsequent to manual tripping of the system control circuit. (All valves were tested for leaktightness after completion of construction.)

Prior to the Wet Critical Experiments, the building isolation system will be tested again to assure proper operation. Each of the sensing devices provided for tripping of the system (high radiation level, high building pressure or temperature, and high reactor coolant temperature) will be checked.

p. Power Systems

A similar test program will be conducted on the components and sub-systems comprising the power system.

Very little operational testing can be accomplished on the secondary sodium system prior to filling with sodium. After filling, the cleanup system (cold trap) will be operated to remove initial contamination. Because of the extensive piping involved, the sodium may be drained into the storage tank and the system refilled several times to enhance cleanup. After the system is clean, the pump will be operated and flow instrumentation, etc., will be tested.

The steam system will be tested concurrently with the testing of the secondary system. The steam system is a relatively conventional system constructed of conventional materials (2.25% chrome-moly); it will be cleaned, and made operational in accordance with standard power plant practice.

The turbine-generator has been operated on 175-psi plant (heating) steam. The turbine control operation and generator synchronization have been tested at low load. Similarly, the cooling water system, cooling tower, and substation operation have been tested.

2. Wet Critical Experiments

Following sodium filling, sodium cleanup and systems testing, the reactor will be loaded to critical. This phase of operations is identified as the Wet Critical Experiments because it is performed in sodium (wet),

and to differentiate it from the Dry Critical Experiments which were performed prior to sodium filling. In many aspects, both series of experiments are similar, follow similar procedures, have similar objectives, and produce similar data. The Dry Critical Experiments and their results are described in Appendix L.

The Wet Critical Experiments will be conducted with the reactor and primary system essentially in normal operating condition; however, as was the case with the Dry Critical Experiments, certain plant changes will be required. These include:

(1) The interlocks requiring sodium flow, and those requiring a specified amount of sodium flow related to a steady power level of operation, will be bypassed.

(2) Power-level-trip settings for Reactor Operation will be <60 kw.

(3) Special high-sensitivity BF_3 counters (Channels G and H) will be employed to assure adequate response at source level and low multiplication. These were tested relative to in-core instrumentation during the Dry Critical Experiments (see Appendix L).

Except for these modifications (and certain precautions relating to the secondary system, steam system, etc.), the reactor system will be in normal operating condition; i.e., the shutdown circuits for Reactor Operation and Fuel Handling will be operative; sensing, indicating, and recording instrumentation will be operative as appropriate; the building containment and isolation systems will be operative, etc.

The approach to critical and initial critical experiments will be performed with no sodium flow. Most subsequent measurements will require no sodium flow; however, flow will be required for two distinct investigations during these experiments. It will be most important to determine whether there is a significant reactivity effect associated with increasing or decreasing coolant flow. Furthermore, it will be of some interest to compare certain reactivity measurements (i.e., control rod calibrations) made with and without sodium flow.

The Wet Critical Experiments will include:

(1) Neutron source and subcritical instrument response.
(2) The critical approach.
(3) Reactivity measurements.
(4) Preliminary power calibration and neutron flux distributions.

Some of the experiments outlined below are deemed essential to, and will be performed prior to, the approach to power. Others, mainly concerned with flux distribution and the detailed material replacement experiments, may be performed either before, during, or after the approach to power. However, all the experiments are low-power (<10 kw) investigations.

a. Neutron Source and Subcritical Instrument Response

The relationship between neutron source strength and low-power instrument response is important to the conduct of the Wet Critical Experiments and to the basic reactor system as it relates to normal fuel-handling procedures. The Dry Critical Experiments developed very useful data relating to neutron source strength and low-power instrument requirements. These experiments, in conjunction with measurements made on the ZPR-III mock-up of EBR-II, will provide a basis for approach to wet critical. The start of core loading is an important check point in this sequence. At that time, the reactor grid plate is completely filled. The 61-subassembly core region is filled with dummy steel subassemblies,* natural uranium subassemblies,** and control and safety rod thimbles. Both the inner and outer blanket regions are loaded with Inner Blanket and Outer Blanket subassemblies. The twelve control rods and two safety rods, containing a total of about 26 kg U^{235}, will be loaded during this initial sequence.

The provision for the two strong sources and one weak source provided considerable flexibility during the Dry Critical Experiments. This same flexibility will be provided during the Wet Critical Experiments. The two strong sources will each have in excess of 400 curies of Sb activity. The weak source activity will not exceed 75 curies. Additional flexibility is inherent in the provision for relocating the neutron source radially relative to the core. The strong neutron source (or sources) will be placed in Sector E (Fig. 54) of the blanket. The source strength, multiplicity of sources and location will be arranged so that:

(1) Startup channels G and H will each record more than 450 unmultiplied counts per minute (see Appendix L).

(2) Low-power channels 1, 2, and 3, will each record more than 60 unmultiplied counts per minute (at a multiplication of less than ten, the requirements of Table IV will be exceeded).

---

*These subassemblies contain only stainless steel. Their function is to fill the core region and provide a solid, tightly-packed system prior to loading subassemblies containing enriched uranium. They are placed in Rows 1, 2, 3, and 4 of the reactor.

**These are core subassemblies containing natural uranium instead of enriched uranium. They are placed in Rows 4 and 5 of the reactor.

b. Approach to Critical

The procedures for Fuel-Handling and Reactor Operation culminating in the wet critical reactor are similar to those successfully used during the Dry Critical Experiments. The only differences in procedures will involve the introduction and removal of subassemblies from the primary tank because of the sodium, and the smaller loading increments of core subassemblies because the wet critical core is at least 20% smaller than the dry critical core.

All enriched subassembly loading is by replacement. A dummy steel, natural uranium core, or inner blanket subassembly must be removed before a core subassembly or a sixth row, core-type subassembly* may be inserted into the reactor grid plate. Only one reactor grid plate position may be vacant at any time. (The only exception may occur if it is necessary to replace a control or safety rod thimble. This replacement is not anticipated during these experiments.)

Reactor criticality will be achieved by gradually raising the control rods one at a time. Initially the reactor will be caused to diverge by control rod insertion on a period of not less than 50 sec. After the initial critical size has been experimentally determined, the loading will be reviewed and altered, if necessary, to provide less than a dollar ($\Delta k/k \approx 0.0072$) of excess reactivity for the Wet Critical Experiments.

Comparison of the wet critical mass with the previously measured dry critical mass will permit an evaluation of total sodium reactivity.

c. Reactivity Measurements

Reactivity effects will be measured to afford a means of evaluating design parameters and to complete the understanding of the neutronics. These measurements will include:

---

*A sixth row, core-type subassembly is identical to a core subassembly except that the lower adapter is designed to fit in the inner blanket zone of the grid assembly. These subassemblies can be readily distinguished from inner blanket subassemblies by letter and number stamped on the top end fixture, by weight, by lower adapter coolant openings, and by inspection of upper blanket elements beneath the top end fixture. Nevertheless, the remote possibility of inadvertent interchange between sixth row, core-type and inner blanket subassemblies dictates that the former be subject to special handling. During these experiments, sixth row, core-type subassemblies will be loaded from the operating floor directly to the reactor. They will not normally reside in the storage rack before being initially inserted into the reactor.

(1) Total reactivity worth of all twelve control rods.

(2) Total reactivity worth of two safety rods.

(3) Total reactivity worth of several single control rods.

(4) Incremental calibration of several single control rods.

(5) The isothermal temperature coefficient of reactivity.

(6) A static calibration of the oscillator rod.

(7) The measurement of the zero-power transfer function.

(8) The reactivity effect, if any, caused by varying the coolant flow at zero power.

(9) The reactivity worth of core and blanket subassemblies (replacement worth and relative to sodium).

(10) The reactivity worth of sodium as a function of position.

The various rod calibrations are required to establish normal incremental reactivity worths for reactor operation, fuel-handling and reactor shutdown. They are also required to provide a method of measuring reactivity changes for experimental purposes; e.g., to determine the isothermal temperature coefficient of reactivity.

The isothermal temperature coefficient is of operational as well as of basic interest. It is needed to determine the reactivity associated with the bulk sodium temperature of the primary system. It will provide a basis for estimating and evaluating the power coefficient of reactivity. In particular, comparison of the wet isothermal temperature coefficient with that measured during the Dry Critical Experiments provides a semi-quantitative measurement of the sodium temperature coefficient under uniform heating.

The static calibration of the oscillator rod will be a "proof test" of the design previously investigated during the Dry Critical Experiments.

The measurement of the zero power transfer function will be a demonstration that the dynamic aspects of the oscillator rod and the dynamic recording equipment meet design requirements.

No appreciable coolant flow reactivity effects are anticipated. This will be determined by observing reactivity changes (if any) as a function of coolant flow.

The reactivity worth of core and blanket subassemblies will be measured to facilitate fuel-handling procedures when core and blanket subassemblies undergo replacement.

Detailed measurements of sodium worth as a function of position will afford in-pile data for kinetic analyses.

d. Preliminary Power Calibration and Neutron Flux Distributions

A preliminary power calibration is necessary to permit realistic, initial, power-level-trip settings. These settings will be revised later by more precise heat balance measurements at substantial reactor power. Low-power flux measurements will be performed.

The preliminary power calibration will be obtained by irradiating a pair of highly enriched uranium foils placed at the core mid-plane adjacent to the core boundary. The foils will be contained in a specially-fitted inner blanket subassembly. During constant power (~100 w) irradiation, the counting rates in Channels 1, 2, and 3, as well as the response of the intermediate Channels 4, 5, 6, and 7, will be noted. Radio-chemical fission analysis of the irradiated foils will determine the total number of fissions per unit time. Subsequently, this may be converted to reactor power level. The results of this calibration may be compared with similar investigations during the Dry Critical Experiments.

Flux measurements will be obtained by irradiating enriched and depleted uranium foils and wires. These will be contained in subassemblies which are specifically designed for these low-power experiments. The reactor core and blanket regions will be flux-mapped to afford complete fission and fertile capture distributions. These results will be used to provide a first estimate of the conversion ratio.

3. Approach to Power

The approach to power is defined as the operational steps or sequences, and the experimental observations and measurements, involved in raising the reactor and system power toward maximum design capability. It is anticipated that this will be accomplished over an extended period of time, and that it may be interrupted by sustained operation at various intermediate power levels. Although the time span and continuity of this operational phase are somewhat indefinite, it will begin following completion of the Wet Critical Experimental Program, and will terminate when design power operation is achieved.

In general, the approach to power consists of a sequence of operations at increasing power levels which are intended to check or prove that: (1) the reactor and the power system are stable in operation; and (2) the complete plant will operate in accordance with design objectives.

Stability evaluations will be made by oscillator experiments and the determination of transfer functions at several power levels. The following "natural" power levels of operation will be required to achieve specific system operational objectives:

Approximate Power Level, Mw	Purpose
10	Place steam system in "normal" operation,* dump steam in condenser.
30	Place complete power system in operation; i.e., turbine-generator, etc.
45	"Three-fourths" power (see Section IV.C.).
62.5	Full power (see Section IV.B.).

*Below about 10% power (6 Mw), the steam system is operated on the "startup feed-water pump;" above this power level the main feed-water pumps are operative.

Table XV lists the tentative power levels and operating conditions at which stability investigations are planned. (It should be noted that results obtained during these investigations may indicate revisions to these plans.)

Table XV

STABILITY INVESTIGATIONS DURING APPROACH TO POWER

Experiment No.	Nominal Power, Mw	Per cent of Full Power	Nominal Coolant Flow, gpm	Per cent of Full Power Coolant Flow	Approximate* Reactor Feedback Ratio
1**	< 0.5	~0	9,000	100	~0
2	5	8	9,000	100	0.08
	5	8	6,550	73	0.11
3	10	16	9,000	100	0.16
	10	16	6,550	73	0.22
	10†	16	3,240	36	0.44
4	20	32	9,000	100	0.32
	20	32	6,550	73	0.44
	20	32	4,310	52	0.61
5	30	48	9,000	100	0.48
	30	48	6,550	73	0.66
	30†	48	4,310	52	0.93
6	45	72	9,000	100	0.72
	45†	72	6,550	73	0.98
7	55	88	9,000	100	0.88
8	62.5†	100	9,000	100	1.00

*Reactor feedback ratio is estimated relative to full power - full flow conditions; this approximate ratio is: per cent of full power/per cent of full flow. Total power = 62.5 Mw; total flow = 9,000 gpm.

**For normalization purposes only (may be repeated periodically).

†Periods of sustained operation.

At each power level, the reactor is first operated at 100% coolant flow and then at reduced flow. At the power levels where sustained operation is indicated (Experiment Nos. 3, 5, 6, and 8), the flow is reduced to normal operational flow for that power as indicated. This provides the proper temperature distributions to permit system operation as required to accomplish the desired operational objectives.

The experimental operations involved in the approach to power will be conducted with the plant in the normal operating condition (shutdown circuits, containment, etc.). The level trips will be set for the appropriate power level and all of the normal operational requirements for reactor operation and fuel handling will be followed.

Various methods have been used to predict the kinetics of EBR-I, Mark-III. The most successful method (see Section IV.I.5.) has been applied to EBR-II. This analysis is used as an aid in determining the initial power level to be used in the kinetic experiments. The initial power and associated coolant flow are chosen so that the amplitude of the reactor transfer function is predicted to be about 8% different from that of the zero power transfer function at a frequency of about 0.2 radian/sec. The chosen power level for EBR-II is about 5 Mw with 33% (3,000 gpm) coolant flow. This is a few per cent more than the minimum coolant flow that can be obtained for extended periods of operation of the pumps. At full flow (9,000 gpm), the amplitude is less than 8% different from the zero power gain. The stability experiments will be initiated with full (9,000 gpm) coolant flow and then reduced.

The initial measured transfer functions at 5.0 Mw with two different flow rates will, to some extent, govern subsequent investigations; however, the program outlined in Table XV is considered appropriate if there is no evidence of reactor instability. If there is evidence of instability, the program will be modified accordingly.

An extremely important aspect of the approach to power pertains to the measurement of the power coefficient of reactivity at various power levels. Similarly, the coolant flow coefficient of reactivity will be measured at various power levels. These coefficients determine the total reactivity change from shutdown to full power.

The kinetic and thermal behavior of the reactor system during scram (with and without cessation of pumping power) will be investigated. The experiments, initially conducted at low powers, will indicate whether any thermal and/or kinetic problems will occur at the higher power levels contemplated for subsequent investigations.

The power coefficient of reactivity as well as the closed loop transfer function feedbacks are temperature dependent. Therefore, if similar temperature distributions prevail at two different power levels with two different total coolant flows, the measured closed loop transfer function feedbacks should be similar. The power coefficient of reactivity will be highly sensitive to coolant flow; in fact it may be approximately inversely proportional to coolant flow.

In addition to demonstrating that the EBR-II reactor system is stable in operation and will operate in accordance with design objectives, the detailed experiments and observations made during the approach to power will demonstrate the validity of predicted performance. These data will have application in the design of other fast reactors.

E. Normal Startup

No significant change has been made in the normal startup procedure.

F. Normal Shutdown

Shutdown procedure is unchanged.

G. Fast Shutdown (Scram)

Reactor scram is effected by certain primary system abnormalities, as listed in Table III. Scram consists of fast shutdown of reactor (by ejection of the control rods), and interruption of power to the secondary system pump. The primary system main pumps remain in operation during the scram process and are later shut down manually by the operator. This section describes the calculated reactor temperature distributions obtaining during this type of scram and also during a scram initiated by primary system main pump failure.

1. Primary Pumps Operative

This case represents the usual type of scram: both primary main pumps remain in operation. An initial condition of full reactor power is assumed, since the most severe temperature transients occur at this power level. A total control rod worth of 0.05 $\Delta k/k$ and an initial rod insertion of 90% are assumed. The resulting reactor temperature variations as a function of time were presented previously [Fig. 77].

Several of the primary system conditions on which the analysis of this case is based have been slightly revised; e.g., total reactor coolant flow rate, initial coolant temperatures, control rod acceleration, etc. Results of the present analysis are shown in Fig. 55; insignificant changes are indicated.

2. Only Auxiliary Pump Operative

This case represents a scram initiated by loss of primary system pumping due to failure of both main pumps, or to loss of electrical power. The primary auxiliary pump continues in operation (even in the event of loss of electrical power, since its power supply is backed up by a floating battery). The same reactor temperatures as considered above were shown previously as a function of time [Figs. 78 and 79].

The primary system conditions on which the analysis of this case is based also have been revised as above. In addition, the substitution of centrifugal pumps for electromagnetic pumps affects this analysis because of the initially slower rate of deceleration of coolant flow. Results of the present analysis are shown in Figs. 56 and 57. Only small changes in temperature maxima are indicated.

H. Shutdown Cooling

Design and operation of the shutdown cooling system are unchanged. The approximate fission product decay power and reactor coolant temperatures existing during long-term natural convection cooling (after several hundred seconds following scram), are unchanged from those given in [Fig. 80]. The actual coolant flow rates (Fig. 58) are also unchanged, but are expressed in per cent of full flow (which value has been increased).

I. Reactivity Coefficients and Nuclear Performance

1. Isothermal Temperature Coefficient of Reactivity

The previously predicted values of the various components comprising the isothermal temperature coefficient are repeated in Table XVI. These are compared with the material replacement data from the EBR-II mock-up on ZPR-III. The measured dry isothermal temperature coefficient between 58°F and 99°F is -2.6×10^{-5} $(\Delta k/k)/°C$ (see Appendix L).

The sum of the predicted fuel and structural components of the temperature coefficient, as given in Table XVI, yields -1.8×10^{-5} $(\Delta k/k)/°C$ without sodium. The agreement between the measured and predicted value is reasonably good because: (1) the temperature distribution in the dry critical reactor may not have been truly isothermal; and (2) the presence and effect of the bond sodium in the Dry Critical Experiments would tend to increase the magnitude of the measured value.

Many of the predicted components of the temperature coefficient may be compared with material replacement data from ZPR-III. However, such comparison is not direct. To demonstrate, an important component in both power and temperature coefficient of reactivity is the effect of sodium density in the reactor core, predicted to be -0.87×10^{-5} $(\Delta k/k)/°C$.

Table XVI

ISOTHERMAL TEMPERATURE COEFFICIENTS OF REACTIVITY
[in $(\Delta k/k)/°C$]

	Predicted [Table XIII]	Inferred from ZPR-III Measurements
Core		
Axial Growth of Fuel	-0.39×10^{-5}	$-0.34 \pm 0.02 \times 10^{-5}$
Radial Growth of Fuel (Displacement of Na)	-0.09×10^{-5}	-0.057×10^{-5}
Axial Growth of Structure (Density Change)	-0.039×10^{-5}	-0.033×10^{-5}
Density Change of Coolant	-0.87×10^{-5}	-0.98×10^{-5}
Radial Growth of Support Structure	-0.97×10^{-5}	-0.92×10^{-5}
Doppler Effect	$+0.04 \times 10^{-5}$ (avg)	-
Bowing	-	-
Gaps		
Density Change of Coolant	-0.38×10^{-5}	-0.33×10^{-5}
Density Change of Structure	-0.036×10^{-5}	-0.04×10^{-5}
Upper and Lower Blanket		
Density Change of Coolant	-0.21×10^{-5}	-0.21×10^{-5}
Radial Growth of Uranium and Jacket	-0.016×10^{-5}	-
Axial Growth of Blanket Uranium	-0.024×10^{-5}	-
Axial Growth of Jacket	-0.021×10^{-5}	-0.0064×10^{-5}
Inner Blanket		
Density Change of Coolant*	-0.2×10^{-5}	-0.30×10^{-5}
Axial Growth of Blanket Uranium	-0.066×10^{-5}	-
Axial Growth of Jacket*	-0.022×10^{-5}	-0.054×10^{-5}
Radial Growth of Uranium and Jacket	-0.07×10^{-5}	-
Radial Growth of Support Structure	-0.17×10^{-5}	-
Bowing	0	-
Outer Blanket		
Density Change of Coolant*	-0.017×10^{-5}	-0.011×10^{-5}
Axial Growth of Blanket Uranium	-0.014×10^{-5}	-
Axial Growth of Jacket*	-0.003×10^{-5}	-0.0012×10^{-5}
Radial Growth of Support Structure	-0.034	-

*The experimental results for these components are difficult to interpret because the radial boundaries, especially between core and blanket, are not well defined.

The experimental investigation on ZPR-III dealt with removing sizeable quantities of sodium from the reactor core to effect a gross density change of sodium. The measured worth was -1.16×10^{-3} $(\Delta k/k)/kg$ of sodium. The mass of sodium in the core is about 29 kg and the coefficient of expansion is given as $2.9 \times 10^{-4}/°C$. Therefore, the effect of sodium density inferred from the ZPR-III experiments is -0.98×10^{-5} $(\Delta k/k)/°C$. The experiment is an attempt to simulate power reactor conditions with a zero-power, fixed-temperature machine. The calculations feature simple

idealized geometric models, but the comparisons between theory and experiment are encouraging. A number of such comparisons are given in Table XVI. Allowing fairly large uncertainties for the values which were not confirmed by ZPR-III experiments, it is believed that the predicted (wet) isothermal temperature coefficient of -3.6×10^{-5} $(\Delta k/k)/°C$ is known to ±30%.

2. Power Coefficient of Reactivity

The power coefficient of reactivity is a function of flow rate and other operating conditions. The previous evaluation [Section IV.I.2.] for full flow between startup (700°F isothermal) and full reactor power (62.5 Mw), is only slightly modified here. The modification occurs principally because the expected bowing effect is smaller.

Some of the significant contributing components may also be compared with pertinent material replacement experiments on ZPR-III. The nature and limitations of such comparisons have been described in Section IV.I.1.

The total temperature increases are related to reactivity changes by combining the data from Table XVI with those from Table XVII. The results are summarized in Table XVIII. Bulk radial expansion is assumed to be proportional to coolant temperature. The effect of bowing is considered next.

Table XVII

AVERAGE REACTOR TEMPERATURES AT FULL POWER WITH FULL FLOW

Component	Average Temperature, °F		Average Temperature Rise, °C*	
	[Section IV.I.2.]	Present Analysis	[Section IV.I.2.]	Present Analysis
Core Coolant	810	820	61	67
Core Fuel	975	976	153	153
Core Cladding	862	871	90	95
Upper Gap	919	935	122	131
Lower Gap	702	705	1	3
Upper Blanket	924	943	124	135
Lower Blanket	705	708	3	4
Inner Blanket	780	770	44	39
Outer Blanket	745	711	25	6
Supporting Structure	700	700	0	0

* From 700°F (371°C) isothermal to full power-full flow.

Table XVIII

POWER-INDUCED REACTIVITY CHANGES AND
POWER COEFFICIENTS OF REACTIVITY (WITHOUT BOWING)*

	No Uniform Radial Expansion		Includes Uniform Radial Expansion	
	[Predicted]	Current**	[Predicted]	Current**
Reactivity Change, $\Delta k/k$				
Total	-0.0020	-0.0019	-0.0027	-0.0026
Core	-0.0014	-0.0013	-0.0020	-0.0019
Power Coeff. Reactivity, $[(\Delta k/k)/Mw \times 10^5$				
Total	-3.2	-3.0	-4.3	-4.2
Core	-2.2	-2.1	-3.2	-3.1

* 700° F isothermal to 62.5 Mw, with 9,000 gpm flow.

** Analysis based on experimental coefficients of Table XVI, and revised temperature distributions of Table XVII.

Bowing of fuel subassemblies and associated radial core expansion under various conditions was estimated in [Appendix A]. The current thermal analysis (Appendix F), concludes that the full-power, effective temperature difference across a fuel subassembly at the core boundary is approximately 50°F. This may be compared with the earlier [Appendix A] temperature difference of 100°F. The relationship between effective thermal core deformation and reactivity is somewhat uncertain and is therefore conservatively estimated. For the EBR-II radial core deformation, $\Delta k/k \approx -(0.075\ r)(\Delta r/r)$, where r is the core radius (in.). The effective core radius and geometry are dependent on the actual critical size.

Table XIX is a summary of the reactivity effects caused by bowing and radial expansion. The two cases are determined by the initial subassembly configurations. The results of both the most probable and most pessimistic configuration are shown. The influence of bowing is small and the major difference between the "most probable" and "most pessimistic" estimates is the range over which the small positive effect ($\sim 1 \times 10^{-5}\ (\Delta k/k)/Mw$) may be operative; i.e., a range of 9 Mw probable, 36 Mw pessimistic. If the predicted reactivity effects are overestimates (as is expected), the effect is negligible. If the effect occurs at all, it is expected to appear as a variation in the magnitude of the strongly negative power coefficient of reactivity as a function of power level.

Table XIX

POSSIBLE INFLUENCE OF BOWING ON THE POWER COEFFICIENT OF REACTIVITY

	Most Probable Configuration			Most Pessimistic Configuration		
Power Range, Mw	0-25	25-34	34-62.5	0-20	20-56	56-62.5
Change in Core Radius, in.	+0.001	-0.005	+0.003	+0.0005	-0.0195	+0.001
Bowing Reactivity Effect, % $\Delta k/k$	-0.0075	+0.038	-0.023	-0.0038	+0.15	-0.0075
Bowing Power Coeff., $[(\Delta k/k)/Mw] \times 10^5$	-0.3	+4.2	-0.8	-0.2	+4.1	-1.1
*Typical Power Coeff., $[(\Delta k/k)/Mw] \times 10^5$	-3.2	-3.2	-3.2	-3.2	-3.2	-3.2
Net Power Coeff., $[(\Delta k/k)/Mw] \times 10^5$	-3.5	+1.0	-4.0	-3.4	+0.9	-4.3
Reactivity Change Through Each Power Range,						
% $\Delta k/k$	-0.088	+0.0086	-0.11	-0.068	+0.031	-0.028
~ inhours	-37	+3.6	-47	-28	+13	-12
Net Power Coefficient from Zero to Full Power, $[(\Delta k/k)/Mw] \times 10^5$		-3.1			-1.0	
Net Reactivity Loss, inhours		~80			~27	

*From Table XVIII; no radial expansion included.

A negative reactivity effect, analogous to bowing and with a comparable time constant, is created by expansion of the control rods and the lower end of the control rod drive shafts (see Section IV.I.5.). This effect has not been included in the estimated power coefficient, nor has it been treated in the detail of the bowing analysis, because it is clearly negative while bowing is a positive effect.

At low power-low flow, the behavior of the reactor is similar to that at high power-high flow. However, the temperature rises in Table XVII will occur at lower powers, hence, the average power coefficient of reactivity from zero power to some power level will change approximately inversely. For example, the required reactivity to go from zero power to full power at full flow, is essentially the same as that required to go from zero power to, say, 20% power with about 20% coolant flow. This implies that only a very small amount of net reactivity is required to go from 20% power-20% flow, to full power-full flow.

3. Critical Configuration

The detailed EBR-II mock-up on ZPR-III (Appendix E) lacked the precision to specify the U^{235} enrichment of the fuel alloy. The significant differences between the critical experiment and the EBR-II are: (1) the mock-up core height was 14 in., as opposed to 14.22 in. for the reactor; and (2) the mock-up had the radial dimensions of a 64-subassembly core. Therefore, the critical assembly data were interpreted on the basis of perturbation measurements and reactor analysis.

The enrichment for the first loading was based on a critical loading of 67 fuel subassemblies, including control and safety rods. This requirement was established to ensure a minimum core size of not less than 61 subassemblies, and to provide a margin of six subassemblies ($<2\%\ \Delta k/k$).

The following conditions were assumed in fixing the fuel alloy atomic enrichment at 48.4 at-%.

(1) The fuel alloy is the 5 wt-% fissium alloy.

(2) The density of the fuel alloy is 17.95 gm/cc.

(3) The density of the blanket uranium is not less than 18.7 gm/cc.

(4) The blanket uranium is depleted to about 0.22%.

(5) The nominal core will contain 67 subassemblies (53 fuel, 12 control, and 2 safety).

(6) Configuration and composition are as given in Table I.

(7) At full power (62.5 Mw) and full flow (9,000 gpm), the reactor is less than 1% $\Delta k/k$ supercritical (with control rods fully inserted).

The fuel alloy density of 17.95 gm/cc was assumed as a result of experience in fabricating prototype fuel elements which yielded a value of approximately 17.95 gm/cc. Measurement of fuel elements in production showed an average density of 17.8 gm/cc (Appendix A).

The enrichment of the fuel alloy was specified on the basis of both experimental and analytical data developed independently. The data were in substantial agreement and well within the uncertainty of the determination. The details of these analyses have been reported by Loewenstein.[17]

The U^{235} in U content was specified at 48.4 at-%. The average enrichment achieved was 48.41 at-% (Appendix A).

The specified enrichment included an uncertainty of 2.5%, which is equivalent to ±1.1 to 1.2% $\Delta k/k$. Therefore, the critical loading at full power and full flow would be expected to contain between 63 and 71 subassemblies. The agreement between the predicted and measured dry critical size (Appendix L) supports the above conclusions; however, the dry critical size slightly exceeded the "most probable" prediction. This observation tends to favor a core size between 67 and 70 subassemblies.

4. Plutonium Production

Breeding of nuclear fuel will be demonstrated initially by burning U^{235} to produce Pu^{239}. (True breeding as demonstrated by simultaneous destruction and creation of Pu^{239} must await a future Pu-fueled loading of the system.)

Although the predicted initial conversion ratio is 1.26, inaccurate representation of some detailed mechanical design features in the analytical model tends to favor a lower value. A value of 1.2 is probably more realistic.

As U^{235} is destroyed, principally in the reactor core, Pu^{239} is created throughout the system. The bulk of the bred Pu (~90%) is distributed throughout the depleted uranium blankets. These are positions of low reactivity worth relative to the location of the destroyed enriched uranium. During a reactor cycle, the reactivity of the system cannot increase. This conclusion is valid even though there is a net increase in the number of fissionable atoms throughout the system.

These considerations do not include fission product poison effects which tend to further reduce the reactivity. However, the overriding consideration in long-term reactivity loss is associated with the reduction in fissionable material (U^{235}) per unit core volume.

Plutonium buildup in the radial blanket subassemblies can have some influence on the critical size of, and the radial power distribution in, the second and subsequent core loadings. If the first reactor core were permitted to achieve an average burnup of 1 at-% and were replaced without replacing any radial blanket subassemblies, a second core loading identical to the first would be critical with one less core subassembly (in the first row of the inner blanket). Actually, core subassembly replacement will be on a fractional core basis; hence, the reactivity due to plutonium buildup will appear through a shift in control rod insertion. Table XX summarizes predicted reactivity effects of bred plutonium in various rows of the radial blankets. The irradiation times required to achieve the specified Pu content are also given.

Table XX

BRED PLUTONIUM REACTIVITY EFFECT IN THE RADIAL BLANKET WITH 1.0 at-% Pu^{239} CONTENT

Subassembly Row No.	Blanket	% $\Delta k/k$	Approximate* Initial Buildup Time, Years
6	Inner	0.72	1
7	Inner	0.42	1.4
8	Outer	0.21	2
9-11	Outer	0.17	3.5
12-13	Outer	0.006	14

*At core midplane with full power (80% plant factor).

The reactor power distribution is influenced slightly by the presence of the bred plutonium in the radial blankets. The details will depend on the exact mode of cycling both core and blanket subassemblies. If, as is expected, the core is cycled more frequently than the radial blanket, there will be a slight shift in power from the core to the radial blanket for a fixed total reactor power. The over-all shift is small; however, localized power density perturbations will be significant, primarily near the core midplane. Table XXI summarizes the perturbation of the virgin reactor fission power densities by the presence of bred plutonium at various radial positions.

Table XXI

BRED PLUTONIUM PERTURBATION OF CORE MIDPLANE FISSION DENSITIES IN DEPLETED URANIUM

Radial* Distance, cm	F(1 at-% Pu)** / F(0.0 at-% Pu)	F(0.0 at-% Pu),** kw/liter	Approximate† Initial Buildup Time, years
Inner Blanket			
22.4	1.22	222	1.0
24.2	1.25	162	1.1
26.0	1.31	111	1.2
27.7	1.37	82	1.3
29.5	1.43	60	1.5
32.8	1.7	31	1.8
Outer Blanket			
36.0	1.9	18	2.3
39.2	2.2	11	3.0
49.0	3.3	2.7	7.2
58.7	4.0	0.89	18
68.4	4.4	0.29	49
78.1	4.7	0.10	125

*From center of core in core midplane (Z = 0).

**F = Fission power density; total power density is obtained by adding core gamma leakage heating.

†To achieve 1 at-% Pu in depleted uranium with full power (80% plant factor) operation.

Note: 1 at-% average core burnup requires approximately 60 days with full power (80% plant factor).

5. Predicted Kinetic Characteristics

Analytical closed-loop transfer functions have been obtained for EBR-II.[18] The temperature-induced reactivity feedbacks in the model

were caused by unrestrained thermal expansion. Bowing, fuel alloy phase transformations, or other non-linear effects, were not included. The Doppler Effect [Appendix B] was neglected. Radial core expansion was assumed proportional to coolant temperature rise. (This assumption is realistic for tightly packed subassemblies.) Clearances existing at low temperatures may be reduced as the reactor heats up. This would be evidenced by an increase in the magnitude of the negative power coefficient of reactivity with increased power at fixed coolant flow.

Reactivity coefficients were used to determine the temperature-induced feedbacks. These were based on material replacement effects of sodium, steel, and fuel, as a function of position in the EBR-II mock-up on ZPR-III (Appendix E and Reference 19). The feedback coefficients are essentially those used for the isothermal temperature and power coefficients of reactivity (Tables XVI and XVIII).

The predicted closed-loop transfer function amplitudes (Fig. 59) and phase lags (Fig. 60) show no evidence of instability. The reactor model did not include any reactivity coefficients with long delay times. Thermal inertia and coolant transit time delays are less than 2 sec.

No prompt positive coefficient was included in the model. The Doppler Effect and bowing are the only known sources for such effects. The former is believed negligible, while the latter may be present. Bowing (Section IV.I.2.) is only significant under the most pessimistic assumptions and is not believed large enough to be highly important, or perhaps even observable.

Another clearly negative effect not explicitly included in the model is caused by the axial thermal motion of control rods relative to the core. This occurs because the core is supported from the bottom of the primary tank and the control rods are supported from the primary tank cover. The bulk of the effect is prompt due to axial expansion of control rod walls as coolant temperature increases. A minor delayed contribution is expected due to heating of the lower end of the control rod drive shafts below the top of the reactor cover.

The possible presence of a very small, second-order, positive component is also recognized. This is caused by the thermal expansion of fuel pins in partially inserted control rods. However, this possible effect is completely dominated by the much larger and reverse effect due to the reactivity reduction caused by the simultaneous thermal expansion of fuel pins in core subassemblies.

In summary, the reactor system is expected to be stable in operation. Moreover, the experimental stability investigations at 30 Mw with 4,310-gpm coolant flow can be used with confidence to predict reactor kinetics

at 62.5 Mw with 9,000-gpm coolant flow. It is also probable that investigations at 30 Mw with 9,000-gpm coolant flow can be used to predict reactor kinetics at full power-full flow.

J. Fuel-Handling, Unloading, and Interbuilding Transfer.

1. General

Except for changes occasioned by the removal of the Disassembly Cell from the Reactor Plant (see Section III.A.), the fuel-handling and unloading operations remain as contemplated in the original report [Page 34]. This section contains operating information which has been developed since release of the original report. The mechanisms and their functions are described in Sections III.A.7., and III.A.9.

2. Fuel-Handling Center

All operations involved in subassembly transfers within the primary tank, and between the primary tank and the fuel-unloading machine are controlled directly, or are supervised by the operator at the fuel-handling console (Fig. 61).

Of principal interest is the main operating panel (center sloping section), which is shown in detail in Fig. 62. On this panel are located the pushbutton-indicator light units necessary for accomplishing the steps involved in subassembly transfers, both within the primary tank and between the primary tank and fuel-unloading machine. The pushbutton-indicator units are arranged in twelve groups or "operating sequences." Except for the preparatory and terminal sequences (those designated A, H, J, and M), each sequence consists of a series of steps, arranged in the order of execution, essential to the transfer of a subassembly from one location (or handling device) to another. For example, the steps in the group designated "Sequence B" extract a subassembly from the reactor and raise it to the proper level for transfer to the transfer arm. Guide lines are provided on the panel to indicate the normal progression from sequence to sequence.

In sequences J, K, L, and M, the legends on certain indicator units refer to "R-M" (fuel-unloading machine), and to "COOL" (argon cooling system). These indicator units inform the console operator of operations initiated elsewhere during the meshing of operations controlled by the console operator with those controlled at the fuel-unloading machine and argon cooling system panels.

In order to perform the individual operations within a particular sequence, the operator first presses the corresponding "sequence button," which sets up the circuits for the operations within that sequence. He then successively presses the operating pushbuttons within the sequence.

Typically, when a pushbutton is pressed, the drive motor associated with the particular motion starts and the button is illuminated with a red indicating light. Upon completion of the motion, the drive motor stops, and the red light is automatically replaced by a green light. The green light signals that the step has been completed, and the following step may be initiated. The indicating light units associated with operations initiated elsewhere, i.e., at the transfer arm or fuel-unloading machine, are identical to the pushbutton units, except that the switching function is omitted. The arrangement of controls in operating sequences results in some duplication of pushbuttons and indicators, but makes it unnecessary that the operator memorize the sequential order of the many steps. It also provides a more readily comprehended picture of the progress of the transfer operation.

Two key-operated switches are provided on the console for energizing the control power for the fuel-handling and fuel-unloading circuits:

(1) The "restricted operations" key switch is used for fuel-unloading operations not involving access to the reactor. It energizes circuits necessary for operation of the storage rack, transfer arm, and transfer port, provided only that the control power key switch in the control room is switched on.

(2) The "unrestricted operations" key switch energizes the control circuits for all fuel-handling and fuel-unloading operations. Before this key switch is effective, many interlocks must be satisfied. In addition, the control room three-position switch, "reactor operate-off-fuel handling," must be switched to "fuel handling." Figure 35 shows the interlocks governing the fuel-handling control power circuit.

During "unrestricted" fuel-handling operations, reactor operating control power is not available to the control room (interlock enforced), even though the "reactor operate-off-fuel handling" key switch is inadvertently switched to "reactor operate."

Upon completion of "unrestricted" fuel-handling operations, the interlock circuits require that the following conditions be met before the control rods may be raised:

(1) The reactor vessel cover must be down and locked to the vessel.

(2) The fuel-handling operator must have completed the terminating sequence of operations.

(3) The "unrestricted operations" key switch on the fuel-handling console must be switched to "reactor."

3. Numerically-Controlled Positioning System

As stated in Section III.A.7., the input information for the numerically-controlled positioning system is contained on punched cards. There are four types of input cards, each of which is identified by color, and by a number punched and typed on the card:

Type	Color	Operating Functions
1	blue	refueler (unloading machine) to storage rack
2	green	storage rack to core
3	red	core to storage rack
4	yellow	storage rack to refueler

At specified points in the fuel-handling cycle, the appropriate input card is manually inserted into the card reader. The card is immediately read and the information is stored. Provided automatic checks indicate a valid input card is being used, and in the proper sequence, motion of the rotating plugs (or storage rack) is initiated when the related pushbutton is pressed. Upon completion of the positioning operation, the coordinates reached are automatically punched on an output card. After completion of all positioning operations specified on a given input card, the input and output cards are visually compared by the operator for agreement between the command coordinates and the actual coordinates.

The completion of an operation directed by the numerically-controlled positioning system is indicated by a green light in the pushbutton unit as in the case of simpler motions where limit switches are used. However, in the former instance, the green light will not appear unless automatic checks indicate that the position is within tolerance, and that the position encoder data are valid.

Provisions are included for individual manual control of the rotating plugs and gripper mechanisms. Manual control is subject to the same interlocks as is the card-directed automatic operation; however, the presence of a valid input card in the card reader is not required.

4. Fuel-Unloading Machine

The fuel-unloading machine is provided with a control panel (Fig. 63) on which are mounted the control pushbuttons, indicators, etc. An operator at this station initiates all motions of the power-operated components of the machine. Normally the motions are terminated automatically by limit switches. Stop pushbuttons are provided, however, for unusual circumstances. Because of the smaller number and lesser complexity of operations performed at the unloading machine, as compared to those at the main operating panel, the pushbuttons and indicators are

not grouped in operating sequences. Extensive interlocking is provided, both among the various functions of the unloading machine, and between these functions and the other fuel-handling mechanisms.

5. Manual Operations

The fuel-handling and unloading procedures include the direct manual operation of certain devices as described below. Although manual operation, when permitted, is not restricted as to direction, the interlock circuits require attainment of the correct position before the next operation may be performed.

a. Transfer Arm

For reasons outlined [Section III.A.7.], the transfer arm is operated manually. Rotation and locking (or unlocking) are physically prevented at other than the proper junctures by electro-mechanical locking devices. During fuel unloading from the primary tank, an additional blocking device prevents rotation of the transfer arm to points above the reactor vessel. At specific points in its rotation, the actual position of the transfer arm is transmitted to indicators at the fuel-handling center.

b. Port Plugs

Manually rotated access port plugs are employed on the primary tank, unloading machine, and interbuilding coffin. These plugs permit passage of reactor subassemblies (a) between the primary tank and the unloading machine, and (b) between the unloading machine and the interbuilding coffin. Again, electro-mechanical locks permit rotation of the plugs only at the proper time. Except for the interbuilding coffin port, their position is indicated at the fuel-handling center.

c. Locking Pins (Fuel-Unloading Machine)

Manually actuated locking pins are used to secure the fuel-unloading machine in position over the primary tank and over the interbuilding coffin.

6. Interbuilding Coffin

The transport of the interbuilding coffin from the pit beneath the fuel-unloading machine tracks, to the air cell in the Fuel Cycle Facility, is accomplished in the following stages:

(1) Transport from the pit to the equipment air lock dolly, using the reactor building crane.

(2) Transport through the length of the equipment air lock on the self-propelled dolly.

(3) Lift through the outer hatch in the air lock, and deposit on self-propelled interbuilding cart, using a fixed hoist at the air lock.

(4) Transfer to the Fuel Cycle Facility. Subassembly cleaning operations are carried out, while the coffin is on the interbuilding cart.

(5) Within the Fuel Cycle Facility, vertical transfer to the fuel-cycle cart, using the building crane.

(6) Transport to a station beneath the air cell on the self-propelled fuel-cycle cart. At this point, the subassembly is extracted from the coffin.

The transport of subassemblies from the Fuel Cycle Facility back to the Reactor Plant follows the above stages in the reverse order. All crane, hoist, and cart operations are manually controlled and under constant supervision.

V. SUMMARY OF HAZARDS CONSIDERATIONS

The previous sections of this report have described the various changes which have developed during the construction of the EBR-II. Other changes, evaluations, and test results relevant to reactor and plant safety are treated in the Appendices. This section summarizes the various hazards considerations.

The previously described changes, additions, and verifications can be divided into two groups on the basis of relevance to safety. Those considered directly related to safety can be summarized as follows:

(1) Reduction of predicted reactivity worth of control rods, safety rods, and core subassemblies, resulting from experimental data and additional analyses (Appendices E and L).

(2) Reduction in acceleration of control rods during scram operation (Section IV.A.2.).

(3) Verification of many predicted reactivity coefficients (Appendices E and L).

(4) Revisions in instrument locations and instrument thimble cooling (Section III.A.5.).

(5) Addition of provision for manual scram of safety rods during reactor operation (Section IV.A.2.).

(6) Addition of rate-of-change control on primary pump flow (Section IV.A.3.).

(7) Reduced temperature difference across subassemblies and consequent reduction in bowing (Appendix F).

(8) Change in nominal core configuration from 61 to 67 subassemblies (Section III.A.1.).

(9) Revisions in reactor power density distribution, coolant flow distribution, and calculated temperatures (Sections IV.B.2. and IV.B.3.).

(10) Provision for limiting ratio of power to coolant flow; ratio does not exceed preset limits (Section IV.A.2.).

The following changes are not considered directly related to safety although they may indirectly enhance safety because of improved operational reliability or convenience:

(1) Removal of Disassembly Cell from Reactor Plant to the Fuel Cycle Facility.

(2) Incorporation of the "subassembly basin" in the primary tank.

(3) Use of mechanical-centrifugal pumps rather than d-c electromagnetic pumps in the primary sodium system.

(4) Use of orifice holes, rather than slots, in the core and inner blanket subassembly coolant inlet adapters.

(5) Change in reactor vessel shape (to uniform diameter), resulting in a simpler structure less subject to thermal stress.

The major safety considerations related to operation of the EBR-II were summarized in ANL-5719 [Section V]. The significant safety features treated can be summarized as follows:

(1) Integrity of primary sodium system (which virtually precludes loss of sodium coolant).

(2) Reliability of reactor shutdown cooling.

(3) Reliability of reactor control system achieved by: (a) redundancy provided by twelve independent control rods and drives; (b) small reactivity worth of each control rod [$< 0.006\ \Delta k/k$]; and (c) independent operation of safety rods during fuel-handling operations.

(4) Prompt negative temperature effect resulting from fuel expansion.

All of these features have been retained or enhanced. The speeds of the various drives which add reactivity (control drives, safety drive, fuel-gripper drive) are unchanged and the reactivity worths of the respective components are less than originally estimated. As a result, the rates of reactivity addition are now smaller. Conversely, the reduction in estimated reactivity worth of the twelve control rods results in some reduction in the shutdown of the reactor (to approximately 3.5% $\Delta k/k$); this is considered adequate in view of the operative reactivity coefficients and the availability of the safety rods ($\sim$1.3% $\Delta k/k$) during shutdown.

The acceleration force on the control drives during scram has been reduced (from 2 g to 1.5 g) to decrease the loading on the control rods. The reduction in speed is small; rod movement of 10 in. from the fully inserted position, corresponding to removal of 73% of total rod worth, now occurs in about 0.18 sec (after start of rod movement) as compared to about 0.16 sec formerly.

The arrangement of the neutron instrument thimbles has been revised to provide four thimbles within the neutron shield for improved low-level detector sensitivity. This improvement has been verified by critical experiments on ZPR-III and by the Dry Critical Experiments.

The addition of rate-of-change control on the primary sodium pump flow reduces the temperature transients which can be effected during flow changes.

The EBR-II nuclear analyses have been compared with, and based on, applicable experimental data from the mock-up investigations on ZPR-III (Appendix E) and the EBR-II Dry Critical Experiments (Appendix L). This has improved the reliability of the predictions of reactor performance. The extensive power-stability investigations conducted on EBR-I, Mark III have provided a better understanding of fast reactor power kinetics (Appendix D).

The predicted isothermal temperature coefficient of the EBR-II is negative, and the power coefficient of reactivity is believed to be prompt and negative over the operating power range; however, small positive power coefficients are possible over certain power level increments due to bowing (Appendix F). If these positive power coefficients do appear, they should be of small magnitude and should exist only over a limited power level range. Under the most pessimistic assumptions, there is always a net decrease in reactivity between startup and any "normal power level" (a power and coolant flow condition resulting in rated coolant outlet temperature, i.e., ~883°F). The power coefficient of reactivity is prompt and negative above any normal power level. Only very small delayed negative temperature effects are operative and these are masked by the much larger prompt negative coefficients. As a result, no significant feedback effects are anticipated which could produce oscillatory instabilities.

Two leak-rate tests have been conducted on the Containment Vessel. The first test indicated the leak rate to be 560 ft^3 (32°F, 36.2 psia)/day, or less. The second and more accurate test, conducted with all vessel penetrations completed, indicated a leak rate of less than 100 ft^3/day. (The specified maximum permissible leak rate was 1000 ft^3/day.)

With respect to possible hazards related to operation of the EBR-II, the following six hypothetical accidents were considered [Page 107] to assess the safety characteristics of the reactor and to estimate the consequences:

"Case 1.

"Assume the reactor is at delayed critical and at zero power conditions (8 watts and 600F) with the safety rods out. These rods are then driven into the reactor in an uncontrolled fashion at their normal speed of two inches per min.

"Case 2.

"Assume the reactor is at delayed critical and zero power conditions with the central fuel subassembly removed. This element is then loaded at regular speed of 6 in. per min for the last 24 in. of motion.

"Case 3.

"Assume the reactor is at delayed critical and zero power conditions and a single control rod is driven into the reactor in an uncontrolled manner at 5 in. per min.

"Case 4.

"Same as Case 3., except that the excursion begins at operating power and full flow.

"Case 5.

"Assume the reactor is at delayed critical and zero power conditions with the central fuel subassembly being loaded. It is dropped and falls into the reactor. This is an accident where reactivity is added rapidly. Two sub-cases are considered: first, where the subassembly is dropped from just above the core, and second, where the subassembly falls the full length of the reactor.

"Case 6.

"Same as Case 2., except that the core subassembly is driven all the way in at the high speed of 72 in./min. (The high speed is employed normally after the subassembly has been raised 24 in.)"

The first four cases involve "uncontrolled" reactivity additions by normal components of the reactor system (at normal speed). In each case, the reactivity increase would be terminated by normal operation of period- and/or power-level trips. Since the reactivity worths of each of the components involved (control rods, safety rods, or central subassembly) are less than previously predicted, the rates of reactivity addition are smaller and more time is available for operation of the safety systems (Appendix F).

In the event the safety devices fail, reactor melting may occur. This is also true of the last two hypothetical accidents (Cases 5 and 6). It should be noted that a combination of malfunctions and/or a gross loss of administrative control are required to achieve these hypothetical conditions.

The consequences of primary pump failure were also assessed [Pages 108-109] and it was found that significant overheating would not occur if the safety systems (reactor scram) were operative. If the safety systems failed to operate (combination of malfunctions), reactor melting would result.

Without implying any credence to the accident, the consequences of a gravity-induced core meltdown subsequent to a loss of sodium were evaluated. Reactivity insertion rates of $200/sec, $600/sec, and $1000/sec, might be realized, depending upon a combination of assumed events (and pessimism). Additional analyses have been performed (Appendix G) to determine the energy yield from accidents involving such rates of reactivity addition. These have resulted in somewhat higher yields as shown in Table XXII.

Table XXII

EXPLOSIVE ENERGY YIELD AS A FUNCTION OF REACTIVITY INSERTION RATE

Reactivity Insert. Rate, $/sec	Explosive Energy Yield, lb of TNT	
	Previous Analysis [Section V.E.]	Present Analysis
200	280	370
600	660	850
1000	1050	1240

An assessment of the prediction of explosive energy yields resulting from these specific reactivity insertion rates indicates they are overestimates of what may actually appear as a result of a core meltdown (see Appendix G). A large fraction of the created energy is assumed to be available for an explosion; the calculation assumes no spatial energy transfer during the excursion which would, in fact, tend to reduce the local pressures.

Although these results indicate an increase in the possible energy yield from such an accident, the magnitude of the changes are within the range of accuracy which can be assigned to these calculations and also are based on pessimistic assumptions as described above. The practical result of applying them to the containment analysis results in a small reduction in the safety factor of the primary containment system which is estimated to be very conservatively designed (Appendix H).

The effect of a single fuel element failure or multiple failures (including propagation of failure) has been evaluated (Appendix F). These evaluations indicate that a relatively large blockage of coolant flow channels can be tolerated without causing fuel element failure. They also indicate that propagation of fuel element failures will be confined within the subassembly and that the progression of failure probably will be retarded short of complete failure of all 91 fuel elements within the subassembly. Failure of a single fuel element (or a few elements) may not produce a detectable reactivity change in the system. Failure of a large number of fuel elements in a subassembly probably will produce a power level scram (increasing power level) or more likely, a power level alarm (decreasing power level). It is quite improbable that such a failure will cause a period trip.

It is also postulated that the propagation of fuel element failures will not progress beyond the subassembly wall, or if this does occur, a significant time delay will obtain before failure is initiated in adjacent subassemblies. It is therefore concluded that it is very improbable that fuel element failure can initiate a serious reactor incident or reactivity change which will not be detected by the reactor control system and terminated automatically if a power increase results. Preliminary TREAT experiments tend to confirm the confining characteristics of the subassembly hexagonal can with respect to failure propagation (Appendix F).

TREAT in-pile test results have been evaluated (Appendix G) as they may apply to EBR-II. It is concluded that the test conditions are sufficiently different from those which might be postulated for the reactor that application of the results is questionable. Also, that extrapolation of the single pin test results to the EBR-II will not result in greater reactivity addition rates and subsequent nuclear explosions than those in the hypothetical gravity-induced core meltdown following loss of sodium.

The radiation hazard to the surrounding area from a hypothetical reactor disaster is unchanged [Section V.G.]. That analysis assumed 50% fission product release to the atmosphere after 135 days of full-power operation. This resulted in maximum external doses of less than 100 r at distances greater than 35 miles from the site. This conclusion is extremely pessimistic because of the assumed magnitude of fission product release. Furthermore, it is not likely that large concentrations of activity can travel 35 miles without being appreciably diluted. Also, the prevailing winds would be expected to direct a concentrated cloud away from the nearest centers of heavy population.

The evaluation of hazards for the EBR-II, as summarized in this section, is essentially unchanged from ANL-5719. The following conclusions can be drawn in summary of these evaluations:

(1) Intrinsic protection of the reactor system from a meltdown accident resulting either from loss of sodium or from loss of heat removal capability is provided by: (a) sodium containment afforded by the primary tank; and (b) natural circulation of sodium through the reactor (augmented by the auxiliary pump), together with natural convection heat dissipation by the shutdown coolers.

(2) Intrinsic protection of the reactor system from a loading accident is provided by: (a) loading the reactor by substitution (minimum void in the reactor); (b) speed control and check points in the fuel-handling sequence; and (c) safety rods which are operational during fuel handling.

(3) A large number of errors and malfunctions in combination must occur to cause a serious accident. Although these requirements make such an accident extremely improbable, it cannot be considered impossible.

(4) Such an accident would be contained unless the energy release were far larger than predicted on the basis of very pessimistic assumptions, and if the safety factors employed in the design of the structural and containment systems failed to provide the expected capability.

(5) If the containment vessel were breached, the consequences would be primarily local because of the isolated location of the plant. The general public would not be seriously endangered.

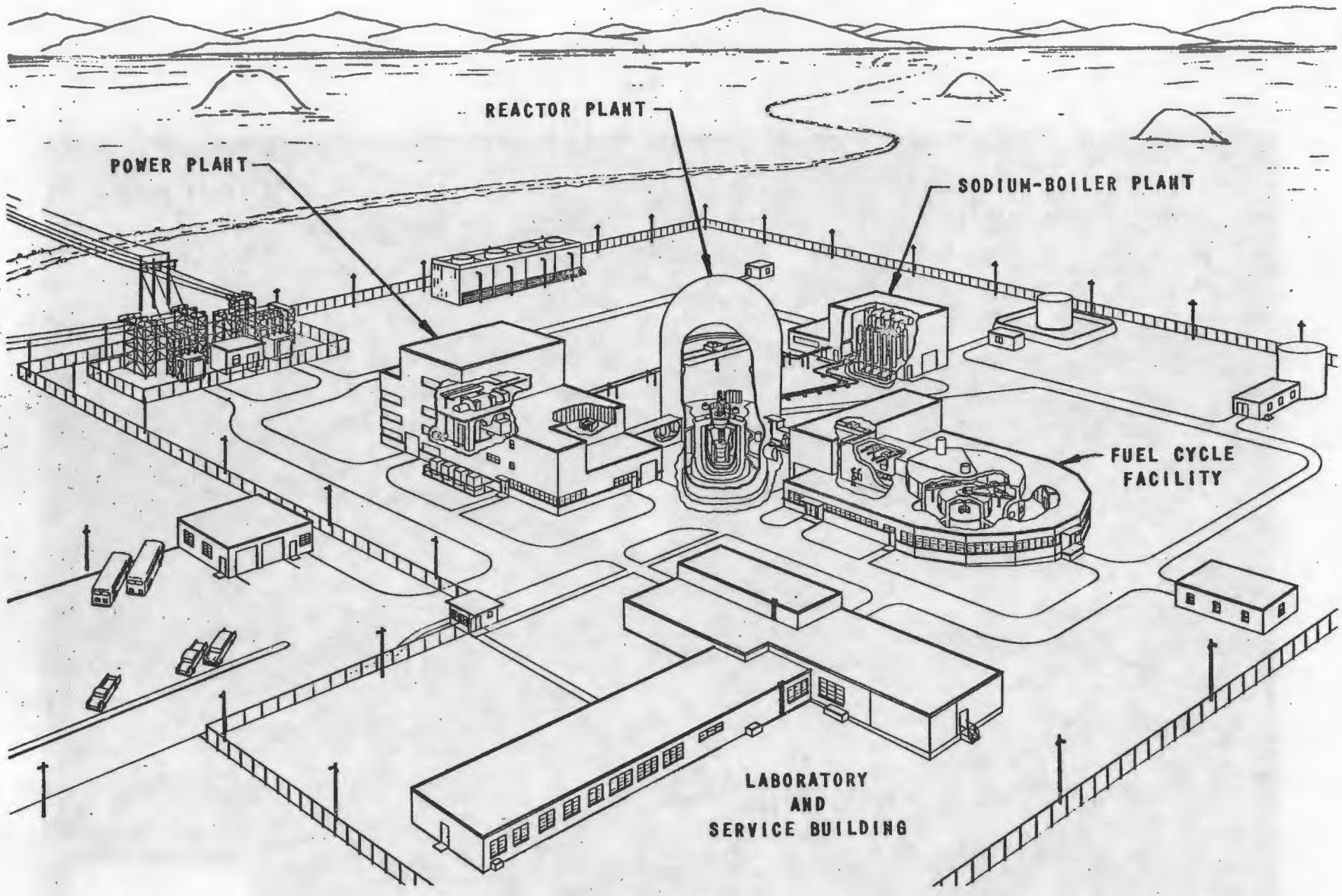

Fig. 2

EBR-II Plant Arrangement

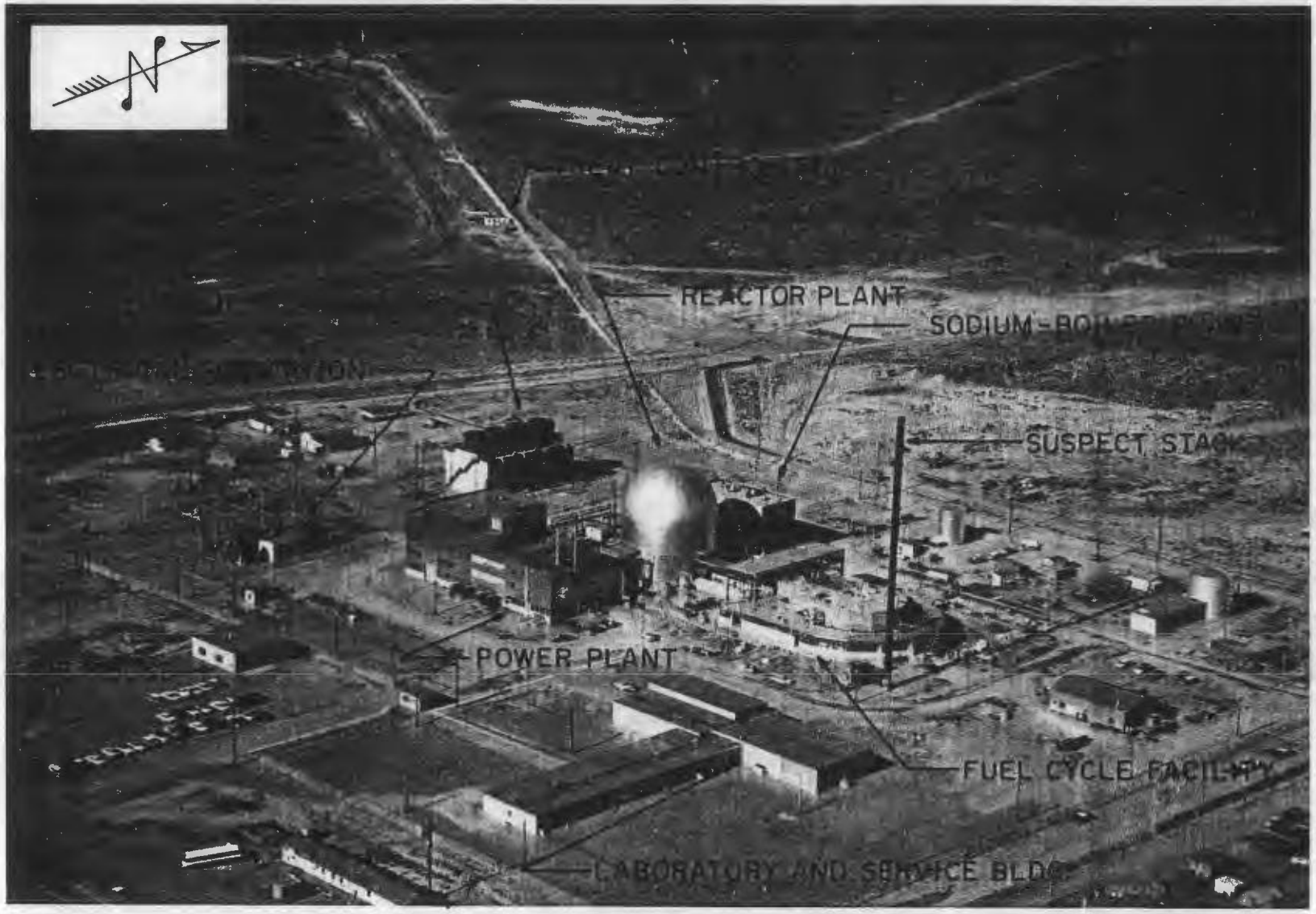

Fig. 1

EBR-II Facility

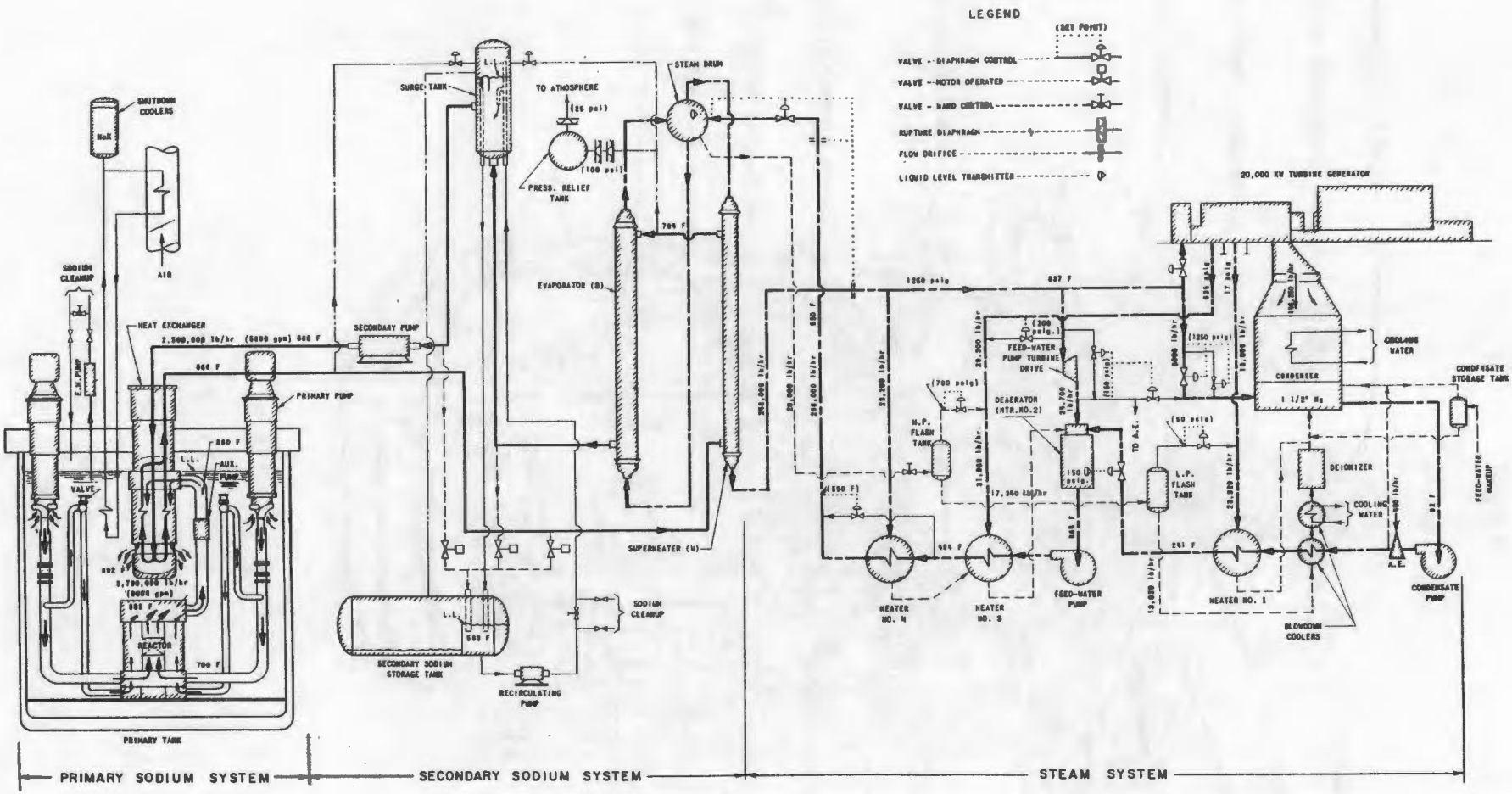

Fig. 3

Simplified Flow Diagram

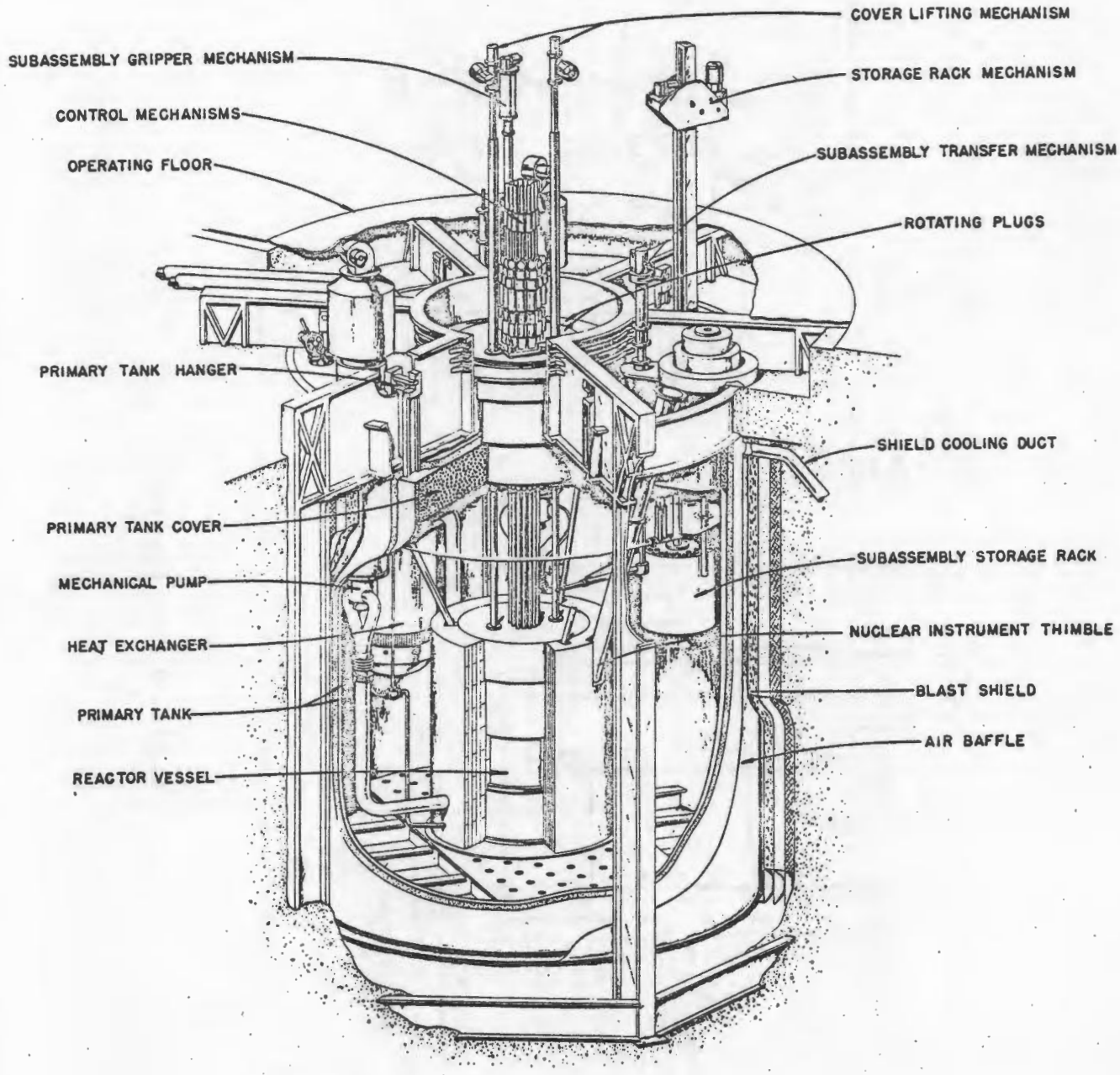

Fig. 4

Primary System

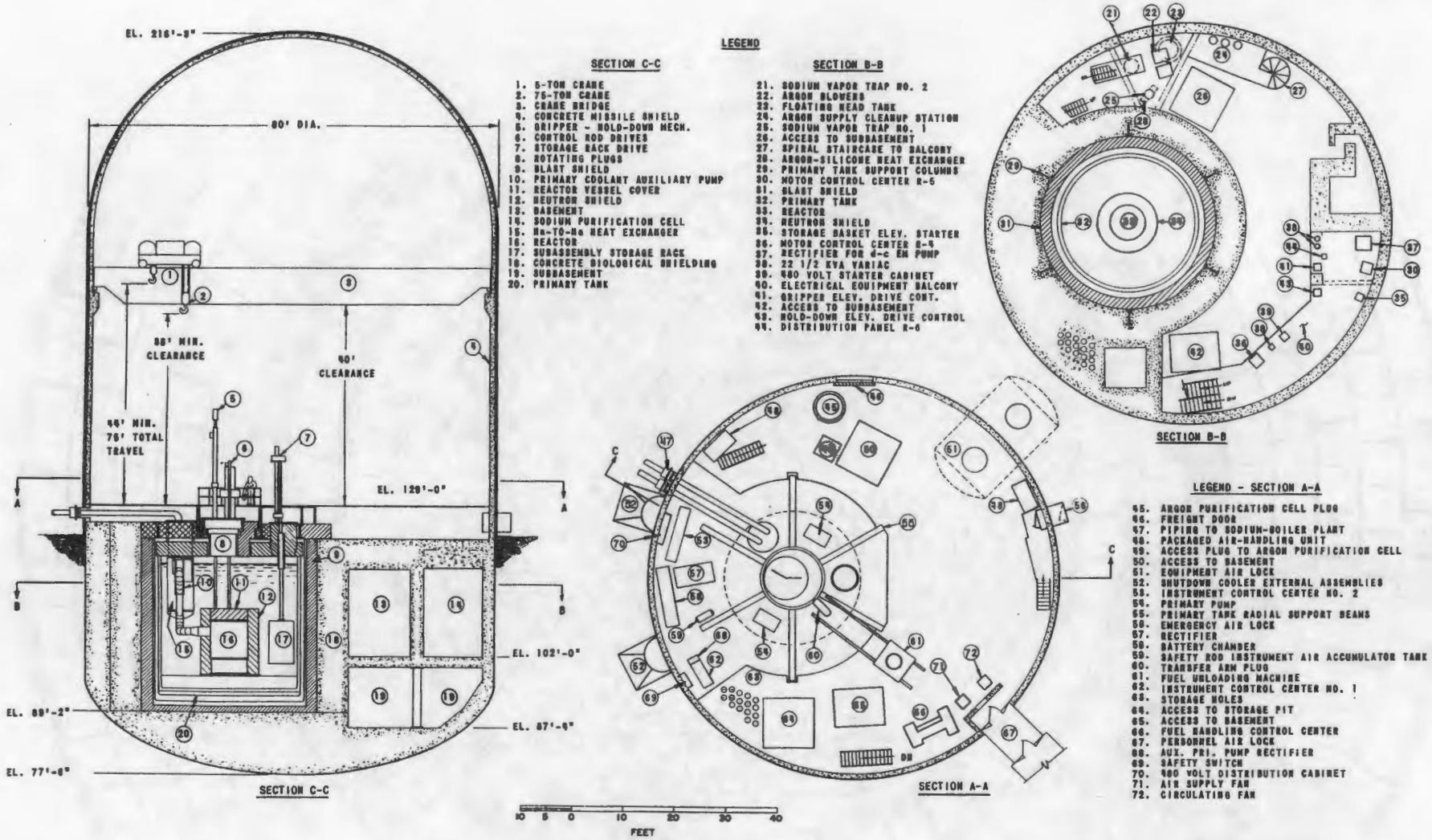

LEGEND

SECTION C-C

1. 5-TON CRANE
2. 75-TON CRANE
3. CRANE BRIDGE
4. CONCRETE MISSILE SHIELD
5. GRIPPER - HOLD-DOWN MECH.
6. CONTROL ROD DRIVES
7. STORAGE RACK DRIVE
8. ROTATING PLUGS
9. BLAST SHIELD
10. PRIMARY COOLANT AUXILIARY PUMP
11. REACTOR VESSEL COVER
12. NEUTRON SHIELD
13. BASEMENT
14. SODIUM PURIFICATION CELL
15. Na-TO-Na HEAT EXCHANGER
16. REACTOR
17. SUBASSEMBLY STORAGE RACK
18. CONCRETE BIOLOGICAL SHIELDING
19. SUBBASEMENT
20. PRIMARY TANK

SECTION B-B

21. SODIUM VAPOR TRAP NO. 2
22. ARGON BLOWERS
23. FLOATING HEAD TANK
24. ARGON SUPPLY CLEANUP STATION
25. SODIUM VAPOR TRAP NO. 1
26. ACCESS TO SUBBASEMENT
27. SPIRAL STAIRCASE TO BALCONY
28. ARGON-SILICONE HEAT EXCHANGER
29. PRIMARY TANK SUPPORT COLUMNS
30. MOTOR CONTROL CENTER R-5
31. BLAST SHIELD
32. PRIMARY TANK
33. REACTOR
34. NEUTRON SHIELD
35. STORAGE BASKET ELEV. STARTER
36. MOTOR CONTROL CENTER R-4
37. RECTIFIER FOR d-c EM PUMP
38. 22 1/2 KVA VARIAC
39. 480 VOLT STARTER CABINET
40. ELECTRICAL EQUIPMENT BALCONY
41. GRIPPER ELEV. DRIVE CONT.
42. ACCESS TO SUBBASEMENT
43. HOLD-DOWN ELEV. DRIVE CONTROL
44. DISTRIBUTION PANEL R-6

LEGEND - SECTION A-A

45. ARGON PURIFICATION CELL PLUG
46. FREIGHT DOOR
47. PIPING TO SODIUM-BOILER PLANT
48. PACKAGED AIR-HANDLING UNIT
49. ACCESS PLUG TO ARGON PURIFICATION CELL
50. ACCESS TO BASEMENT
51. EQUIPMENT AIR LOCK
52. SHUTDOWN COOLER EXTERNAL ASSEMBLIES
53. INSTRUMENT CONTROL CENTER NO. 2
54. PRIMARY PUMP
55. PRIMARY TANK RADIAL SUPPORT BEAMS
56. EMERGENCY AIR LOCK
57. RECTIFIER
58. BATTERY CHAMBER
59. SAFETY ROD INSTRUMENT AIR ACCUMULATOR TANK
60. TRANSFER ARM PLUG
61. FUEL UNLOADING MACHINE
62. INSTRUMENT CONTROL CENTER NO. 1
63. STORAGE HOLES
64. ACCESS TO STORAGE PIT
65. ACCESS TO BASEMENT
66. FUEL HANDLING CONTROL CENTER
67. PERSONNEL AIR LOCK
68. AUX. PRI. PUMP RECTIFIER
69. SAFETY SWITCH
70. 480 VOLT DISTRIBUTION CABINET
71. AIR SUPPLY FAN
72. CIRCULATING FAN

Fig. 5

Reactor Plant - Operating Floor and Balcony Equipment Layout

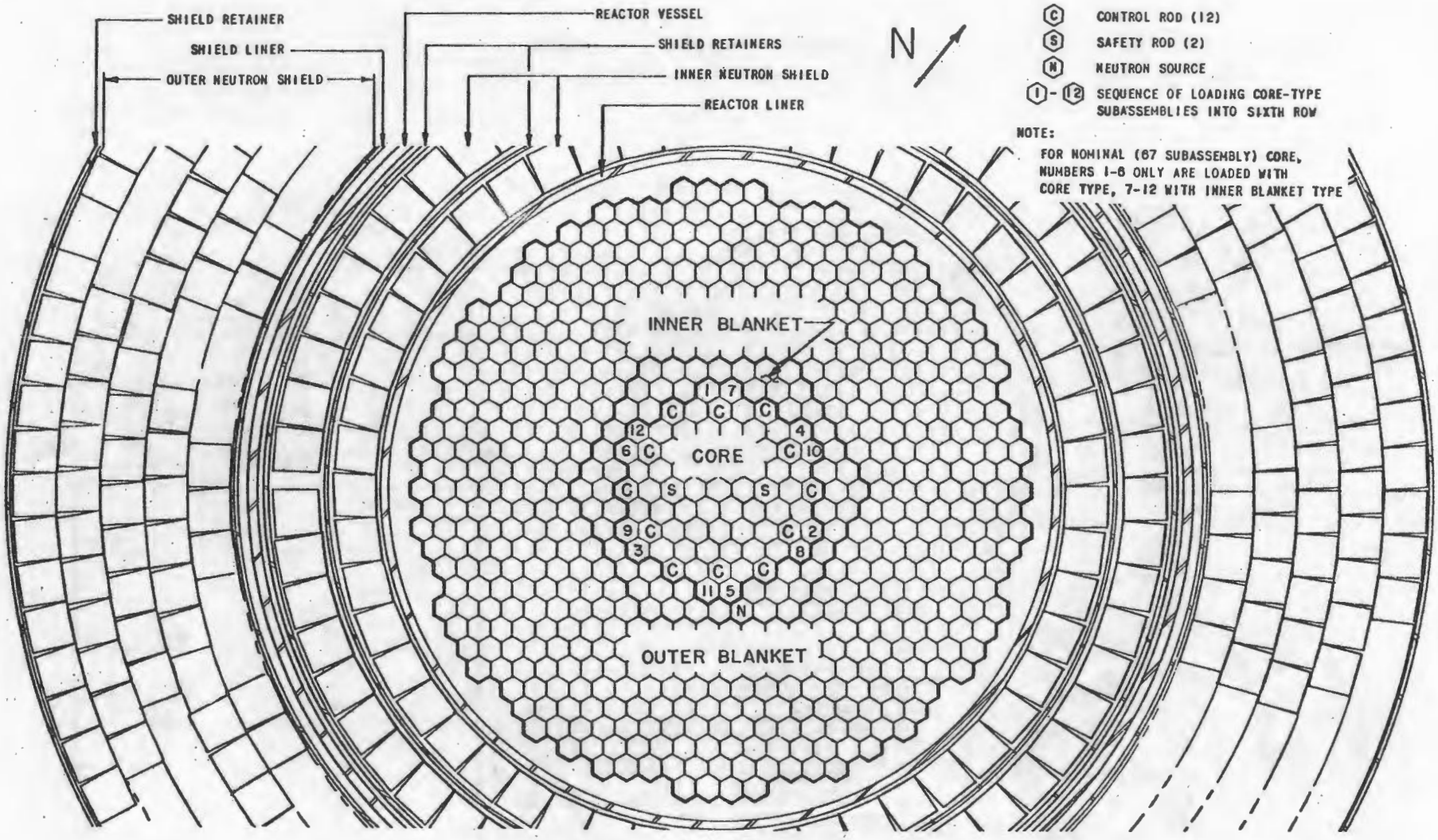

Fig. 6

Reactor Arrangement

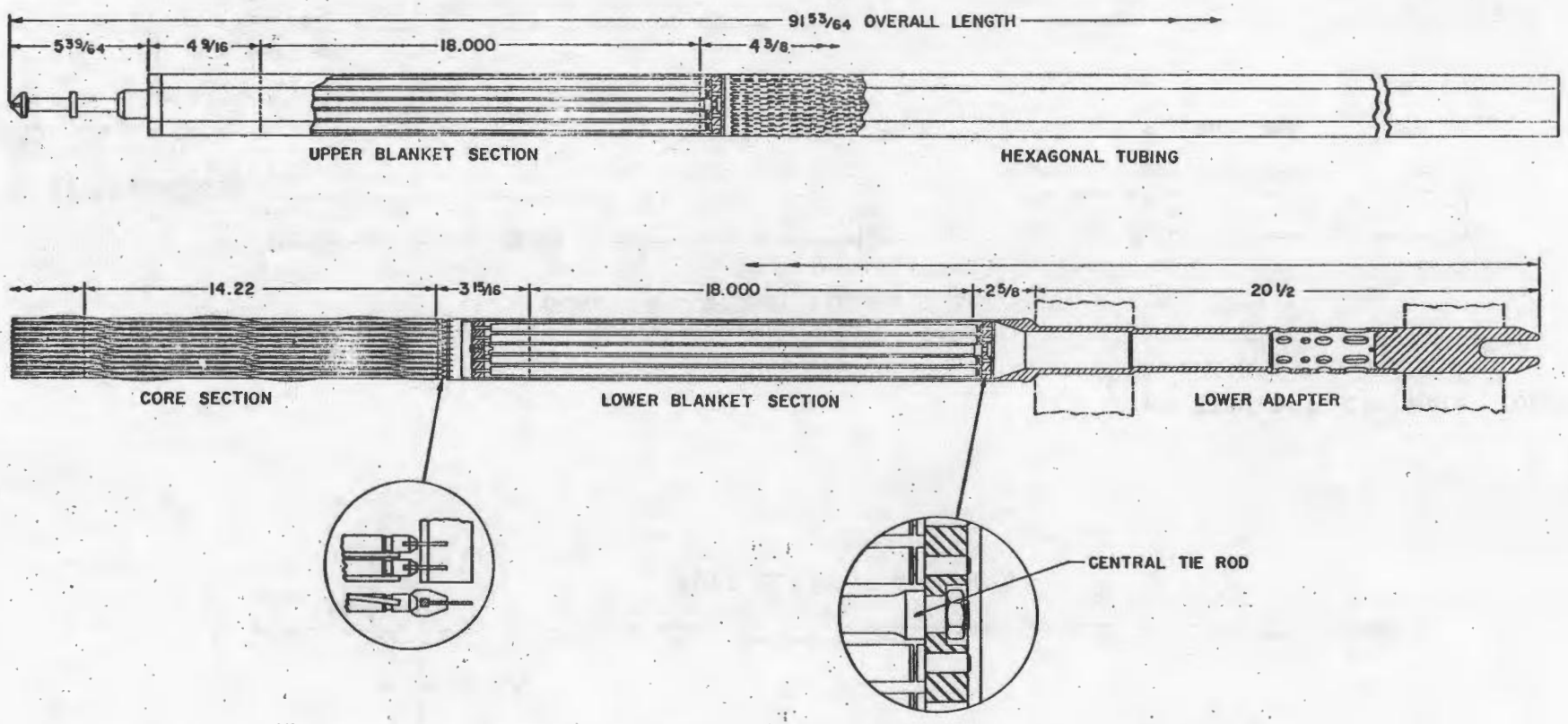

Fig. 7

Core Subassembly

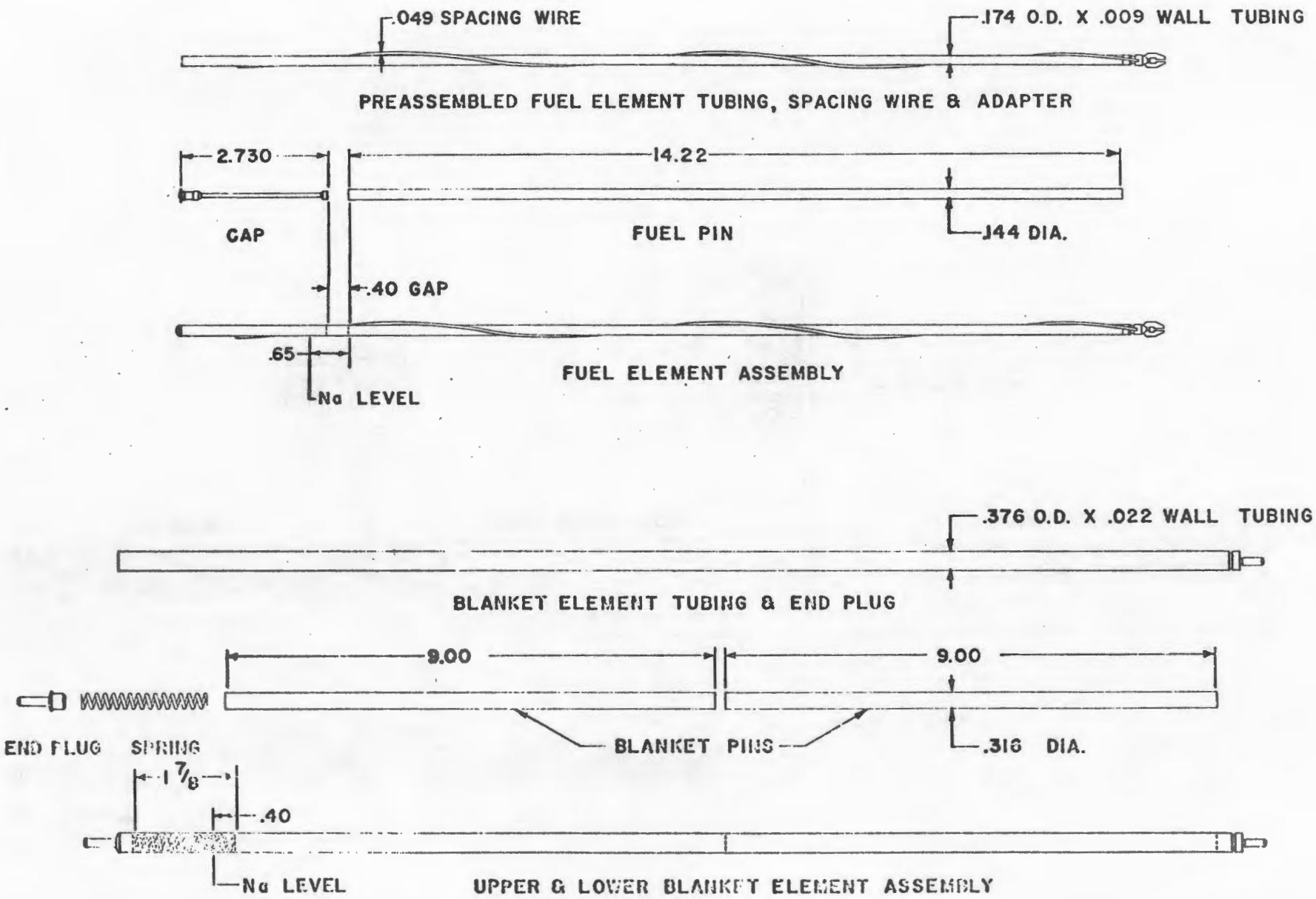

Fig. 8

Core Subassembly Elements

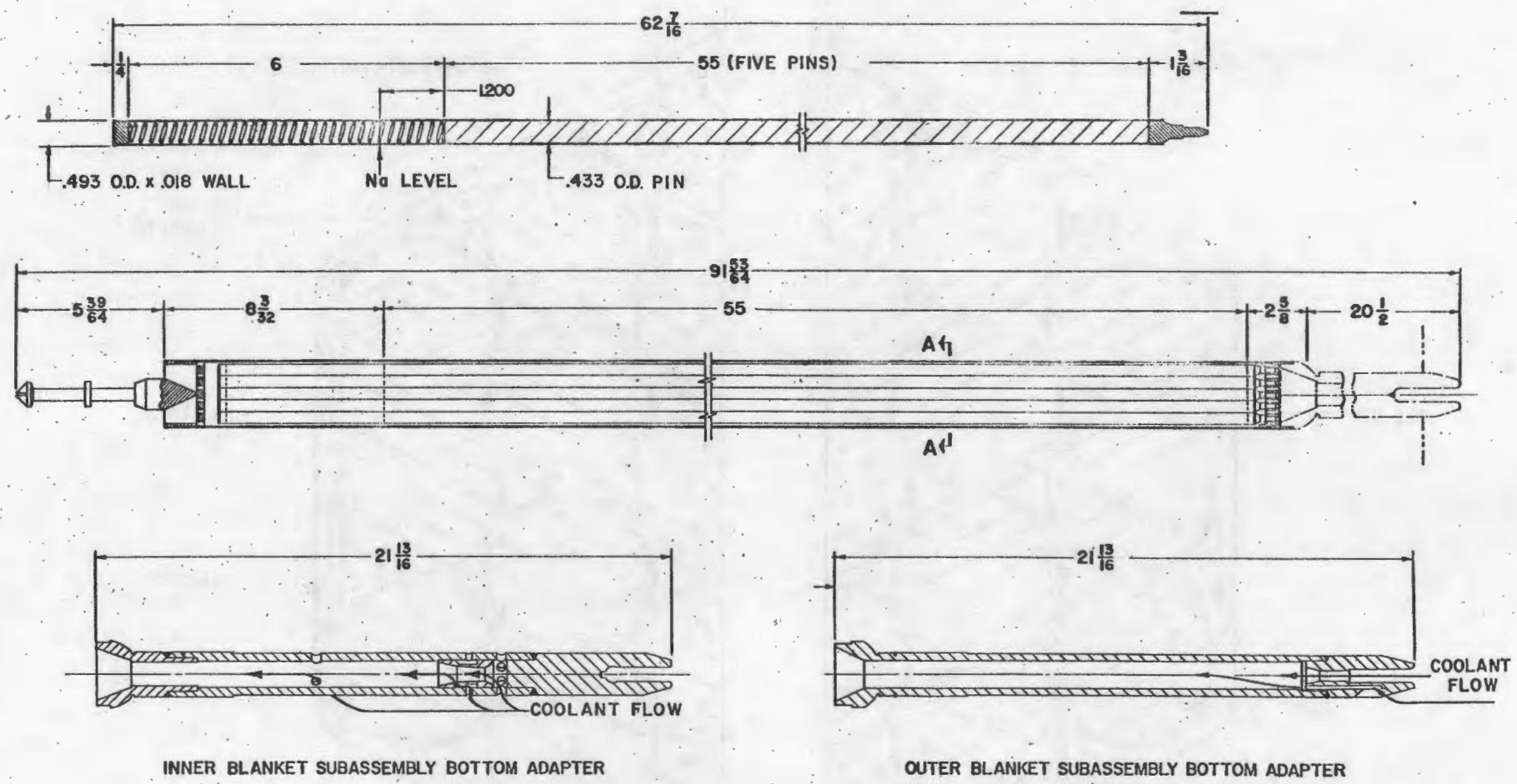

Fig. 9

Inner Blanket and Outer Blanket Subassemblies

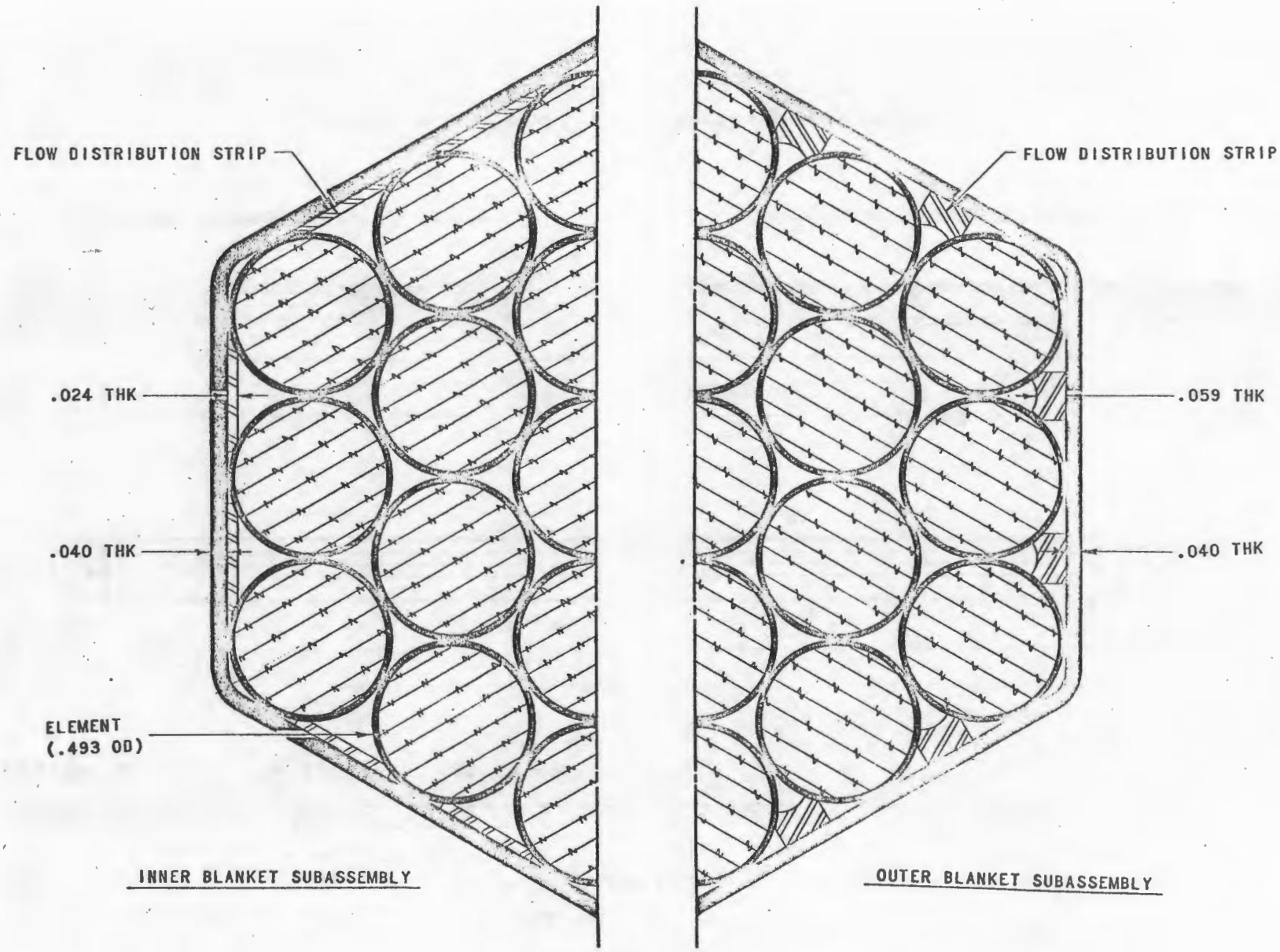

Fig. 10

Inner Blanket and Outer Blanket Subassembly Cross Sections

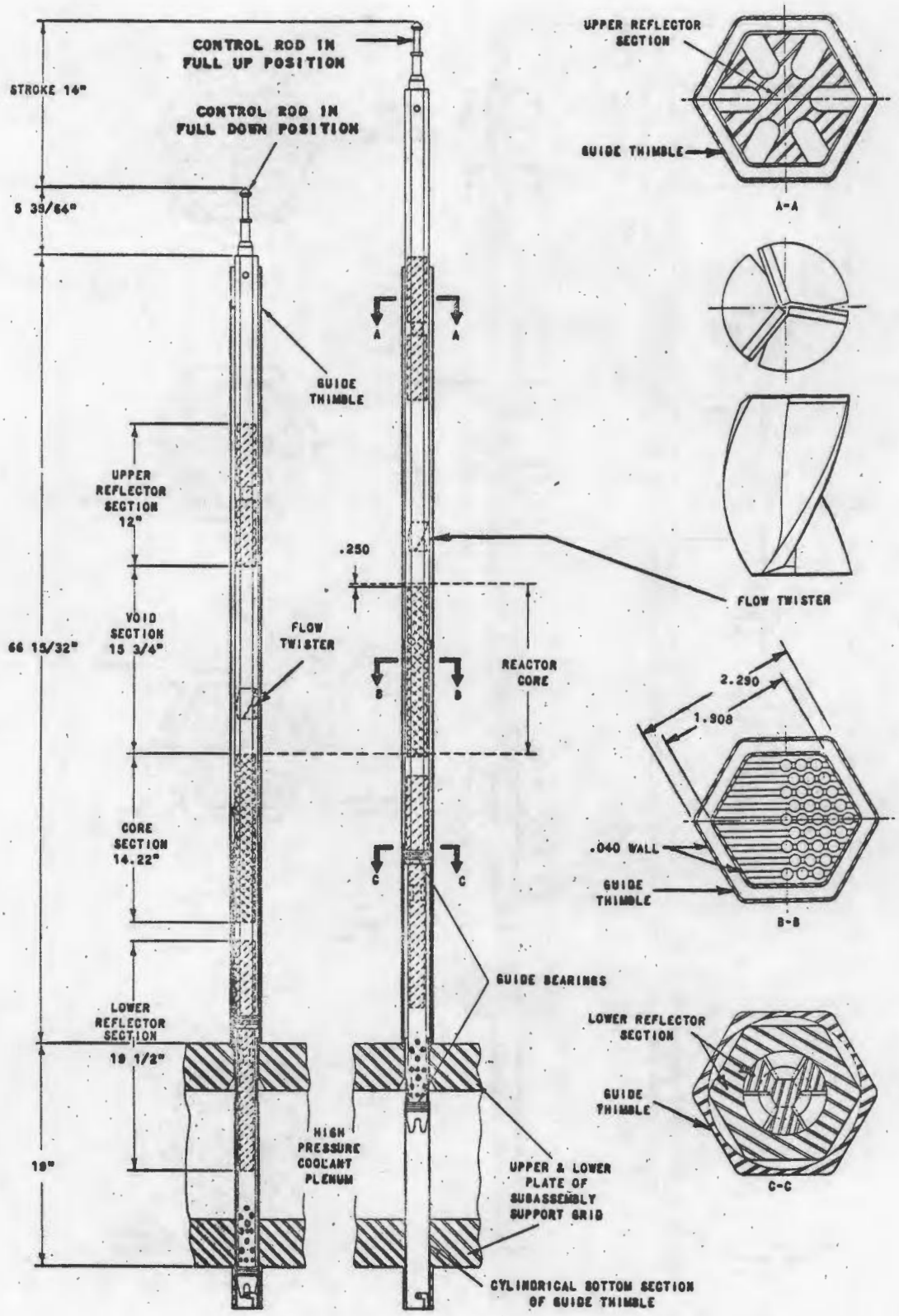

Fig. 11

Control Subassembly

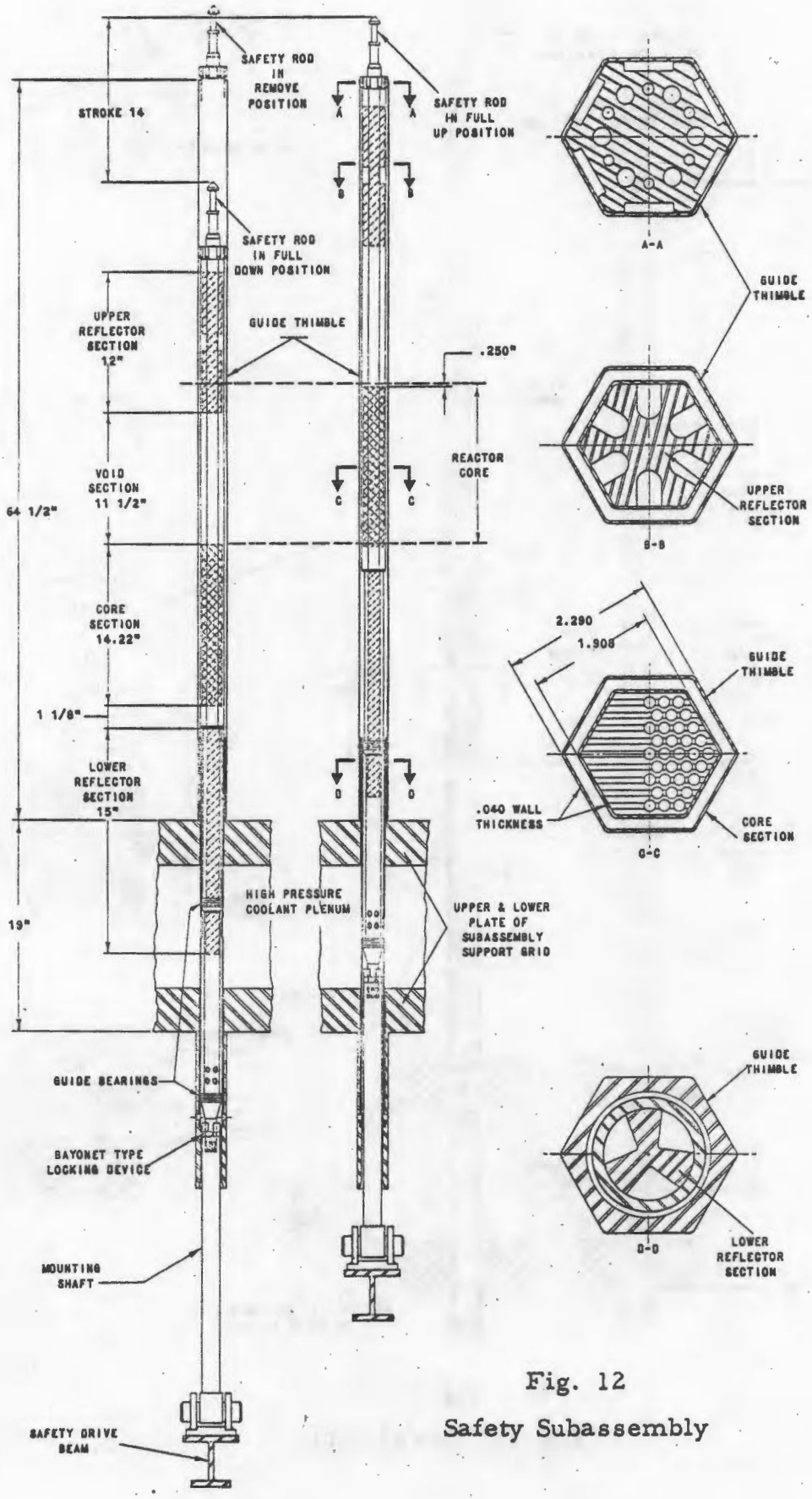

Fig. 12

Safety Subassembly

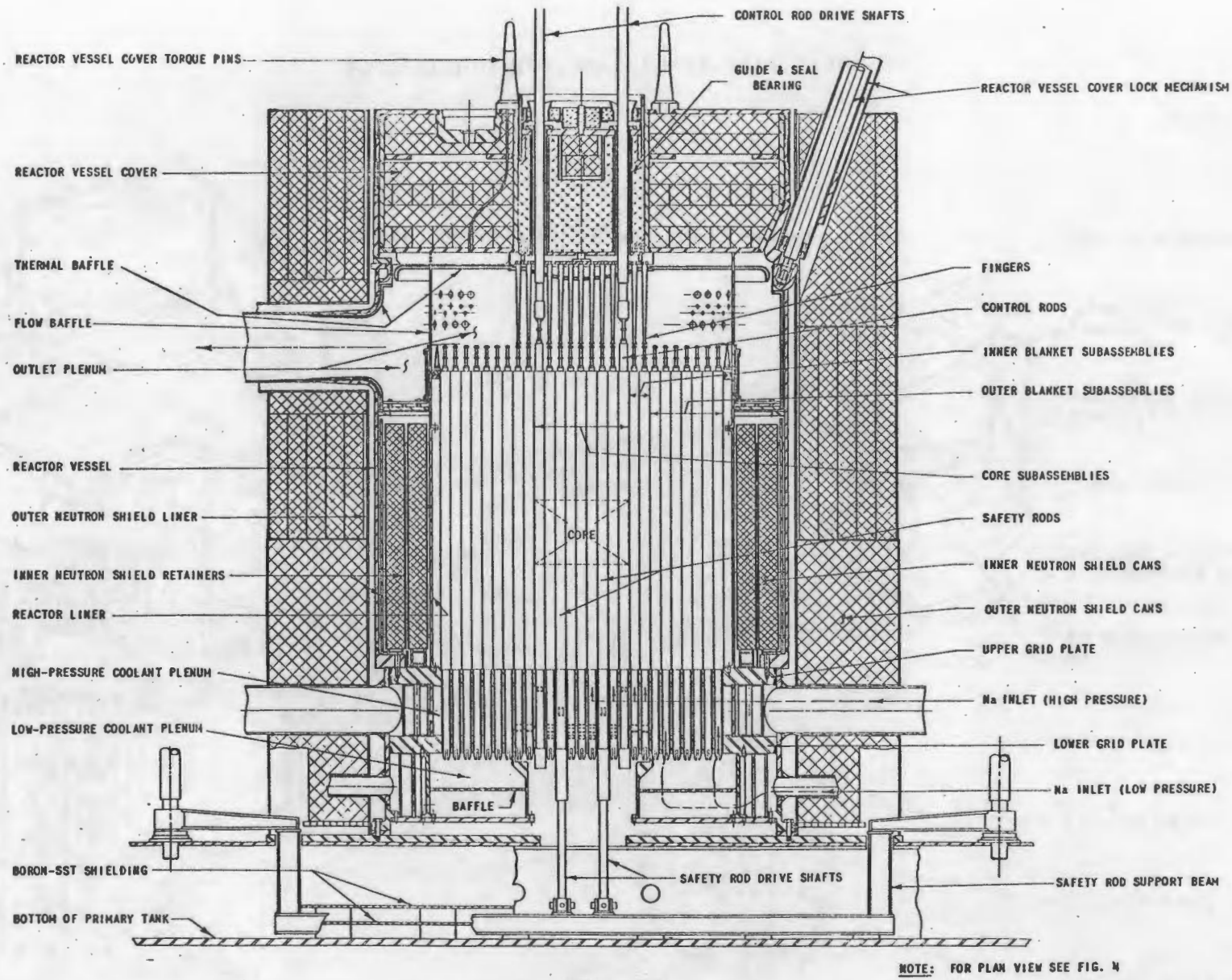

NOTE: FOR PLAN VIEW SEE FIG. 4

Fig. 13

Reactor Vessel Assembly

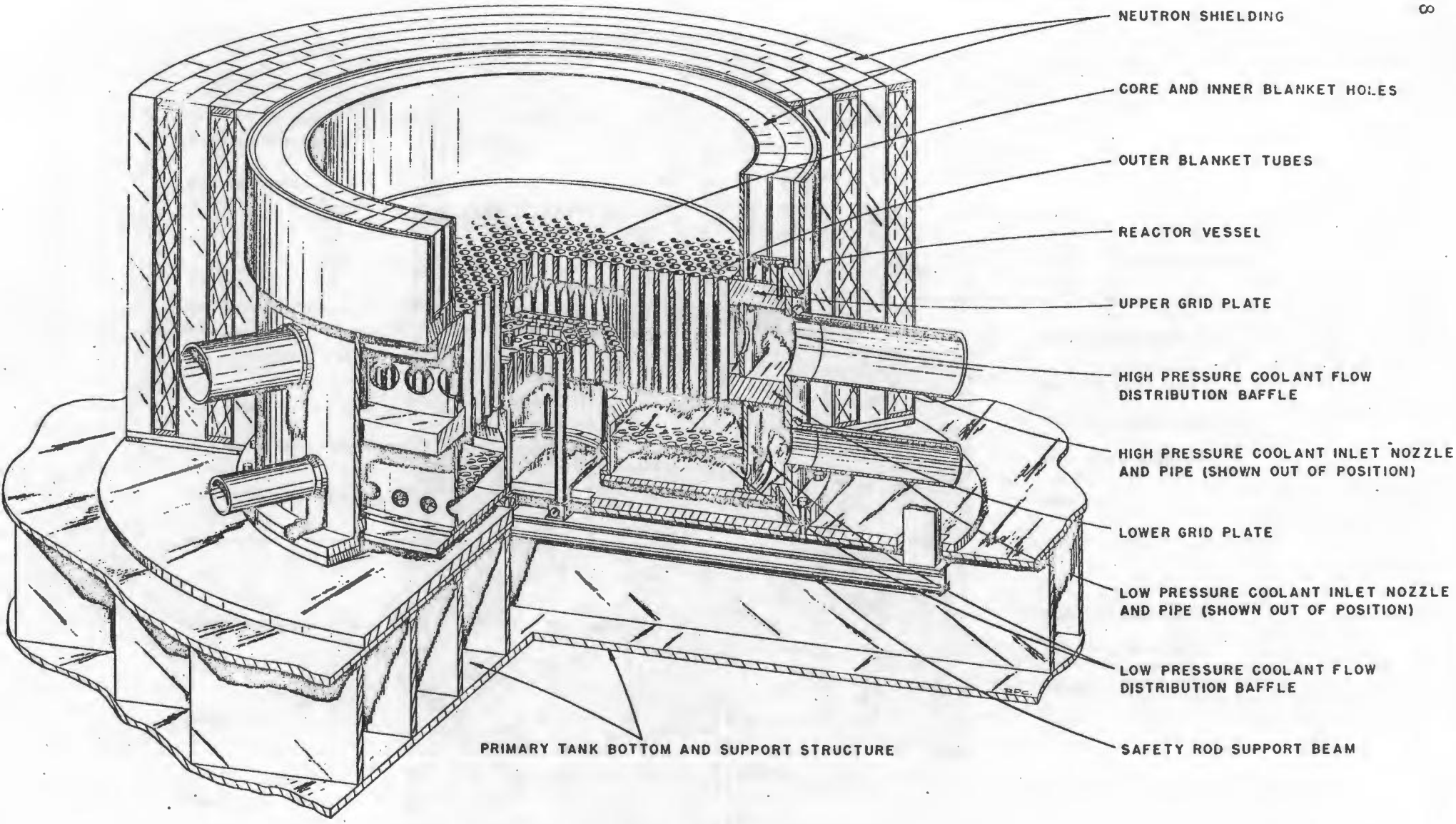

Fig. 14

Pictorial of Reactor Vessel Grid Assembly

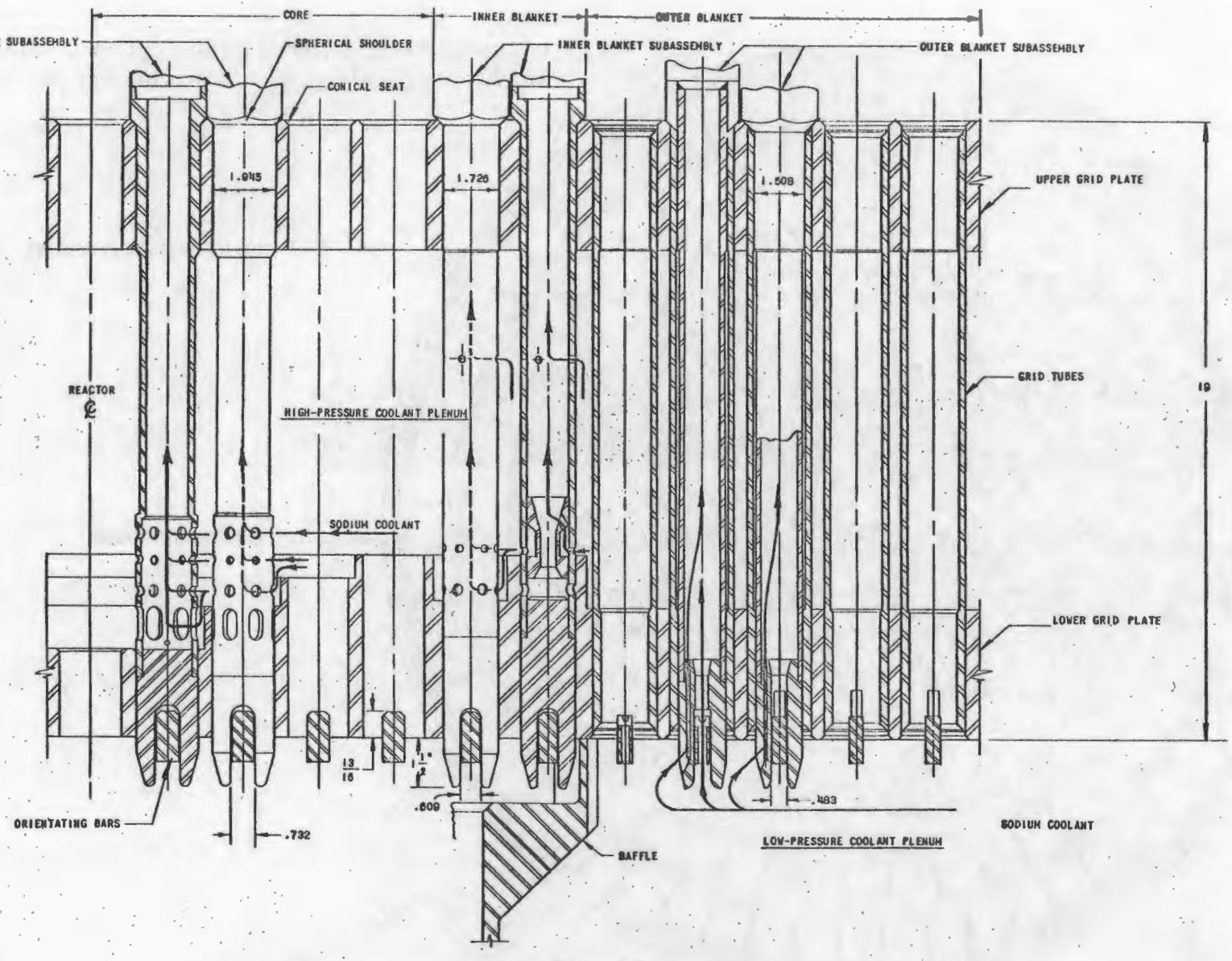

Fig. 15

Section of Reactor Grid Plenum

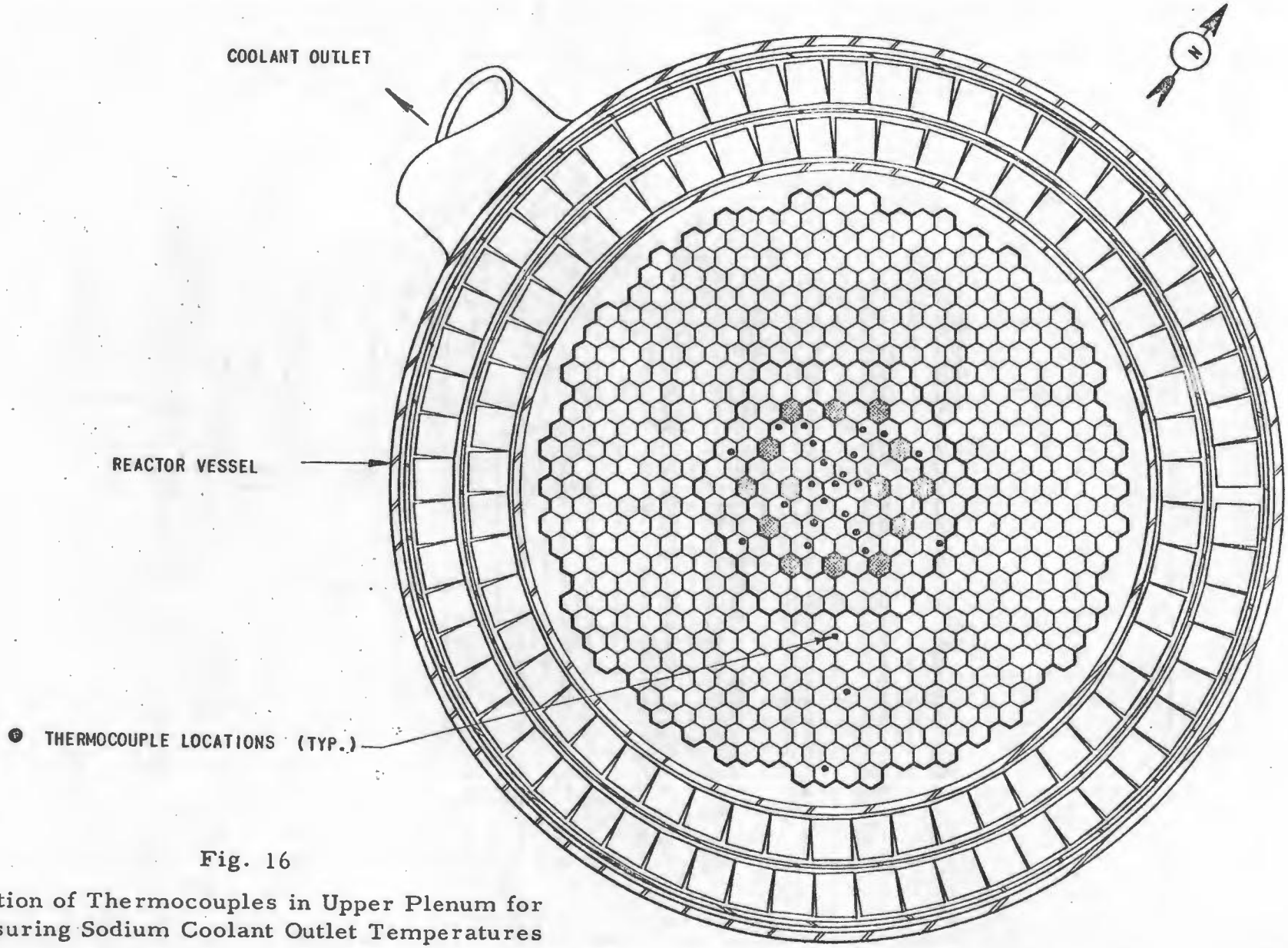

Fig. 16

Location of Thermocouples in Upper Plenum for Measuring Sodium Coolant Outlet Temperatures

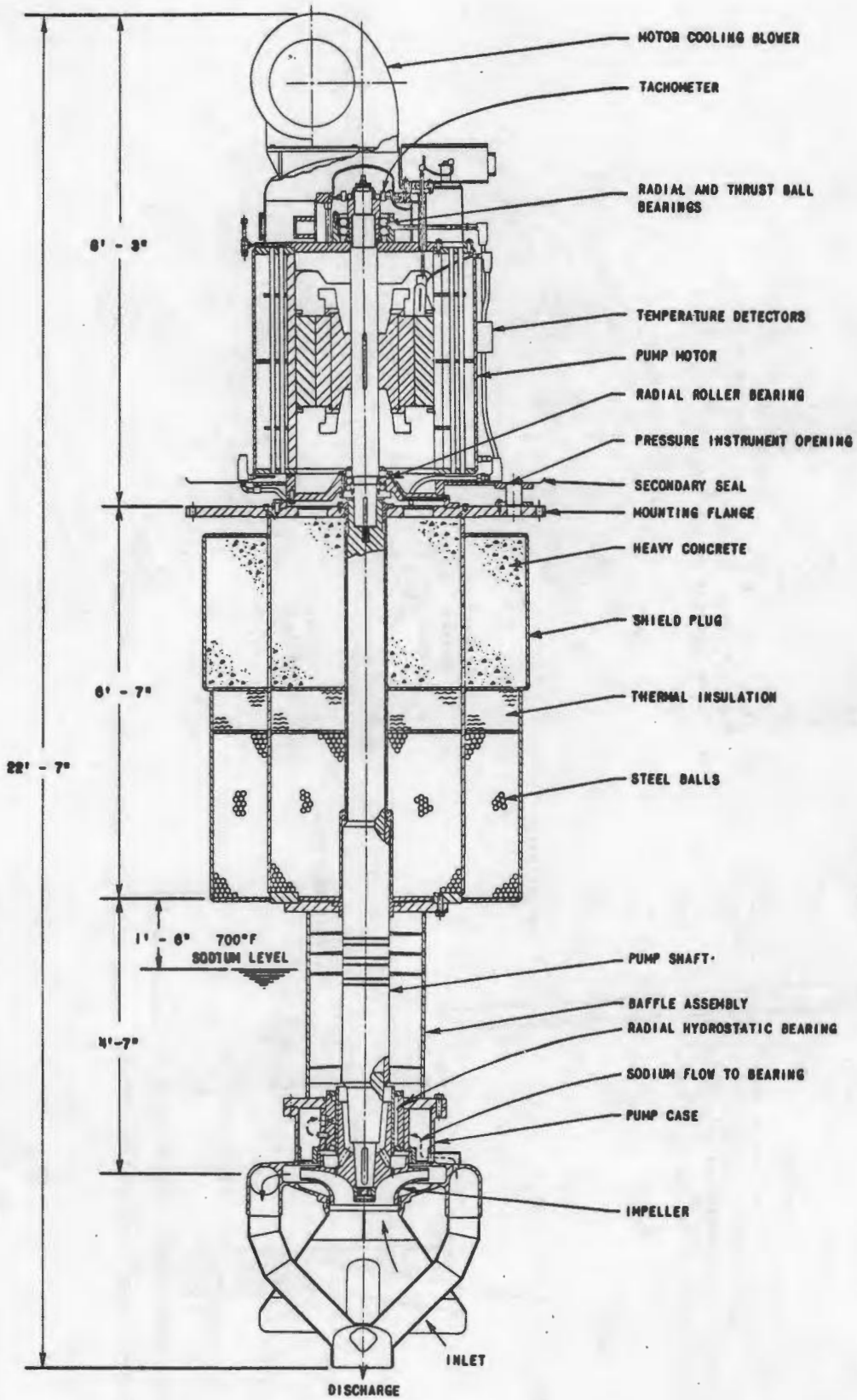

Fig. 17

Primary System Mechanical Sodium Pump

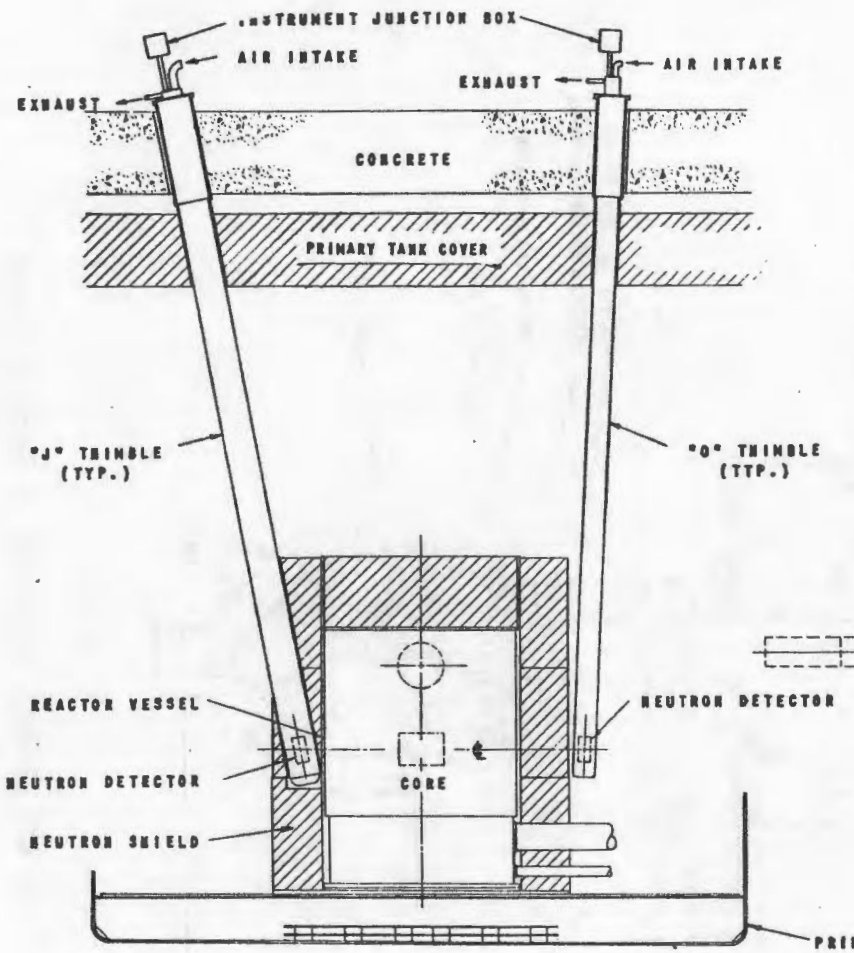

THIMBLE NO.	NUCLEAR INSTR. CHANNEL NO.	NEUTRON DETECTOR
O1	11	C.I.C.
O2	8	C.I.C.
O3	10	C.I.C.
O4	9	C.I.C.
J1	1 & 2	F.C. & F.C.
J2	3 & 4	F.C. & C.I.C.
J3	7	C.I.C.
J4	5 & 6	C.I.C. & C.I.C.

F.C. = FISSION COUNTER
C.I.C. = COMPENSATED ION CHAMBER

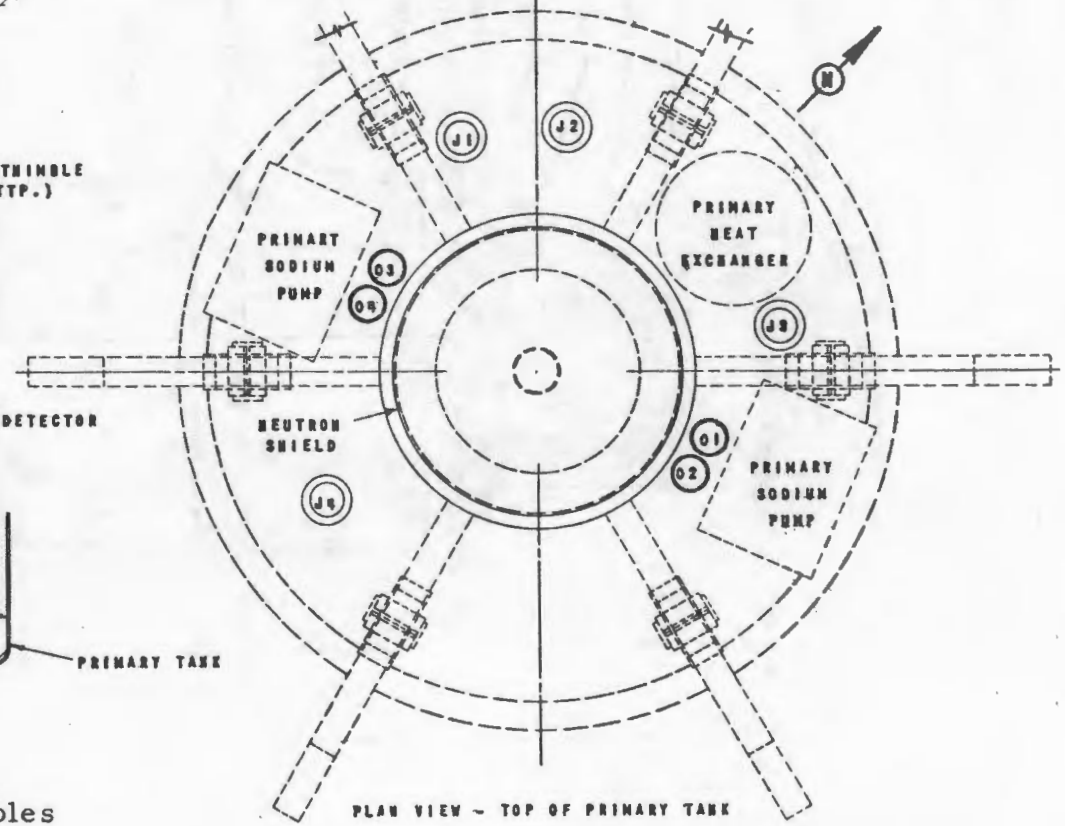

Fig. 18

Location of Nuclear Instrument Thimbles

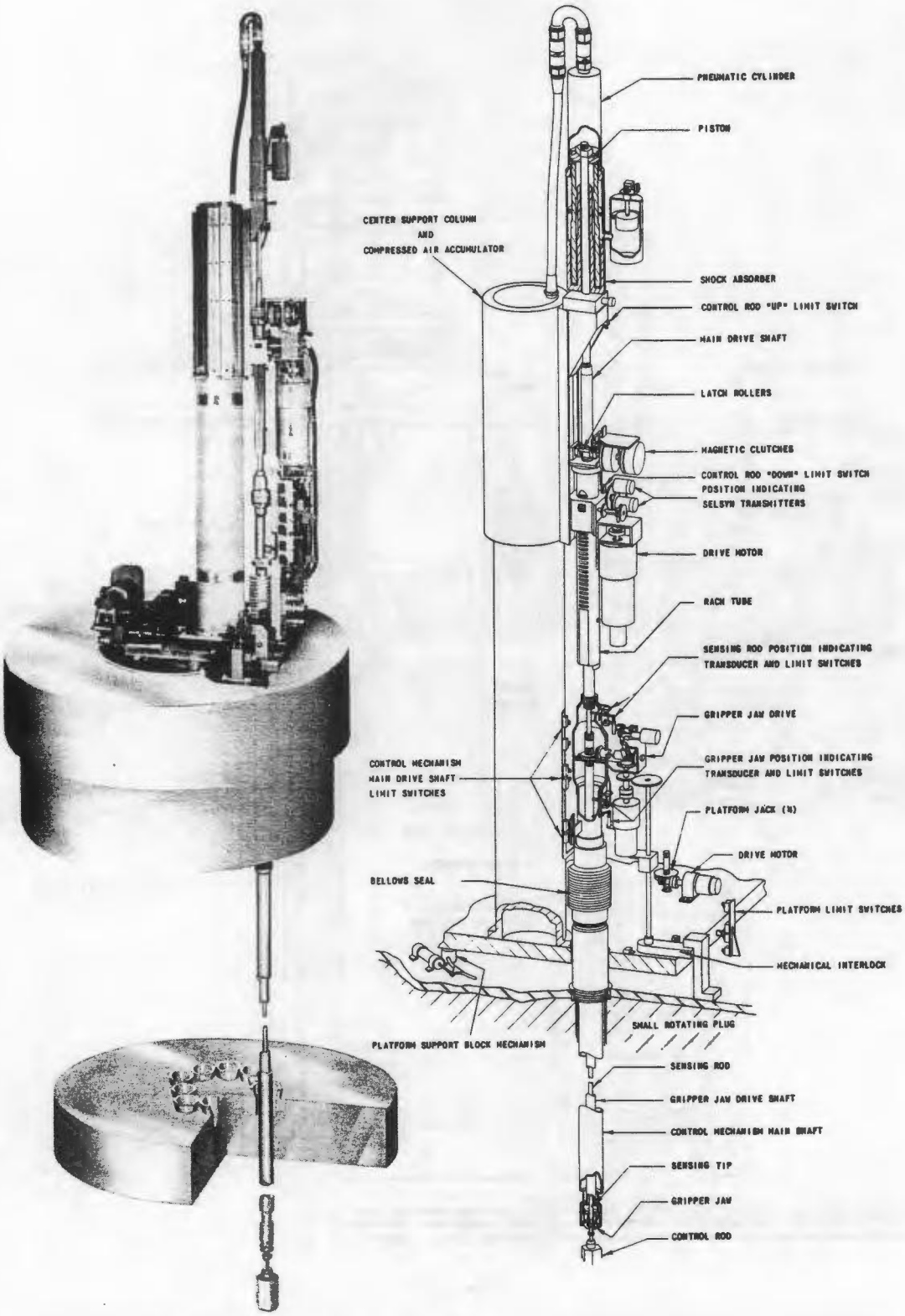

Fig. 19

Control Rod Drive Mechanism

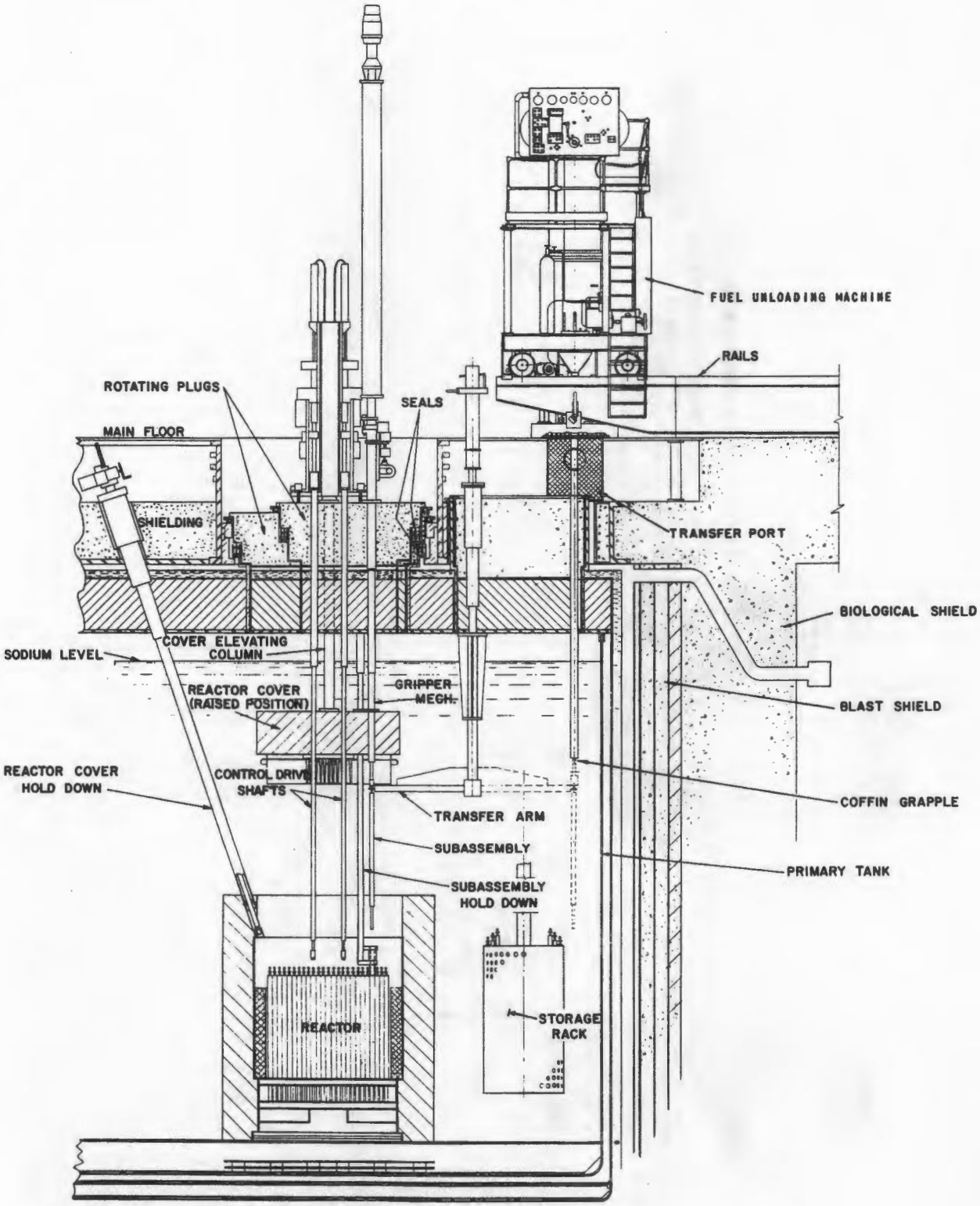

Fig. 20

Principal Components of Fuel Handling and Unloading Systems

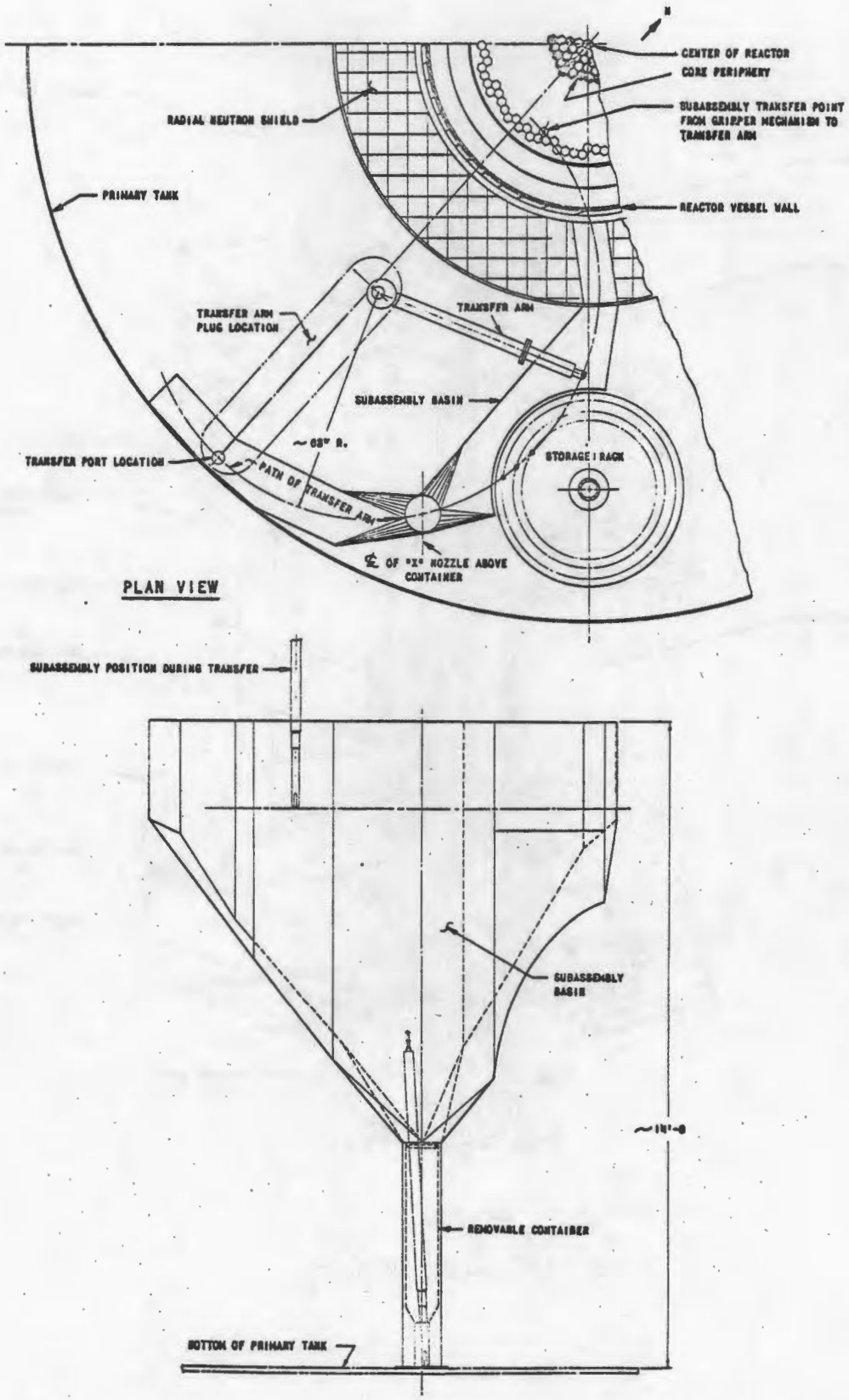

Fig. 21

Subassembly Basin

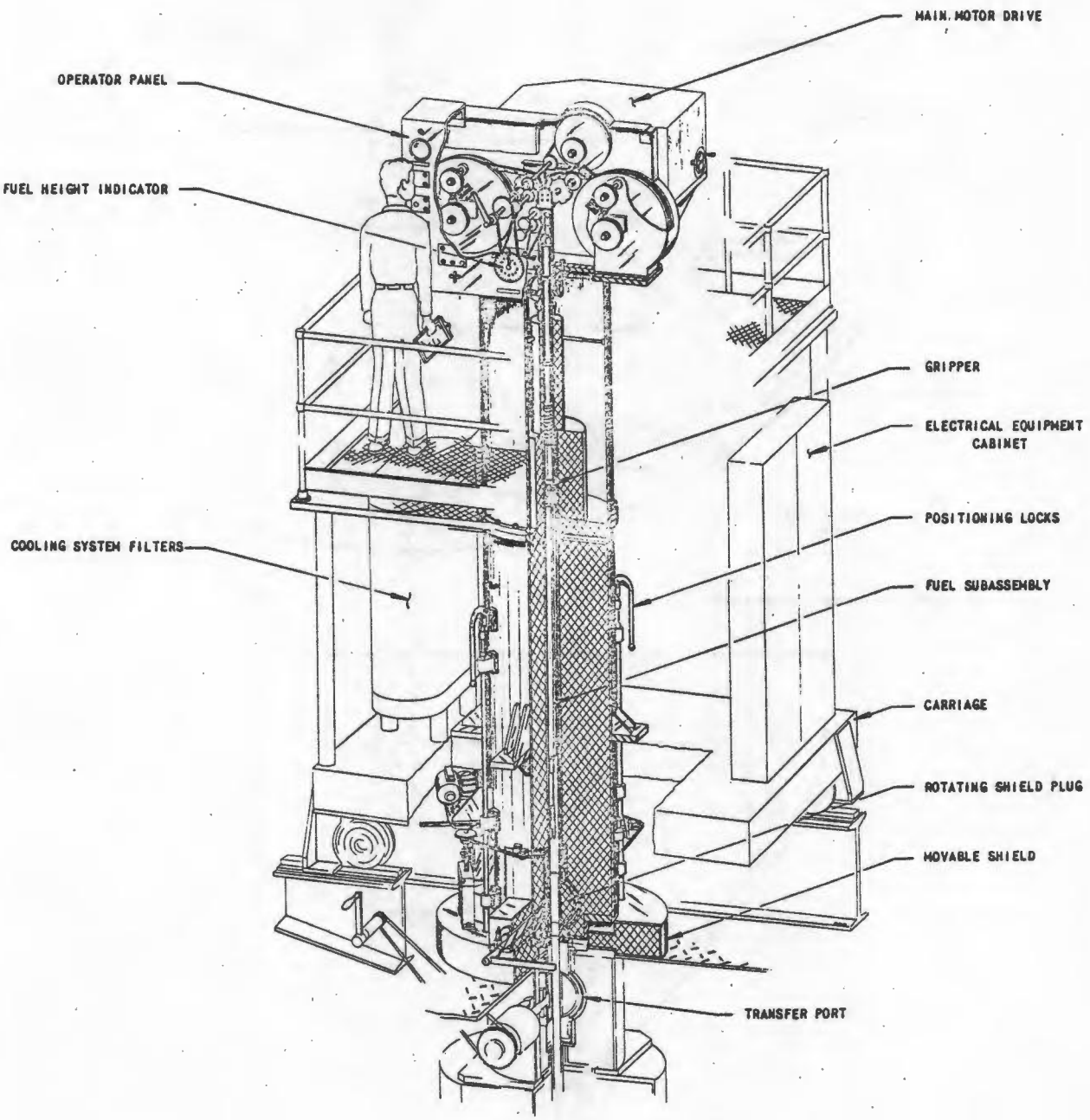

Fig. 22

Fuel-Unloading Machine

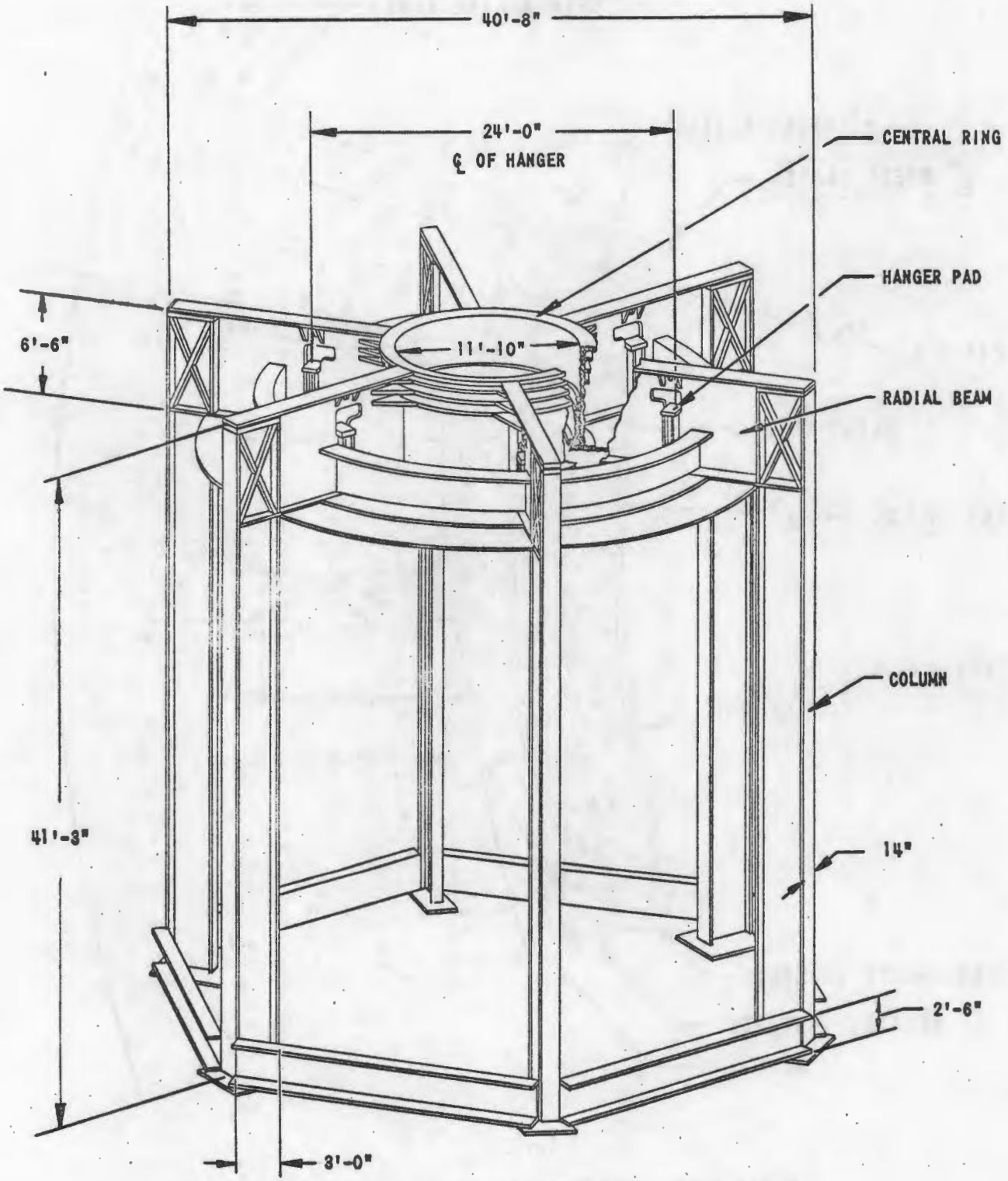

Fig. 23

Primary Tank Support Structure

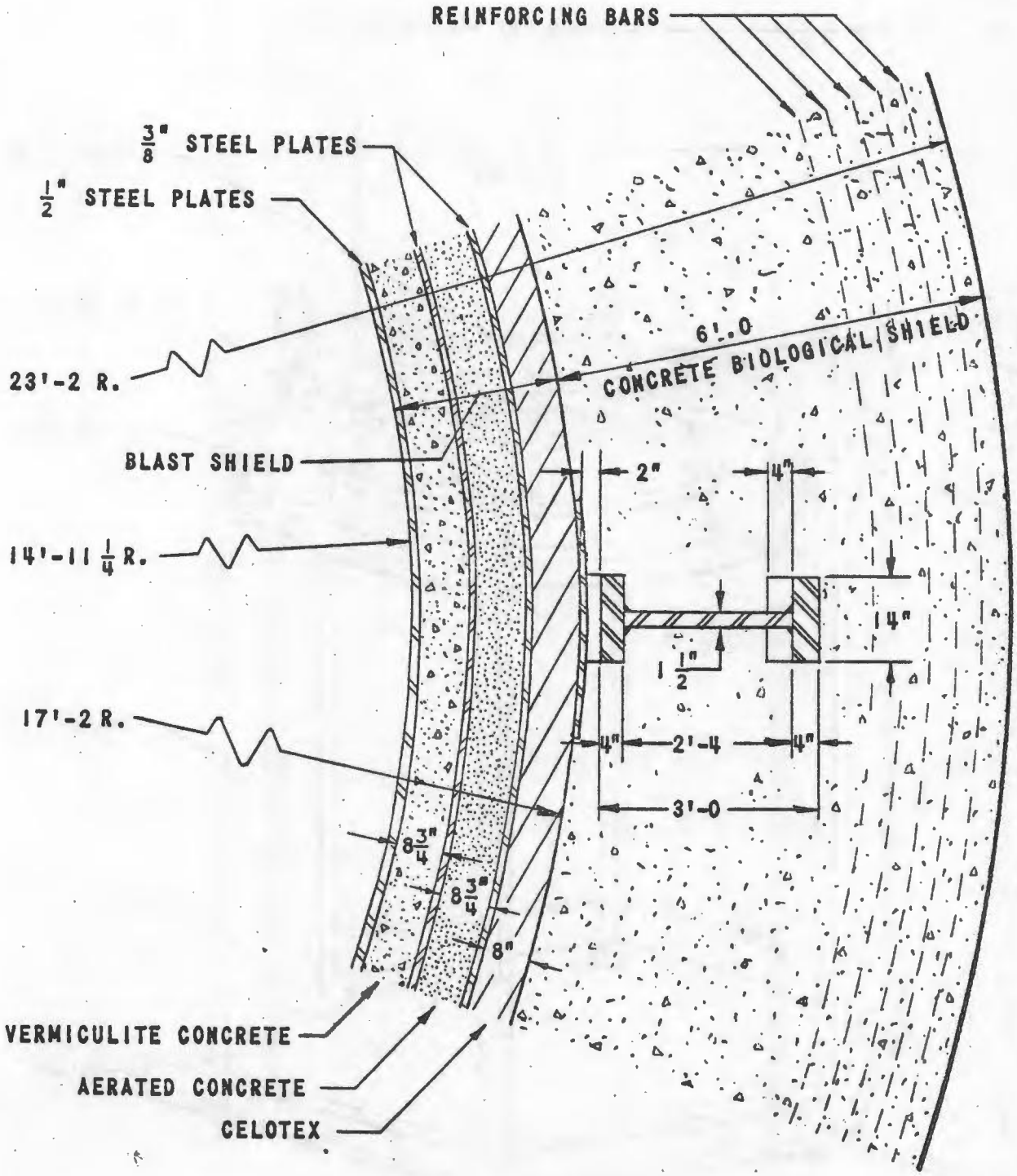

Fig. 24

Blast Shield and Typical Column Detail for Primary Tank Support Structure

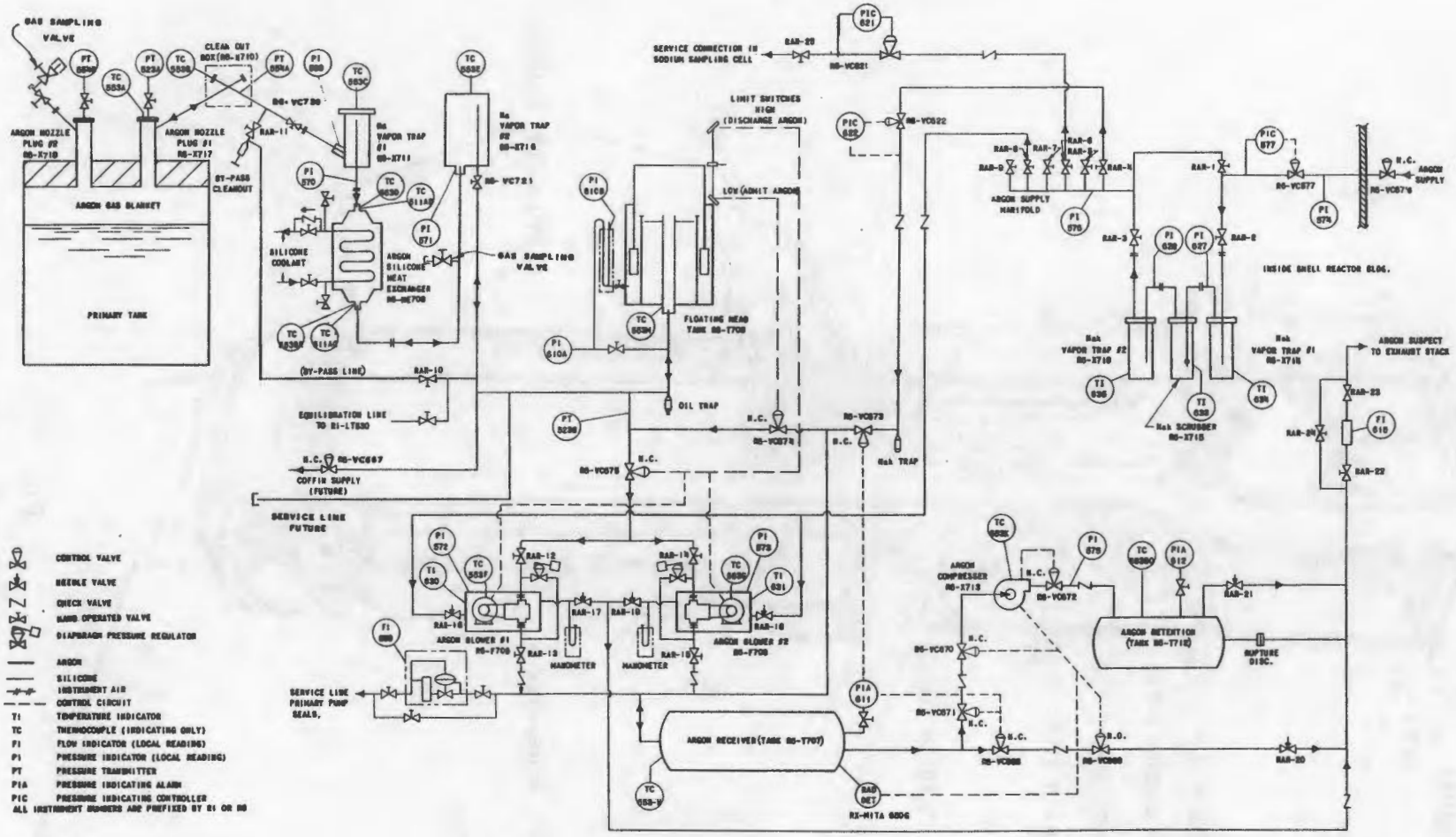

Fig. 25

Argon Blanket Gas System

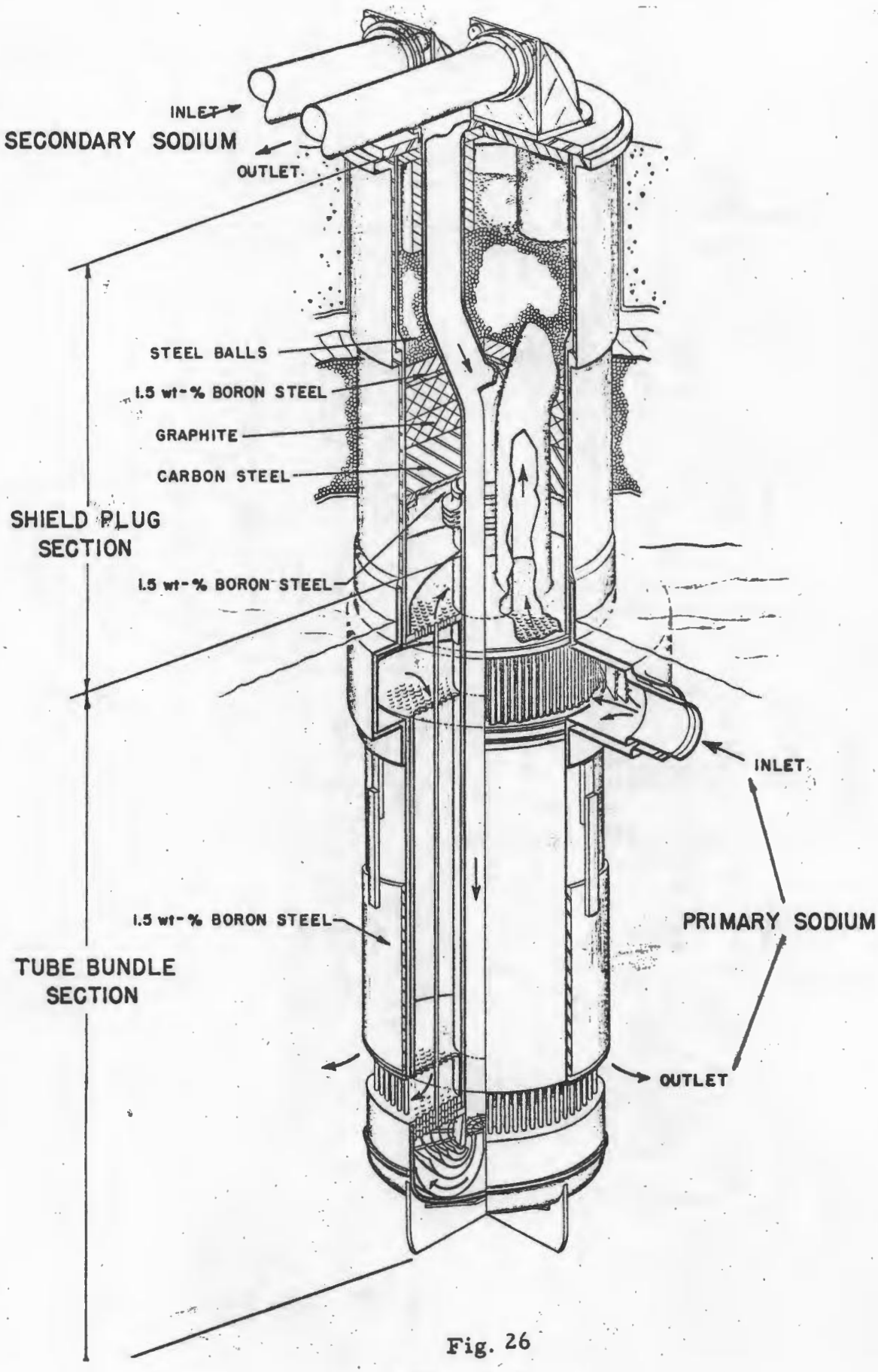

Fig. 26

Heat Exchanger

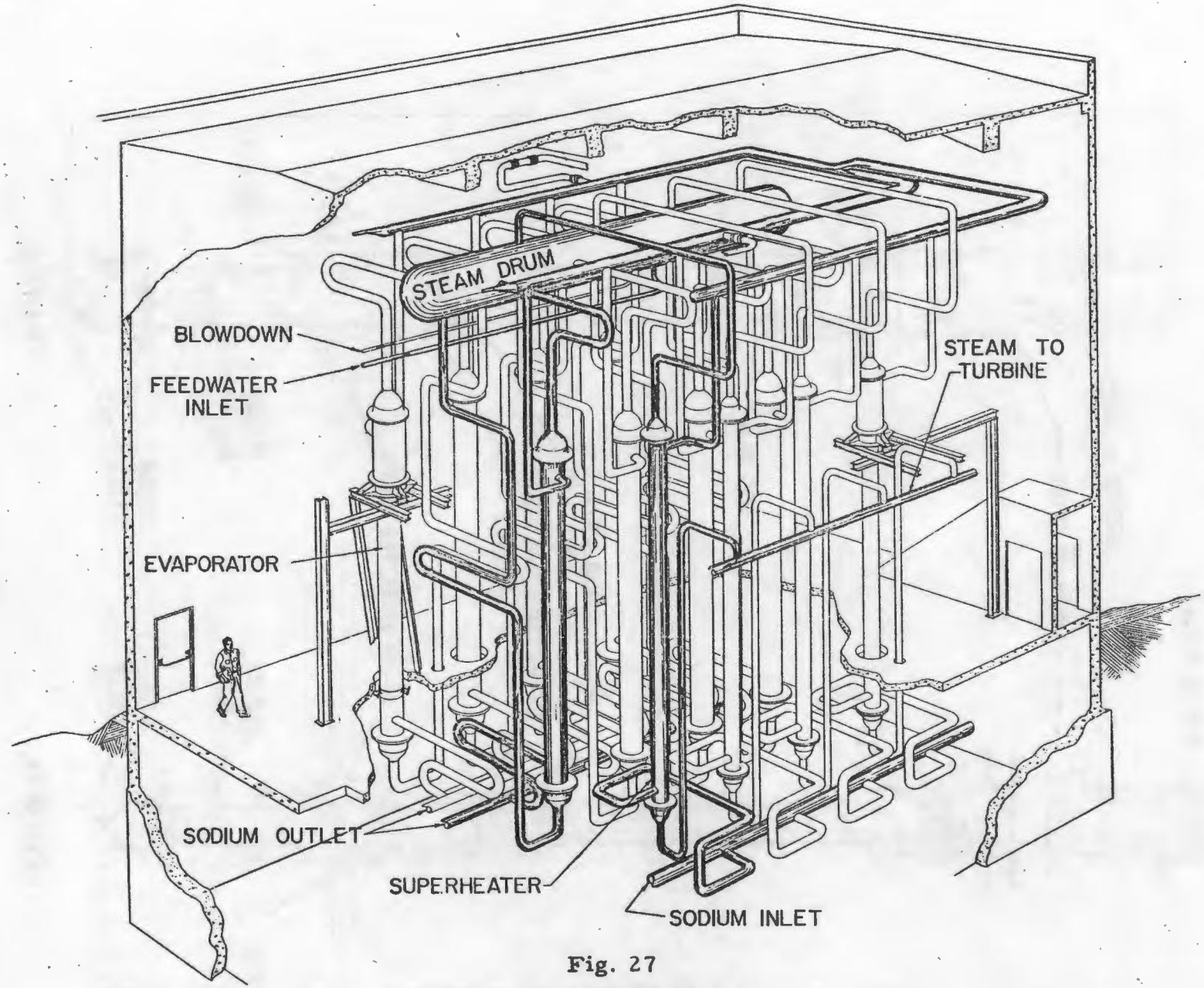

Fig. 27

Steam Generator

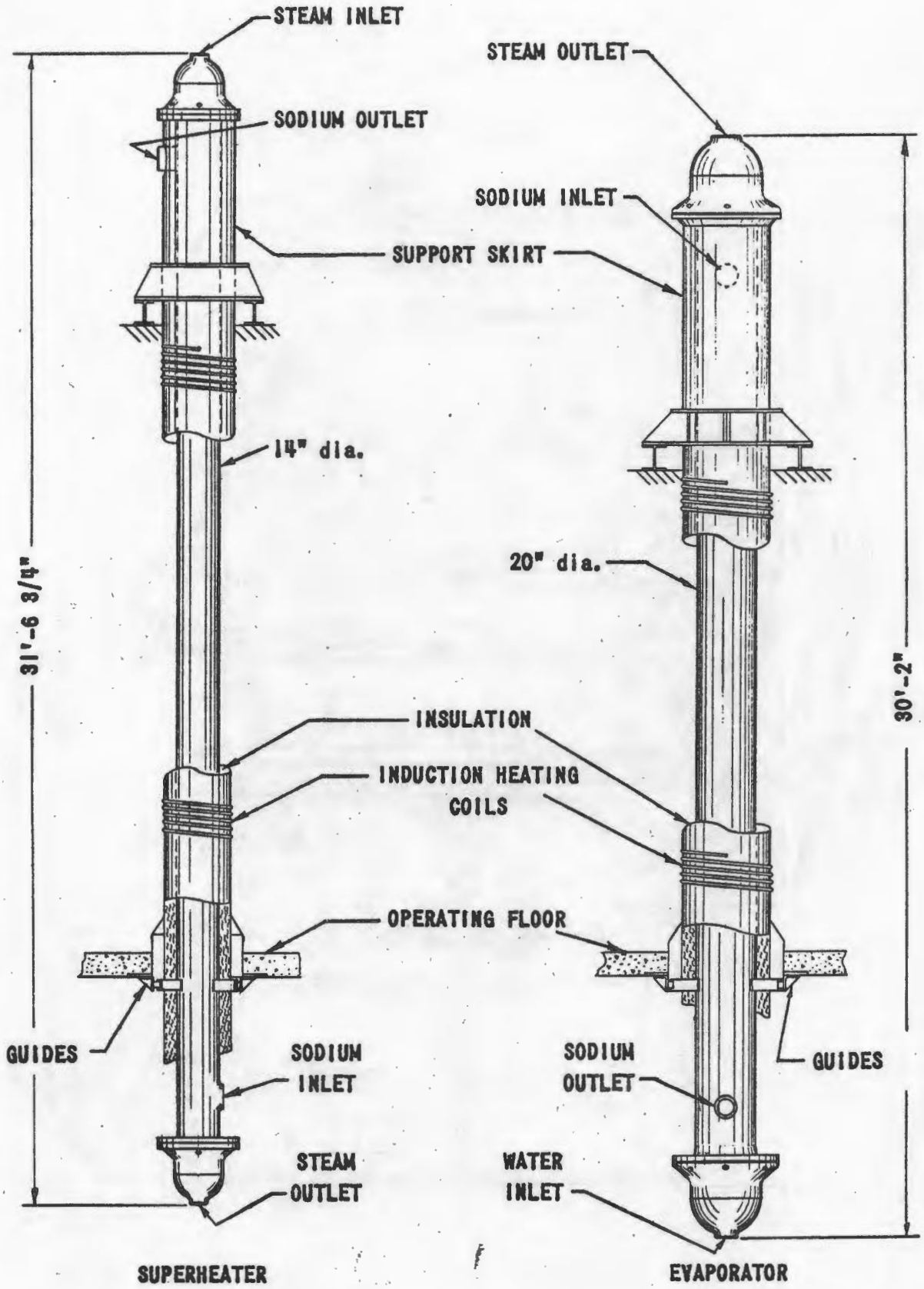

Fig. 28

Superheater and Evaporator Assemblies

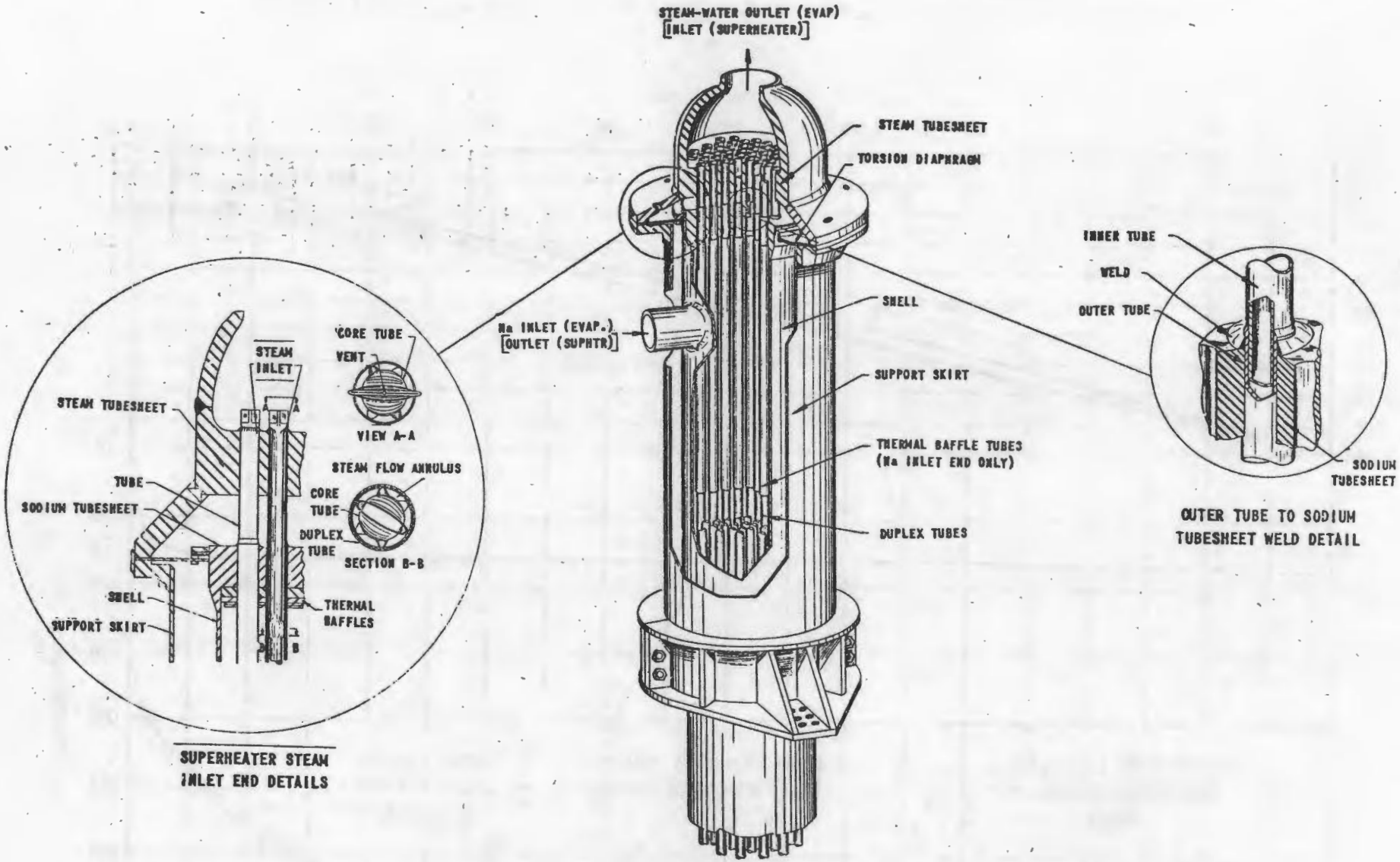

Fig. 29

Superheater and Evaporator Details

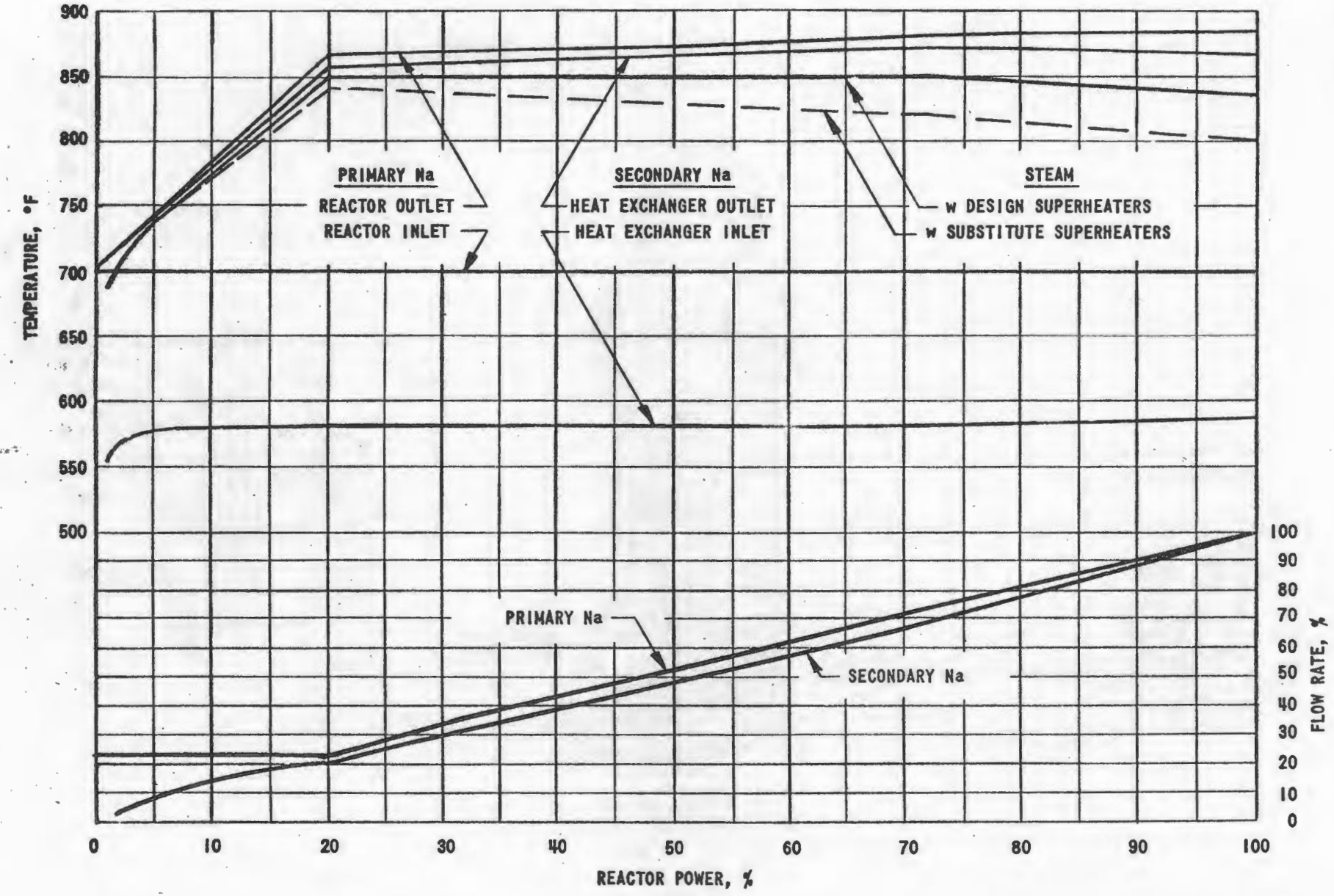

Fig. 30

Major System Temperatures and Flow Rates as Functions of Reactor Power

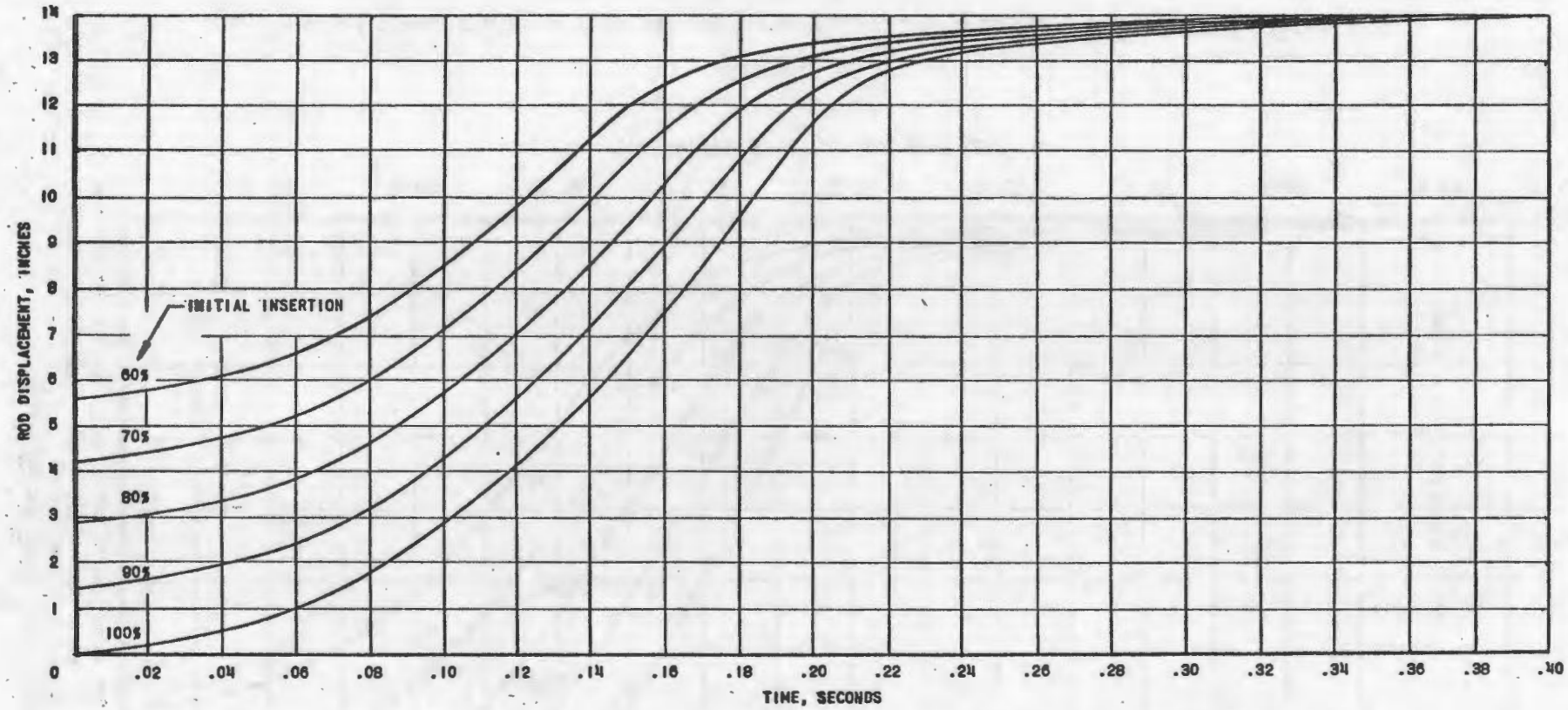

Fig. 31

Control Rod Displacement vs Time after Start of Rod Movement
(Maximum Acceleration of 1.5 g)

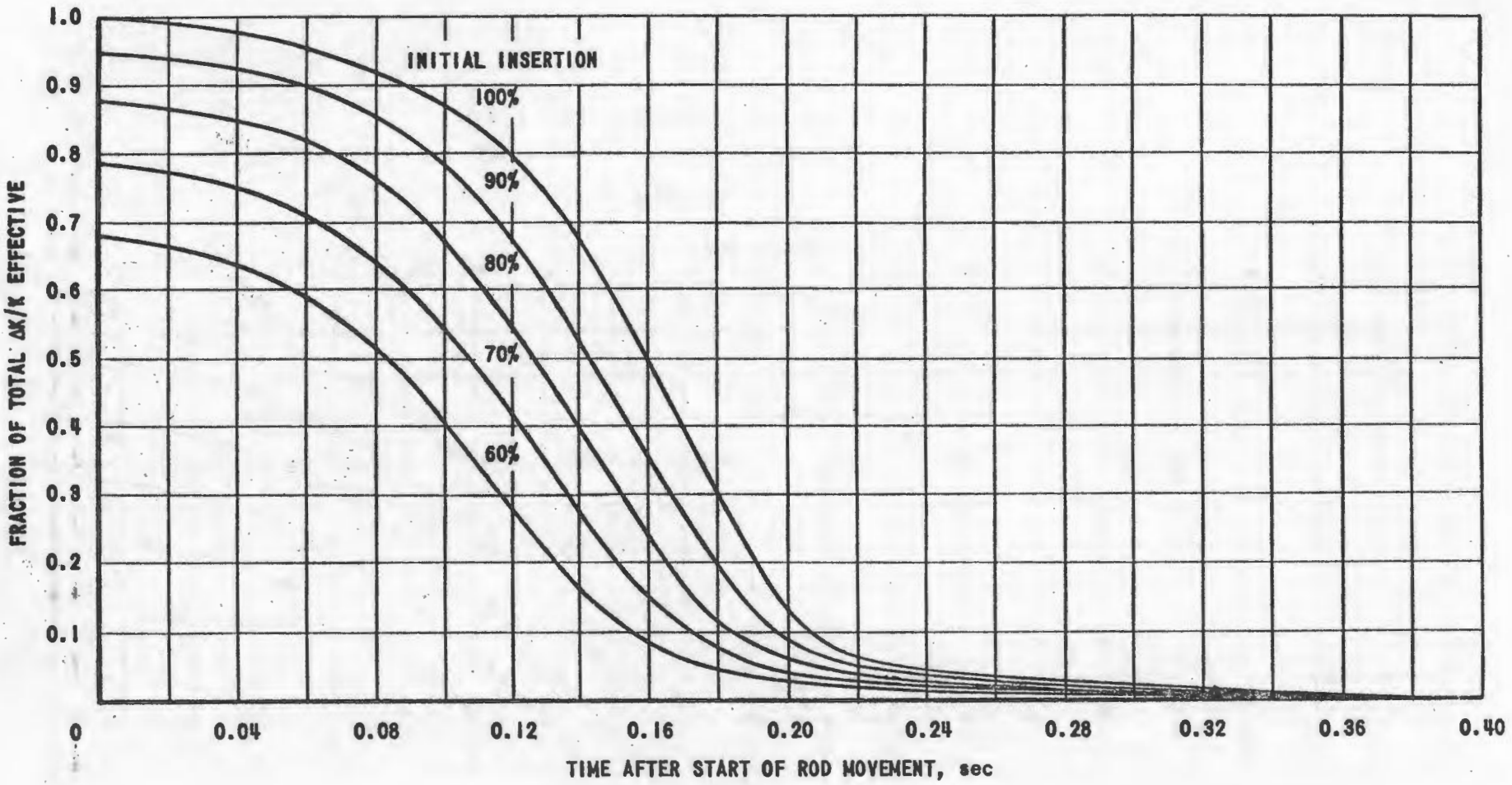

Fig. 32

Fraction of Total Control Rod Worth Effective vs Time after Start of Rod Movement
(Maximum Rod Acceleration of 1.5 g)

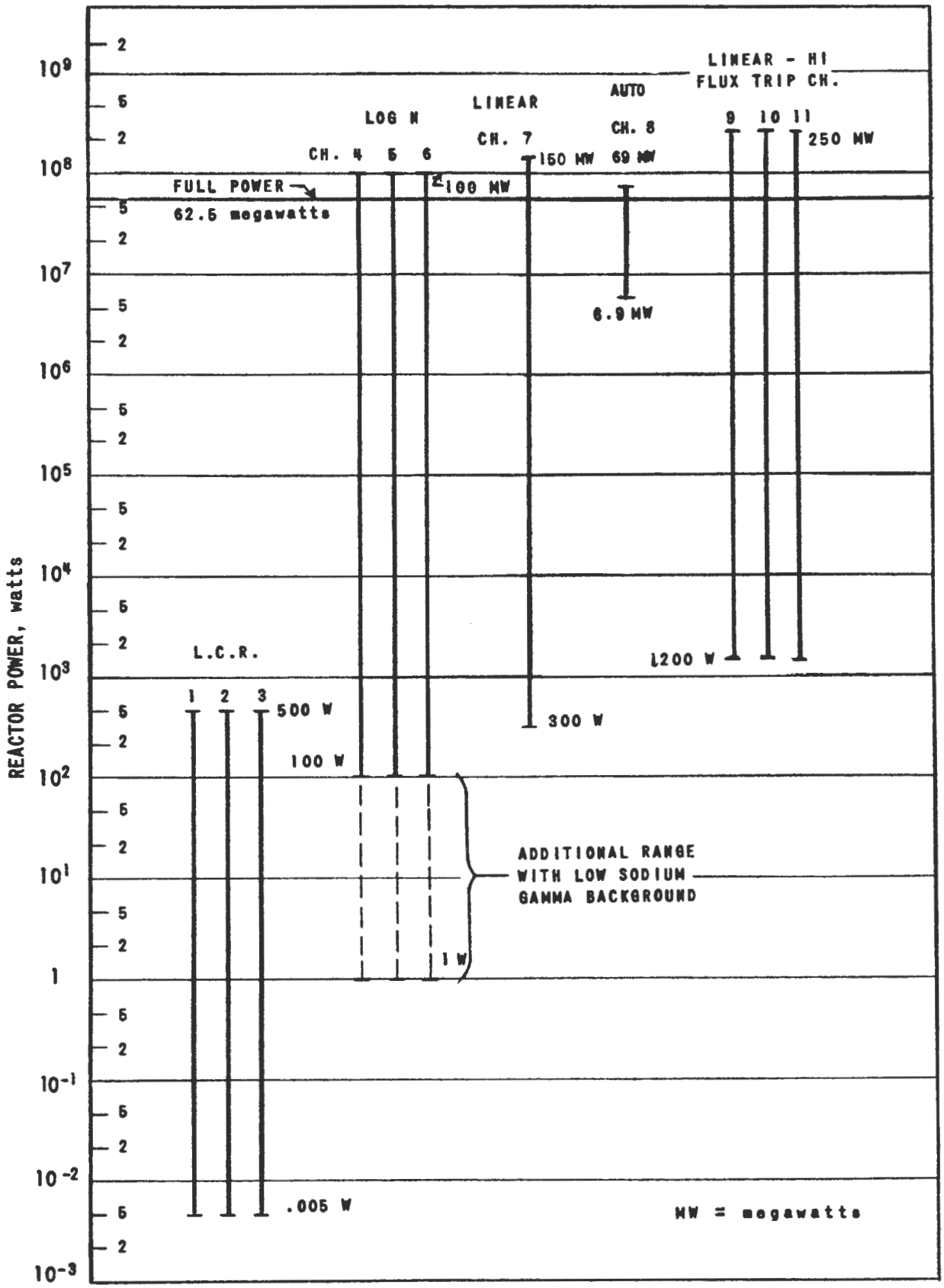

Fig. 33

Nuclear Instrument Range Chart

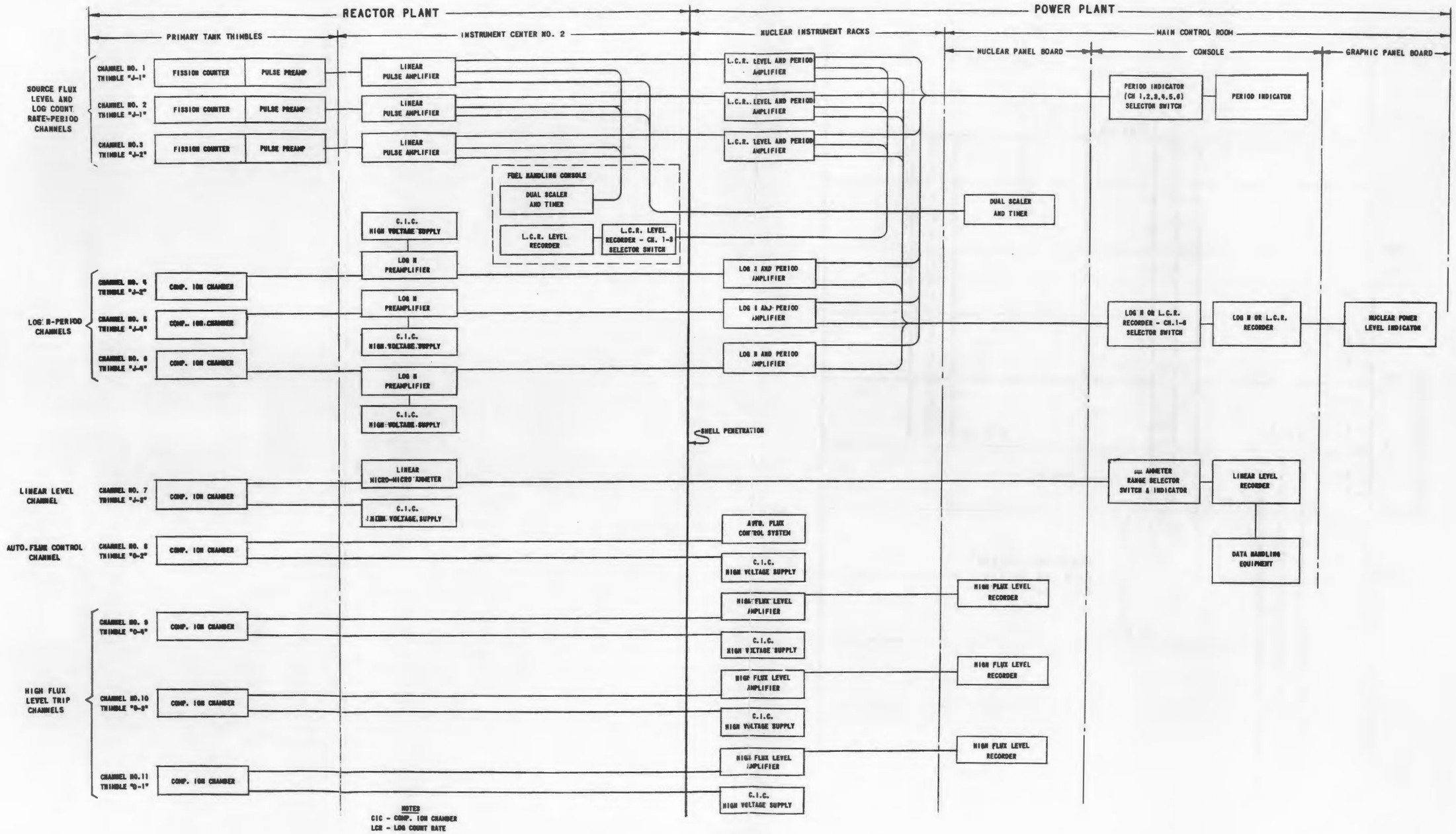

Fig. 34

Nuclear Instrumentation Block Diagram

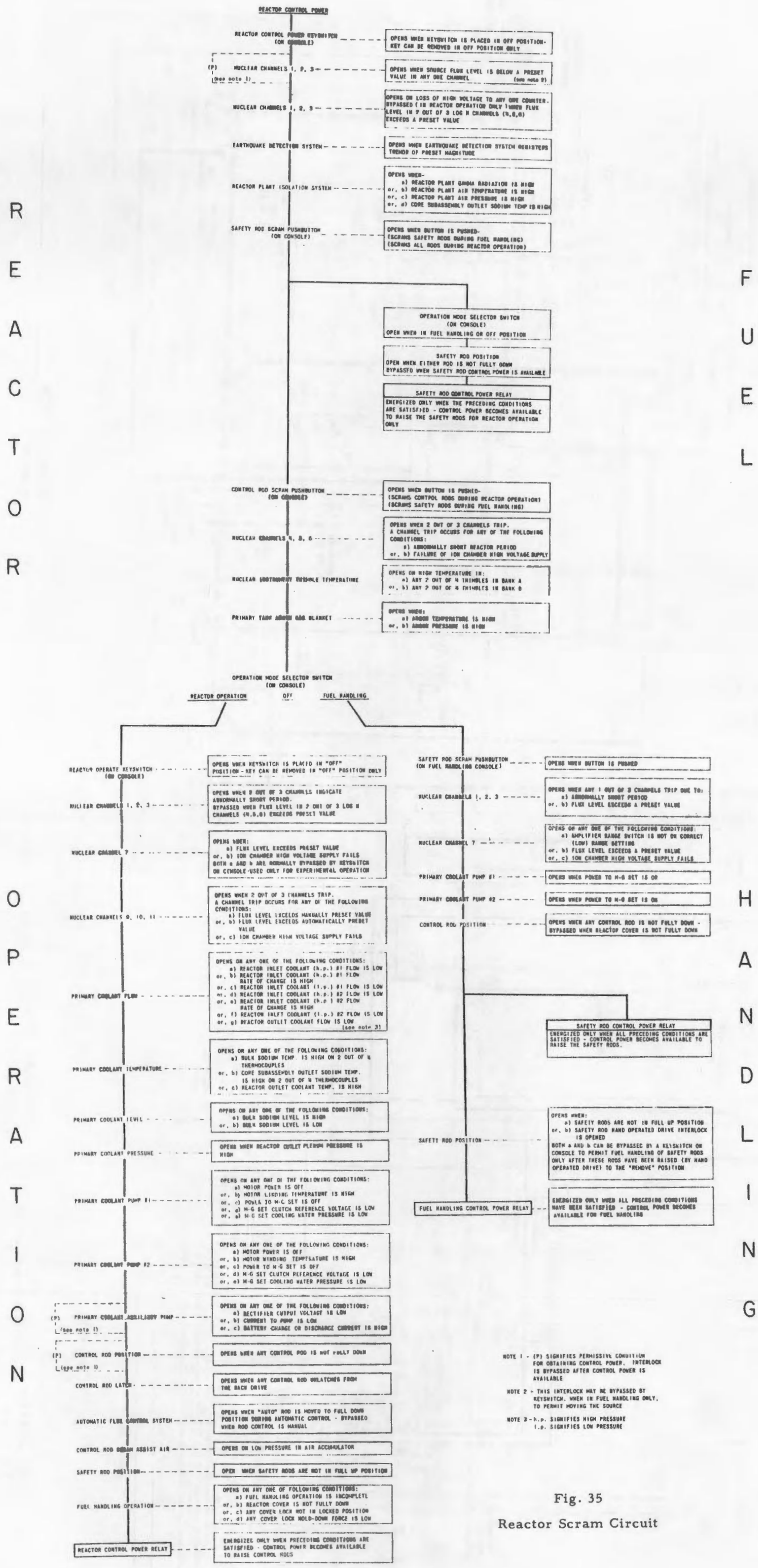

Fig. 35

Reactor Scram Circuit

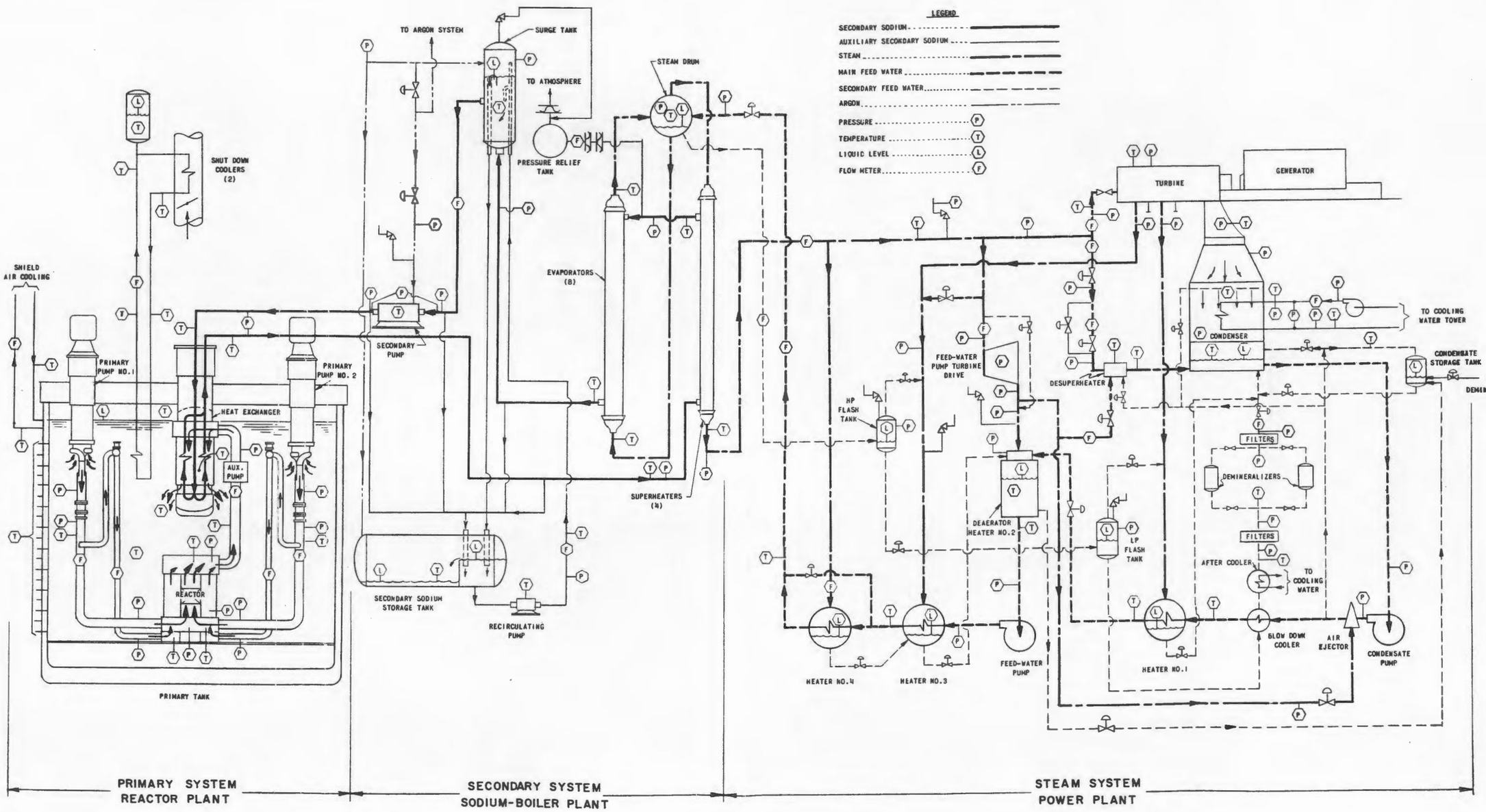

Fig. 36

Simplified Instrument Flow Sheet

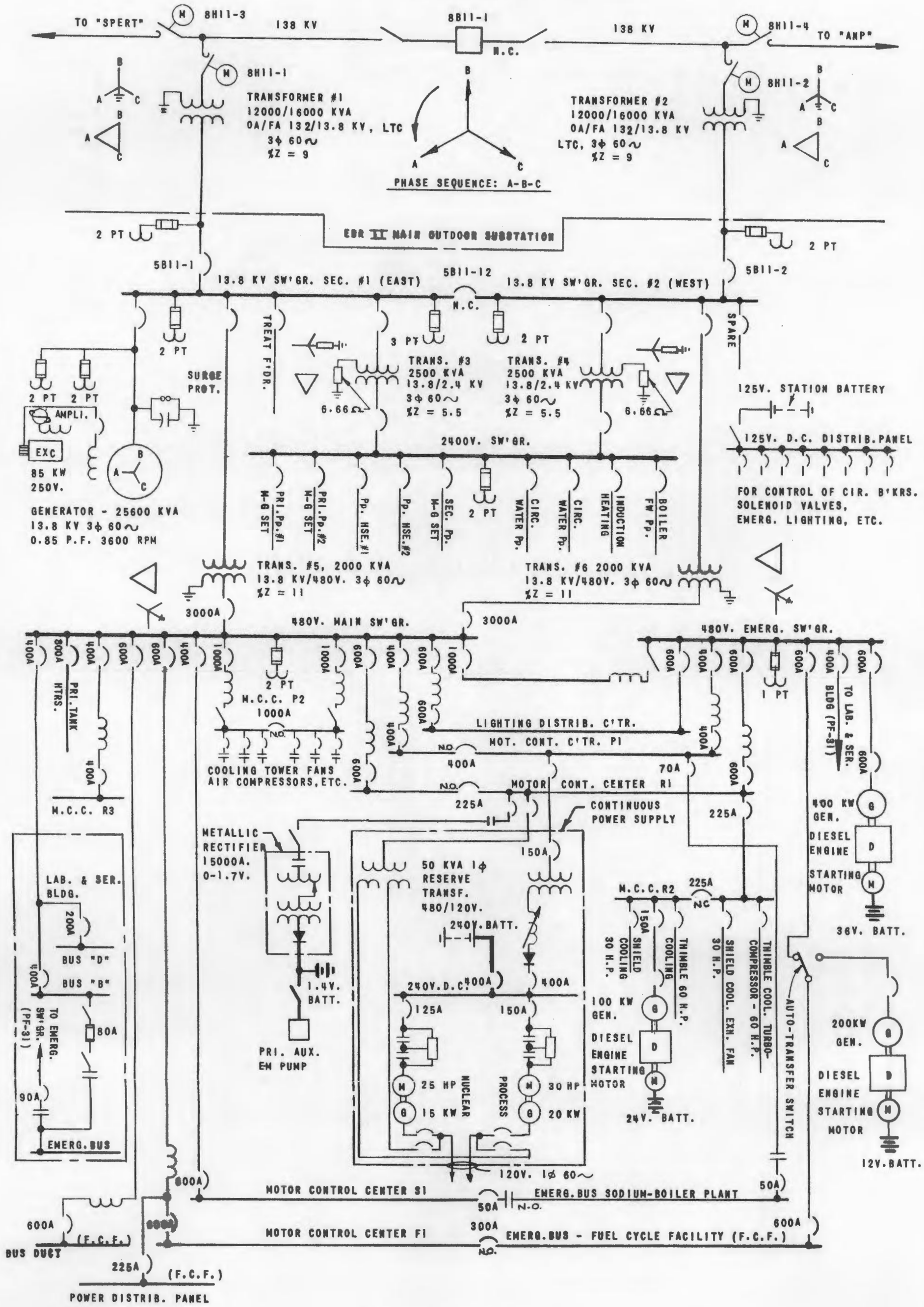

Fig. 37

Single-Line Diagram of EBR-II
Electric Power Distribution

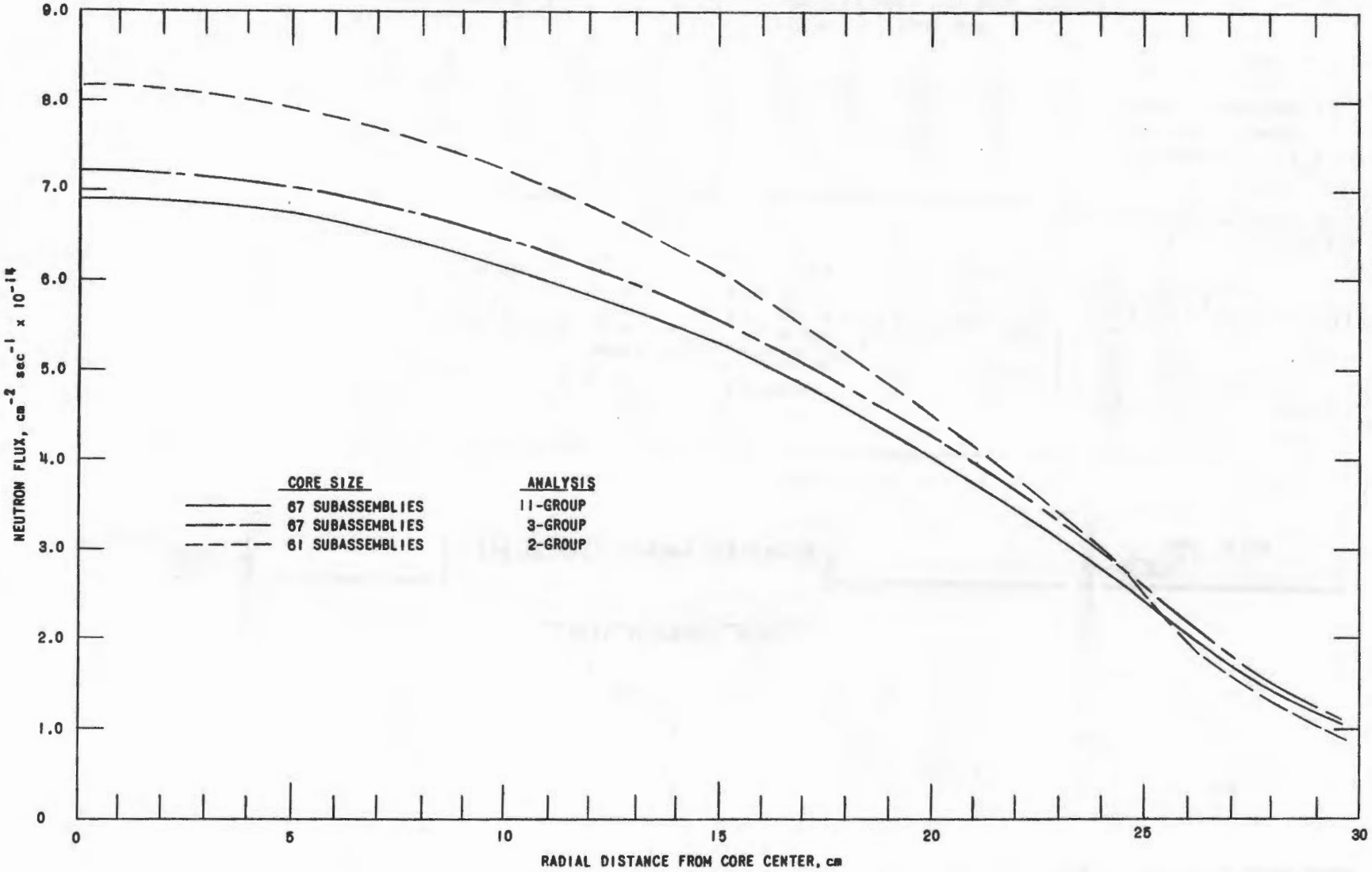

Fig. 38

High-Energy (>1.35 Mev) Neutron Flux
at Core Midplane, 62.5 Mw

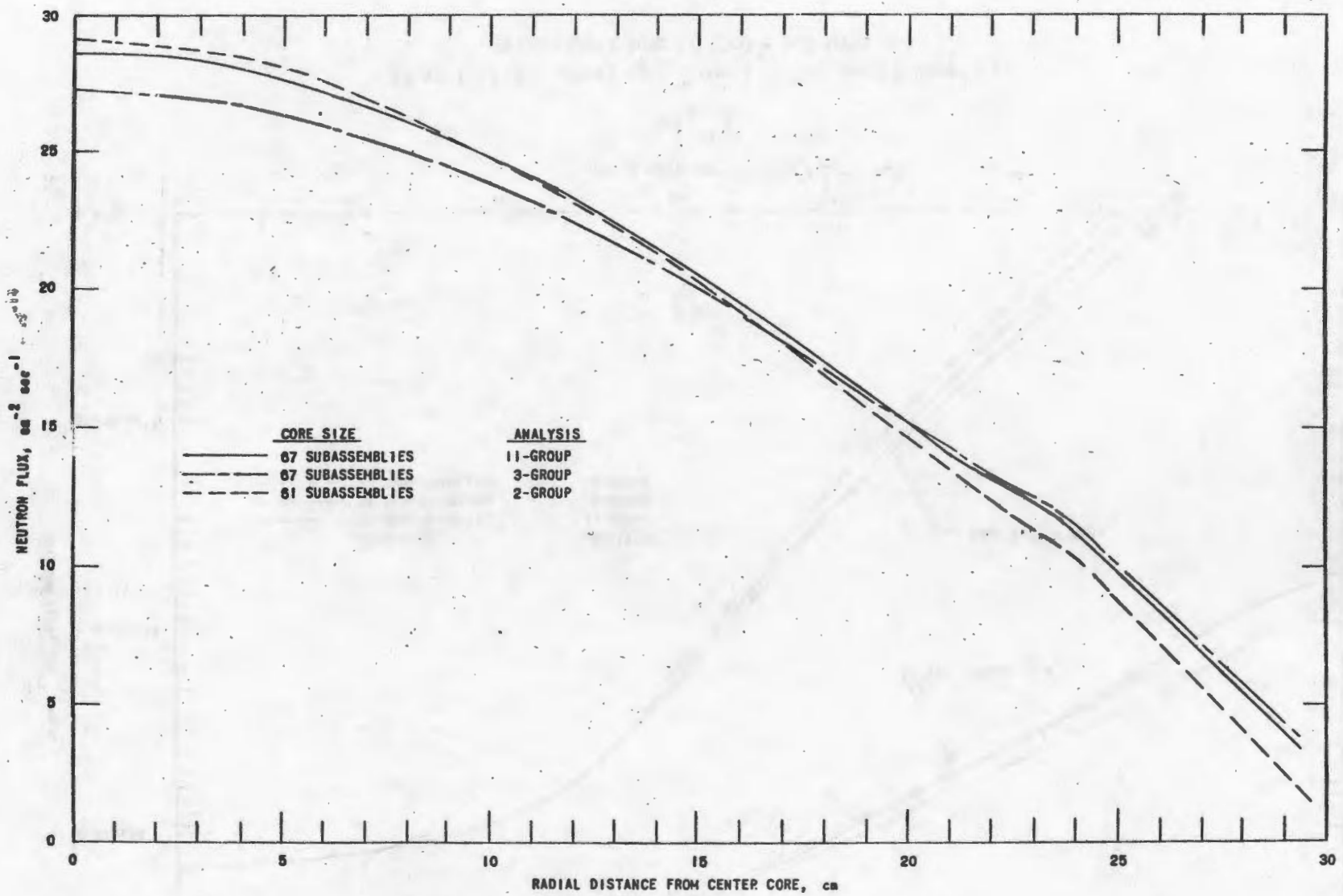

Fig. 39

Low-Energy (< 1.35 Mev) Neutron Flux
at Core Midplane, 62.5 Mw

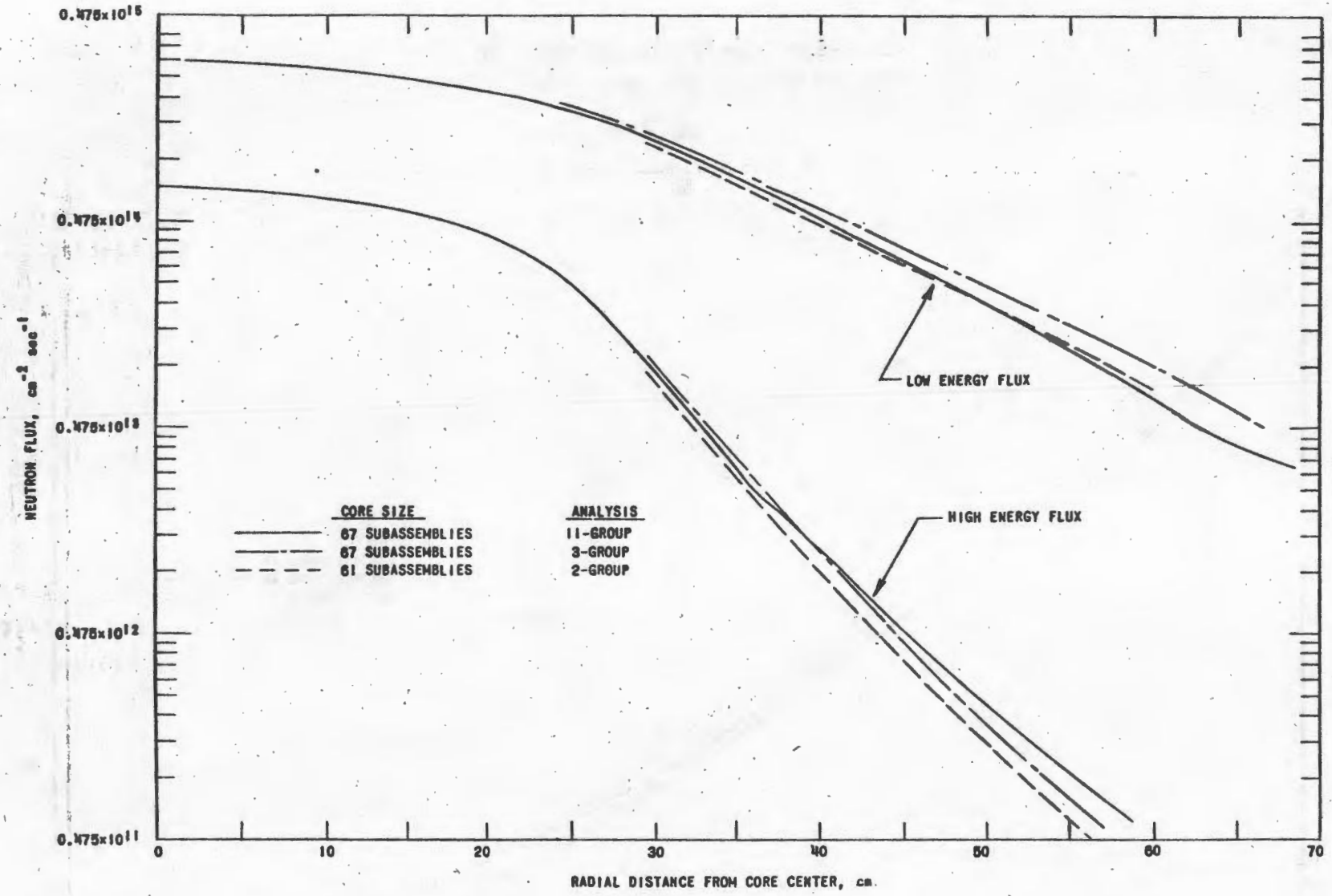

Fig. 40

High (>1.35 Mev) and Low (<1.35 Mev) Energy
Neutron Flux at Core Midplane

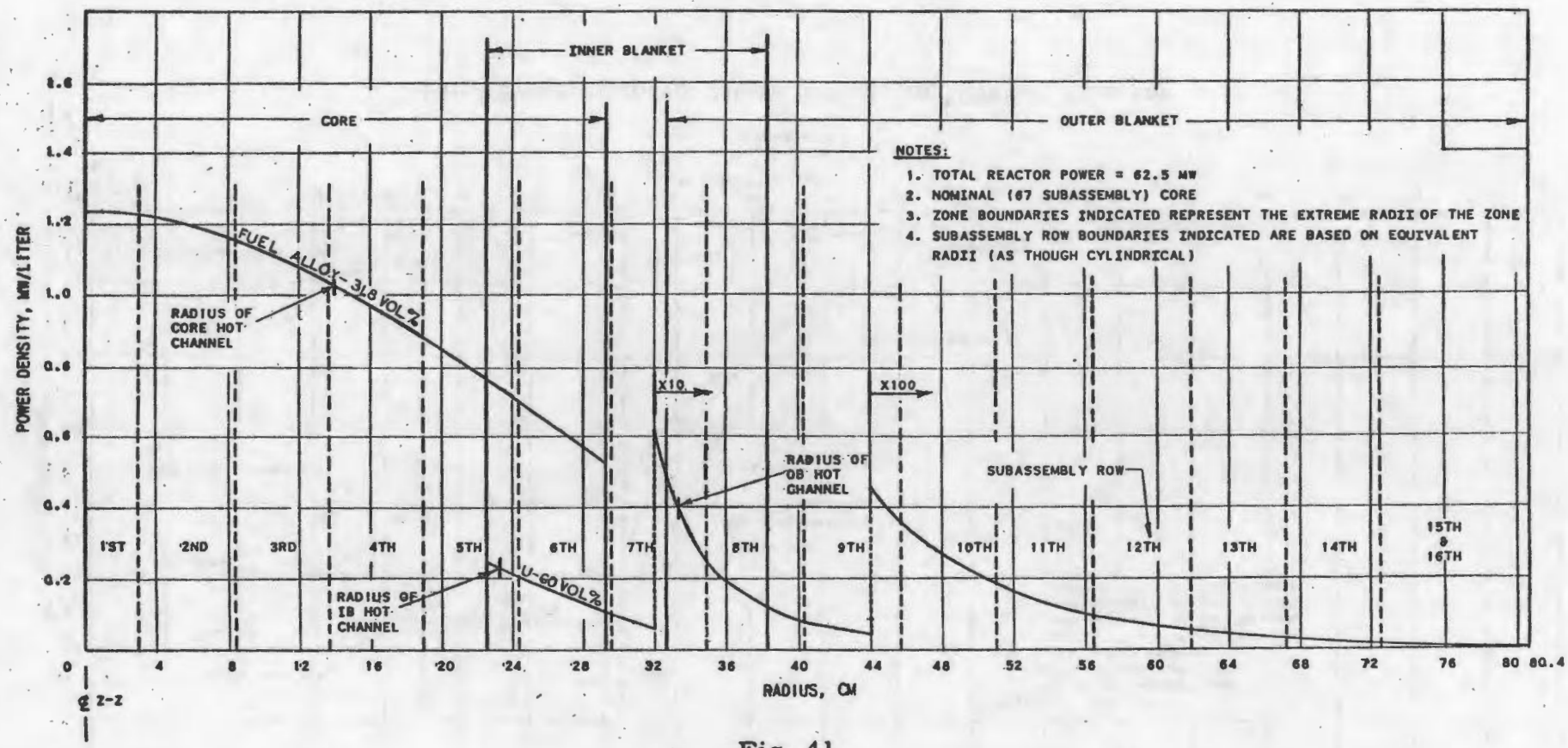

Fig. 41

Radial Power Density Distribution at Center Plane of "Clean" Reactor (Z = 0)

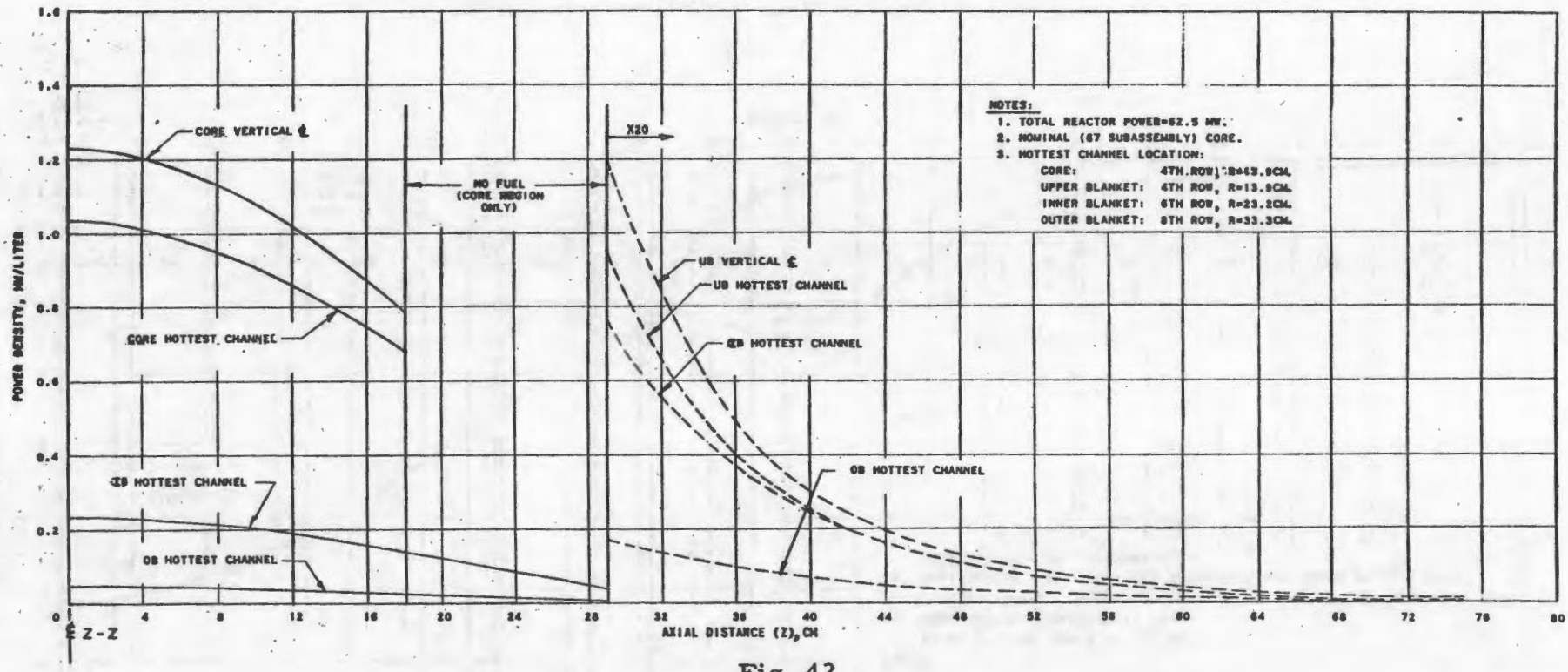

Fig. 42

Axial Power Density Distributions in "Clean" Reactor

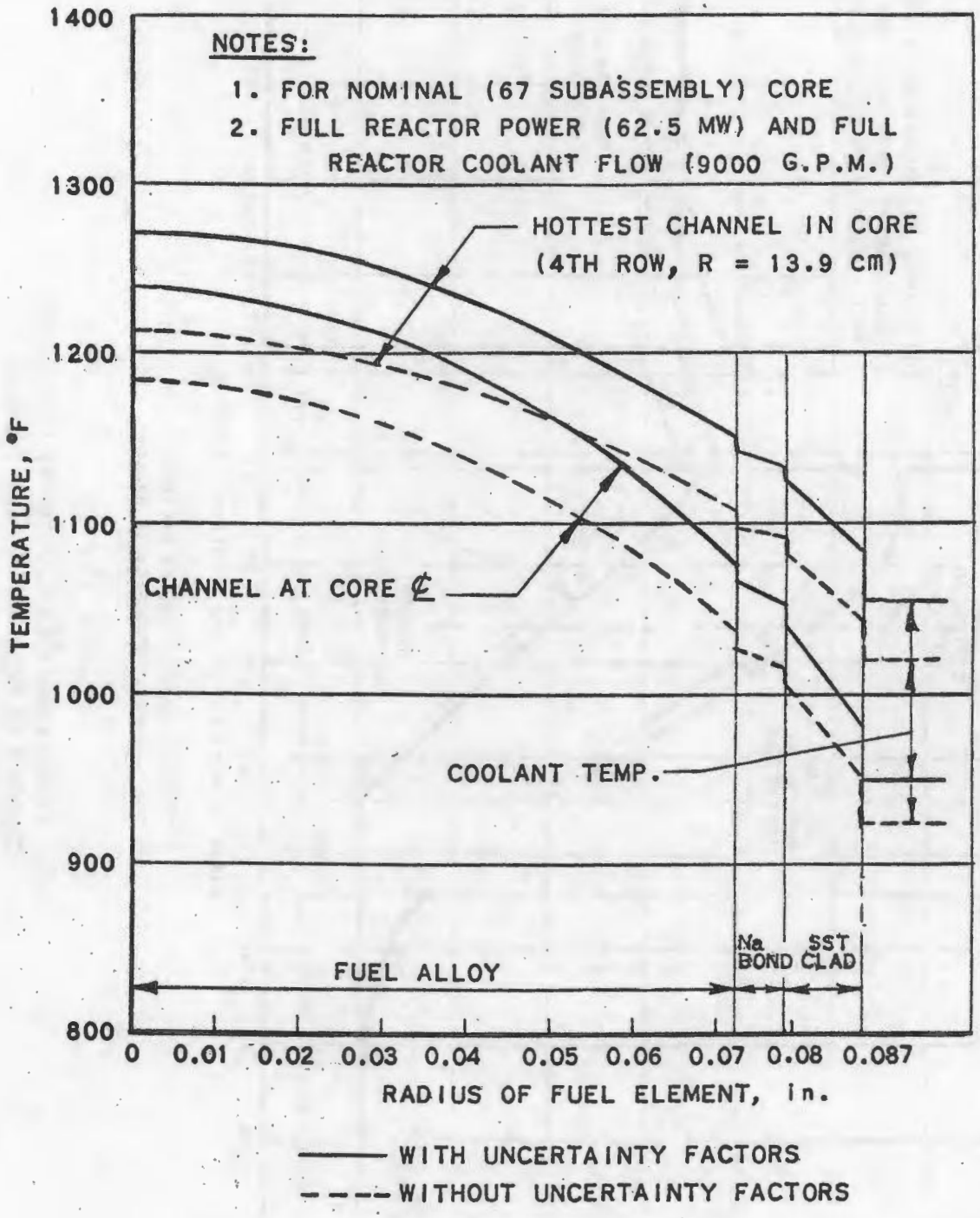

Fig. 43

Radial Temperature Distribution through Fuel Element at Point of Maximum Fuel Temperature

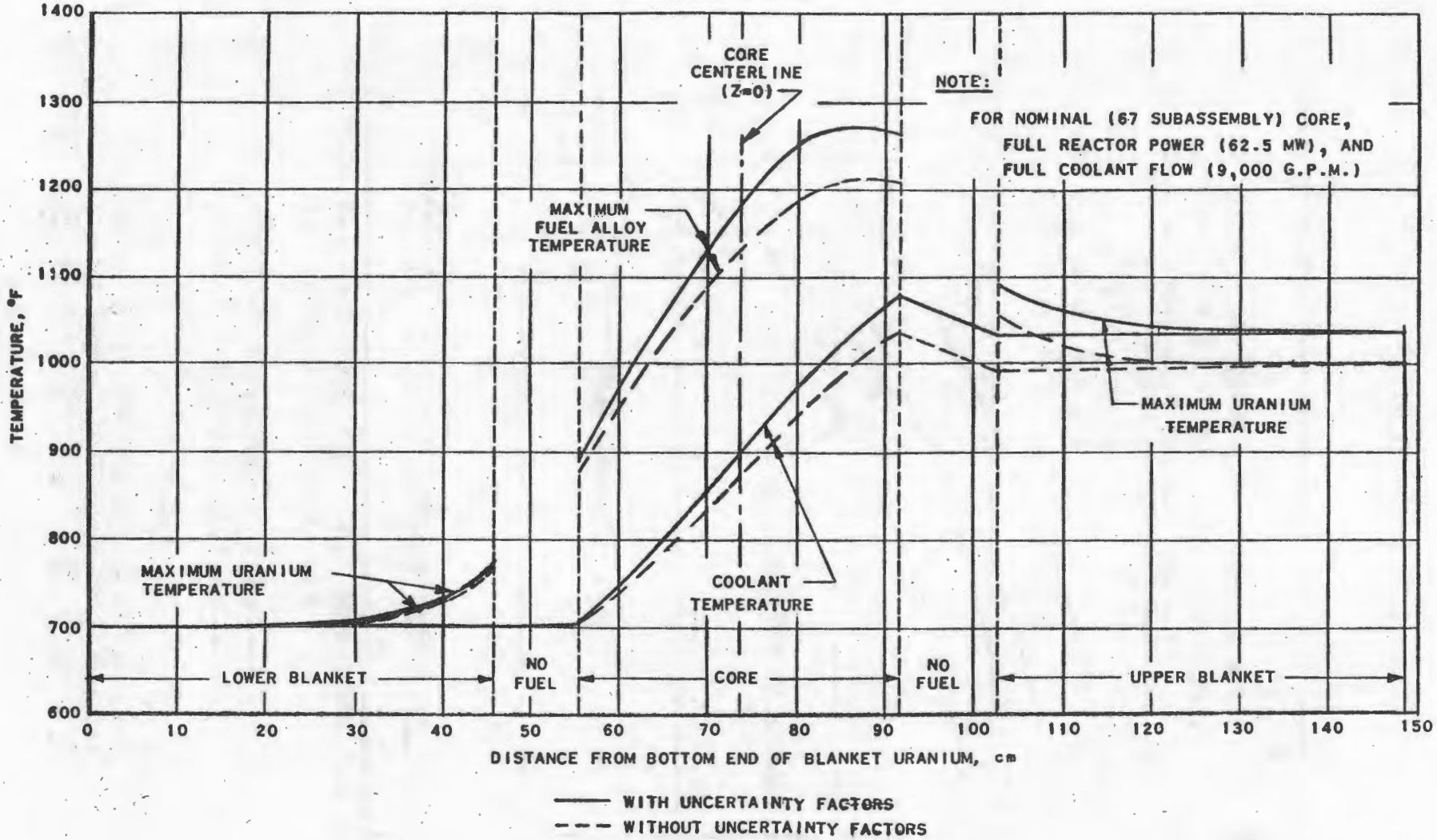

Fig. 44

Axial Temperature Distributions in Hottest Channel of Core and Upper Blanket (4th Row, R = 13.9 cm)

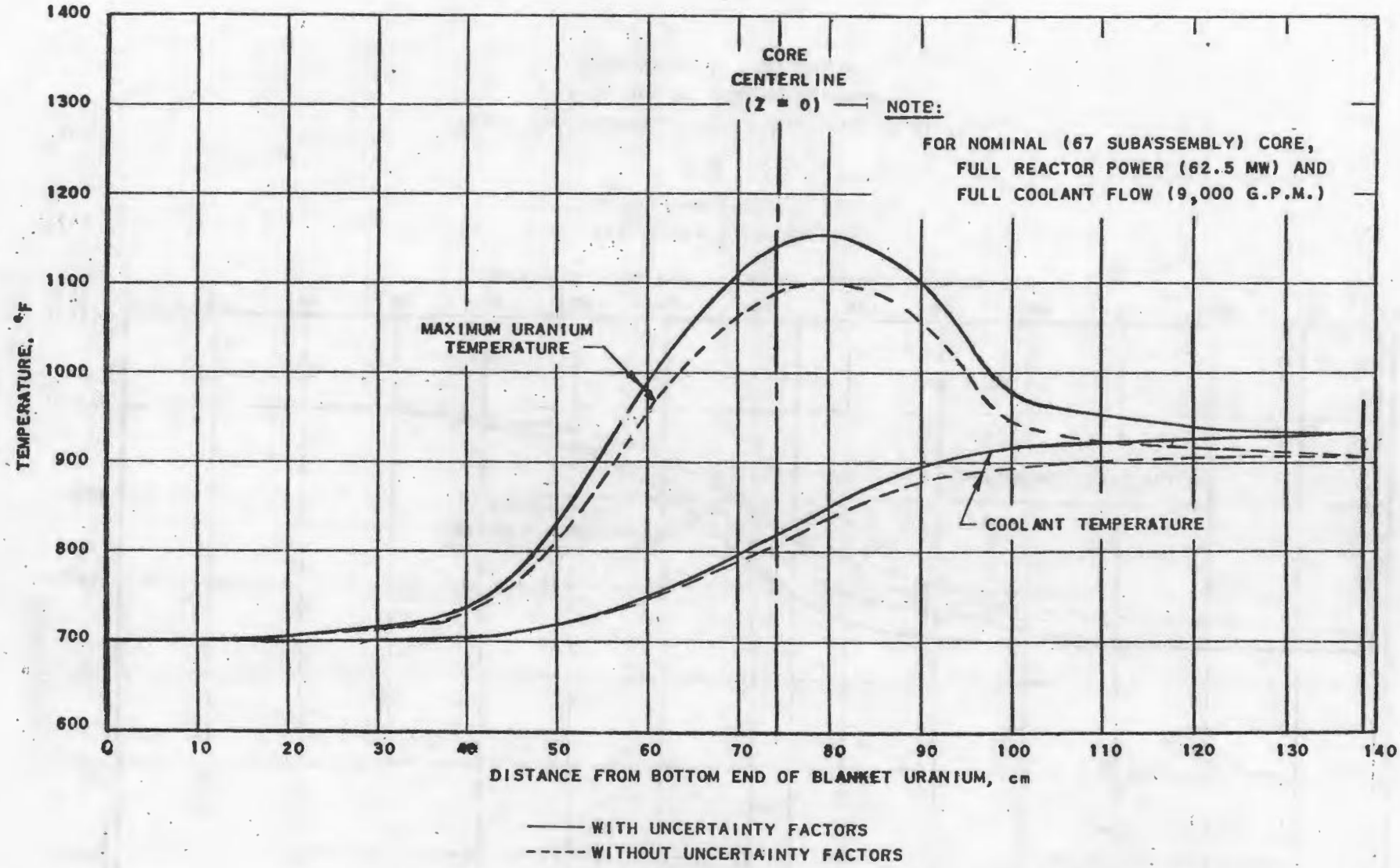

Fig. 45

Axial Temperature Distributions in Hottest
Channel of Inner Blanket
(6th Row, R = 23.2 cm)

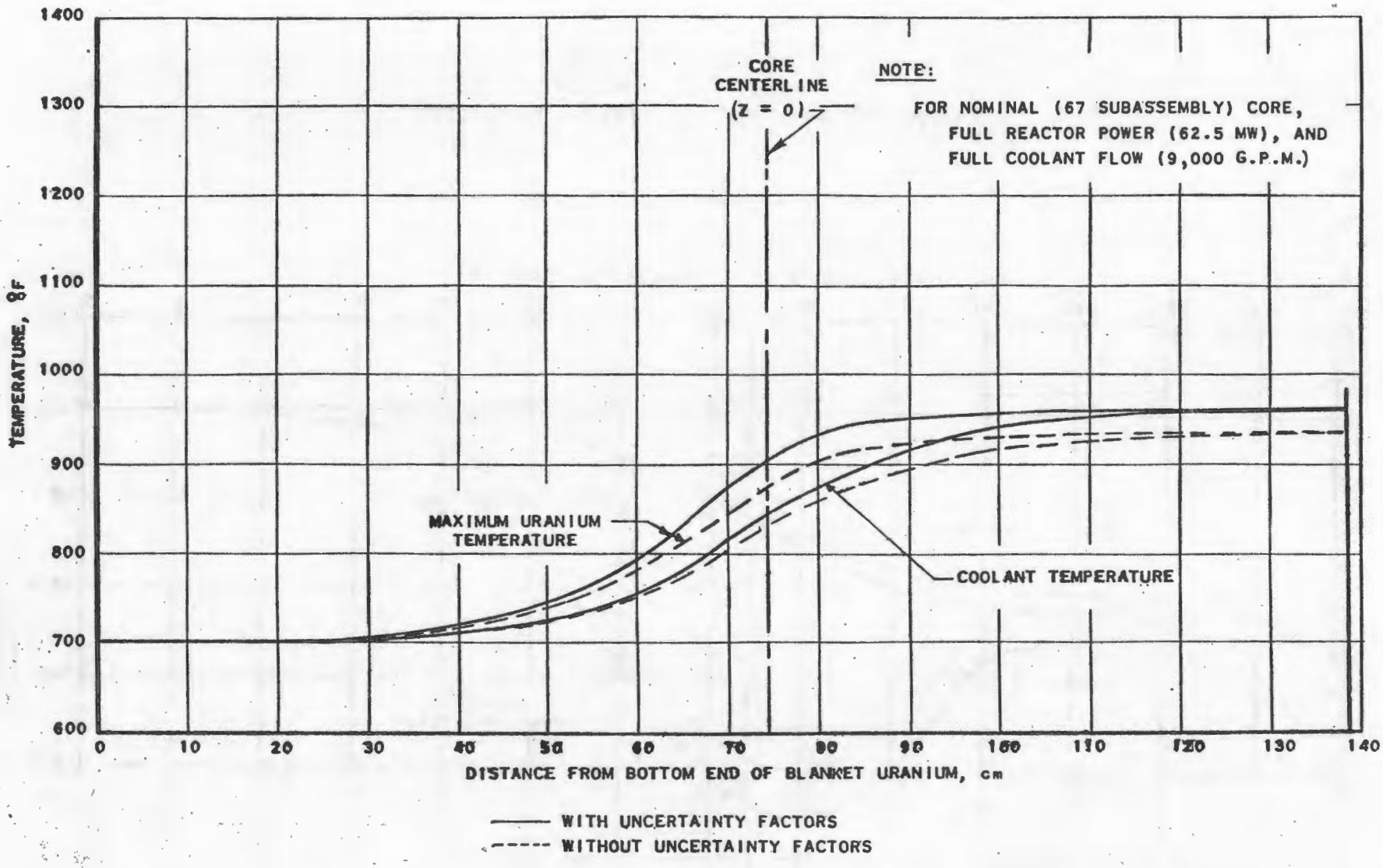

Fig. 46

Axial Temperature Distributions in Hottest Channel of Outer Blanket (8th Row, R = 33.3 cm)

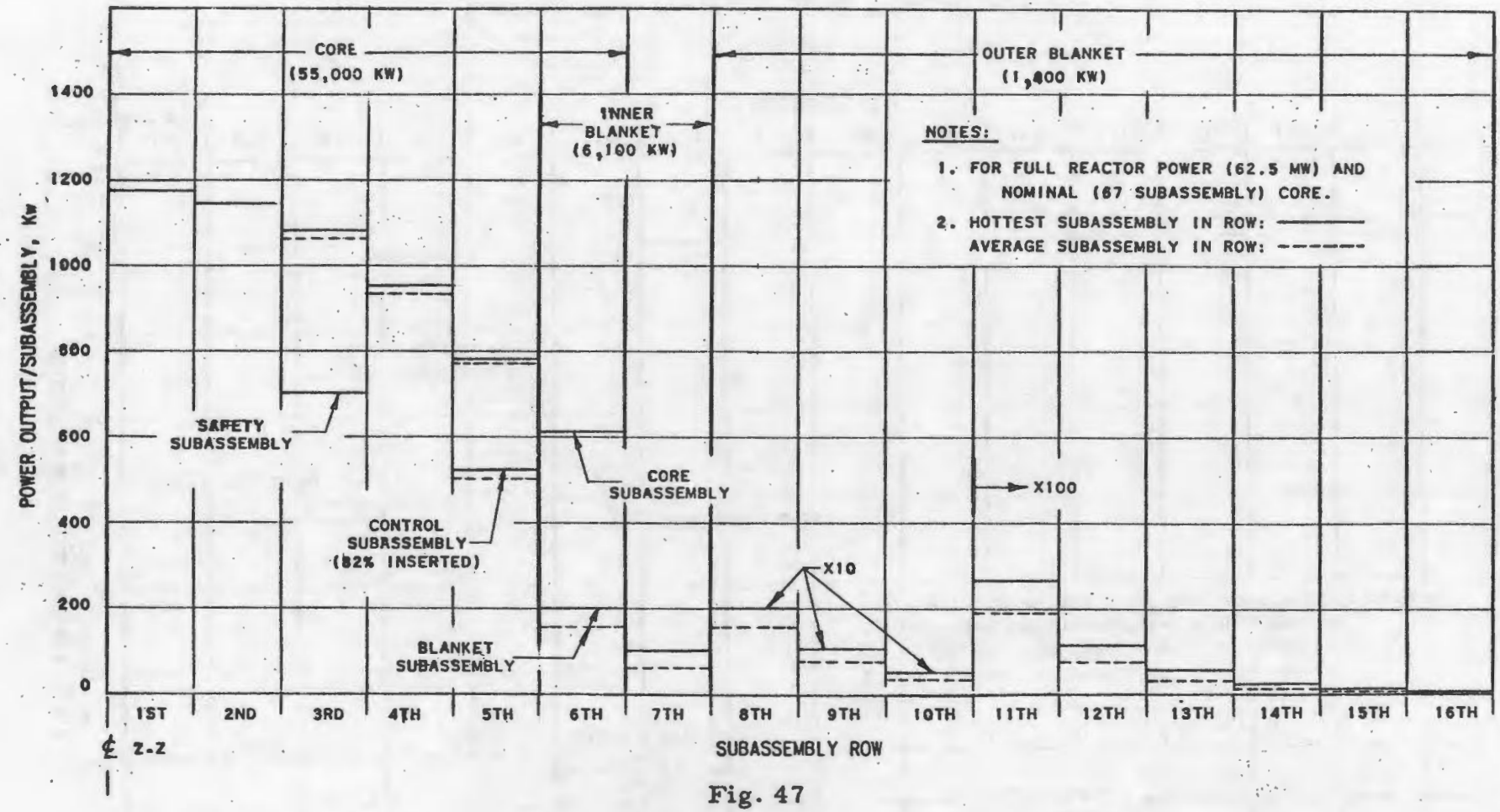

Fig. 47

Power Output per Subassembly
for "Clean" Reactor

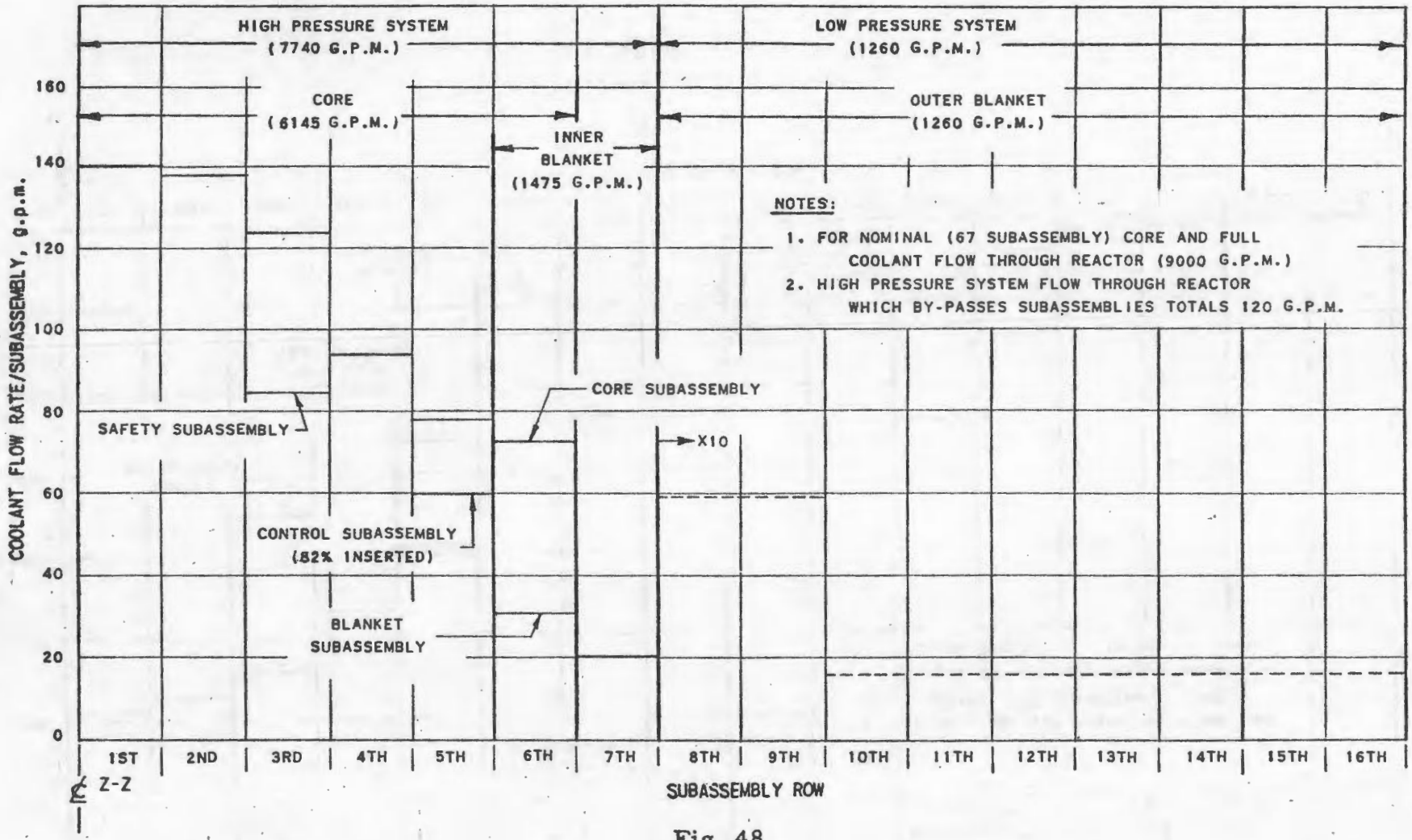

Fig. 48

Coolant Flow Distribution in "Clean" Reactor

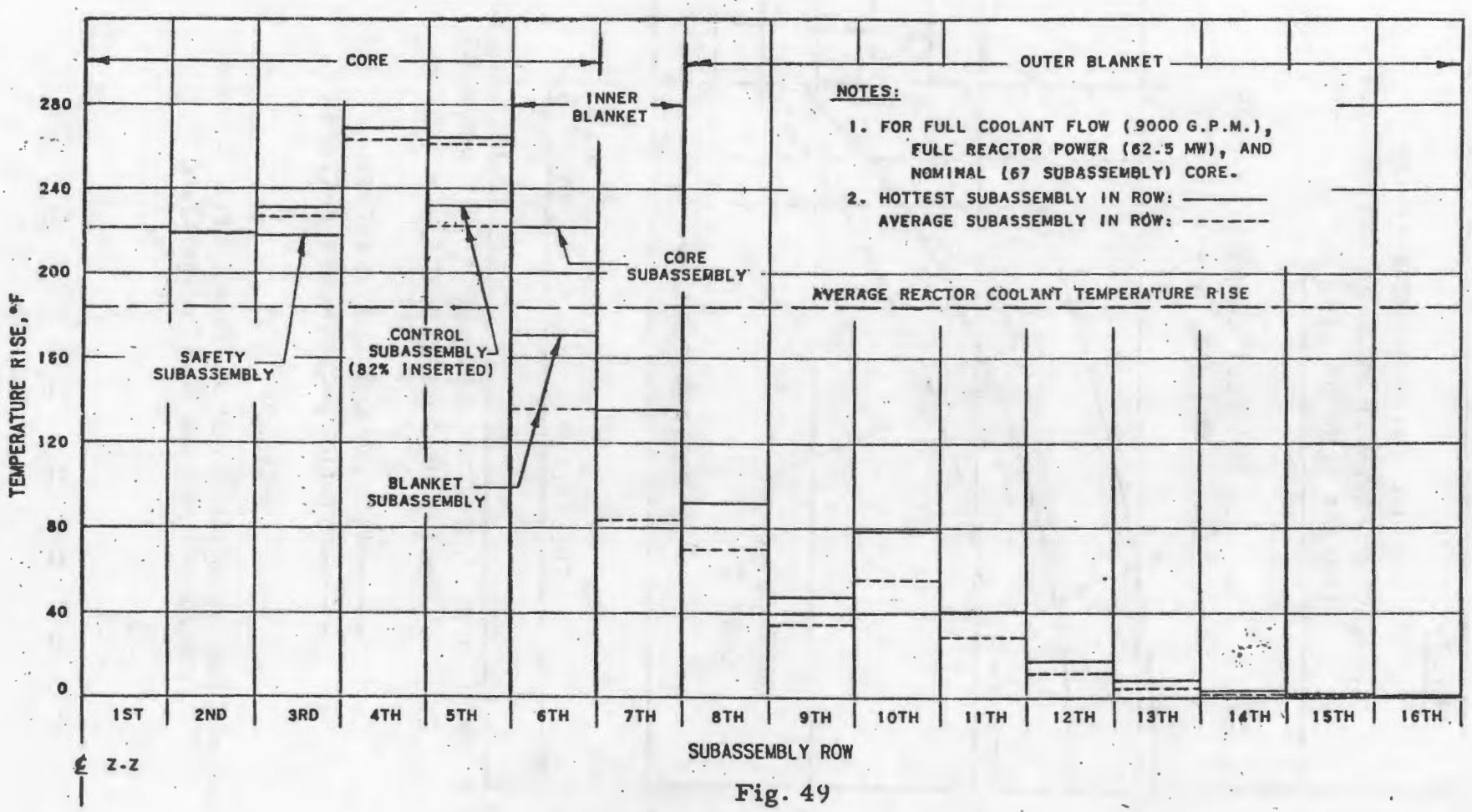

Fig. 49

Mixed Mean Coolant Temperature
through Each Subassembly for "Clean" Reactor

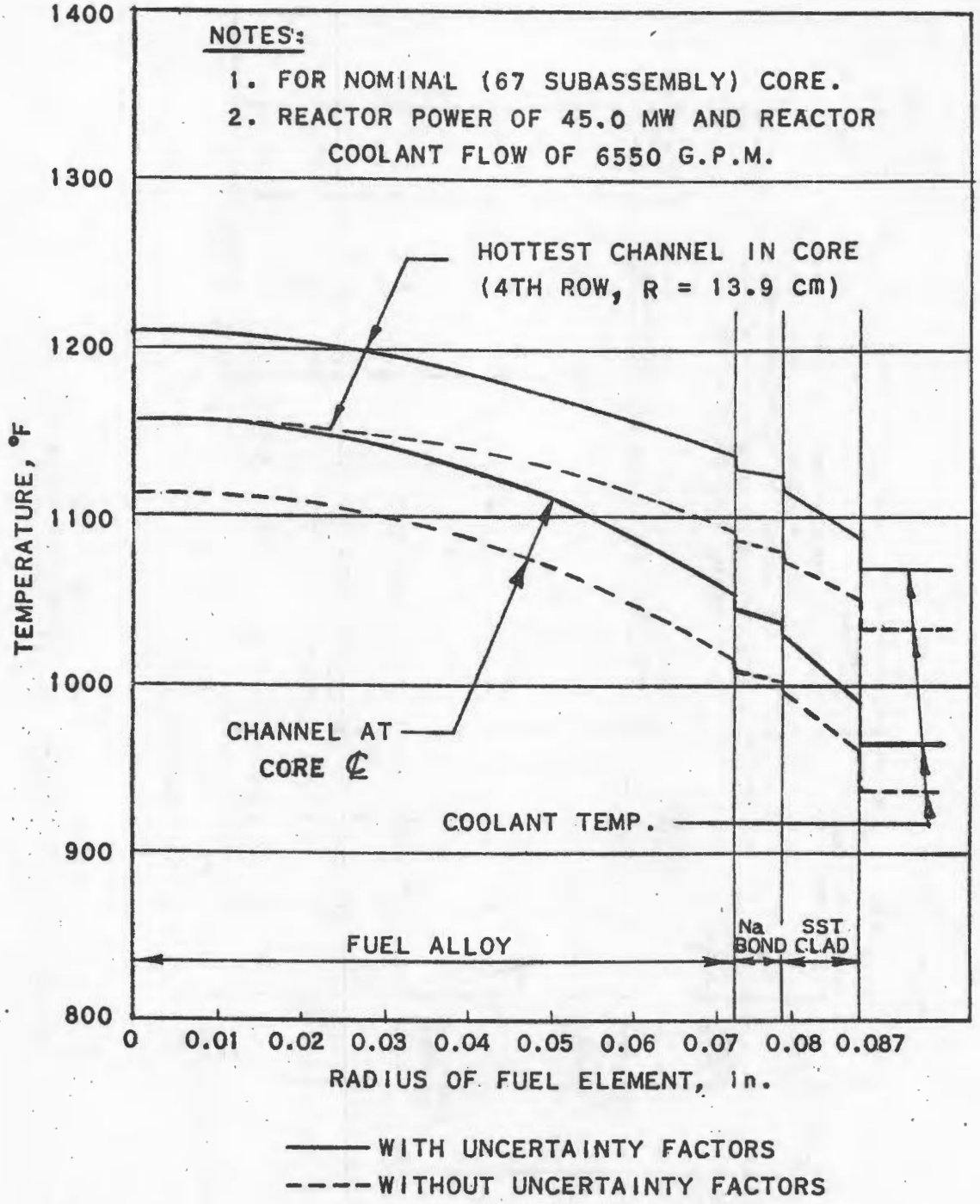

Fig. 50

Radial Temperature Distributions through Fuel Element at Point of Maximum Fuel Temperature

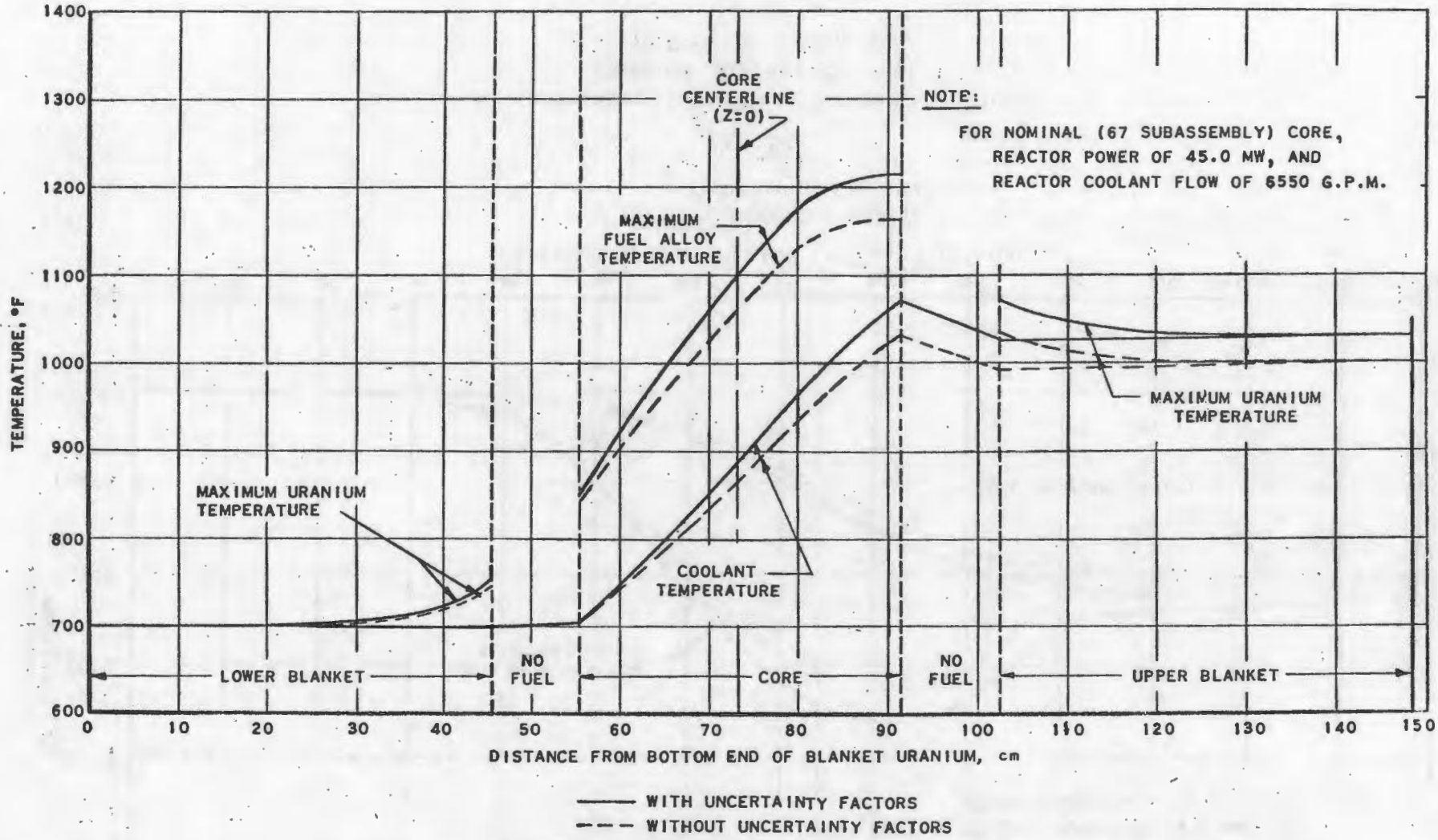

Fig. 51

Axial Temperature Distributions in Hottest Channel of Core and Upper Blanket (4th Row, R = 13.9 cm)

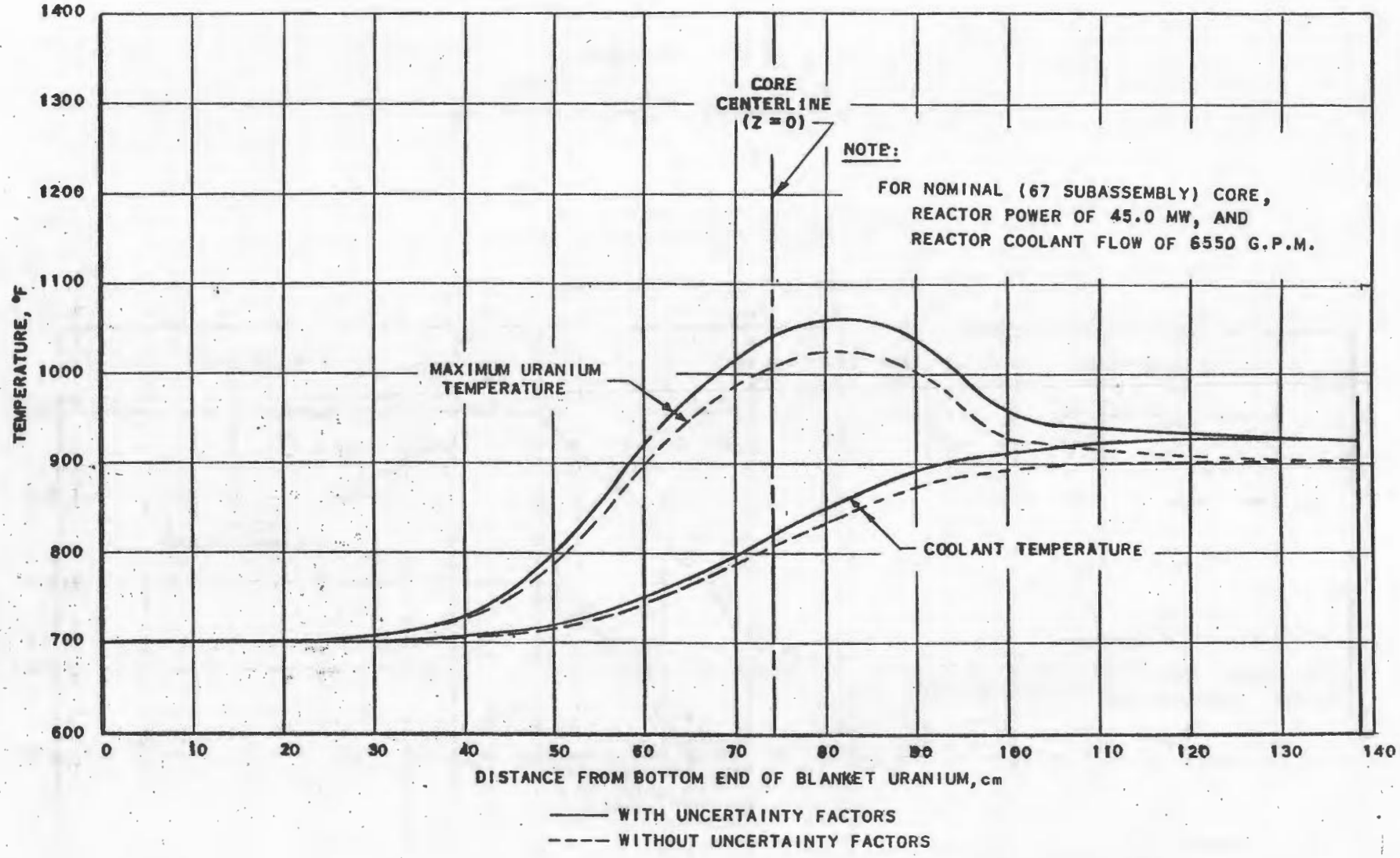

Fig. 52

Axial Temperature Distributions in Hottest Channel of Inner Blanket (6th Row, R = 23.2 cm)

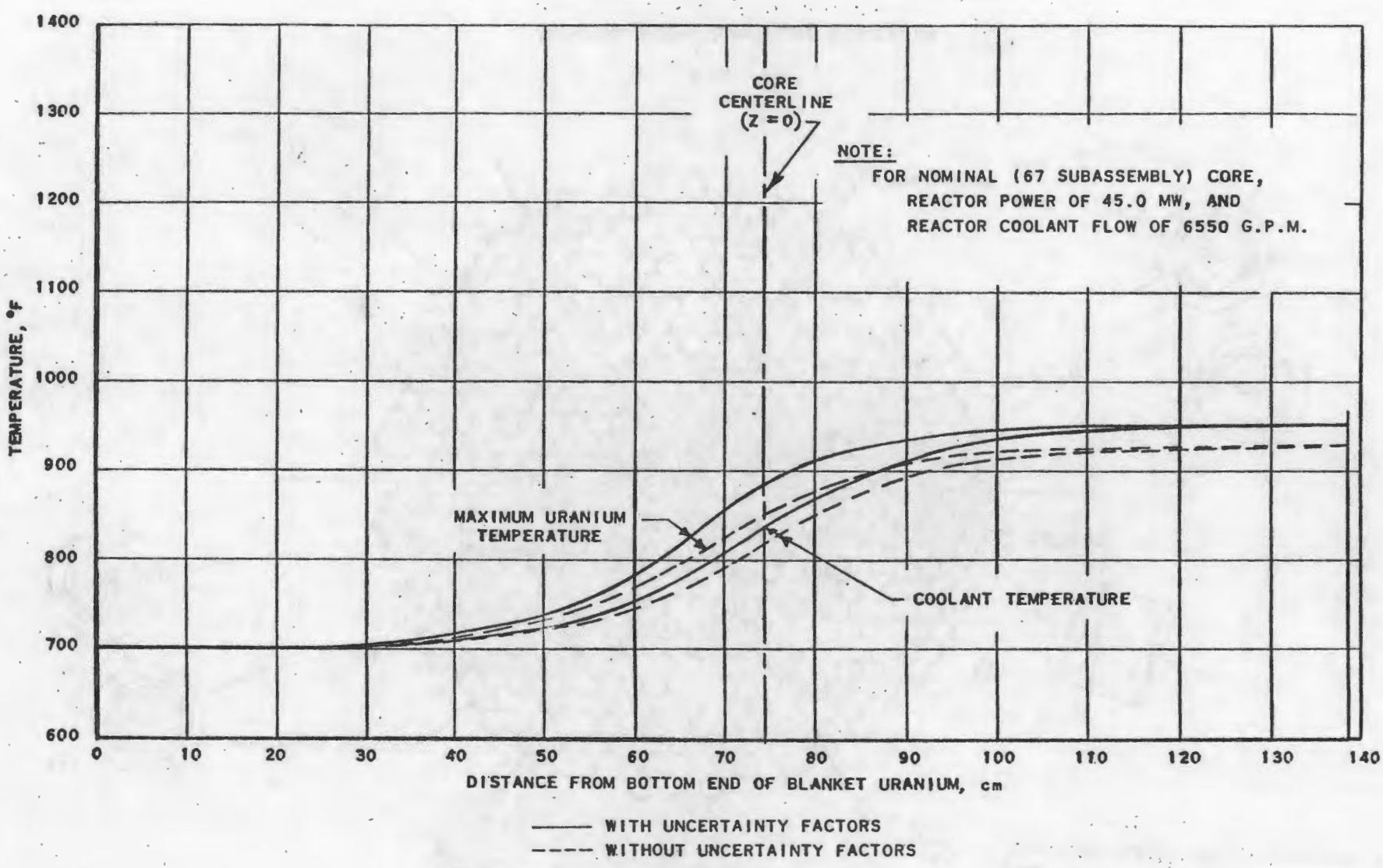

Fig. 53

Axial Temperature Distributions in Hottest Channel of Outer Blanket (8th Row, R = 33.3 cm)

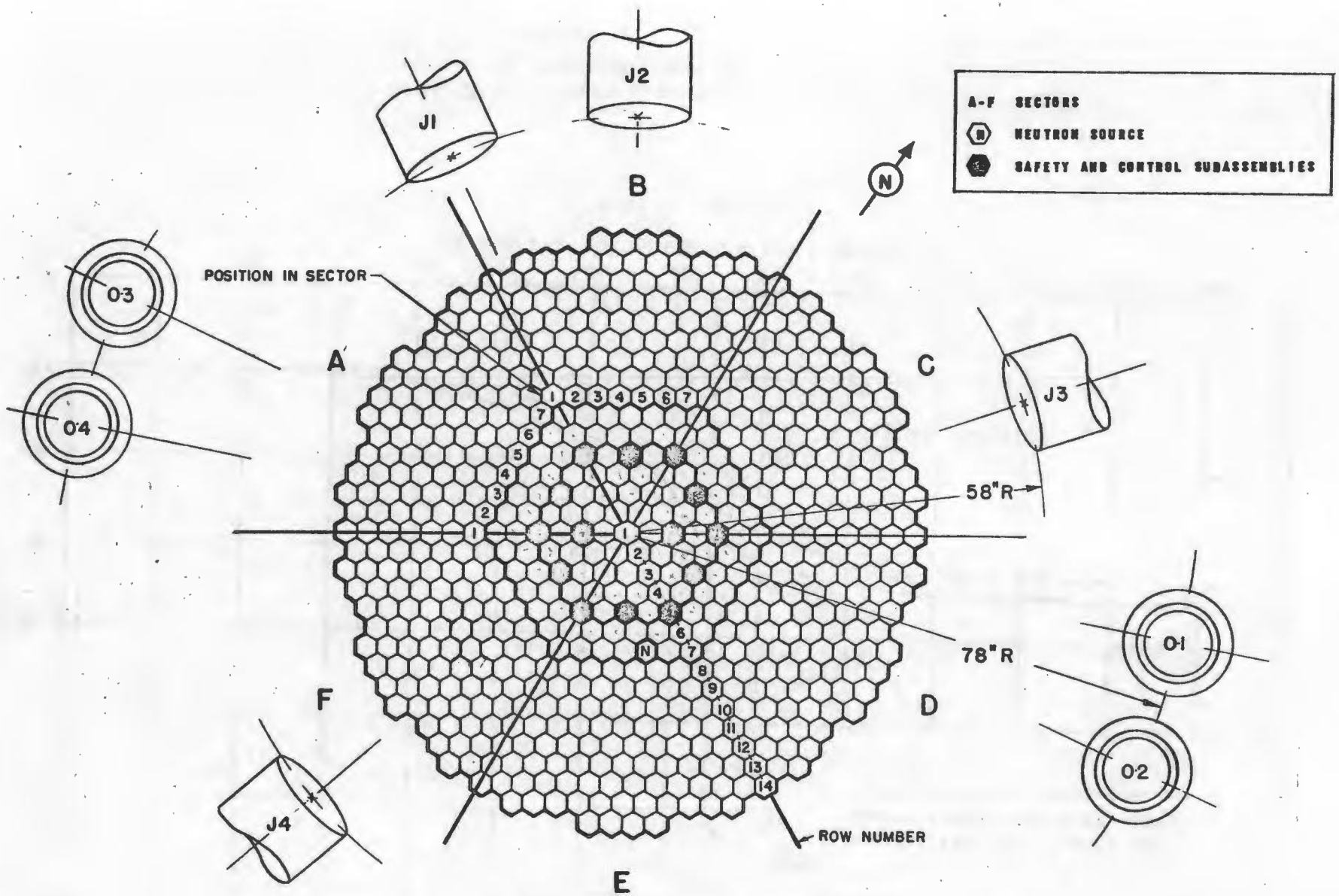

Fig. 54

Subassembly Locating Diagram

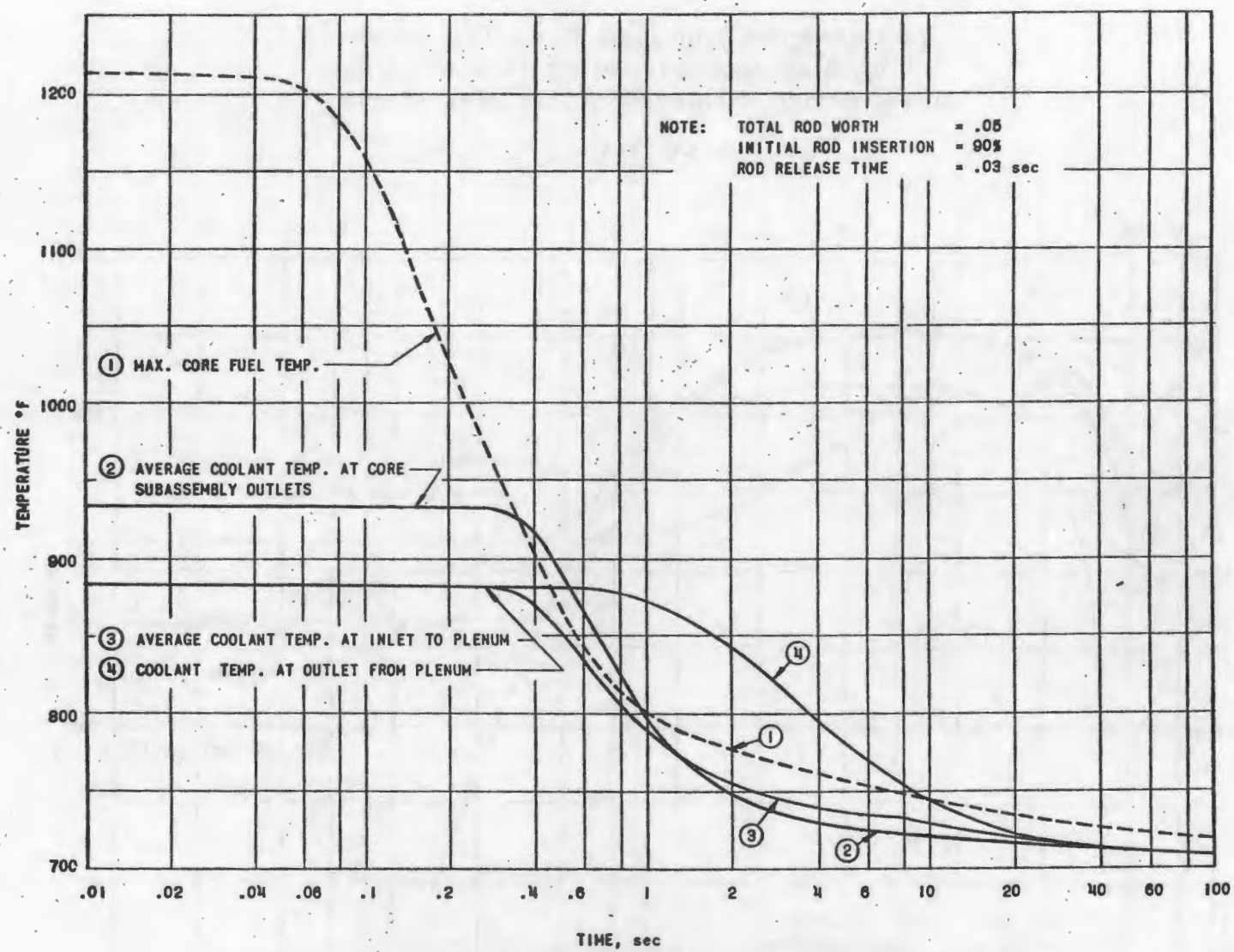

Fig. 55

Various Reactor Temperatures during Scram vs Time after Scram Signal Reaches Control Rods (All Pumps Remain in Operation)

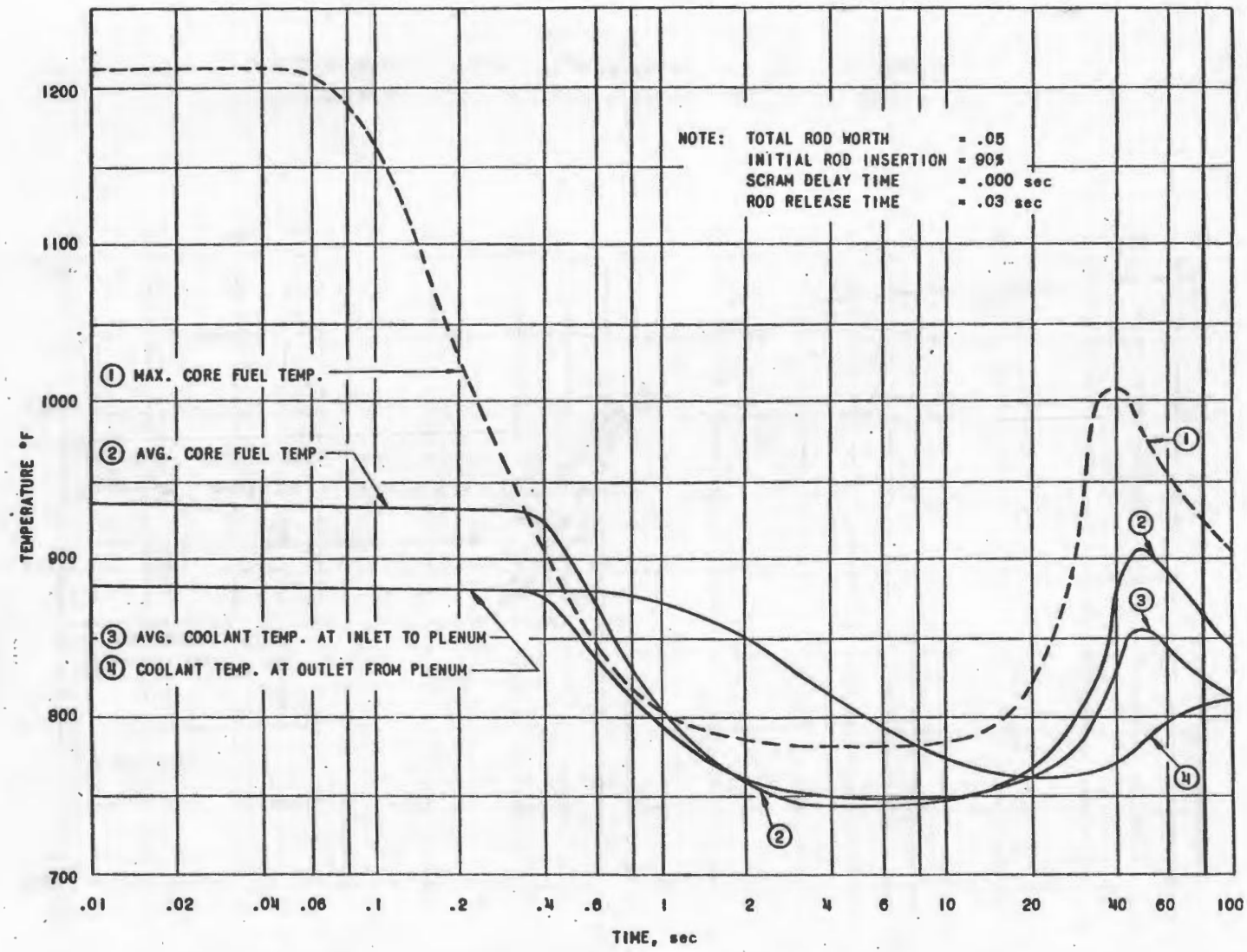

Fig. 56

Various Reactor Temperatures during Scram vs Time after Failure of Both Main Pumps (Auxiliary Pump Continues in Operation)

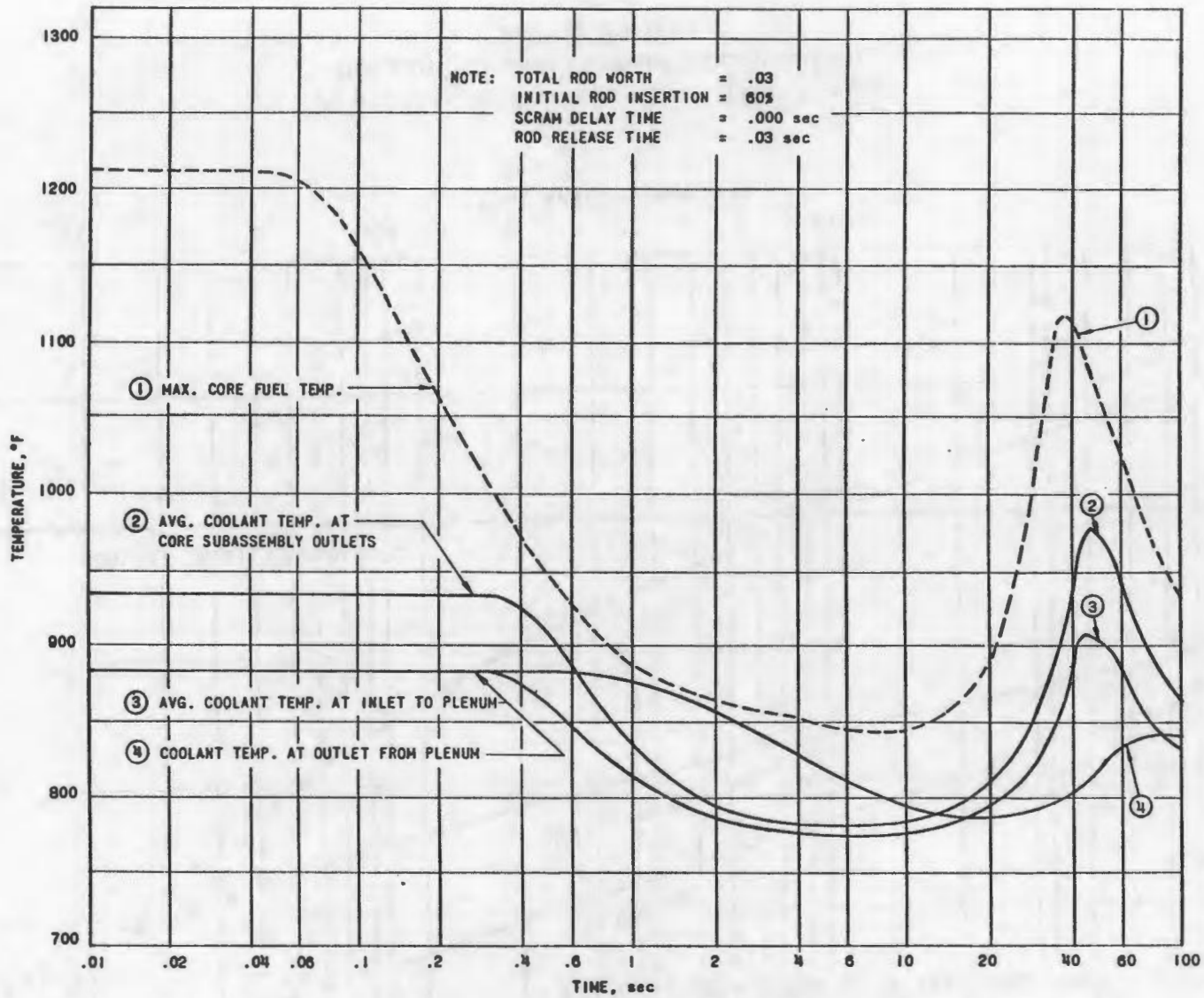

Fig. 57

Various Reactor Temperatures during Scram vs Time after Failure of Both Main Pumps (Auxiliary Pump Continues in Operation)

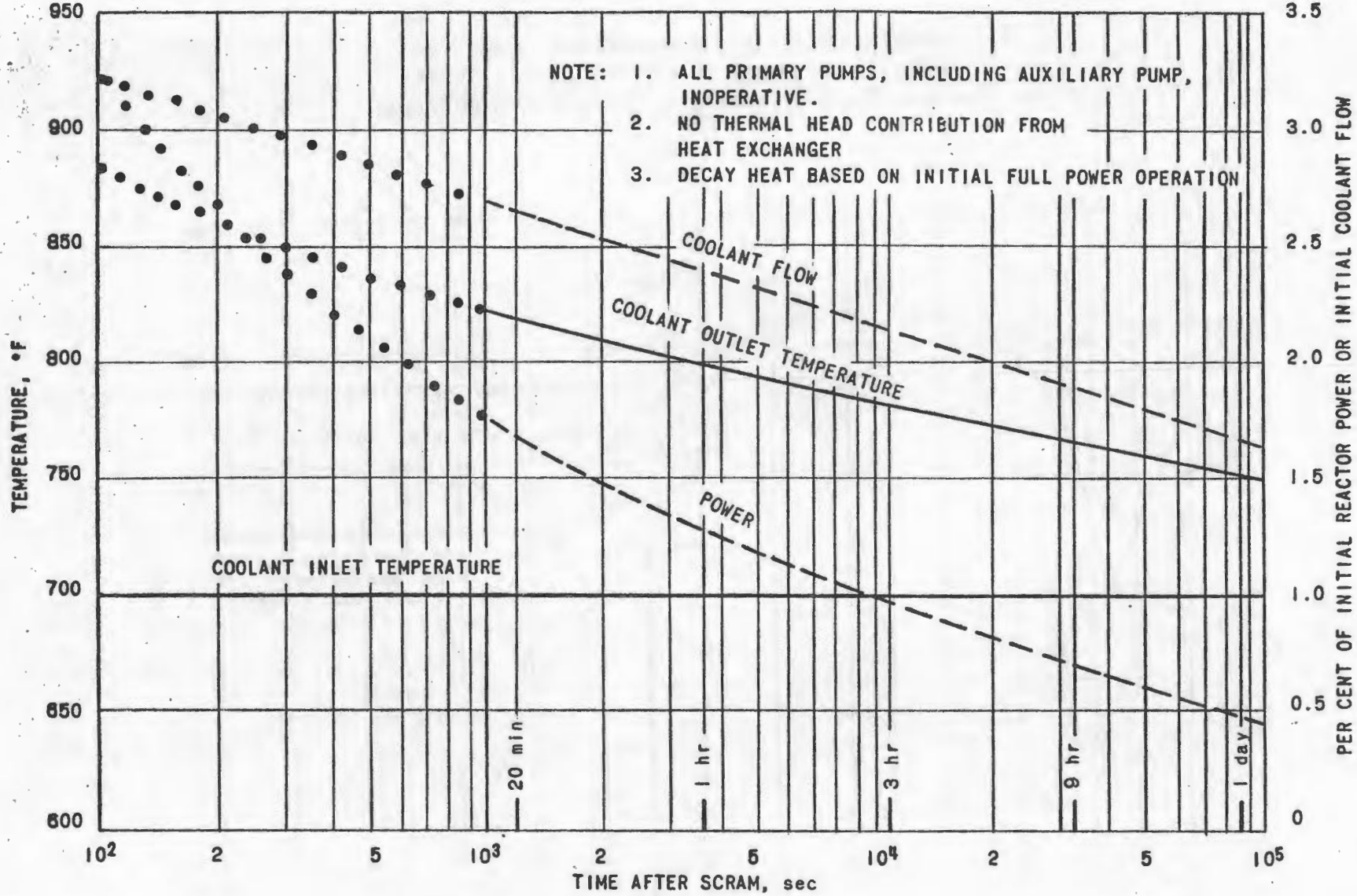

Fig. 58

Approximate Reactor Conditions during the Long-Term (Natural Convection) Cooling Process

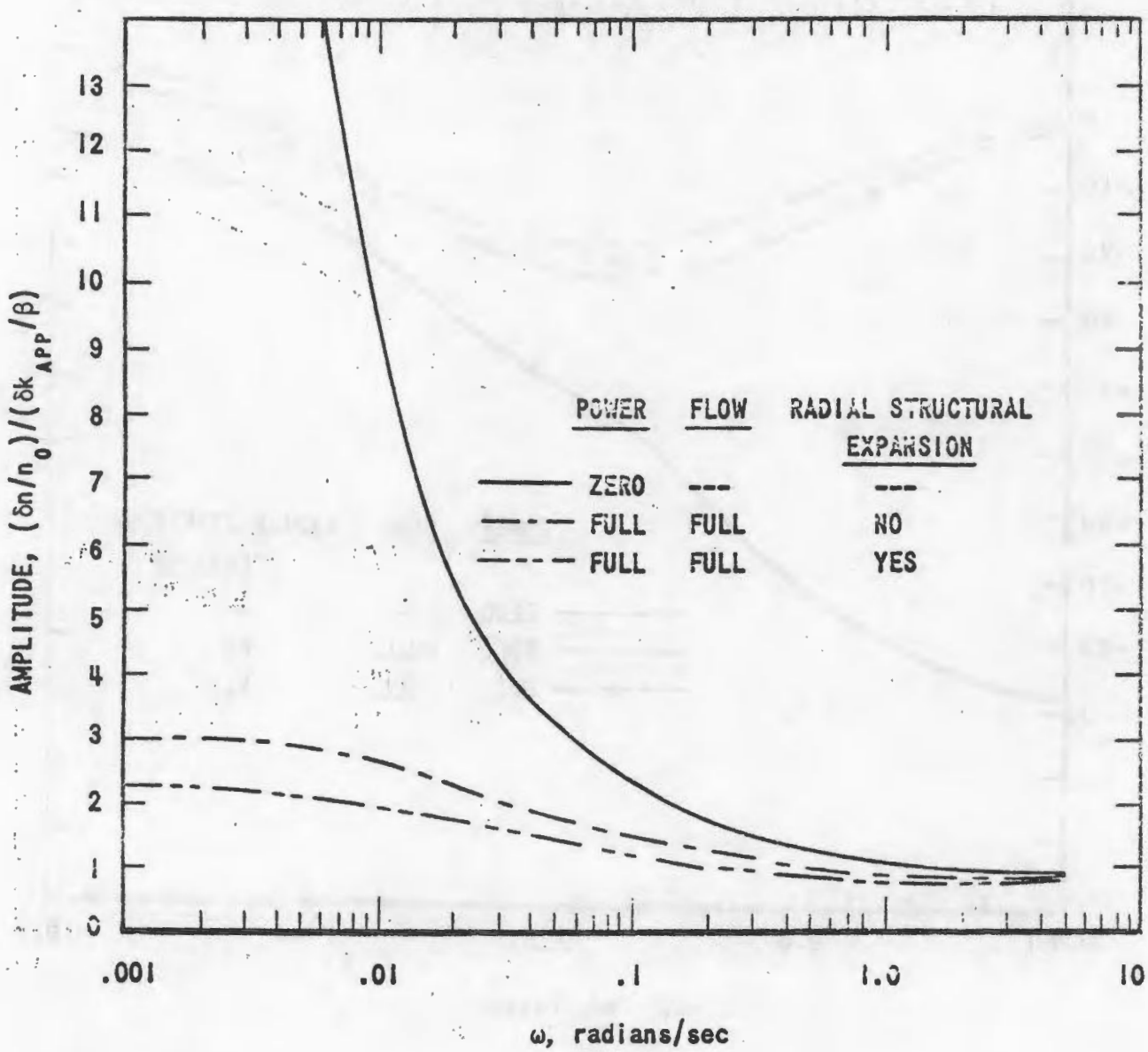

Fig. 59

Amplitude of EBR-II Closed-Loop Transfer Function

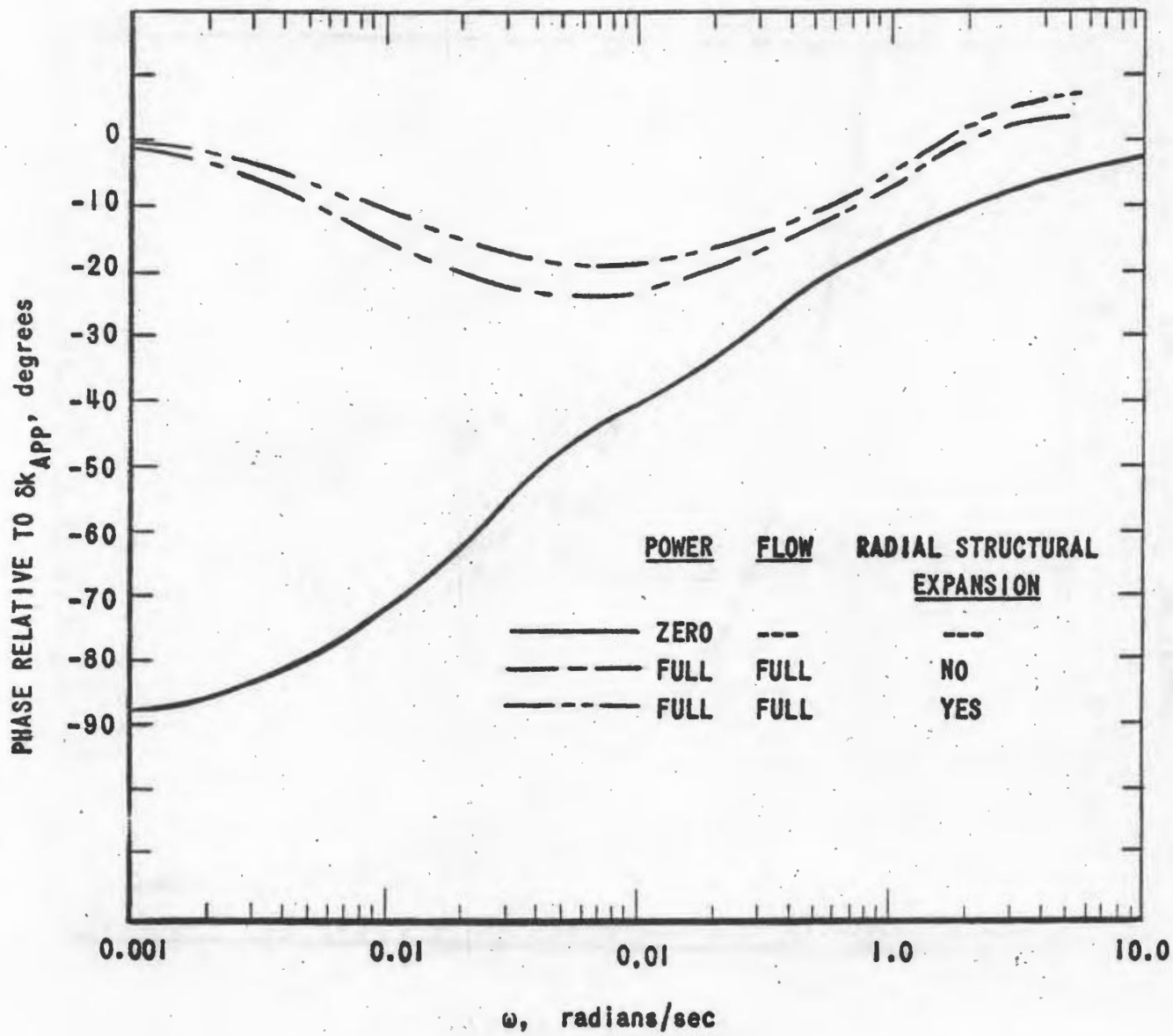

Fig. 60

Phase of EBR-II Closed-Loop Transfer Function

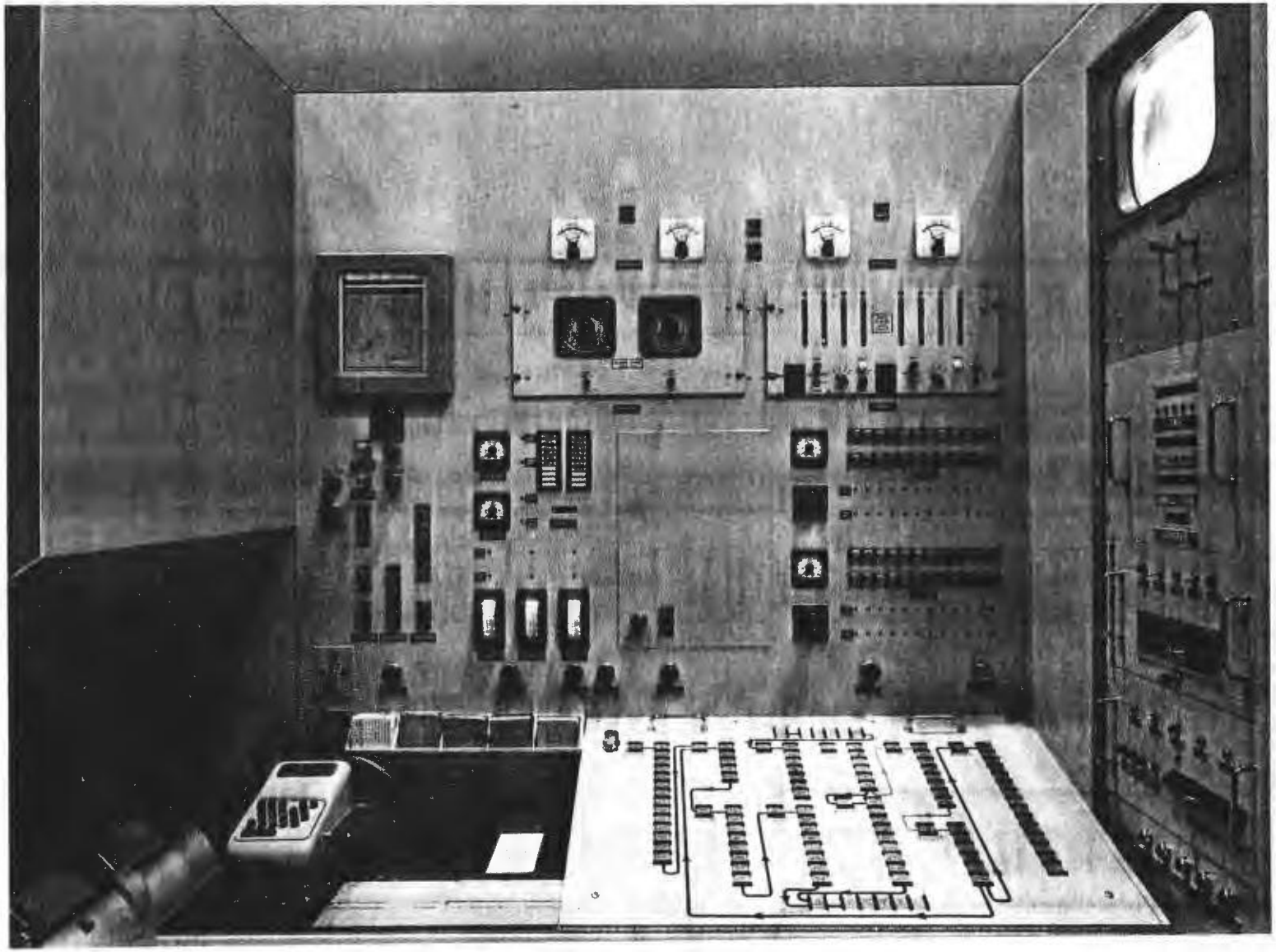

Fig. 61

Fuel-Handling Console

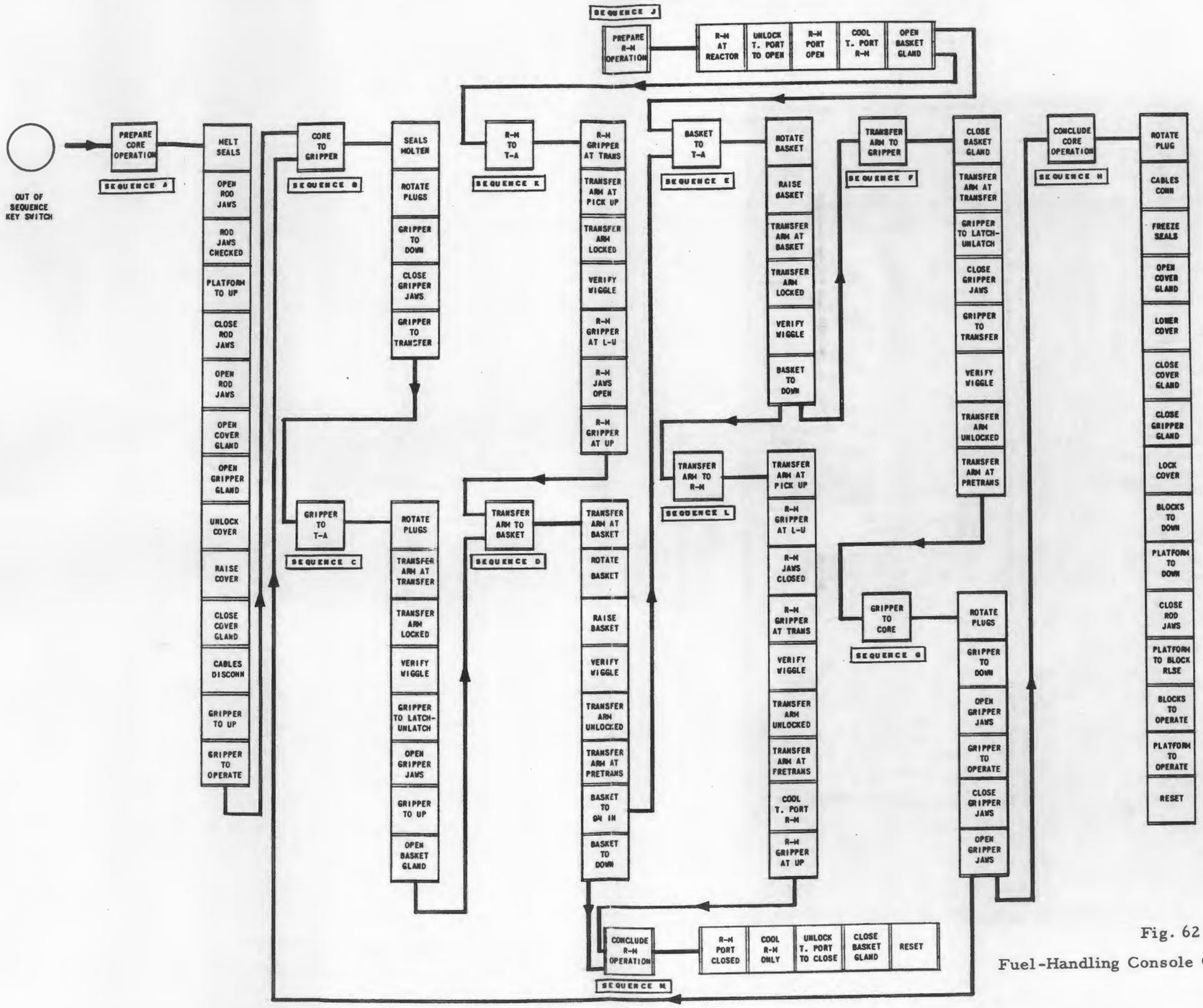

Fig. 62

Fuel-Handling Console Operating Panel

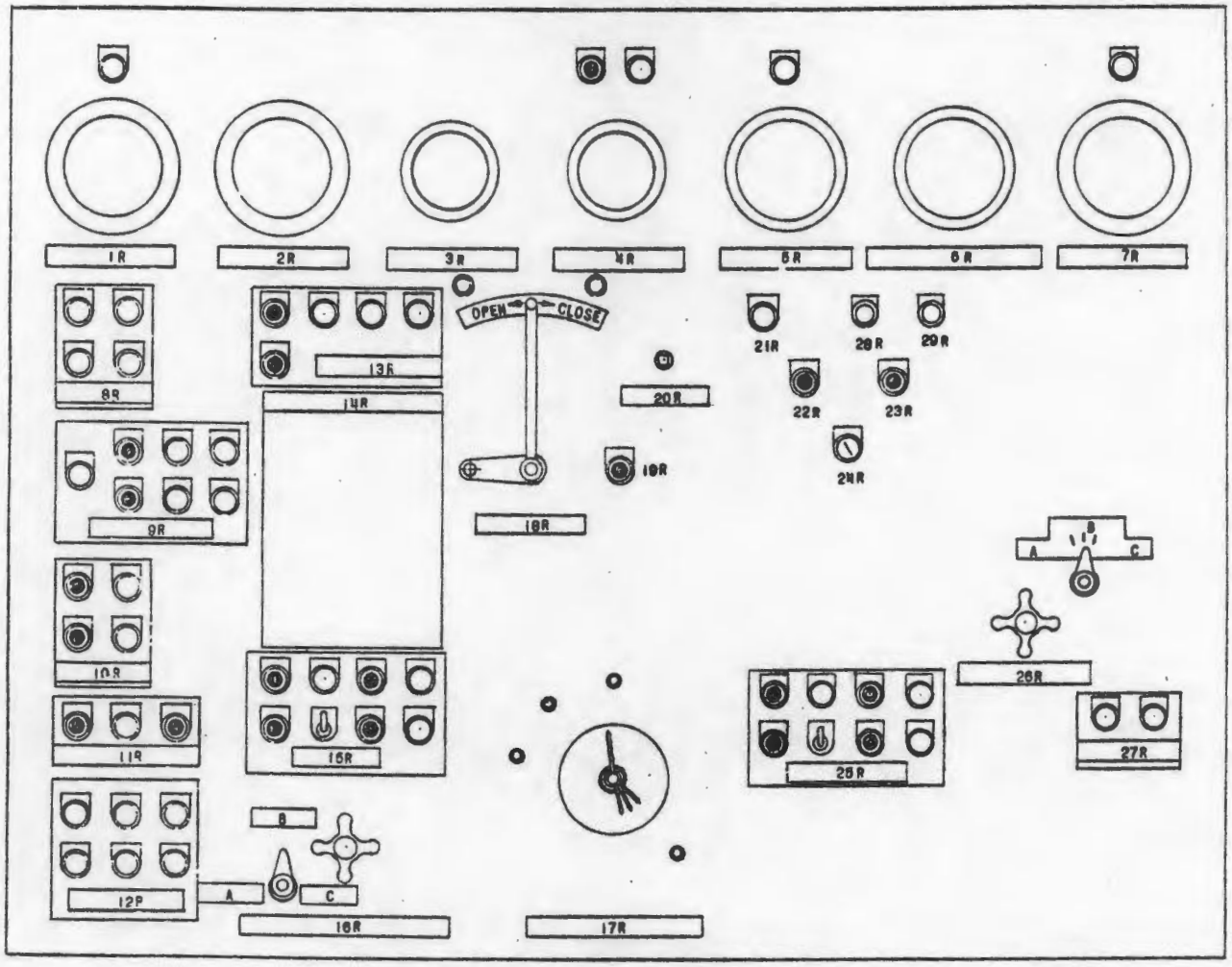

1R - ARGON TO FUEL PRESSURE INDICATOR & ALARM LIGHT
2R - ARGON FROM FUEL PRESSURE INDICATOR
3R - ARGON TO FUEL TEMPERATURE INDICATOR
4R - ARGON FROM FUEL TEMPERATURE INDICATOR RESET PUSHBUTTON & ALARM LIGHT
5R - ARGON FLOW INDICATOR & ALARM LIGHT
6R - DEMISTER DIFFERENTIAL PRESSURE INDICATOR
7R - PURGE CHAMBER PRESSURE INDICATOR & INDICATING LIGHT
8R - LOCATER PINS POSITION INDICATING LIGHTS
9R - BOTTOM SHIELD UP & DOWN PUSHBUTTONS & INDICATING LIGHTS
10R - BOTTOM SEAL RAISE & LOWER PUSHBUTTONS & INDICATING LIGHTS
11R - AIR PURGE & TEST PUSHBUTTONS & INDICATING LIGHT
12R - PORT PLUG POSITION INDICATING LIGHTS
13R - COOLING SYSTEM ON & OFF PUSHBUTTONS & INDICATING LIGHTS
14R - OPERATING INSTRUCTIONS
15R - CARRIAGE MOTOR OFF & ON, CLUTCH & BRAKE PUSHBUTTONS (N) & INDICATING LIGHTS
16R - CARRIAGE SPEED CONTROL KNOB & DIRECTION INDICATOR (A) TO REACTOR (B) NEUTRAL (C) TO COFFIN
17R - FUEL HEIGHT INDICATOR & GRIPPER POSITION INDICATING LIGHTS
18R - GRIPPER JAW HANDLE & INDICATING LIGHTS
19R - EMERGENCY STOP PUSHBUTTON
20R - SENSING CHAIN ADJUSTMENT
21R - SPRING MOTOR FAILURE ALARM LIGHT
22R - BUZZER SILENCER PUSHBUTTON
23R - BUZZER TEST PUSHBUTTON
24R - KEY SWITCH
25R - GRIPPER DRIVE MOTOR OFF & ON, CLUTCH & BRAKE PUSHBUTTONS (N) & INDICATING LIGHTS
26R - GRIPPER DRIVE SPEED CONTROL KNOB & DIRECTION INDICATOR (A) UP (B) NEUTRAL (C) DOWN
27R - FUEL TRANSFER ARM POSITION INDICATING LIGHTS
28R - COFFIN POSITION INDICATING LIGHT
29R - FUEL IMPROPERLY SEATED INDICATING LIGHT

Fig. 63

Fuel-Unloading Machine Control Panel

APPENDIX A

PROPERTIES OF FISSILE AND FERTILE MATERIAL

The EBR-II fuel is a (metallic) fissium alloy.[13] Most of the fuel irradiation experiments have been on the reference fuel for the first core (injection-cast, uranium-5 wt-% fissium alloy). Also, several specimens with variations in the amount and composition of the fissium addition have been irradiated to determine the suitability of the reference alloy. Over 100 small specimens and 17 full-length pins[20] have been irradiated in the MTR and CP-5 reactors.

The results of these irradiations have been generally encouraging. It appears that the EBR-II fuel operational objectives of 1 to 2 at-% burnup at a maximum central metal temperature of approximately 650°C probably can be realized. Varying the composition of the fissium by adding extra zirconium has little effect. This also is encouraging because the zirconium content in the EBR-II fuel will increase with repeated recycling. Not unexpectedly, the dimensional stability of the uranium-fissium alloys improves as the fissium content is increased to 10 wt-%.

The details of the EBR-II, Core I fuel element production are given in ANL-6274[21] and ANL-6276.[22] The production methods for the Core I elements were developed for ultimate application in the Fuel Cycle Facility. Development of these methods and required equipment is described in ANL-6272.[23] A prototype facility to test the methods and produce Core I elements is described in ANL-6092.[24] Fuel alloy preparation for Core I is described in ANL-6290.[25]

1. Fuel and Fuel Element Fabrication

The first loading for EBR-II was fabricated at Argonne utilizing, to the maximum extent practicable, the fabrication techniques and prototype fabrication equipment that will be used subsequently in the Fuel Cycle Facility for recycle. These operations have been reported in detail in References 21 to 24, and are briefly summarized here.

The enriched fissium alloy fuel pins were precision injection cast to size in vycor molds. The average physical and geometric properties of the as-cast fuel pins are given in Table A-1.

Table A-1

AVERAGE FUEL PIN DATA
(Enriched Uranium-Fissium Alloy)

Weight, gm	Length, in.	Pin Diameter, in.	Density, gm/cc (Calculated)
67.36	14.225	0.1438	17.795

The fuel tubes were fabricated to an inside diameter tolerance of 0.1555 to 0.1565 in. The tubes were divided into ten groups with average inside diameter increments of 0.0001 in. Fuel pins and fuel tubes were matched to produce an essentially constant sodium bond annulus (average) thickness. The bond sodium was extruded and weighed to provide the proper bond volume. Sodium bond level (height above fuel pins) was then verified by radiography.

Each fuel element was non-destructively tested for bond integrity with a cyclograph. The criterion for rejection of elements was bond defects approximating and exceeding 0.0625 in. diameter. Each completed fuel element was helium leak tested twice (two methods).

2. Thermal Cycling of EBR-II Fuel Alloy

Samples of unirradiated, injection-cast, EBR-II fuel alloy were thermal cycled between 370°C and 670°C, the approximate maximum anticipated EBR-II fuel temperatures during shutdown and operation, respectively. The sequence consisted of two hours at 370°C and one hour at 670°C, with 30-minute transfer times. The rather long holding times were used to obtain a significant degree of phase equilibrium at the two temperatures. Table A-2 summarizes the thermal cycling data. It can be seen that unirradiated fuel does not exhibit any appreciable deformation after as many as 500 cycles.

Table A-2

THERMAL CYCLING OF EBR-II FUEL ALLOY
BETWEEN 370°C AND 670°C

No. of Cycles	Change in Length, %	Change in Density, %
58	0.44* (0.30)*	-0.74 (-0.71)
150	0.65 (0.51)	-0.67 (-0.68)
300	0.66 (0.64)	-0.95 (-0.89)
500	0.75 (1.05)	-0.98 (-1.33)

*The two sets of data compare results for samples taken from the top or (bottom) of the fuel pin.

3. Irradiation Stability of EBR-II Fuel Alloy

A summary of typical irradiation results on EBR-II fuel alloy is given in Table A-3. These data extend the information contained in

[Table VI] and Reference 20. Higher total burnups at anticipated reactor operation temperatures permit a more realistic evaluation of irradiation stability for the EBR-II fuel alloy.

There is some evidence to suggest that the rate at which fuel is destroyed (fission rate) has some bearing on irradiation effects. From Table A-3 it can be seen that many of the samples were subjected to fission densities similar to those expected in EBR-II.

Table A-3

IRRADIATION EFFECTS ON EBR-II FUEL ALLOY
(Uranium - 5 wt-% Fissium)

In-Pile Thermal Cycling	Original Length, in.	Burnup, at-%	Maximum* Irradiation Temp., °C	Length Change, %	Diameter Change, %	Volume Change, %	% Volume Change / at-% Burnup	Sample Fission** Density [Fiss/cm²/sec] x 10^{-13}
Extensive	1.00	0.18	360	0.3	-0.4	0.6	3.3	6.5
Extensive	1.00	0.25	280	0.1	0.2	1.0	4.0	6.5
?	14.22	0.30	320	6.9	-	1.01	3.4	3.8
Moderate	1.00	0.45	290	1.7	0.2	0.9	2.0	5.0
Extensive	14.22	0.54	620	-	7.0	7.45	13.8	2.5
Moderate	1.00	0.71	420	2.1	-0.4	1.7	2.4	8.2
Moderate	1.00	0.78	>700	-	7.0	29.0	37.0	27.9
Extensive	14.22	0.92	620	-	-	13.2	16.3	3.1
Moderate	1.00	1.0	600	2.8	-0.4	2.3	2.3	10.8
Moderate	1.00	1.0	440	0.3	2.4	1.6	1.6	6.2
Moderate	1.00	1.1	630	5.2	-0.9	2.1	2.0	9.9
Moderate	14.22	1.3	430	-	-	3.57	2.7	10.8
Moderate	1.00	1.8	>700	2.0	2.3	9.0	5.0	11.4
Moderate	14.22	2.0	420	2.63	-	3.92	2.0	7.2
Extensive	1.00	0.35	670	6.27	4.8	15.9	45.0	5.8
Extensive	1.00	0.35	670	4.39	5.9	16.2	46.0	5.8

*Maximum nominal fuel alloy temperature in EBR-II is 656°C.

**Maximum and average fission densities in EBR-II are 1.2 x 10^{14} and 7.2 x 10^{13}, respectively.

Additional irradiation stability data on assembled EBR-II fuel elements have been obtained on samples irradiated for subsequent tests in TREAT. These samples were not disassembled after irradiation; the post-irradiation measurements (Table A-4) apply to the external dimensions of the fuel tube assembly. Comparison of data in Tables A-3 and A-4 shows that the EBR-II fuel element can accommodate substantial burnup without the resultant fuel alloy growth causing significant changes in the fuel element dimensions.

Table A-4

IRRADIATION EFFECTS ON EBR-II FUEL ELEMENTS (DIMENSIONAL CHANGES OF FUEL TUBE)
(5 wt-% Fissium Fuel Alloy)

Burnup, at-%	Maximum Temperature, °C		Bulk Volume Change, %	Diameter Change,* in.	% Volume Change / at-% Burnup	% Diameter Change* / % Burnup
	Fuel Alloy	Stainless Steel Clad				
0.58	580	550	+0.25	+0.00023	+0.43	+0.22
0.58	580	550	~0	~0	~0	~0
0.58	580	550	~0	~0	~0	~0
0.88**	440	420	+0.26	+0.00023	+0.30	+0.15
0.88	460	420	+0.35	+0.00031	+0.40	+0.20
1.4	500	480	+0.34	+0.00030	+0.24	+0.12
1.4	500	480	+0.34	+0.00030	+0.24	+0.12
1.4	500	480	+0.17	+0.00016	+0.12	+0.06
1.7	600	570	+0.43	+0.00038	+0.25	+0.13
1.7	600	570	+0.34	+0.00030	+0.20	+0.10
1.7	600	570	+0.26	+0.00023	+0.15	+0.08

*Inferred from bulk volume change. It is assumed that all volumetric growth is diametral.

**This sample represents five fuel elements under the same conditions and with similar post-irradiation properties.

The EBR-II will be an irradiation facility for its fuel in a truly fast neutron flux. A total of 105 fuel elements with special identification, have been distributed throughout 15 core subassemblies. These fuel elements, which are identical to the remainder of the loading, have been very carefully measured for weight, length, diameter, and density. It is intended that the subassemblies containing these fuel elements will be located in core positions with coolant outlet thermocouples. These subassemblies will be removed at intervals and the seven special fuel elements contained in each will be examined to determine the behavior of the fuel as operation proceeds and to aid in establishing the allowable fuel burnup.

4. Phase Characteristics of EBR-II Fuel Alloy

The phase characteristics of uranium-fissium are similar to those of the U-Mo-Ru ternary system.[13] For reactor operation, the interesting phase transformation is that from the predominantly alpha phase to the predominantly gamma phase. This transformation occurs at about 550°C (~1020°F). The temperature distribution in the fuel pins suggests that the center of the pins would be predominantly gamma phase, while the surface of the pins would be predominantly alpha phase. It is believed that material being irradiated at alpha-phase temperatures tends to at least partially transform to gamma phase. If this is the case, after a small amount of irradiation, the gamma phase may be present in greater amounts than in unirradiated pins.

The transformation kinetics of the 5 wt-% fissium alloy are relatively slow and have no bearing on instantaneous reactor conditions. A complete transformation from alpha to gamma phase would exhibit itself as a long-term reactivity drift. The complete transformation would result in a 1.4% density decrease. If this density change is isotropic, the long-term reactivity drift will require about 0.14% $\Delta k/k$ compensation. This is equivalent to the insertion of about 5 in. of control rod.

5. Blanket Uranium

Both the radial and axial uranium blankets (where the bulk of the breeding takes place) contain unalloyed beta-treated, depleted (~0.2% U^{235}) uranium metal pins (min. density = 18.7 gm/cc). The pins are contained in stainless steel tubes with a static sodium bond in the annulus between the pin and the tube.

Fuel alloy burnup limitations dictate the removal of axial blanket uranium because it is contained in the same subassembly. Since the anticipated fuel alloy burnup will not exceed 2 at-%, the burnup in the axial blanket uranium will not exceed 0.1 at-%. Consequently, there is no anticipated irradiation problem for the axial blanket; the nominal uranium temperature does not exceed 1050°F (566°C).

Nominal uranium temperatures in the outer blanket will not exceed 932°F (500°C). Maximum localized burnup of uranium and buildup of plutonium are estimated at 0.02 at-% and 0.1 at-%, respectively, per reactor core cycle (1.0 at-% burnup of the fuel). Most of the outer blanket is subjected to both lower temperatures and burnup rates, thus allowing long in-pile residence.

Operation of the inner blanket subassemblies may be limited by irradiation damage; consequently, the subassemblies may require recycling more frequently than desired for optimum plutonium production, economics, etc. Maximum local burnup and plutonium buildup are estimated at 0.09 at-% and 0.2 at-%, respectively, per reactor core cycle. The calculated maximum uranium (nominal) temperature is 1100°F (593°C). At this temperature, substantial uranium swelling might be expected. It is thought, however, that the blanket element clad (0.018 in. thick stainless steel) will restrain swelling sufficiently to enable achievement of a few tenths per cent burnup. Only a small number of subassemblies will be subject to this high temperature and correspondingly limited in burnup.

About 90% of all plutonium production in EBR-II occurs in the blanket regions. The over-all breeding characteristics of the system are independent of the blanket cycle, but economics are not. The inner blanket will provide an irradiation environment to permit evaluation of blanket alloys. It is also a convenient location for experimental irradiation of fuel and structural materials.

6. Enrichment of EBR-II Fuel Alloy - Analysis After Fabrication

The enrichment (U^{235} content in U) of the EBR-II fuel alloy was specified at 48.4 at-% (48.08 wt-%). This requirement is based on both experiment and analysis (see Section IV.I.3.).

Eighty-five process batches, each containing 10 kg of 5 wt-% fissium alloy were prepared.[25] In each case, calculated uranium enrichments (based on constituents in the 10-kg batch), were compared with batch sample analyses. Table A-5 lists the specified U^{235} and U contents and the corresponding results from fuel alloy batch analyses.

Table A-6 shows the typical fissium alloy, uranium, and U^{235} content of completed core subassemblies.

Table A-5

URANIUM CONTENT AND URANIUM ENRICHMENT OF THE 5 wt-% FISSIUM ALLOY
(Data from Reference 25)

	Specified	Obtained from Batch Analyses*
Wt-% U^{235} in U	48.08 ± 1.2	48.09 ± 0.10
At-% U^{235} in U	48.40 ± 1.2	48.41 ± 0.10
At-% U^{235} in Fissium	42.99 ± 1.06	42.88 ± 0.23
Wt-% U in Fissium	95.00 ± 1.0	94.90 ± 0.1
At-% U in Fissium	88.82 ± 0.95	88.58 ± 0.28

*Average for 85 batches (ingots). Individual batches differ by less than 1.1% from the average values.

Table A-6

FISSIUM ALLOY, URANIUM, AND U^{235} CONTENT OF TYPICAL CORE SUBASSEMBLIES

Subassembly No.	Total Weight, gm			Subassembly No.	Total Weight, gm		
	Fissium Alloy	Uranium	U^{235}		Fissium Alloy	Uranium	U^{235}
C-100	6123.80	5817.58	2801.05	C-113	6142.99	5835.84	2808.83
C-101	6116.30	5810.44	2858.28	C-114	6170.76	5862.02	2821.27
C-102	6123.94	5817.74	2798.32	C-115	6198.86	5888.54	2834.09
C-103	6140.09	5833.08	2807.00	C-116	6196.70	5886.26	2833.26
C-104	6136.76	5829.91	2805.00	C-117	6199.65	5889.59	2833.95
C-105	6130.37	5823.80	2804.16	C-118	6213.74	5903.06	2841.97
C-106	6127.56	5821.18	2801.18	C-119	6189.54	5879.96	2830.10
C-107	6132.90	5826.25	2804.10	C-120	6207.19	5896.78	2838.46
C-108	6114.54	5808.80	2794.80	C-121	6212.98	5902.23	2841.74
C-109	6118.87	5812.90	2798.81	C-122	6169.16	5860.62	2820.65
C-110	6134.24	5824.38	2802.48	C-123	6172.59	5867.46	2823.64
C-111	6132.16	5830.30	2806.23	C-124	6208.09	5897.64	2840.55
C-112	6140.08	5830.05	2806.58	C-125	6203.66	5893.48	2855.40

APPENDIX B

COMPONENT TESTS

1. Mechanical Stability and Integrity of Core Subassemblies

A series of investigations were conducted to determine and to assess the mechanical integrity of the fuel elements and subassemblies. Some of these experiments were conducted in conjunction with other investigations such as the determination of pressure drop, flow characteristics, etc. Of particular concern was the stability and integrity of these units under the hydrodynamic and mechanical forces which would (or could) be exerted during reactor operation.

a. Hydrodynamic Tests in Water

A clear plastic hexagonal tube was constructed with the internal dimensions of the EBR-II core subassembly. The standard complement of 91 fuel elements was assembled into this test section and the unit installed in the water test loop. The loop was operated at varying flow rates and pressures, and high-speed motion pictures were taken to determine if vibration of the fuel elements was induced under any conditions which could be generated in the reactor. There was no observable vibration. At the conclusion of the test, examination of the fuel elements revealed no evidence of vibration such as galling or wear.

The exit coolant from blanket subassemblies flows radially outward in the upper plenum of the reactor. Accordingly, test apparatus was constructed to provide flow across the top of a blanket subassembly to determine if significant vibration of the subassembly could be induced by the flow past the subassembly upper adapter. A series of runs was conducted at varying flow velocities and varying flow patterns without developing any indication of vibration. (Subsequent investigations on the scale model test at The Franklin Institute revealed that the actual flow across the top of the subassemblies was considerably lower than had been estimated.)

b. Hydrodynamic Tests in Sodium

Tests were conducted on core subassemblies and control subassemblies in a 4-inch pipe sodium loop primarily to determine flow characteristics and pressure drop (as described in Appendix C). A second objective of these tests was to determine the behavior of the fuel elements in their closely-packed configuration within the subassembly under the approximate thermal and hydrodynamic conditions which will exist in the reactor. It should be emphasized that these tests were conducted under isothermal temperature conditions, as the reactor temperature gradients could not be simulated.

Two core subassemblies were tested. The first was run for approximately 600 hr with sodium temperatures of 300°F to 875°F, and average sodium velocities from 2 to 25 fps. The second was run for 732 hr at sodium temperatures of 500°F to 960°F, and sodium velocities from 3 fps to 26.2 fps. There was no evidence of fuel element warpage or vibration (rubbing) as can be seen in Figs. B-1 and B-2.

The tests on the control subassembly included operation of the control rod. This test accumulated 580 hr of operation with a sodium flow of 150 gpm at 950°F through the subassembly, plus 160 hr of operation with flow rates of 20 to 150 gpm at 600°F to 950°F. During this period, the control rod was mechanically cycled 1,680 times (between "full up" and "full down" positions) at the high-flow, high-temperature conditions. Engagement and disengagement of the control drive gripper and the control rod was performed twice each week for 17 weeks. Again, there was no evidence of distortion of the fuel elements or the control rod, and no evidence of wear on the moving parts of the control rods other than a trace wiping of the aluminum bronze lower bearing.

c. Mechanical Strength of Core Subassemblies

In addition to the normal operating forces, the subassembly is exposed to "push" and "pull" forces during fuel-handling operations. Of particular interest was the tensile strength of the subassembly; excessive pulling forces might be required in the event of "sticking" in the reactor. Forty subassemblies, with the internals omitted but with standard upper and lower end fittings spot welded to the hexagonal tube in accordance with production methods, were pull tested to destruction. The minimum room-temperature tensile strength obtained was 12,000 lb, and all failures occurred by tearing the hexagonal tube at the spot welds. Twenty similar tests were conducted on control and safety rods with failure occurring at tensile loads of 13,000 to 16,000 lb. This provides a large safety factor over the 400-800-pound maximum load limit for which the gripper mechanism is normally set (and the 3000-4000-pound maximum limit to which it could be set, if required).

d. Mechanical Strength of Fuel Elements

The fuel elements are attached to a parallel plate grid consisting of T-shaped plates to which the end fittings of the fuel elements are "hooked" (see Fig. 7). The strength of this connection was determined in a tensile testing machine; it was found that a tensile force in excess of 180 lb per element was required to cause separation. The mode of failure in each case was by spreading of the horseshoe-shaped fuel element tips with the tip springing free of the T-bar without tearing metal. The only pulling force exerted on the fuel elements is the hydrodynamic force of the coolant flowing around them, and the strength far exceeds the maximum

force which can be imposed. It should also be noted that during the flow testing of subassemblies described earlier there was no evidence of separating or loosening of this connection.

2. Control Rod and Safety Rod Drive Mechanisms

a. Control Rod Drive Mechanisms

Two control rod drive mechanisms were built for purposes of testing under a variety of operating conditions. The first of these drive units was similar to the final design except for a slightly different gripper mechanism and a somewhat shorter drive shaft. Also, the gripper-sensing device was not included. A control subassembly (rod and thimble) similar to the final design was included as part of the test equipment. This drive mechanism was cycled approximately 300 times in air. One complete cycle consisted of raising, and then lowering, the control rod the entire 14-inch stroke permitted by the drive unit. The drive mechanism was then installed in a sodium loop and tested for a period of approximately four months. The sodium temperature was varied from 300°F to 900°F during these tests. A total of 13,000 cycles were successfully completed during the four-month period.

The second control rod drive mechanism tested was identical to the final design of the units for the reactor with the exception of having a shorter drive shaft and other minor modifications to accommodate the experiment in the available laboratory space. The control rod and thimble were identical to the final design for the reactor. The drive unit successfully completed 21,000 cycles in air, and 1,700 cycles in sodium. The temperature of the sodium was varied from 300°F to 960°F during these tests. In addition to these cycle tests, approximately 35 scram cycles (a portion of these in sodium) and 15 rod-gripping operations were accomplished. A scram cycle consisted of raising the rod the full 14 in. inside the thimble and then effecting a scram release (disengagement) which rapidly ejected the rod drive downward with the force of gravity plus the force derived from the scram-assist cylinder. Pneumatic cylinder assist pressures up to 50 psig were used. (Pressure of about 25-35 psig will be used in reactor operation.) The rod-gripping operations consisted of gripping and releasing the control rod upper adapter by means of the gripper mechanism.

Although only twelve control rod drive mechanisms are required for the EBR-II, fourteen drives of final design were fabricated. All fourteen drives were briefly tested by the fabricator prior to shipment. This testing was accomplished in air by the previously described general methods of stroke cycling, scram cycling, and rod-gripping operations.

Certain of the time displacement data obtained from control rod scram tests are summarized in Fig. B-3. Time is computed from the instant a scram signal is received at the rod drive. The scram tests were made with air cylinder pressures of 0, 25, and 50 psig. The data from the 0-psig and 50-psig tests, only, are presented as a pair of curves at each pressure. The data from all fourteen drive units fell between the two curves at the specified air pressure. It will be noted that the two curves for the 50-psig pressure converge at approximately 0.3 sec after receipt of the scram signal and show that all control rods had completed their full 14-inch stroke within this time. However, the curves for the 0-psig pressure do not converge within the time scale of the graph. This is due to the longer time required to traverse the last 5 in. of the stroke during which the rod is being decelerated by the hydraulic dashpot. The dashpot is designed to decelerate the total rod and drive mass in 5 in. after being accelerated at about 2 g. At the lower acceleration rate experienced with zero pressure, the rod enters the dashpot zone at considerably lower velocities and, because of the fixed characteristics of the dashpot, requires much more time to traverse this portion of the stroke. The result is that more than 0.5 sec are required for the rods to drop the full 14 in.; however, the first 10 in. of rod travel is accomplished in approximately 0.23 sec (about 0.07 sec longer than with 50-psig assist). It is intended that the scram-assist air pressure employed in the EBR-II operation provide a rod acceleration of 1.5 g. It may be estimated from the displacement-time curves that the required air pressure is approximately 25-35 psig. (The exact pressure will be obtained from curves based on subsequent tests in sodium.)

Of the fourteen drives fabricated, thirteen were shipped to the construction site and one was retained at the Laboratory for further testing. This unit was tested extensively and operated very satisfactorily in air (room temperature and heated), and in sodium. The tests included the following operations:

Environment	Operating Cycles	Gripper Operations	Scram Cycles
Air (room temp)	900	20	120
Air (800°F)	700	6	5
Sodium (750°F)	1100	18	80

After installation of the twelve rod drives in the reactor, each unit was tested extensively in air for all functions and correctness of all control wiring. This testing was conducted immediately prior to approach to dry critical and during the Dry Critical Experiments.

b. Safety Rod Drive Mechanism

The complete safety rod drive mechanism was tested as a unit prior to shipment to the EBR-II site. These tests were performed in air at room temperature. The mechanism was scrammed approximately 100 times using simulated safety rods. A curve of safety rod displacement vs time during scram is presented in Fig. B-4. The total time required for complete scram travel is about 0.320 sec, with the first 9 in. of travel occurring in approximately 0.2 sec. The shock absorbers of the drive mechanism were tested separately, in addition to testing of the complete unit. In these tests, the shock absorbers were scram cycled approximately 50 times, using weights equal to those of safety rods.

After installation of the safety rod drive mechanism in the reactor, it was retested prior to the approach to dry critical. This was done to insure proper mechanical operation and correctness of control wiring.

3. Fuel-Handling System Components

a. Packing Gland

Sealing of the reactor vessel cover-lifting column shafts, the storage rack shaft, and the gripper and holddown shafts, to prevent loss of the argon blanket gas is complicated by the fact that large axial movements of the shafts occur and, except for the cover-lifting columns, the shafts also rotate.

To meet these requirements, each shaft is sealed with a compression-type packing gland which differs only with respect to shaft size. The packing gland is motorized for remote-controlled operation. It is mounted on a standpipe which bolts to the flange of the nozzle (in the primary tank cover or small rotating plug) through which the shaft passes. Figure B-5 shows a complete packing gland assembly.

The packing gland is enclosed in a separate housing for ease of installation and maintenance. It consists of two sets of four split standard form, asbestos rings. Each ring is 0.5 in. square in cross section and contains a graphite lubricant. The two sets of rings are separated by a metallic spacer; this provides a gap for bleed-in of argon gas to reduce the leakage rate, if necessary.

When the shafts are not in use, a pressure plate is driven down to exert a uniform compressive force on the packing and the shafts are tightly sealed. Prior to either rotation or translation of the shafts, the pressure plate is driven up to reduce the amount of compression in the packing. The prime objective of the design is to provide adequate sealing whether the shafts are stationary or in operation.

A full-scale prototype packing gland assembly was tested for four months under simulated operational conditions to verify the leak integrity of the seal under both conditions of packing compression. The assembly was mounted on a tank containing sodium. An argon gas blanket was maintained above the sodium vessel. The temperature was maintained at 750°F and the argon gas blanket slightly pressurized. The pressure connection was then sealed off from the gas supply and the pressure in the vessel observed and recorded for several days. The following leak test rates were measured by this method:

(1) With the packing gland tight and with no bleed-in of gas to the gland, the leak rate was 0.001 ft^3/hr for a blanket gas gauge pressure of 2 in. water.

(2) With the packing gland loose (such that movement of the shaft through the gland was possible) and with no bleed-in of gas to the gland, the leak rate was 0.003 ft^3/hr for a blanket gas gauge pressure of 2 in. water.

Both leak rates are acceptably low.

b. Rotating Plug Freeze Seals

The purpose of these seals is to prevent gases from leaking into, or out of, the primary tank around the peripheries of the rotating plugs. Each seal consists primarily of a vertical circular "blade" (skirt) attached near the periphery of each plug, and a mating trough attached to each plug stationary support. The blade moves within the trough, which contains a low-melting point "Cerrotru" alloy (58% bismuth - 42% tin; M.P. 281°F). The alloy expands upon freezing.

An approximate model of the seal (about 36 in. diameter and 12 in. high) was constructed and is shown in Figs. B-6 and B-7. Various tests were made on this model, including alternate freezing and melting cycles, determination of heating and cooling requirements and ease of rotation, and leak testing. Preliminary experiments indicated that upon freezing, the "Cerrotru" separated from the vertical surfaces of the blade and trough, permitting gas leakage under pressure. Accordingly, a system in which only the upper half of the alloy in the trough was frozen was pressure tested and found to be a satisfactory solution.

With the seal in the half-frozen state the model successfully sustained pressure differentials up to 5 psi (the normal pressure differential will be only a few inches of water). Even in the molten condition the seal was capable of withstanding a pressure differential of approximately 0.5 psi. Based upon these preliminary tests, the two rotating plug seals were designed to incorporate the following features:

(1) "Fire-Rod" heaters (for melting the "Cerrotru") are located at two different levels within the blade. The heaters at the upper level are used only to heat the seal to the molten condition. The heaters at the lower level, which are in direct contact with the "Cerrotru," are used for maintaining both the half-frozen condition and the molten condition.

(2) At each level, the heaters are spaced circumferentially about 7 in. apart; heaters at the upper level are spaced midway between the lower level heaters. The lower level heaters are connected by a heavy copper ring to reduce circumferential temperature gradients.

(3) The seals are cooled by flow of shield cooling air past one side of each trough.

(4) Thermocouples are provided for measuring "Cerrotru" temperatures at four different levels. At each level, the thermocouples are spaced circumferentially about 15 in. apart. The first (top) level of thermocouples must indicate that the "Cerrotru" is safely above the melting point before plug rotation is permitted. The fourth (bottom) level thermocouples provide overheat protection. A portion of the third level thermocouples are used for controlling the molten condition. A portion of the second level thermocouples are used for controlling the half-frozen condition. The remainder of the second and third level thermocouples are used for verification of the half-frozen condition and for alarm (in the control room) if the condition is abnormal.

To test the operation of this seal design, a mock-up of the seal, full-scale in the vertical and radial directions, and about 2 ft long in the circumferential direction, was constructed and operated. Some of the information gained from the mock-up, and from extensive supplementary analyses and electrical analog studies, is listed below:

(1) The heaters can maintain any condition desired, using only a fraction of their rated capacity. This should insure long heater life.

(2) In the half molten-half frozen condition, the temperature difference from bottom to top of the alloy was only about 35°F, a situation tending to aggravate control problems. Analysis of the design indicated that the addition of cooling fins to the upper half of the trough exposed to the cooling air should increase this ΔT to 50°F. Fins were therefore provided on the seal troughs.

(3) Changing the seal from the half molten-half frozen condition to the completely molten condition takes about 1 hr. The seal returns to the half molten-half frozen condition from the completely molten condition (all heaters off) in about 1.5 hr.

(4) In the half molten-half frozen condition, the third and fourth (bottom) level thermocouples, which are in the molten region, indicate very little change in temperature so long as any part of the seal is frozen. The second level thermocouples do indicate the condition of the seal and are employed to control the half molten-half frozen condition.

(5) Setting the completely molten condition control point at about 350°F will insure that it is impossible for frozen alloy (281°F) to exist anywhere between the indicating thermocouples.

c. Gripper Mechanism Load Limit Tests

An important design feature of the gripper mechanism is the force-limiting function which controls the push and pull force applied to a subassembly during fuel handling. The device used to effect force limiting is complicated by the fact that it is necessary for the device to differentiate between the force applied on the subassembly by the mechanism, and the force required to move the gripper shaft. The latter force has two components: the friction between shaft and packing gland (variable), and the weight of the shaft. A friction compensator device is employed to differentiate between these two components. The design allows a wide range of force-limit settings (approximately 400-4,000 lb) which are easily adjusted.

A prototype of the force-limit assembly was operated for about 200 cycles at several force-limit settings over the approximate range 400-800 lb, to verify the accuracy and reproducibility of this design feature. It was found that the actual force-limit setting was reproducible and accurate to within 50 lb, which is adequate.

d. Gripper Tests in Sodium

The gripper mechanism gripping device [Fig. 30] (which engages the upper adapter of the subassemblies), and the two gripper bellows (one of which provides the sodium seal between the main shaft and the jaw-actuating shaft, the other between the jaw-actuating shaft and the sensing-rod shaft) were thoroughly tested in sodium at 800°F.

The test cycle employed consisted of lowering the gripper into a tank of sodium, closing the jaws over the top end of a simulated subassembly, raising the subassembly, lowering it, releasing the gripper jaws, and raising the gripper. This operation was performed for about 15,000 cycles. Upon conclusion of the test, the gripper jaw assembly was removed and inspected. It was found to be in satisfactory condition with insignificant evidence of wear.

The gripper bellows were cycled through a 2.25-inch stroke (design value) while submerged in the 800°F sodium. The bellows developed a small leak (noted by a loss in pressure within the vessel) after 9,540 cycles. This performance was considered adequate since the test was estimated to represent at least twenty years of normal operation in EBR-II.

4. Fuel-Unloading System Components

a. Fuel-Transfer Port Tests

The fuel-transfer port (Fig. B-8) provides access to the primary tank for refueling operations. It is employed to seal the opening into the primary tank to prevent entry of air and the escape of blanket argon gas. The fuel-transfer port is, basically, a large valve. When closed, it provides a gas seal for the fuel transfer opening in the primary tank. When open, it provides access to the primary tank through which the fuel-unloading machine gripper may pass to insert or remove subassemblies.

A second function of the port is to shield personnel on the operating floor from radiation streaming upward through the fuel transfer tube from the primary tank.

To accomplish these objectives, a special type of valve is used. It may be described as a short cylinder, supported on shafts extending from each end, with a hole through the cylinder along one of the diameters. When the cylinder is rotated in its housing until the hole lines up with the openings in the housing, there is an unobstructed path through the valve into the primary tank. When the cylinder is rotated 90° from this open position, the hole is at right angles to the openings in the housing and closes them completely. The cylinder is filled with lead to provide approximately 10 in. of lead shielding above the hole into the primary tank.

The gas seal is effected by four "O" rings set in grooves, in the curved surface of the cylinder. One "O" ring encircles each end of the 3 in. dia. hole through the cylinder. These seal when the port is open, reducing the possibility of either argon gas leaking out into the reactor building, or inleakage of air into the primary tank. The remaining two "O" rings are set 90° from each of the above "O" rings to seal the openings in the housing when the port is closed.

The shafts supporting the rotating port are sealed with silicone "O" rings to provide a back-up seal to the four "O" rings on the rotating port.

Several tests were conducted on both a mock-up and the actual fuel-transfer port to verify the leak-tightness of the seals. The mock-up tests were conducted with a helium leak detector, using a wide range of conditions of pressure and seal cleanliness to assure the validity of results. These are summarized as Tests Nos. 1, 2, and 3.

Test No. 1

The section of the port above the seal was pumped down to a vacuum of approximately 100 microns and helium was introduced into the section of the port below the seal. All sealing surfaces and the "O" ring were clean and dry. No leakage of helium could be detected.

Test No. 2

The lower section of the port, below the seal, was pressurized with helium to 20 in. of water. The helium detector was introduced in the section above the seal. The "O" ring and sealing surfaces were clean and dry. No leakage could be detected.

The above procedure was then repeated several times using helium pressures of 15 in., 10 in., and 5 in. of water pressure, respectively. No helium leakage could be detected under any of these conditions.

Test No. 3

To determine what effect a deposit of sodium oxide on the sealing surfaces would have on leakage, a quantity of metallic sodium was burned in the lower section of the port mock-up. The oxides of the sodium deposited on all interior surfaces including the "O" ring and its sealing surface. The port was then closed and the lower section pressurized with helium as in Test No. 2. No leakage could be detected past the seal. Additional checks were made by opening and closing the port repeatedly, probing frequently with the leak detector. No leakage could be detected.

Test No. 3 was then repeated after burning more sodium in the lower section of the port until the "O" ring and its sealing surface appeared to be completely covered with flakes and granules of sodium oxide. This is probably the worst condition conceivable for seating and sealing the "O" ring. No leakage was detected past the "O" ring under these conditions. This concluded the series of tests on the mock-up fuel-transfer port.

Leakage tests were then conducted on the fully-assembled fuel-transfer port. All tests were performed by pressurizing the interior of the port housing with helium to 20 in. of water, and using the probe (sniffer) attachment of the leak detector. These tests are summarized as Tests Nos. 4, 5, and 6.

Test No. 4

All interior openings in the port housing were sealed, including the lower mounting flange, the top flange (or mating surface for the refueling machine) and argon cooling gas inlet and outlet pipes. Helium was introduced through the argon cooling inlet pipe to the interior of the housing until a pressure of 20 in. of water was obtained. The helium detector probe was passed over all weld joints, bolted joints, machine screw penetrations, and shaft seals. Helium leakage was detected at two locations where shoulder screws (which position the lower "O" ring seats) penetrate the housing. A silicone grommet was installed on each shoulder screw and no further leaking was detected. The housing was then re-checked completely and found to be leaktight.

Test No. 5

The general test procedure was similar to Test No. 4, except that the temporary seal at the top flange (mating surface) was removed and the rotating port was closed. The housing was again pressurized with helium as in Test No. 4, and the probe inserted in the fuel transfer opening in the top flange. No leaks were detected at the rotating port "O" ring seal.

Test No. 5 was repeated several times, by opening and closing the port, to determine if "O" ring seal on the rotating port would seat properly after being removed. No leakage was detected after any of the rotations.

Test No. 6

A further check was made to determine if any small leaks existed which were not found by the preceding tests. The procedure used in Test No. 5 was followed and the helium gas pressure was maintained for 1 hr. Subsequently, the detector probe was passed over all welds, bolted joints, seals, etc. No leakage was detected at any point.

b. Fuel-Unloading Machine Tests

The fuel-unloading machine has been described briefly in Section III.A.7.b., and is shown in Fig. 22. It is used to transfer subassemblies between the primary tank and the interbuilding coffin (which, in turn, provides transport to the Fuel Cycle Facility). The following tests were conducted (or are being conducted) on specific parts of the fuel-unloading machine and the machine assembly:

(1) Gripper Drive Assembly Test

The gripper drive assembly enables the fuel-unloading machine to reach into the primary tank or the interbuilding coffin; to grip a subassembly by its upper adapter; to raise or lower it about 26 ft; to cool it or to heat it during this motion; to release it in the proper sequence; and to indicate the distance of vertical travel and the (subassembly engagement) sensing information on the control panel.

The tests on the gripper drive assembly included the gripper chain, gripper travel, sensing features, gripping and releasing, indicator readings, and over-all performance checks. All tests were performed satisfactorily in dry air: 45 cycles at room temperature; 20 cycles at 400°F; and 10 cycles at 750°F.

Similar tests will be conducted with the gripper end submerged in sodium at 750°F.

(2) Carriage (Dolly) Travel Test

A self-propelled carriage operates on rails between the transfer port location and the interbuilding coffin station. It is used to transport the shield coffin and other parts of the fuel-unloading machine between these points. In order to test the carriage under the proper load, lead bars were added to bring the total weight to approximately 34 tons. The carriage deflections, rails, the drive, and the carriage stops, were checked and performed satisfactorily.

(3) Retractable Shield Actuating Mechanism

Attached to the bottom of the shield coffin is a doughnut-shaped shield ring. This ring is lowered over the upper end of the transfer port or the interbuilding coffin with the aid of four locating pins whenever a fuel subassembly is transferred. The 2.5-inch vertical movement, the drive assembly, and the rotating pin alignment, were tested with satisfactory results.

(4) Rotating Shaft Seal Tests

Eight rotating shafts extend into the sealed upper plenum of the gripper drive assembly. Six shafts use "Eccentric Shaft Seals" and two use "Double 'O' ring hydrostatically pressurized seals." Both types of seals were tested repeatedly at room temperature, and at operating speeds, using helium or freon at 7 psig. There was no detectable leakage after 48 hr of operation.

(5) Leak Test of Gripper Drive Assembly

The leak-tightness of the complete gripper drive assembly was tested using 7-psig freon at room temperature. (Since this assembly consists of many parts, great care was taken in preparing and tightening all joints.) There was no detectable leakage after a 7-day period.

(6) Cooling System Tests

The cooling system provides the proper cooling (or heating) of a subassembly during transit. The system also removes some of the sodium adhering to the subassembly as it is removed from the sodium-filled primary tank. Assembly and testing of the cooling system components are still in progress.

A test of the complete cooling system will be conducted after completion of testing of the components. The pressure drop through the gripper and subassembly within the fuel-unloading machine has been measured with air at room temperature and has confirmed the analytical predictions.

5. Sodium Pumps

a. Primary System Mechanical Centrifugal Pumps

Two mechanical centrifugal pumps are used as the main coolant pumps in the EBR-II primary coolant system. Each has a maximum capacity of 5,000 gpm at 85 psi of 700°F sodium. The approximate EBR-II full-power requirement of each pump is 4,730 gpm at 56 psi head.

Each pump was given a comprehensive performance test with water at the vendor's plant. The tests were performed using the individual variable speed power supply and control system provided for each pump. Tests were run over a wide range of pump speeds; the results corrected to sodium are shown on Fig. B-9. The flow acceleration and deceleration rate was adjusted to meet the specified 0.3 to 0.5%/sec of the actual flow rate throughout the full speed range of the pumps. The water tests on each pump totaled about 30 hr of operation, including several starts. Disassembly and inspection following the tests revealed no evidence of malfunction and all parts were in excellent condition.

Each of the pump motor assemblies was tested with a helium mass spectrometer to assure the required leak tightness. (All electrical connections are solid conductors equipped with hermetic seals where they penetrate the pump motor frame.)

A sodium test on these pumps was not warranted because performance and life of a similarly constructed 5,000 gpm mechanical centrifugal test pump has proved most satisfactory.[26] The 5,000-gpm test pump employs a standard rigid coupling which requires a longer shaft for coupling purposes than the EBR-II pumps, but the latter require a relatively longer shaft to traverse the radiation shielding between the pump and the pump motor. The hydrostatic bearing in the test pump is also very similar, except that the EBR-II pump has additional hydraulic pads within the hydrostatic pressure pockets. The test pump has a two-speed, 480-volt, a-c motor, and an auxiliary drive to provide operation at 10% of rated speed. Each EBR-II pump 480-volt, a-c motor is capable of variable speed over a range of 10% to 100% of rated speed with adjustable acceleration and deceleration rates. Each pump is powered by a motor-generator set with an eddy current coupling which provides variable frequency and voltage.

The reported test results[26] were based on 7,500 hr operation of the test pump. The total operating time with sodium now is 16,100 hr. This consists of 7,100 hr at full speed (1,750 rpm); 3,700 hr at half-speed; and 5,200 hr at 10% speed. During the last 3,200 hr of full speed and 800 hr of half-speed operations, no inert gas was passed down along the pump shaft to retard the upward diffusion of sodium vapor, except when the test loop temperature was altered. Gas flow was used during changes in loop temperature to maintain the desired pressure levels within the sealed loop. The test pump has been started a total of 251 times.

Inspection of the pump after operation revealed that it was in excellent condition. No significant amount of sodium or sodium oxide had passed the upper labyrinth seal toward the motor enclosure. There was no evidence of corrosion or cavitation on the pump parts. All surfaces exposed to flowing sodium were in excellent condition.

Of perhaps greatest interest was the condition of the "hydraulic bearing" which operates with sodium under pressure from the pump outlet. No hydrostatic-centering forces exist until some pump discharge pressure is established. During this brief interval after pump startup, the bearing functions as a sodium "lubricated" journal bearing. The wear on the bearing was measured to be 0.001 to 0.002 in. There were also small grooves, perhaps 0.002 to 0.003 in. deep, which have not propagated or increased in subsequent operation. Neither the wear nor the light scoring affect operation since the normal diametral clearance is about 0.017 in. (The EBR-II pumps are provided with additional pads in the hydraulic bearing which should result in even less wear.)

b. Primary System d-c Electromagnetic Auxiliary Pump

The EBR-II primary coolant system includes one 14-inch, direct-current electromagnetic auxiliary pump. The pump has a capacity of about 500 gpm at about 0.25 psig. When powered by batteries alone, e.g.,

during an unexpected complete power failure with subsequent scram, the flow will continue at a minimum of 300 gpm for about 20 min. The approximate EBR-II head requirement for a 500-gpm flow is 0.22 psig.

A 14-inch prototype primary auxiliary pump was constructed and assembled into a test loop designed to match approximately the desired hydraulic performance of the pump. Pump flow was read with an electromagnetic flowmeter. The differential head across the pump was read directly with an oil-filled manometer, using a balanced level, twin-seal pot arrangement. Power to the pump was supplied by a rectifier.

The test data produced a head-capacity curve which is a straight line with the head decreasing slowly from 0.30 psi at zero flow, to 0.24 psi at 600 gpm. Tests on the actual EBR-II nickel-cadmium battery discharging through a resistance simulating the 14-inch auxiliary pump application, provided data to estimate the discharge characteristics of the EBR-II installation as shown in Fig. B-10. Based on this available power and pump test data, the EBR-II primary system auxiliary pump flow rate variation with time has been plotted on the same figure. Thus when only battery power is available, the primary system coolant flow will continue for a period sufficient to prevent overheating and to insure a smooth transition to natural circulation of the primary sodium coolant.

c. Secondary System a-c Linear Electromagnetic Pump

The EBR-II secondary coolant system features one 12-inch alternating-current, linear induction electromagnetic pump. This pump has a capacity of 6,500 gpm at 53 psig. The approximate EBR-II full-power flow requirement of the pump is 5,900 gpm at 45 psig of 585°F sodium.

Performance and life tests were conducted on an identically constructed, slightly smaller capacity (5,000 gpm), a-c, linear electromagnetic pump. The reported test results[26] were based on 5,600 hr operation at 5,000 gpm with sodium at 850°F, plus an additional 1,000 hr at lower flow rates and temperatures. The total operating time with sodium now is 8,700 hr at full capacity at 850°F, plus an additional 1,100 hr at reduced flow rates and temperatures.

One of the major attributes of this type of pump is the very fine flow control which can be achieved. Refinements were made in the control system for the M-G power supply and stable flow rates down to approximately 7 gpm were achieved. This type pump is also capable of reverse flow. This characteristic will be useful in the EBR-II secondary system as a coolant "brake" to control natural circulation rates.

The reliability of the pump is best illustrated by the post-test inspection results. Twelve of the approximately eighty pump tube supports were observed to be broken. These supports prevent the flat section of the pump tube from collapsing while the pump contains a vacuum as encountered during sodium filling operations, etc. The loss of three thermocouple tubes from other portions of the test loop may have caused the pump tube support failures. The broken thermocouple tubes were 0.25 in. diameter stainless steel tubing of 0.0625 in. wall thickness, and about 3 to 5 in. long. These had circulated through the pump and test loop with no adverse effect on pump operation.

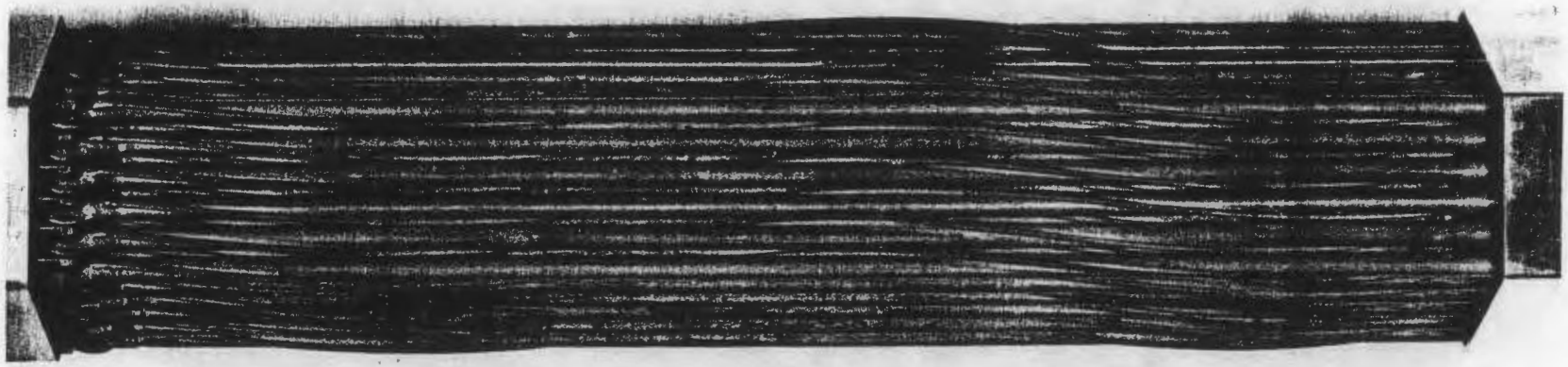

Fig. B-1

Core Subassembly (91 Fuel Elements) Exposed for 732 hr in Sodium at 500°F - 960°F and 3fps - 26.2 fps

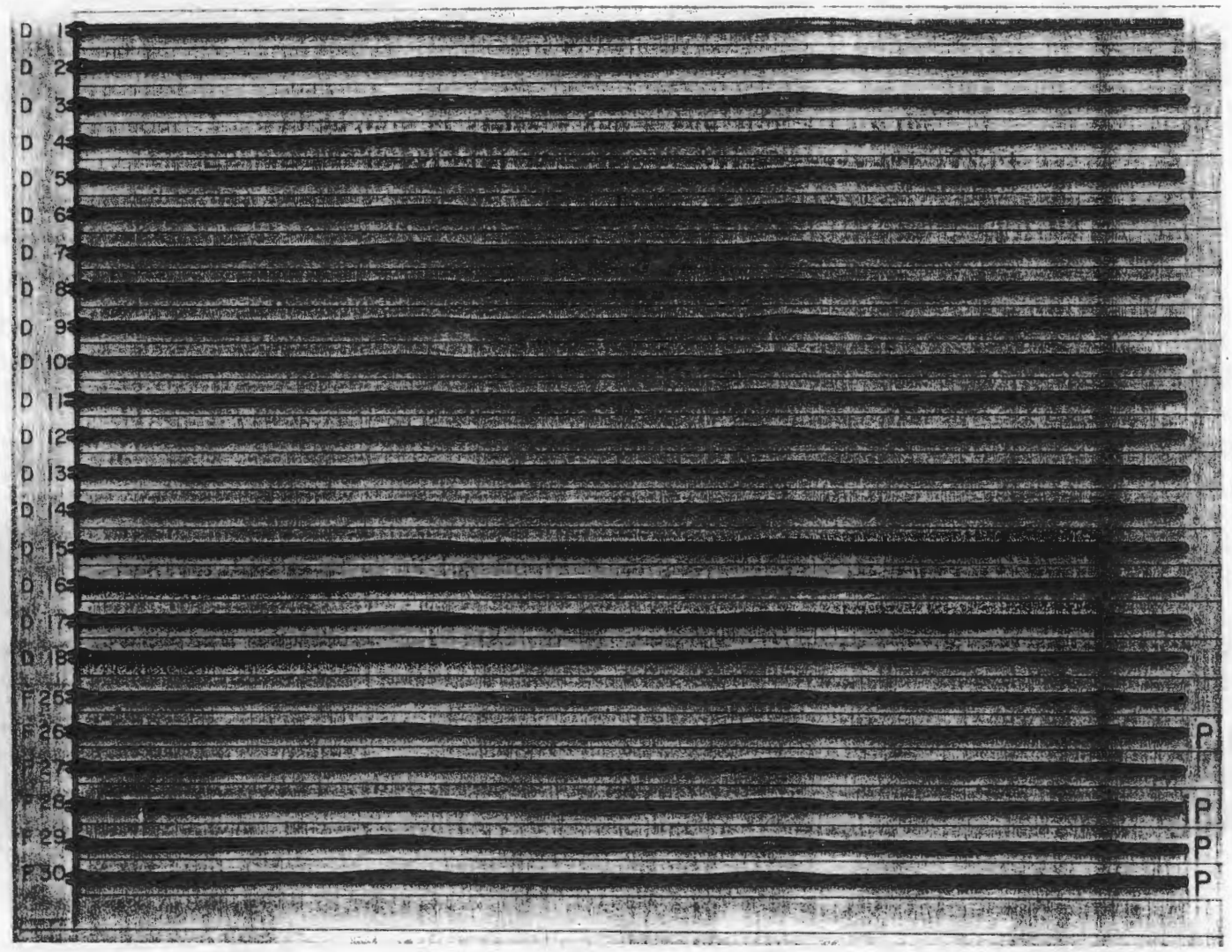

Fig. B-2

Typical Appearance of Fuel Elements Removed from Core Subassembly (Fig. B-1)

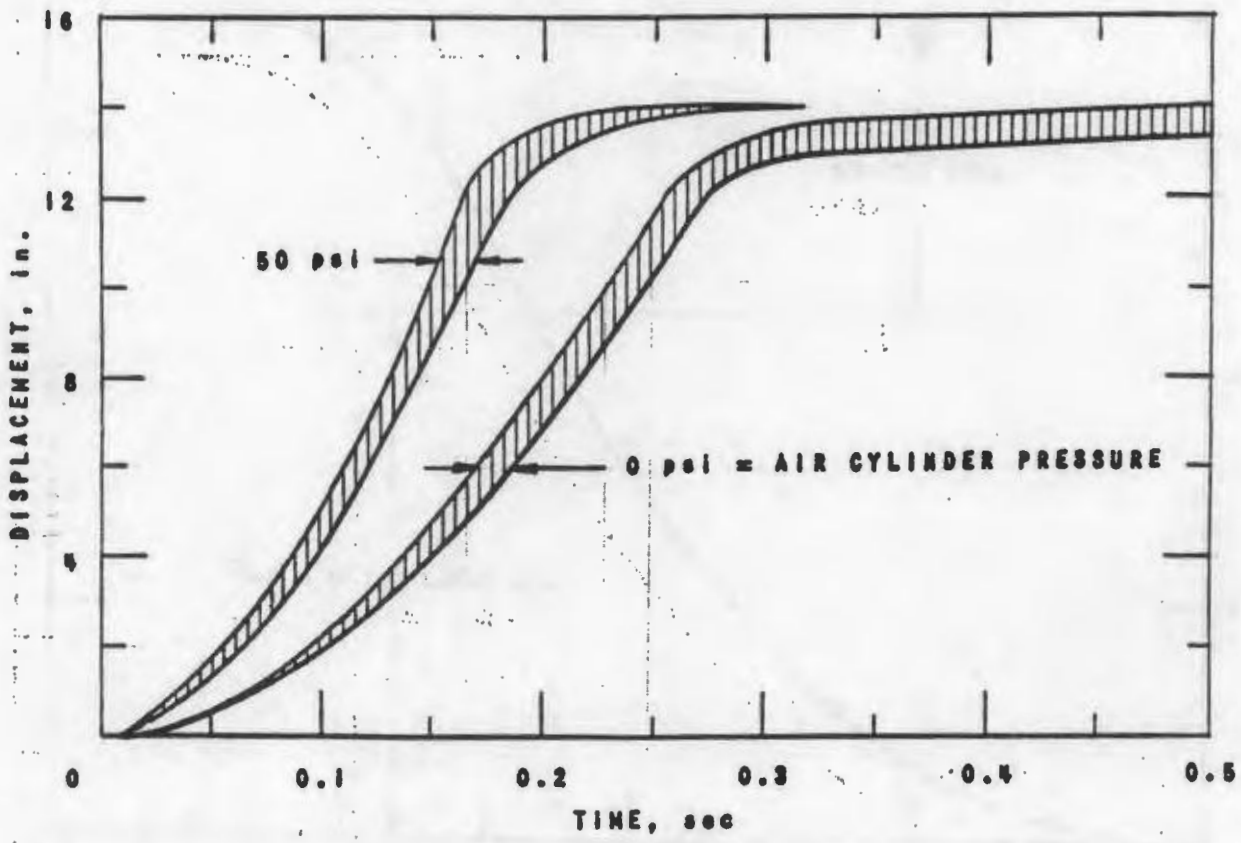

Fig. B-3

Displacement vs. Time for Control Rods during Scram

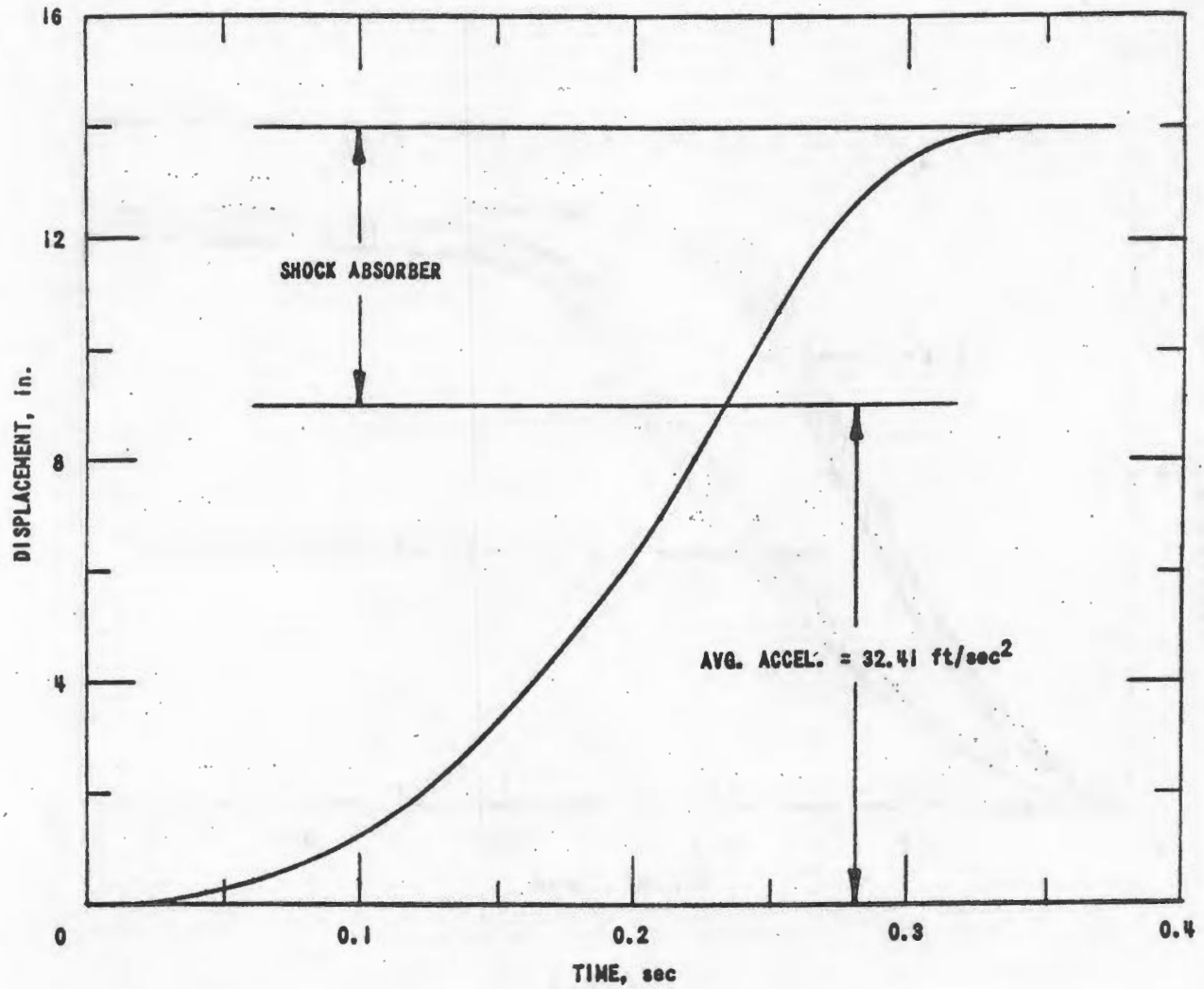

Fig. B-4

Displacement vs. Time for Safety Rods during Scram

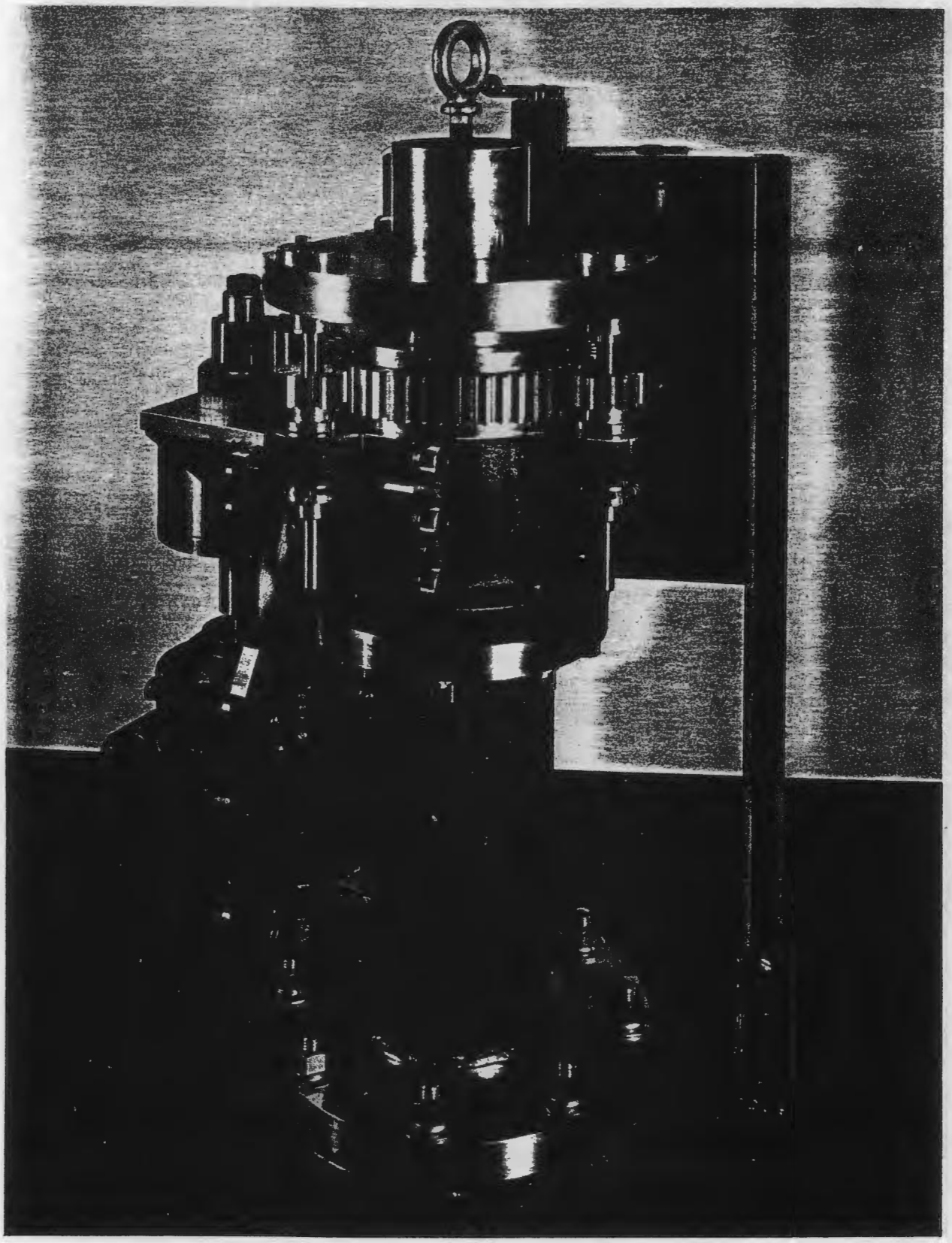

Fig. B-5

Shaft Seal Packing Gland Assembly

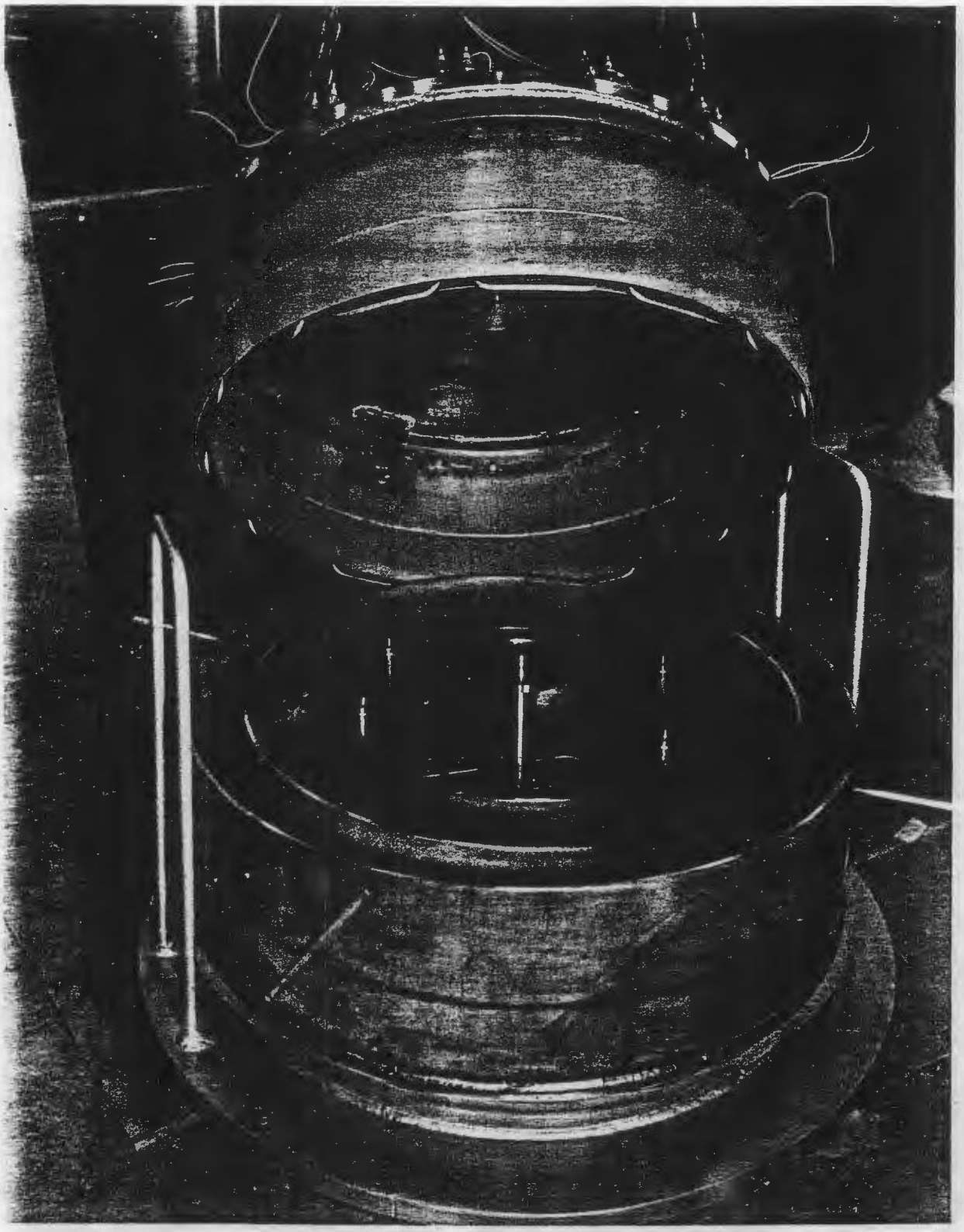

Fig. B-6

Experimental Model of Rotating Plug Freeze Seal (Test Head Open)

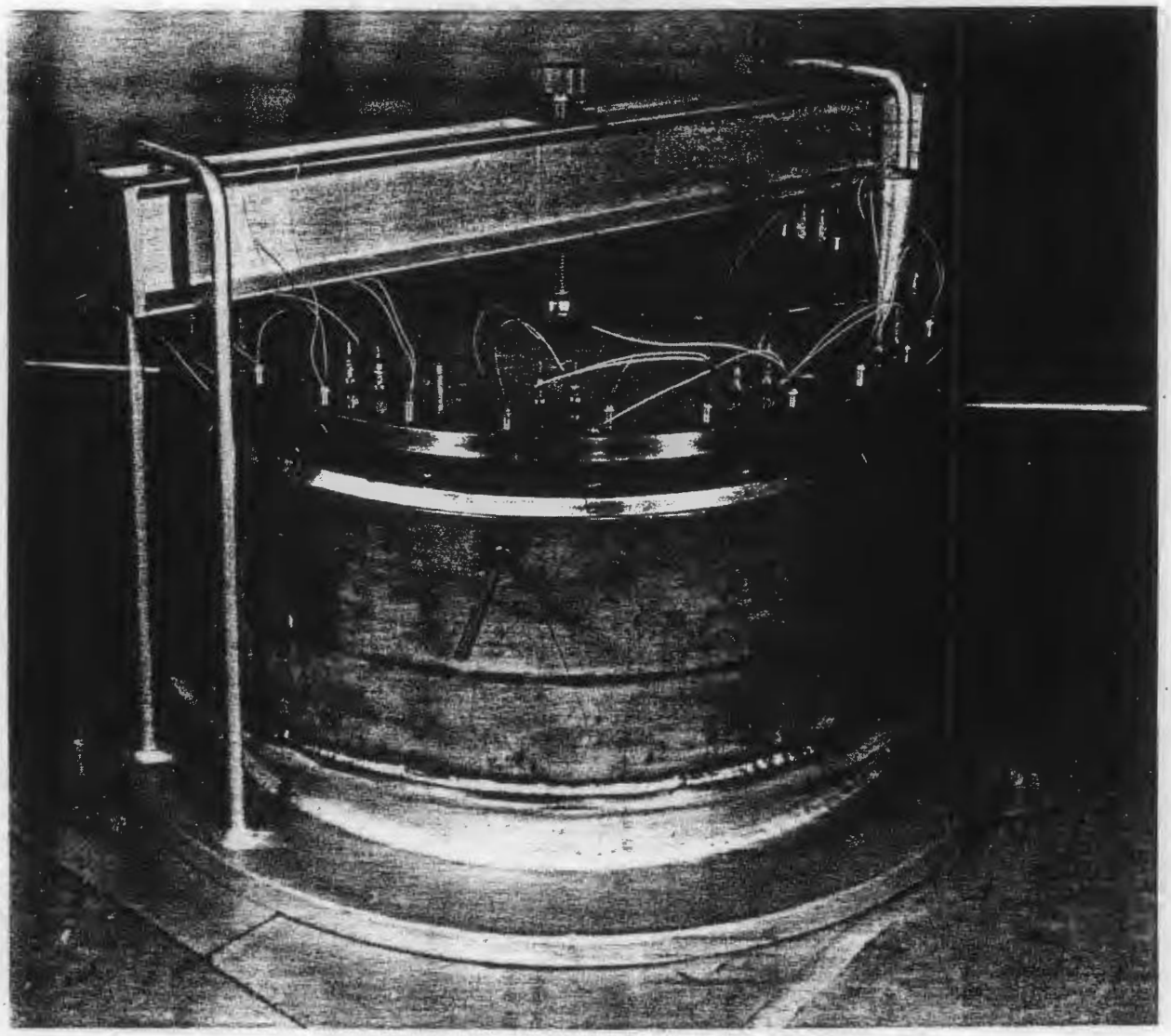

Fig. B-7

Experimental Model of Rotating Plug Freeze Seal (Test Head Closed)

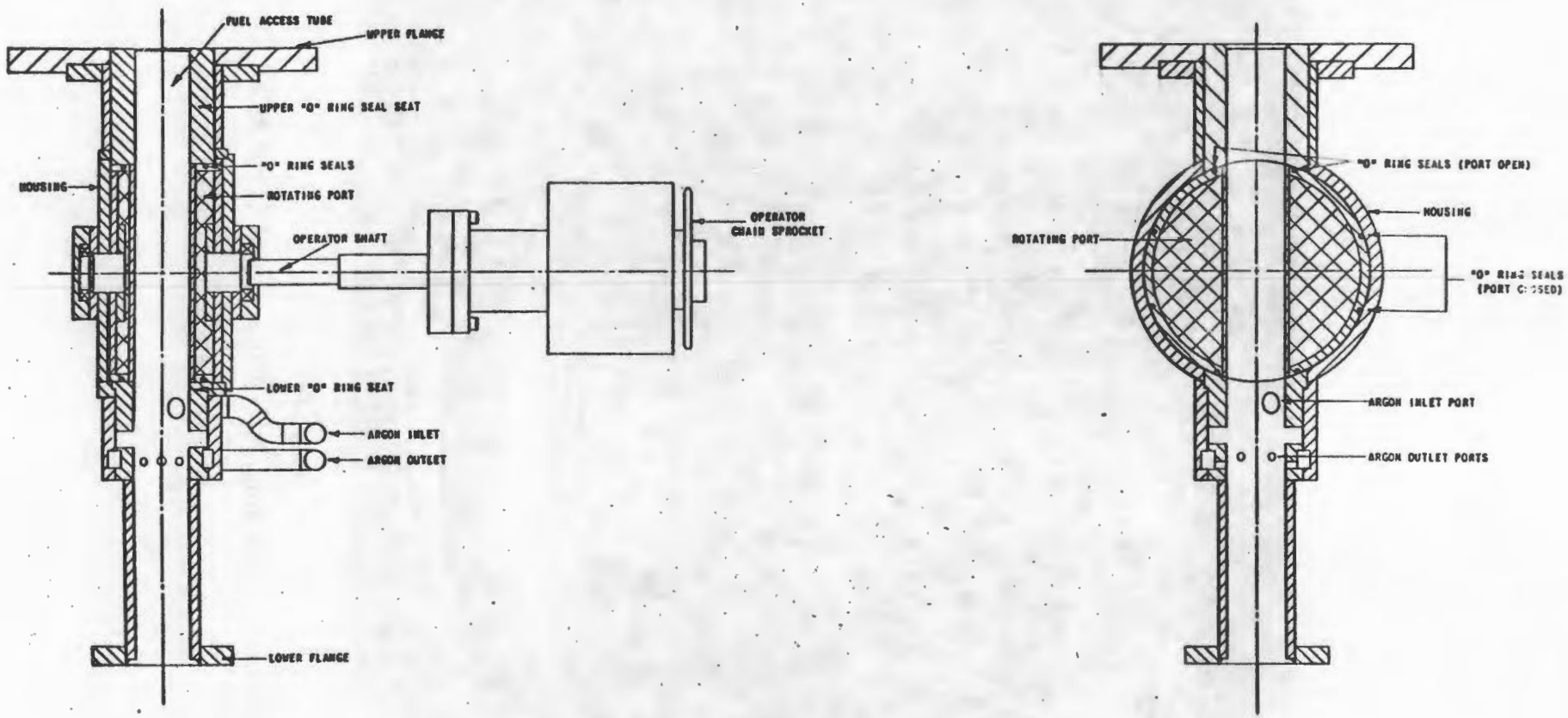

Fig. B-8

Fuel-Transfer Port

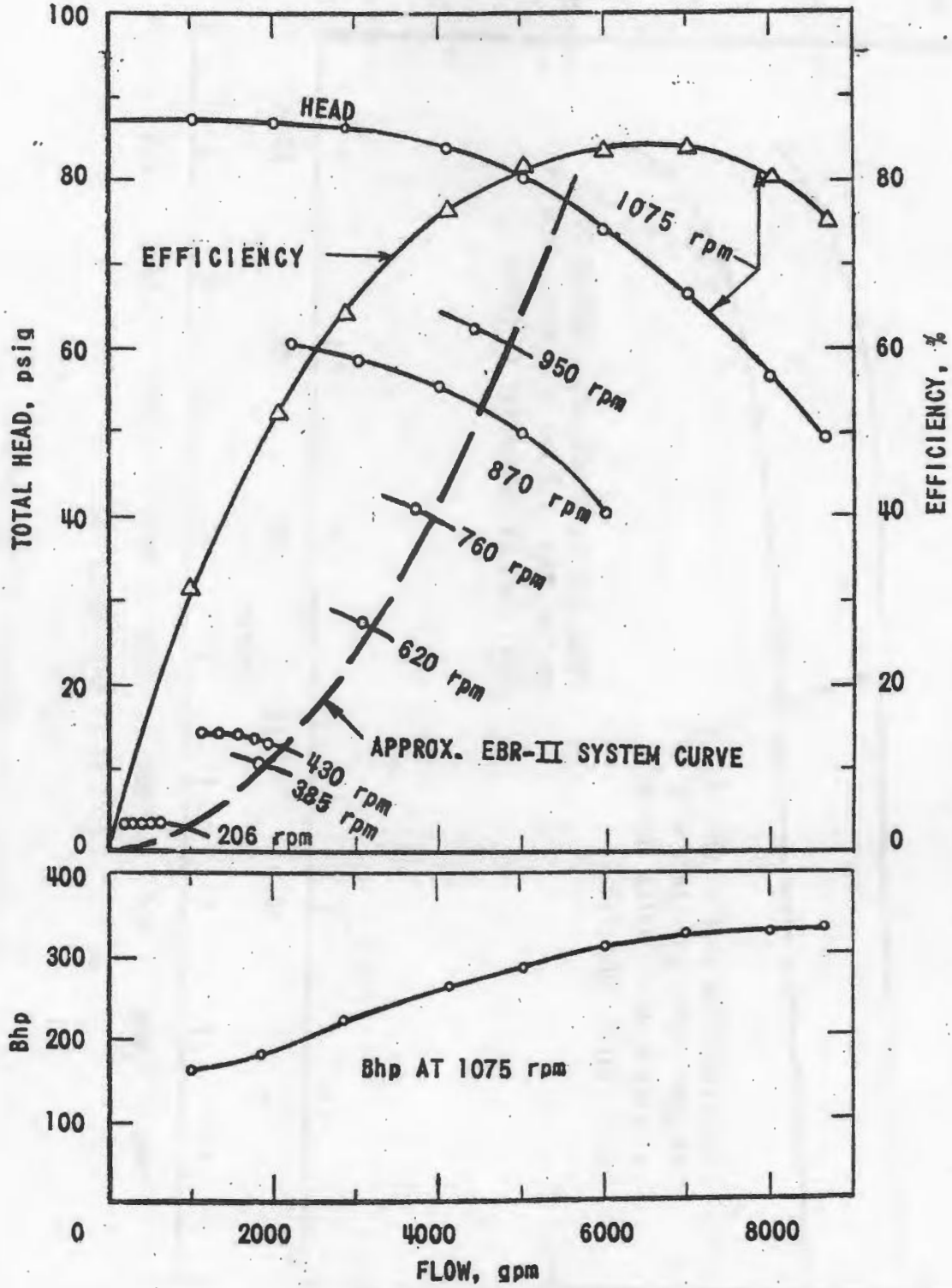

Fig. B-9

Operating Characteristics of Primary Pump with Sodium at 700°F

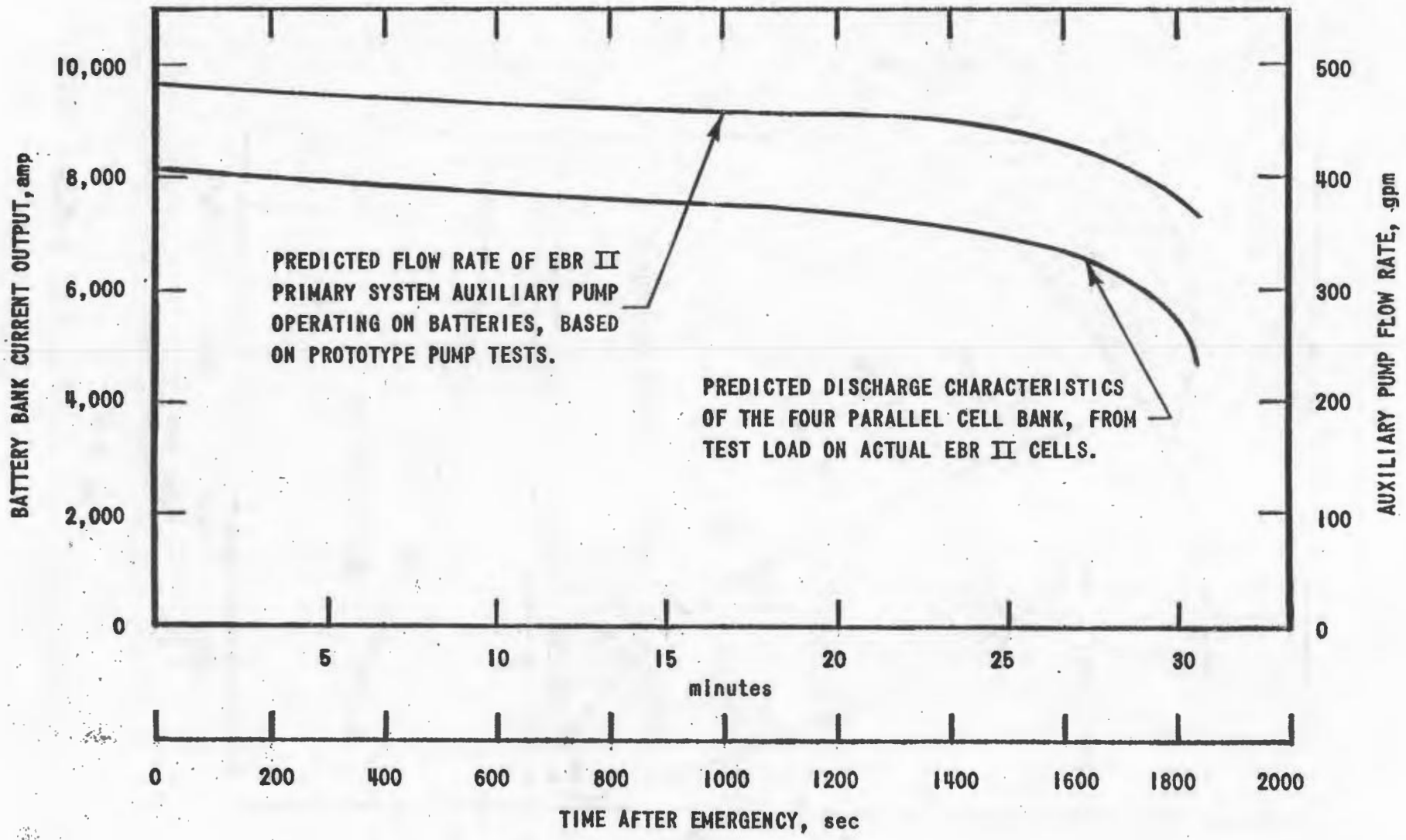

Fig. B-10

Auxiliary Pump Flow on Battery Power

APPENDIX C

REACTOR COOLANT FLOW DISTRIBUTION

1. General

A major objective in the development of EBR-II has been to achieve high steam temperature and, consequently, high reactor coolant outlet temperature. As an aid to this end, the reactor employs a coolant "orificing" system. This system provides an optimum coolant flow rate through each individual subassembly, the magnitude of the flow rate being dependent upon the subassembly location in the reactor. The design details of the system are described in the body of the report (see particularly Figs. 7, 9, 14, 15, and 48).

To assure that the proper coolant flow rate through each subassembly will be realized in the reactor, numerous experimental tests have been conducted. Included were tests on full-scale subassemblies, model subassemblies, and a model reactor. These and certain supplementary tests are briefly described in this Appendix.

2. Preliminary Tests

Preliminary flow rate vs. pressure drop tests were conducted on complete, full-scale subassemblies of both the core type and control type. Pressure drops across the various subassembly sections (lower blanket, core, etc.), as well as across the entire subassembly, were obtained. The influence on flow rate of the control rod position in its thimble also was established. Most of these tests were run both in a sodium loop and in a water loop. Although the subassembly lower adaptors (containing the flow "orifice" holes) employed were of preliminary design, these tests served to: (1) establish fairly closely the pressure drop across the reactor which would be required; (2) enable approximation of the orifice hole sizes needed; and (3) confirm the validity of conversion of water flow test data to sodium flow.

3. Proof Tests

By repeatedly testing in a water loop, revising the orifice hole sizes, retesting in a loop, etc., the correct orifice hole arrangement can be determined for each type of subassembly. That is, the subassembly lower adaptor can be designed by this process to provide the desired flow rate for any condition of hole exposure (or reactor grid step height) for a given pressure drop across the subassembly. The question arises, however, as to what the effective pressure drop across each individual subassembly (or row of subassemblies) in the core and inner blanket region of the reactor might actually be. Because of variations in pressure conditions

within the reactor outlet and inlet plenums, the effective pressure drop would be expected to vary from row to row and, perhaps, even between subassemblies of the same row. In the upper (outlet) plenum, which is of considerable depth, only small pressure differentials would be expected. But in the lower (high-pressure) plenum, substantial differentials could occur because of the reduced plenum depth and the abrupt changes in flow area produced by the lower grid steps. More importantly, the close positioning of the subassembly lower adaptors within the lower plenum could produce very high local pressure drops, particularly in the immediate vicinity of the inlet (orifice) holes. In these locations, the flow areas are small and the flow velocities are very high. The resulting pressure drops in these entrance regions could decrease substantially the effective pressure drops across affected subassemblies. Moreover, since the inlet holes of a given subassembly "face" those of the adjacent subassemblies and draw coolant from the same local regions, the decrease in effective pressure drop experienced would be influenced not only by the flow rate of the given subassembly but by those of all the adjacent subassemblies as well. These numerous, combined effects could not be calculated with reasonable accuracy and were therefore determined by experimental means as described below.

Extensive water loop tests first were conducted at Argonne on full-scale subassemblies to establish, tentatively, the lower adaptor (orifice) hole design for the core, inner blanket, outer blanket, safety, and control subassemblies.

A water test program on a simulated reactor then was carried out by The Franklin Institute under Argonne direction and was reported in detail in Reference 27. In this program, a full-scale test loop, a six-tenths scale test loop, and a six-tenths scale model reactor were employed.

In the model reactor, all EBR-II reactor vessel dimensions affecting flow were duplicated to scale. The model grid assembly may be seen in Fig. C-1, including the stepped portion of the lower grid plate in the core and inner blanket region. Six-tenths scale model subassemblies also were constructed for installation into the model reactor. Each model subassembly was provided with a lower adaptor (equipped with orifice holes) and an upper adaptor (the handling fixture) which were built precisely to scale. Between the lower and upper adaptors, a round tube containing a specially designed flow restrictor was used to simulate hydraulically the prototype subassembly body (the hexagonal can with its fuel and blanket elements, grids, etc.). The flow restrictor was designed as an orifice-type flow sensor, so that measurement of pressure drop across the restrictor could be correlated accurately with flow rate through the subassembly. The core and inner blanket zones of the model reactor were fully loaded with model subassemblies. In the outer blanket zone only two model subassemblies per row were installed, the remaining grid holes

being fitted with simple orifice plugs to provide the correct total outer blanket flow rate. Fig. C-2 shows the installation of the model subassemblies; in this figure the flow-sensing connections to individual subassemblies can be seen. The complete model reactor test facility is shown in Fig. C-3.

The first tests at The Franklin Institute consisted of determining flow rate vs. pressure drop curves for each type of subassembly, using the full-scale test loop and the same full-scale subassemblies earlier tested by Argonne. This was done to obtain independent verification of the Argonne data.

Secondly, flow rate vs. pressure drop (across the subassembly) curves for most of the six-tenths scale subassemblies of each type were determined using the six-tenths scale test loop. This was done to assure that the hydraulic characteristics satisfactorily simulated those of the actual subassemblies. Simultaneously, flow rate vs. pressure drop (across the internal orifice) curves were obtained, so that the actual flow rate through each subassembly later could be determined with the subassemblies positioned in the model reactor.

Following the above tests and installation of the six-tenths scale subassemblies in the model reactor, comprehensive flow distribution measurements were made under a variety of reactor flow conditions. During this testing, the total flow rate through the reactor and the flow rate through each of the individual subassemblies were measured simultaneously. This was done for various total reactor flow rates, for various total subassembly row flow rates (varied by plugging different groups of subassemblies), and for both normal and single-pump operation. The major conclusions which resulted from the tests were as follows:

(1) The effective pressure drops across subassemblies at each of the two rows of the inner blanket are essentially equal, but in the core zone the effective pressure drops vary significantly from row to row. As an illustration, the approximate effective pressure drop at each subassembly row for the case of reactor flow distribution as shown in Fig. 48 is indicated below.

Zone	Subassembly Row Number	Effective* Pressure Drop, %
Core	1	93
Core	2	93
Core	3	95
Core	4	85
Core	5	83
IB	6	100
IB	7	100

*Referred to pressure drop at rows 6 and 7.

(2) The effective pressure drops at the various rows in the core are interdependent, as expected. If the row-by-row flow distribution is changed, as by revision of core subassembly design, the effective pressure drop distribution is also changed. To enable future minor revisions in flow distribution in the EBR-II, a set of empirical equations was developed from the reactor model test data. These equations relate the effective pressure drop existing at each row to the total flow rate in that row and in other influencing rows. By iterative solution of these equations, the complete flow distribution within the core and inner blanket zones for any subassembly design (orifice hole size) can be calculated. To effect the solution it is necessary only to determine experimentally the flow rate vs. pressure drop curves for the full-scale subassemblies (in a water loop, converting analytically to sodium). The form of the equations is shown below.

$$\text{Eff. } \Delta P_5 = \Delta P_{6,7} + aQ_5^2 + bQ_5Q_4 + cQ_4^2 + dQ_{1-4}^2$$

$$\text{Eff. } \Delta P_4 = \Delta P_{6,7} + eQ_5^2 + fQ_5Q_4 + gQ_4^2 + hQ_4Q_3 + iQ_{1-3}^2$$

$$\text{Eff. } \Delta P_3 = \Delta P_{6,7} + jQ_4^2 + kQ_3^2 + lQ_{1-2}^2$$

$$\text{Eff. } \Delta P_{2,1} = \Delta P_{6,7} + mQ_{1-2}^2$$

where $\Delta P_{6,7}$ is the pressure drop across subassemblies at rows 6 and 7, or the plenum-to-plenum pressure drop. The coefficients (a-m) are constants and were evaluated from the model test data but are not presented here. Q_{1-2} is the total flow rate in rows 1 and 2; Q_3 is the total flow rate in row 3; Q_4 is the total flow rate in row 4; and Q_5 is the total flow rate of the core-type subassemblies in row 5. (Flow through the control subassemblies is not included in Q_5 because the flow inlet holes are positioned higher than those for the other subassemblies and they are not strongly involved in the flow interactions between subassembly rows. The effective pressure drop across control subassemblies was found to be approximately equal to that for rows 6 and 7.) It should be noted that the equations are valid only for core subassembly orifice hole locations as presently employed (Fig. 7).

(3) Flow distribution within the core and inner blanket zones does not change significantly with change in total flow rate (within the range of interest, approximately 10% to 100% of full flow).

(4) Flow distribution is essentially unaffected by single-pump versus two-pump operation. Although single-pump operation is not contemplated for EBR-II, the model tests showed that less than a 3% variation from average flow rate might be expected for subassemblies of a given row, whether located closest to the active inlet or diametrically opposite it.

(5) Dye studies of flow patterns in the upper (outlet) plenum of the model showed that extremely little lateral flow across the outer blanket subassembly upper adapters will occur in EBR-II. The main flow occurs at an elevation above the tops of the adapters. Accordingly, no tendency for subassembly vibration induced by flow past the adapters is anticipated.

4. Special Tests

In addition to the coolant flow distribution tests described above, a number of special-purpose tests were conducted. The more significant of these are described below.

(1) One objective of the control subassembly design is to achieve automatic variation of flow rate with control rod position (insertion) such as to maintain a nearly constant maximum fuel temperature. With this arrangement, maximum utilization is made of the total core coolant flow, and minimum thermal cycling of the hottest fuel in the (regulating) rod is experienced. The lower adapter of each rod is provided with an external taper; when the rod moves axially within the thimble, a flow annulus of varying area is presented. By repeated water loop tests and modifications of a full-scale control subassembly, the optimum details of adapter taper, inlet hole number and arrangement, and inlet hole size were determined. The flow rate vs. insertion curve for the final design is shown in Fig. C-4.

(2) An important factor in determination of temperature distributions within the core is the coolant mass flow distribution within the core section of a subassembly. To determine the mass flow rate associated with each fuel element, it is necessary to know the flow area associated with each and the velocity profile across the section. The flow area is easily ascertained. The velocity profile across such an array, however, cannot be calculated with accuracy and resort must be made to experiment.

A model subassembly was constructed, complete with 91 model fuel elements. This was a precise scale model except for shortened blanket sections and an added taper at the top end of the fuel elements, neither of which would affect flow distribution through the active core section. Pitot-static probes, which measure local static and total pressure simultaneously, were selected as the primary sensing devices. The smallest probe of this type which appeared usable, including plugging and response considerations, was of 0.042 in. outside diameter. Because the actual core subassembly has only 0.019 in. wide (straight line) gaps available for probe traverses, it was necessary to employ a model scale factor greater than two. Because water was to be used in the model instead of

sodium, Reynolds Number criteria and available pump size limited the model scale factor to not more than three. An intermediate scale factor of 2.874 was selected which permitted use of a readily available rod diameter (0.500 in.) for the fuel elements.

The model was installed in a water loop constructed of copper pipe. Figure C-5 shows the model assembly of lower blanket, fuel element grid and core section, and upper blanket (separate). Figure C-6 shows two probes and probe supports assembled for testing. Extensive measurements of velocity distributions were accomplished, complete traverses being made from wall to wall in various directions and at several elevations within the core section. Data were taken at each elevation at approximate 0.054-inch intervals of traverse with probe positions being known within approximately 0.015-in.

It was found that the average velocity of the coolant associated with each of the 61 interior fuel elements ranges from 97% to 100% of the average coolant velocity within the core section. The average velocity of the coolant associated with each of the 30 peripheral fuel elements is approximately 102% of the average coolant velocity within the core section. The coolant mass flow rate associated with each interior element ranges from 82% to 84% of the average mass flow rate per element of the core section (total mass flow rate divided by 91). Because of the relatively large flow area existing between the peripheral fuel elements and the subassembly wall, the mass flow rate associated with each peripheral element is about 136% of the average mass flow rate per element of the core section. These tests and results are described in detail in Reference 28.

(3) As noted in the body of the report (Table XII), leakage of coolant from the flow system to the primary tank bulk sodium occurs at several locations. Several tests were conducted to establish the magnitude of these leakages.

The 47 core-type subassemblies in rows 1 through 5 have a diametral clearance of 0.0085 in. between the lower adapter of each subassembly and the lower grid plate. Coolant under pressure in the inlet plenum leaks through these clearance annuli, returning to the bulk sodium in the primary tank. Using a test loop (sodium), the leakage between a core subassembly and a simulated grid support was measured by collection of the leakage flow in a tank. Measurements were made with a number of pressure differentials across the simulated lower grid plate. Based on these experimental data the total leakage for the EBR-II core subassemblies in rows 1 through 5 was established at 75 gpm of 800°F sodium at full reactor flow. Similar tests on control and safety subassemblies established the total leakage between the rods and their thimbles and between the thimbles and lower grid plate to be about 125 gpm at full reactor flow. The same experimental data enabled calculation of leakage between the 66 inner blanket subassembly lower adapters and the lower grid plate (105 gpm at full reactor flow).

In an experimental sodium test loop, a labyrinth-type seal was installed, simulating the seal on a control rod drive shaft where it passes through the reactor vessel cover. Leakage rates were measured by allowing seal leakage to flow through an overflow pipe to a collection tank. A curve of flow versus pressure drop was obtained and compared to calculated values. Using these data and the final dimensions of the control rod drives, the gripper, the holddown, and the spare gripper labyrinth, the total leakage around these mechanisms was estimated to be about 57 gpm. Total leakage from the reactor upper plenum, including that at the split line between vessel and cover, is estimated at 105 gpm.

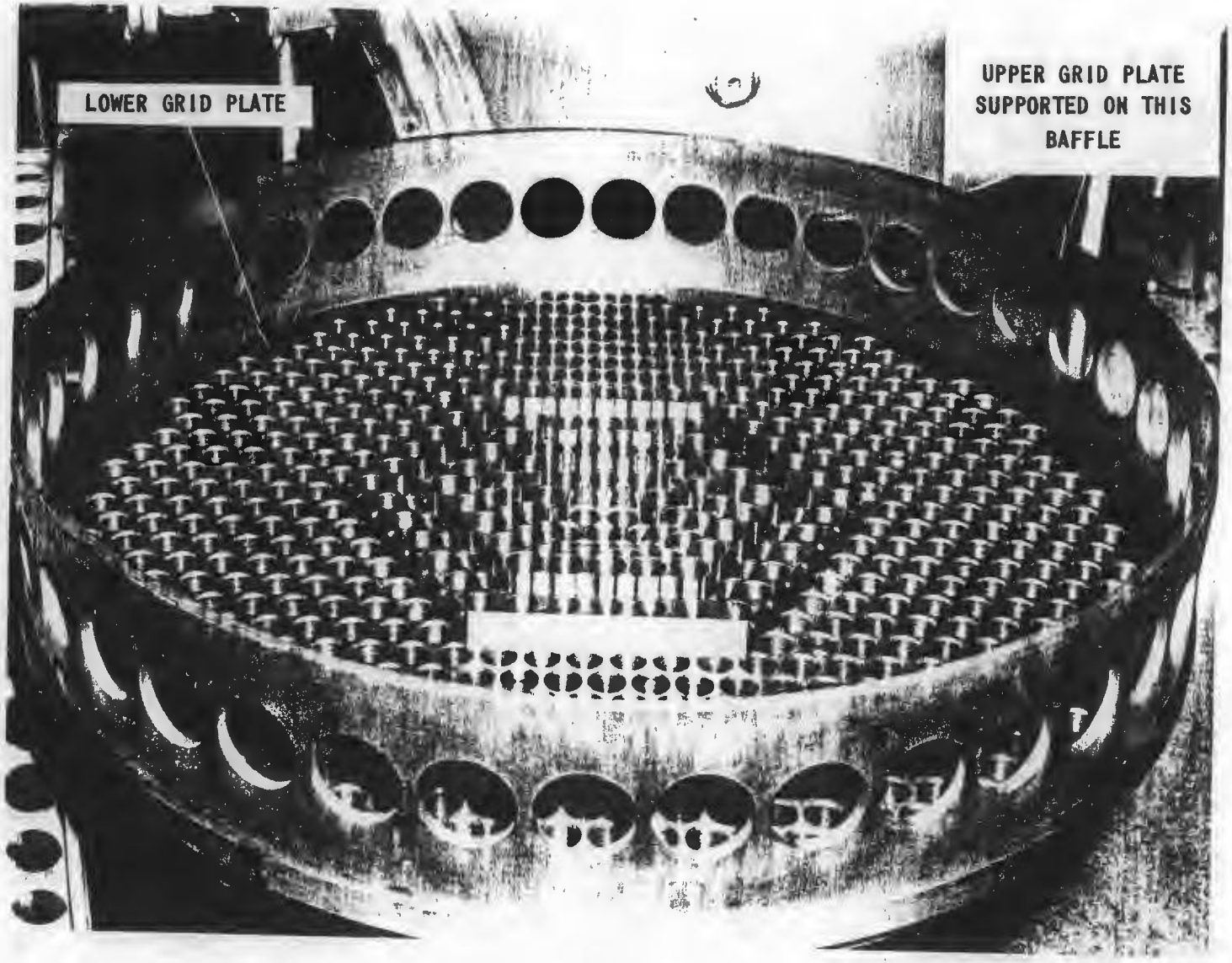

Fig. C-1

Reactor Test Model Grid

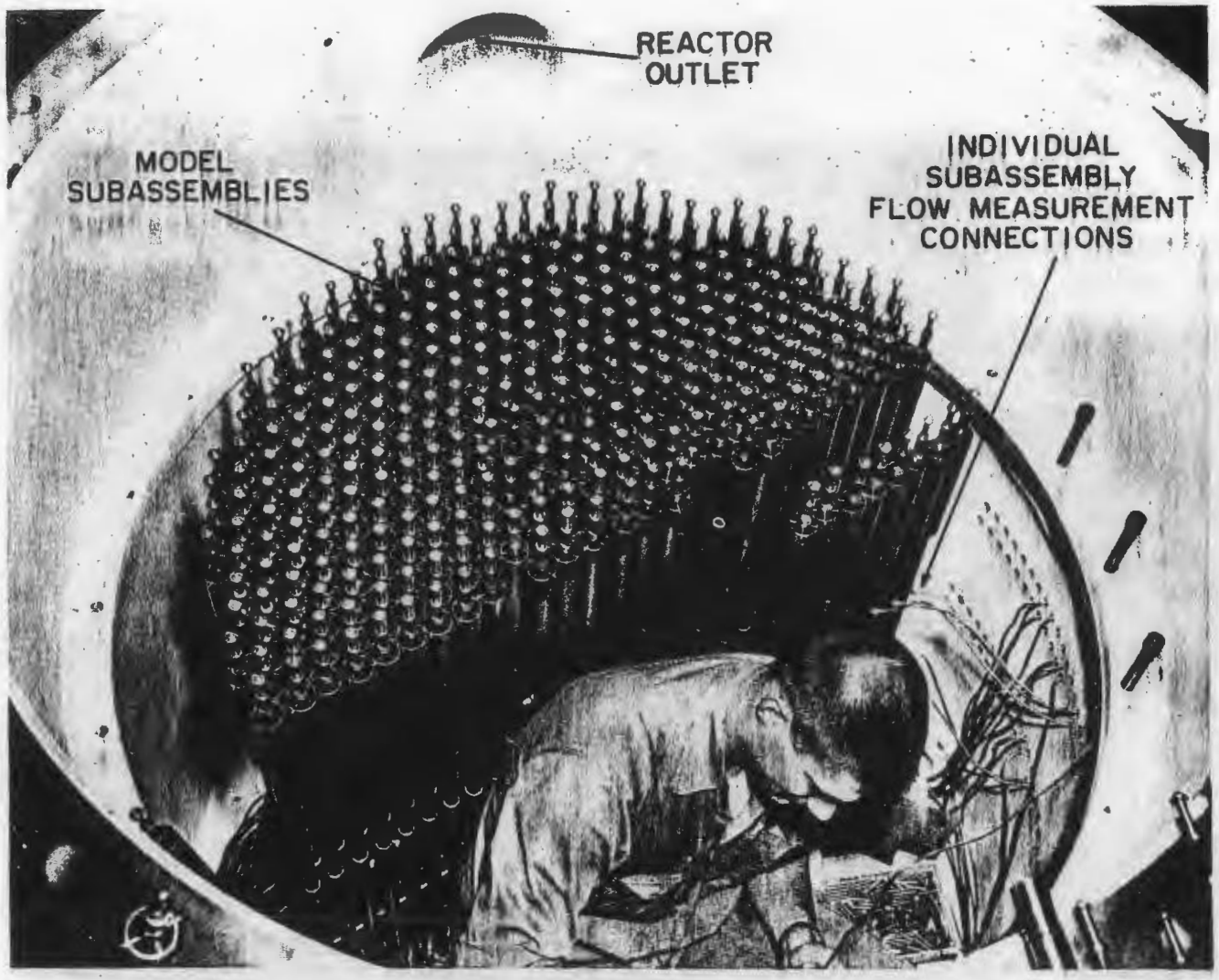

Fig. C-2

Installing Model Subassemblies in Reactor Test Model

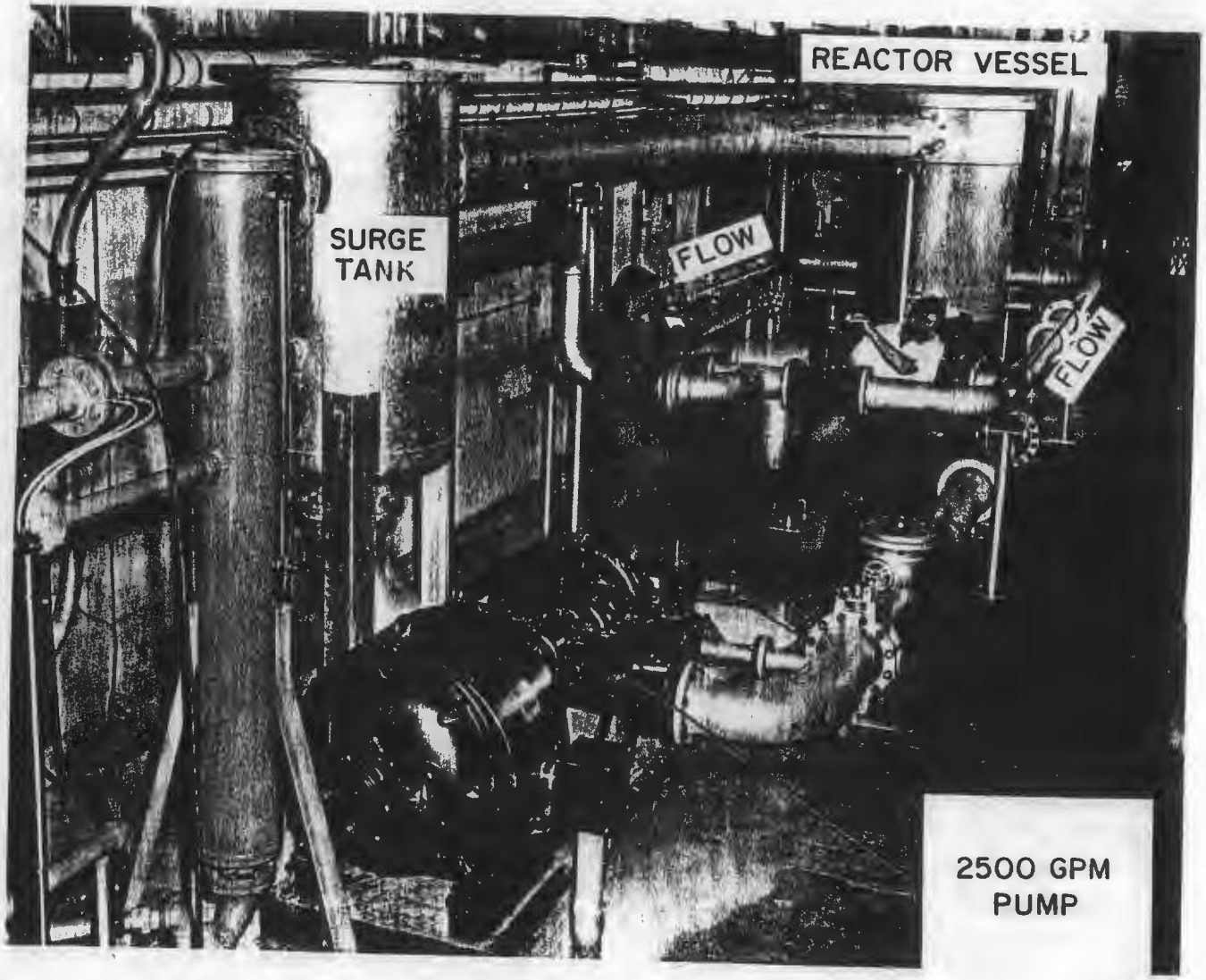

Fig. C-3

Six-Tenths Scale Reactor

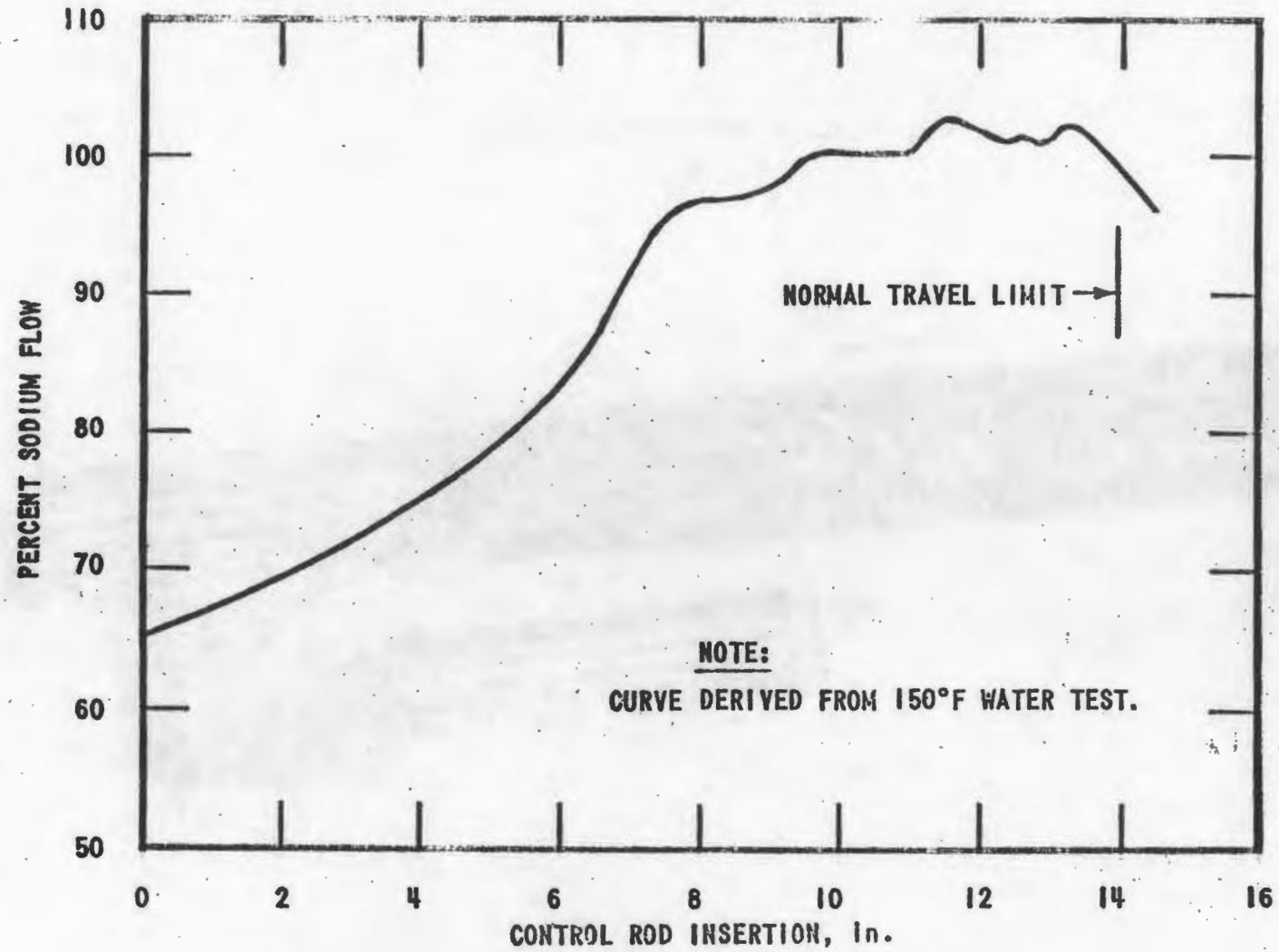

Fig. C-4

EBR-II Control Rod Flow Variation with Insertion

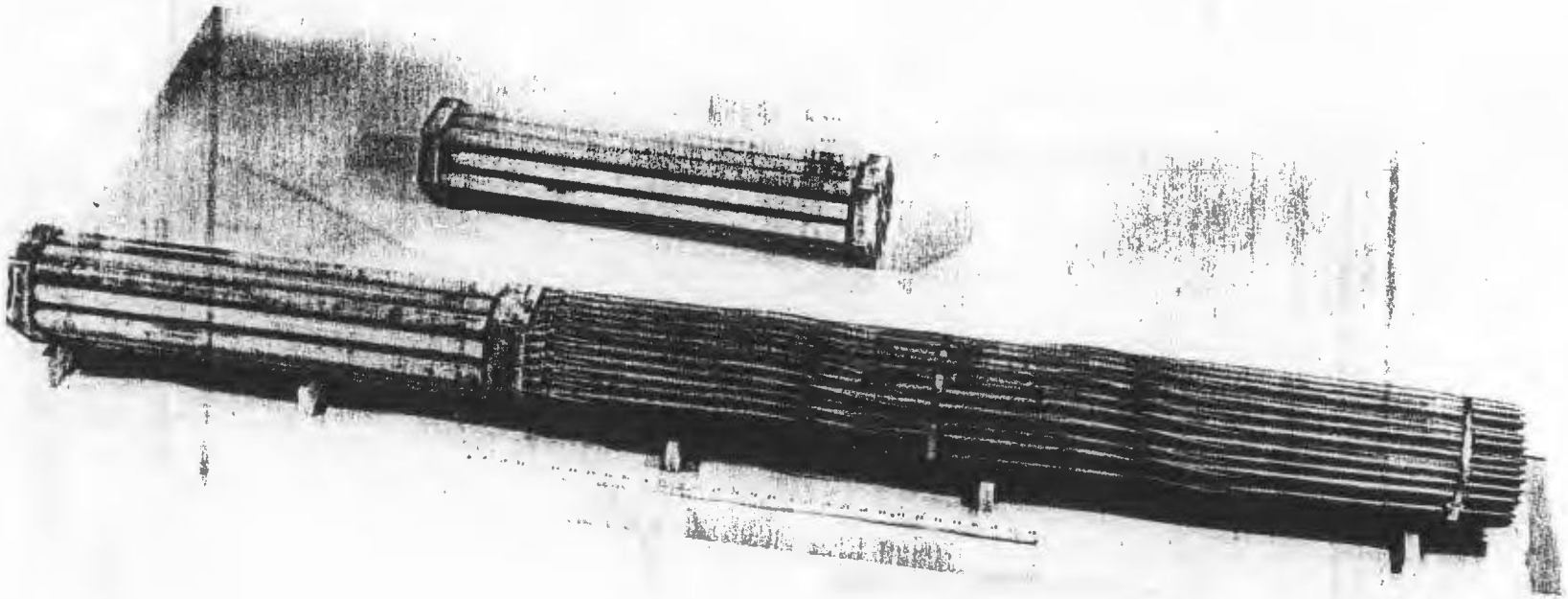

Fig. C-5

Model Subassembly Components

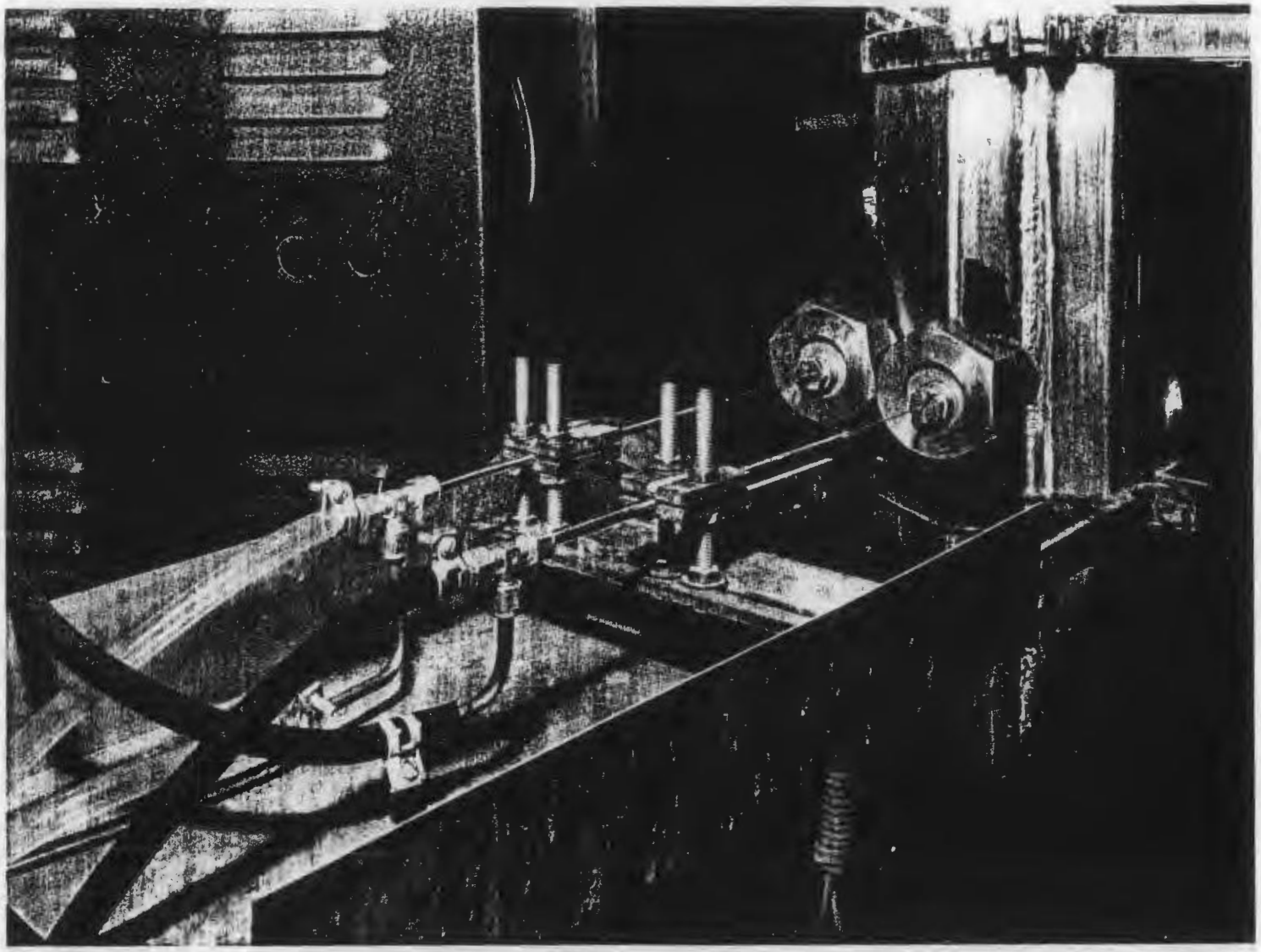

Fig. C-6

Model Subassembly Probes and Supports

APPENDIX D

STABILITY STUDIES ON EBR-I, MARK-III CORE

The stability studies on the EBR-I, Mark-III core have been completed and a final report issued.[29] The following is a summary of the results obtained.

From the results of stability studies it may be concluded that the operational characteristics of a fully-ribbed and rigid Mark-III core loading were governed by feedback processes which guarantee safe and stable operation under normal operating conditions. The stabilizing ribs increased stability in two ways:

(1) The ribs provided strong radial coupling between fuel rods, and between fuel rods and hexagonal cans, with the consequence that a large radial contribution to the power coefficient of reactivity was realized.

(2) The ribs eliminated, for all practical purposes, positive feedback effects arising from the inward bowing of fuel rods during power increases. Absolutely no evidence of positive reactivity effects was noted for the fully-ribbed and rigid core.

The extrapolations of full power, full flow test data indicated that the reactor could be brought into a resonant condition only at power levels exceeding 1,000 Mw. Nominal full power operation was limited to 1.2 Mw by design. The hypothetical instability condition was only of academic interest since the limiting power level was not controlled by instability but by heat removal capability. In a practical sense, the fully-ribbed Mark-III loading could never have been made unstable.

The observed non-linearities in the power coefficient of reactivity posed no serious operational problems over the range of power levels associated with the tests. Except for the region between zero power and 200 kw, where the power coefficient was small, but still negative, the power coefficient was always very strongly negative. Non-linearities were relatively unimportant as related to system stability. They did, however, complicate the interpretation of test data in terms of a single unified model which could be applied over wide ranges of power, flow and temperature conditions. The origin of the non-linearities appears to have been a consequence of power and temperature sensitive clearances existing between fuel rods and hexagonal cans (as many as 36 fuel rods can be accommodated in a single hexagonal can), and between the hexagonal cans. Attempts to define such systems mathematically were further frustrated by differences between the expansion coefficients of fuel and structural materials. The association of such extremely tenuous clearance systems

with power coefficient non-linearities cannot be placed on a firm analytical basis. The descriptive interpretation of the effects caused by such clearance systems is nevertheless important, not only for an understanding of Mark-III behavior, but as a guide for non-linear phenomena in other fast reactors.

The power coefficient was also shown to be sensitive to inlet coolant temperature. Significantly larger static and dynamic power coefficients of reactivity were associated with increased coolant inlet temperatures. Feedback time dependence was insensitive to variations in coolant inlet temperature. This effect was probably due to the strong temperature dependence of the uranium-zirconium fuel alloy expansion coefficient. The effects of increased feedback at higher temperatures were relatively minor.

The influence of structural feedback was also observed in Mark-III, fortunately to a much smaller degree than in the earlier Mark-II design. At the higher inlet temperatures, approximately 13% of the static power coefficient was associated with a feedback process operating with a 400-second time constant. Because of the extremely long time constant, it is assumed that the physical process was associated with some massive portion of the structure at some downstream location. The existence of this delayed component had little effect on stability because it could not be observed with frequencies greater than 0.003 cps.

Attempts to enhance and measure possible feedback effects arising in the radial breeding blanket were unsuccessful. It may be concluded that the assumed possible feedback mechanisms due to the pre-heating of inlet coolant by the transfer of heat between core outlet and blanket inlet in series coolant flow were non-existent or extremely small. Pre-heating conditions were similar for both Mark-II and Mark-III; therefore it may be concluded that strong blanket feedback mechanisms were not the source of the Mark-II delayed negative component.

As the coolant flow was reduced (at constant power), three feedback phenomena varied:

(1) The power coefficient increased inversely proportional to the change in flow rate.

(2) The time constant for fuel expansion increased.

(3) The effective transport lag increased.

All of these changes tend toward instability since they tend toward increased feedback amplitudes and phase lags at the important frequencies. Extrapolations of one-third coolant flow test data concluded that the reactor would

reach resonance instability near 10 Mw; this is more than twenty times the power level consistent with one-third flow. Coolant flow reductions at constant power tend to lower the indicated resonance power level. Extreme flow reductions were inadvisable, not only because of the lowered resonance power level but also because fuel element temperatures might have exceeded design limits.

The results of removing the stabilizing ribs from fuel elements demonstrated the existence of a strong positive reactivity effect which was associated with the inward bowing of fuel rods. The extrapolation of kinetic data obtained by removing the stabilizing ribs from one-third of the fuel elements gave $+ 2.06 \times 10^{-6}$ $(\Delta k/k)/kw$ for the full core with ribs removed. Since the prompt negative component of reactivity associated with fuel, coolant, and blanket expansion was $- 2.21 \times 10^{-6}$ $(\Delta k/k)/kw$, the response of the "non-ribbed" reactor would have still been governed by a very small, but negative, prompt power coefficient.

Removal of stabilizing ribs also produced an increase in the magnitude of the delayed structural component of the power coefficient. An empirical model describing the dynamic and static behaviors of the partially-ribbed core gave $- 2.21 \times 10^{-6}$, $+ 0.543 \times 10^{-6}$, and $- 0.873 \times 10^{-6}$ $(\Delta k/k)/kw$ for the respective prompt negative, rod-bowing, and delayed structural components of the power coefficient. These values may be correlated with those deduced empirically for the prompt negative and delayed structural power coefficient components for the fully-ribbed core, namely $- 2.21 \times 10^{-6}$ and $- 0.330 \times 10^{-6}$ $(\Delta k/k)/kw$, respectively. The magnitude of the positive component due to rod bowing was equal to the increase in the magnitude of the negative structural component of the power coefficient. Rib removal, therefore, introduced two feedback processes: (1) rod-bowing which was prompt and positive; and (2) a negative and extremely delayed structural component. It was clear, however, that the strong increase in the negative structural term did not affect the resonance stability of the partially-ribbed core (and the same is indicated for extrapolations to the non-ribbed core), since reactor oscillations at low frequencies (~ 0.02 cps) could not sense this delayed effect.

The Mark-III core, whether fully-ribbed and rigid, fully-ribbed and loose, and even partially ribbed, was extremely stable, a major departure from Mark-II experience. The most undesirable feature of Mark-II had been the prompt positive, rod-bowing reactivity effect. The inclusion of stabilizing ribs and a system of tightening rods in the Mark-III eliminated, or at least minimized beyond detection, similar effects in Mark-III.

The presence of a delayed negative component to the power coefficient of reactivity was another important observation in Mark-II. This appears to have been the result of delayed expansions in the structure of

the lower shield plate.[30] Experiments with a dummy shield plate have established the existence of radial movements of the shield plate ligaments which, because of their contiguity with the fuel rod extensions, effectively modified the core size following power changes. This effect was clearly negative and operated with a time dependence consistent with that analytically deduced from the Mark-II test data. Structural features such as the Mark-II shield plate were eliminated in Mark-III and no significant, long-delayed reactivity coefficient was observed in Mark-III.

In summary, the Mark-II instability was enhanced by the prompt positive and delayed negative power coefficient components which were the result of design peculiarities. The elimination of the perforated shield plate system and the addition of the stabilizing ribs to the Mark-III fuel rods has resulted in a reactor whose performance was stable under all credible operation conditions.

APPENDIX E

CRITICAL EXPERIMENTS ON ZPR-III

The EBR-II critical experiments on ZPR-III were designed to provide detailed neutronic information.[19] These experiments were performed with mock-ups of the EBR-II reactor configuration simulating the normal power loading (with sodium coolant). In addition, a large number of experimental investigations were made on systems similar, with respect to size and composition, to the EBR-II.[31] The experimental data have been well correlated with analysis;[17,32] hence, the significant neutronics of the EBR-II are believed to be well understood.

The ZPR-III critical experiments utilized low-density aluminum to simulate the sodium coolant volume of the reactor system. Gross and detailed substitution experiments with canned solid sodium, and aluminum of different densities, confirmed the validity of the use of aluminum and that coolant removal reduces reactivity.

1. Critical Mass and Reactivity Effects

The critical mass of the reactor configuration which most closely resembles the geometry and composition of the EBR-II was measured to be 165 kg U^{235}. This critical configuration was predicted within a few kg U^{235}.

The average reactivity worth of a mock-up reactor control rod was measured to be 0.37% $\Delta k/k$.

The reactivity worth of a mock-up core subassembly, relative to low-density aluminum (simulating the displacement of sodium), is principally a function of radial position in the core. These measurements are listed in Table E-1. Also listed are the reactivity worths of Inner Blanket subassembly mock-ups relative to low-density aluminum.

Table E-1

REACTIVITY WORTHS OF CORE AND BLANKET SUBASSEMBLIES AS A FUNCTION OF POSITION

(ZPR-III Mock-up Experiments)

Reactor Row Number (Fig. 54)	Subassembly Type	Reactivity Worth, % $\Delta k/k$
1	Core	1.53
2	Core	1.48
3	Core	1.31
4	Core	1.05
5	Core	0.77
6	Blanket	0.18
7	Blanket	0.04

A number of detailed experiments were performed to determine the reactivity worth of various materials uniformly distributed throughout the reactor core and reflector regions. These were used to convert the data from the "aluminum-cooled" ZPR-III, to the sodium-cooled reactor. The pertinent measurements are given in Table E-2. Additional measurements are reported in Reference 19.

Table E-2

REGIONAL MATERIAL REPLACEMENT EXPERIMENTS

[in % $(\Delta k/k)/kg$ of Material x 10^2]

Material	Core	Reactor Region*		
		Axial Structural Gaps**	Reflectors	
			Radial	Axial
Aluminum	7.4	5.8	3.7	1.6
Stainless Steel	2.3	2.7	2.0	0.8
Sodium	11.6	6.4	5.8	3.7
U^{235}	33.5	-	-	-
U^{238}	1.5	-	-	-

*Core contains enriched uranium. Reflector regions contain depleted uranium. Structural gaps contain no uranium.

**The axial structural gaps are located between the core and the axial reflector.

Additional distributed material replacement experiments were utilized to determine the reactivity effects of fission products, including the 5 wt-% metal fission products in the fissium fuel alloy. These are given in Table E-3, along with measurements on synthesized fission product compositions and some structural materials of potential future interest.

Table E-3

MATERIAL REPLACEMENT EXPERIMENTS

(Distributed throughout EBR-II Core)

Material	Reactivity, $\%(\Delta k/k) \times 10^2/kg$	Material	Reactivity, $\%(\Delta k/k) \times 10^2/kg$
Molybdenum	+2.4	Physicum II*	-2.5
Ruthenium	-0.2	V	+5.9
Rhodium	-5.6	Nb	+0.29
Palladium	-2.0	Al_2O_3	+13
Physicum I*	-3.3		

*Synthesized fission product mock-ups (see Reference 31).

2. Power Distribution

Uncertainties in the predicted power distribution were estimated by comparing predicted with measured fission distributions from ZPR-III. Predicted fission distributions were obtained from the multigroup, two-dimensional (r,z) analysis:

$$F(r,z) \equiv \int_0^\infty \sigma_f(E)\ \phi(E,r,z)\ dE \quad ,$$

where σ_f is the fission cross section; ϕ is the neutron flux; and E is the energy. These calculations used the eleven-group constants from Reference 32.

Figures E-1 and E-2 compare experimental with theoretical radial and axial fission distributions, respectively. Since these experimental data are insufficient for an absolute power calibration, they are normalized to the predicted U^{235} fission density at the center of the core. The slight dip at $r \approx 11$ cm for the experimental U^{238} fission distribution in Fig. E-1 is attributed to the presence of the safety rods. These were not properly described in the two-dimensional (r,z) analysis. Since the U^{238} fissions predominate in the inner regions of the radial blanket, it can be seen that fission densities in this region are reasonably well predicted.

The deviations between theory and experiments in and near the gap regions indicated in Fig. E-2 must be attributed to an inadequate understanding of the neutron cross sections of aluminum and stainless steel. However, since very few fissions ($< 2\%$) occur in the axial reflectors, these deviations between theory and experiment are not significant in determining the reactor power distribution.

3. Neutron Source and Instrument Thimble Experiments

Experiments were conducted to determine the attenuation and spectral shift of neutron flux from the center of the core to the "J" and "O" thimbles (Fig. 54) where the flux monitoring fission counters and ion chambers are located. The "J" and "O" thimbles are located 58 in. and 78 in., respectively, from the reactor centerline at the central core plane. The unperturbed neutron flux can be estimated within, and outside of, the graphite neutron shield under the postulate of no thimble and uniform shield. However, the presence of the "J" thimbles (15 in. OD) appreciably complicates such an estimate and reduces the accuracy of the predicted result. The other aspect of these investigations dealt with determining the neutron yield of an Sb-Be neutron source of the type to be employed in the

EBR-II. Estimates of neutron yield are extremely uncertain. The objectives of these experiments were to determine:

(1) The required Sb activity in the Sb-Be neutron source.

(2) The geometric and compositional arrangement outside of the radial blanket and around the "J" thimbles to optimize low-power fission counter response.

Two independent series of experiments were conducted. The first series dealt with the early design of the neutron shield and reactor vessel [Figs. 8, 20, and 21]. The second series of experiments investigated several geometrical and compositional arrangements adjacent to the "J" thimbles in the final design configuration (Fig. 18). Only those results pertaining to the final reactor configuration are cited here.

An absolute fission counter was placed at the core center and another at the radial core boundary during each investigation. Additional counters were placed throughout the radial blanket and neutron shield. However, the information of primary interest was that of J-1 and J-2 thimble fission counter response relative to the absolute fission counter response, and thus relative to reactor power. Table E-4 summarizes experimental counter response data for a critical reactor producing one watt of thermal power.

Table E-4

INSTRUMENT THIMBLE FISSION COUNTER RESPONSE

(Critical reactor; 1 watt)

Location	Counter Response, cps	Cadmium Ratio	Comment*
J-1, -2	730	1.9	A
J-3, -4	395	2.4	A
0-1, -2, -3, -4	~20	~5	A
Core Center	170	1.0	B
Radial Core Boundary	82	1.0	B

*A = Fission Counter (Same as those in Channels 1, 2, and 3 described in Section IV.A.2.c.)

B = Absolute Fission Counter (Contains ~0.8 mg U^{235}).

The neutron shield configuration adjacent to the J-1 and J-2 thimbles was investigated in a subcritical assembly. With a 10-curie Sb-Be neutron source located at the reactor core-inner blanket interface, subcritical count rates were obtained in the mock-up J-1 thimble as well as at the core-inner blanket interface (across the core from the source). The source location duplicated the Dry and the Wet Critical experimental arrangements with the core between the source and the "J" thimble. The experimental results are summarized in Table E-5. The ZPR-III mock-up experiments cited here as well as similar Dry Critical investigations (Appendix L) showed that sufficient counter response would be obtained in the "J" thimbles for very low reactor multiplications with a strong Sb-Be neutron source. These results obviate the need for in-core instrumentation during the Wet Critical Experiments, or special provisions to enhance counter response in the "J" thimbles. The latter were also investigated on ZPR-III.

Table E-5

SUBCRITICAL COUNT RATES IN J-1 THIMBLE

(Source Strength ~10 curies)

Approximate		Fission Counter Response, cps	
k_{eff}	Multiplication	J-1 Thimble*	Core-Reflector** Interface
0.97	33	11	~3
0.94	16	6	~2

*Fission Counter (Same as those in Channels 1, 2, and 3 described in Section IV.A.2.c.).

**Absolute Fission Counter (Contains ~0.8 mg U^{235}).

4. Other Experiments

The foregoing experiments represent a small fraction of studies performed on the EBR-II mock-up on ZPR-III. General investigations included the effect of inhomogeneity, neutron lifetime, spectral indices, and a large number of material replacement experiments.

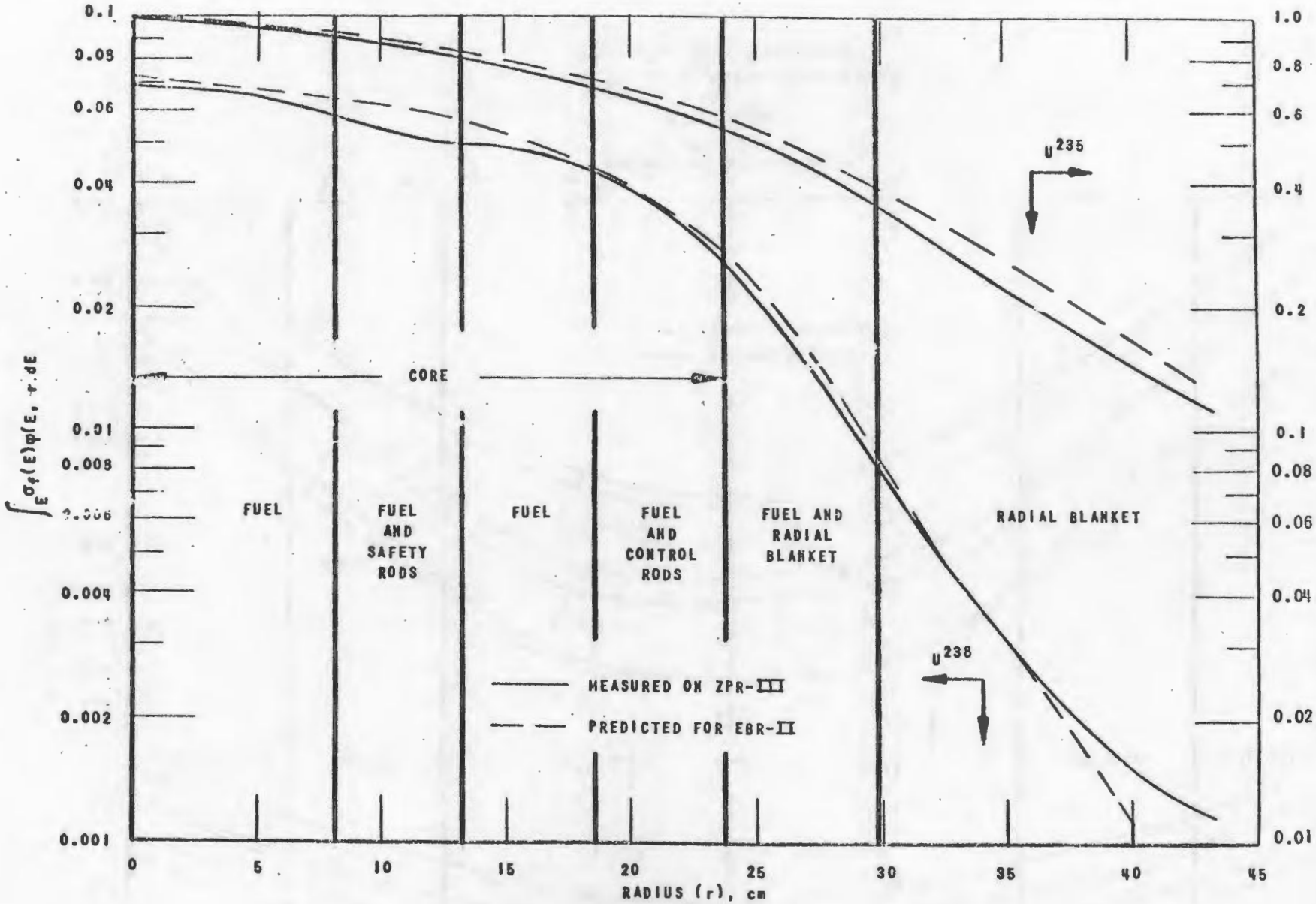

Fig. E-1

Radial Fission Distributions at Core Midplane

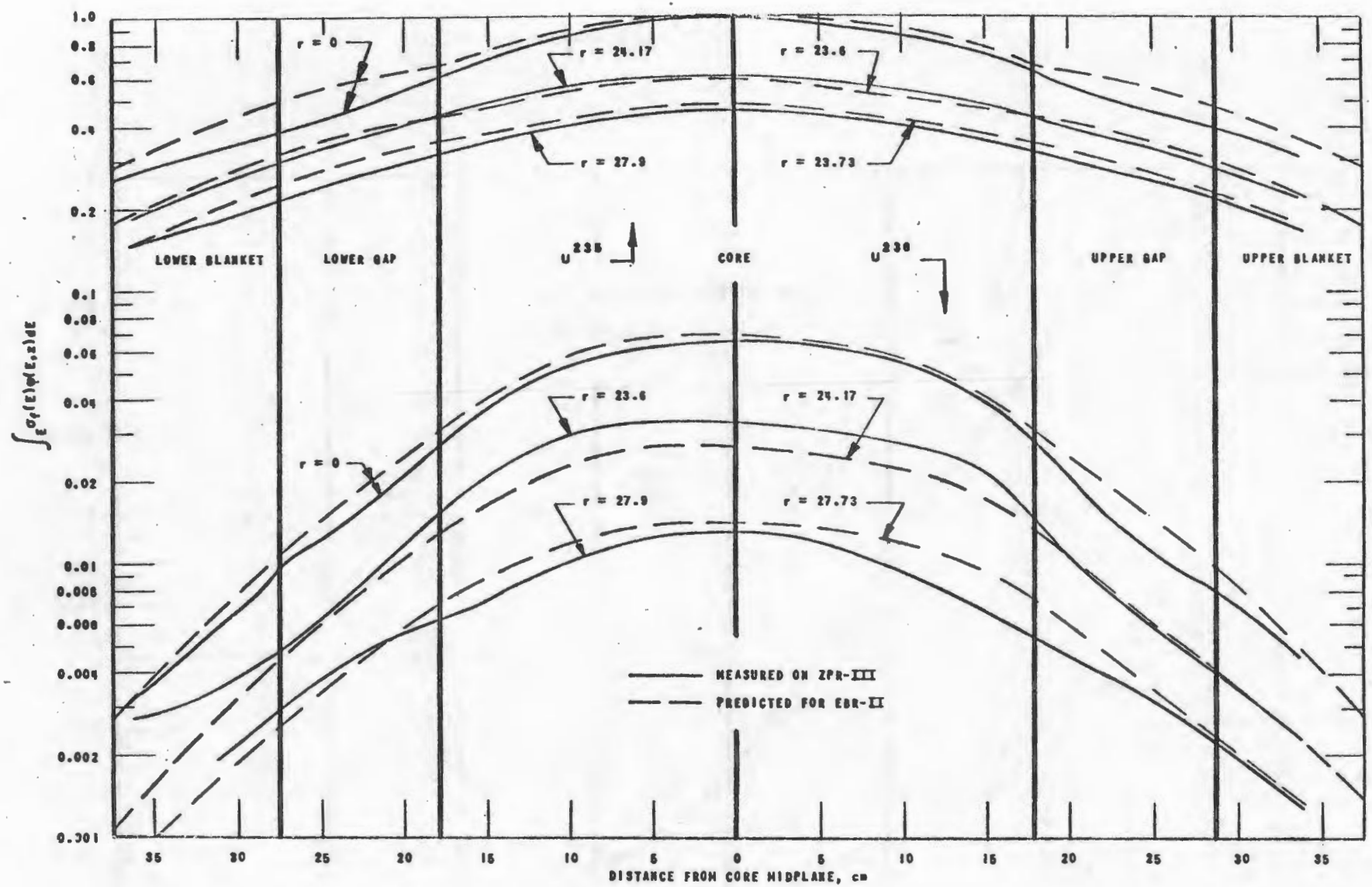

Fig. E-2

Axial Fission Distributions at
Three Radial Positions

APPENDIX F

EFFECTS OF OPERATIONAL ABNORMALITIES

1. Nuclear Accidents

Several cases of reactor mismanagement and/or malfunction were assumed and analyzed earlier [Appendix A-1, p. 198]. The six assumed hypothetical conditions were described as follows:

"Case 1.

Assume the reactor is at delayed critical and at zero power conditions (~8 watts and 600°F) with the shutdown safety rods out. These rods are then inserted into the core at their normal speed of 2 in./min.

"Case 2.

Assume the reactor is at delayed critical and zero power conditions with the central fuel subassembly removed. This subassembly is then loaded at regular speed of 6 in./min for the last 24 in. of travel.

"Case 3.

Assume the reactor is at delayed critical and zero power conditions and a single control rod is driven in at 5 in./min.

"Case 4.

Same as Case 3 except we begin excursion at operating power and full flow.

"Case 5.

Assume the reactor is at delayed critical and zero power conditions with the central fuel subassembly being loaded. It is dropped and falls into the reactor. This is an accident where the reactivity is added rapidly. Two cases are considered, first where the subassembly is dropped from just above the core, and the second where the subassembly falls the full length of the reactor.

"Case 6.

Same as Case 2 but the fuel subassembly is driven all the way in at high speed (72 in./min)."

An analytical evaluation [Appendix A-1] of these accidents showed that the first four cases involving "uncontrolled" reactivity additions by normal components of the reactor system (at normal speed) are terminated by normal operation of period and/or power level trips. In the event the safety devices fail, reactor melting may occur. This is also true of the last two hypothetical accidents (Cases 5 and 6). It should be noted that a combination of malfunctions and/or a gross loss of administrative control are required to achieve these hypothetical conditions.

These conclusions, based on kinetic analyses, contained uncertainties because neither the reactivity insertion rates nor the thermal feedbacks had been verified experimentally. The conclusions have been strengthened by measuring the total and incremental reactivity worth of control, safety, and core subassemblies on the EBR-II mock-up on ZPR-III as well as during the Dry Critical Experiments. The measurements of the EBR-II dry isothermal temperature coefficient and gross and detailed material replacement experiments on ZPR-III have indirectly verified the predicted prompt reactor shutdown coefficients.

Table F-1 summarizes expected reactivity insertion rates for the reactor and compares these with the original predictions used to establish the mechanical drive speeds. Measured results from ZPR-III and the dry critical reactor are shown for comparison. Total reactivity worths of control, safety and core subassemblies were originally predicted [Appendix A-1] slightly higher than are now estimated on the basis of subsequent experiment and analysis. Therefore, the actual reactivity insertion rates, with the same mechanical drive speeds, are less than those used in the accident analyses.

Table F-1

NORMAL RATES OF REACTIVITY INSERTION

	Control Rod				Two Safety Rods				Loading Central Core Subassy.		
		Measured				Measured					
	Original Prediction[a]	EBR-II Mockup on ZPR-III[b]	EBR-II Dry Critical[c]	Present Estimate[d]	Original Prediction[a]	EBR-II Mockup on ZPR-III[b]	EBR-II Dry Critical[c]	Present Estimate[d]	Original Prediction[a]	Measured EBR-II Mockup on ZPR-III[b]	Present Estimate[d]
Total Reactivity Worth, % Δk/k	<0.6	0.37	0.35	0.4	2.0	1.36	1.03	1.3	~2.0	1.5	1.5
Drive Speed, in./min	5.0	(5.0)	5.0	5.0	2.0	(2.0)	2.0	2.0	6.0	(6.0)	6.0
Effective Stroke, in.	14.0	(14.0)	14.0	14.0	14.0	14.0	14.0	14.0	-	-	-
Rate of Reactivity Addition, % (Δk/k)/sec:											
Average	0.003	0.0022	0.0021	0.0024	0.005	0.0032	0.0025	0.0031	0.015	0.011	0.011
Maximum	<0.006	0.0040	0.0030	<0.0041	<0.010	0.0055	0.0036	0.0053	0.02	0.018	0.018

[a]Multigroup calculations in ANL-5719. (For more recent calculations see Reference 17.)

[b]The drive speeds are inferred. Only static incremental measurements were performed (see Appendix E).

[c]See Appendix L and Reference 2.

[d]These values are appropriate for reactor startup.

The lower reactivity insertion rates provide more time for an accident to be terminated if the predicted prompt shutdown coefficients are operative. Verification of the predicted prompt temperature-induced shutdown coefficients is inferential. The measured dry isothermal temperature coefficient is -2.6×10^{-5} $(\Delta k/k)/^{\circ}C$; this may be compared with a corresponding predicted value of -1.8×10^{-5} $(\Delta k/k)/^{\circ}C$. This comparison may be used only to show that the predicted shutdown coefficients have the right order of magnitude. More detailed comparisons between predicted and measured reactivity effects are based on ZPR-III material replacement experiments. Table F-2 compares predicted reactivity effects due to changes in reactor density and geometry [Table A-1], with data from material replacement experiments with the EBR-II mock-up on ZPR-III. The predicted core reactivity coefficients are in substantial agreement with the measured values. These are the more important shutdown coefficients in a slow excursion, while the core fuel expansion alone is most important for a fast excursion.

Table F-2

REACTIVITY EFFECTS OF CHANGES IN MATERIAL DENSITY

$\left(\text{in units of } \frac{\Delta k}{k} \Big/ \frac{\Delta \rho}{\rho}\right)$

	Uranium[a]		Sodium[a]		Stainless Steel[a]	
	Original Prediction[b]	Measured	Original Prediction[b]	Measured	Original Prediction[b]	Measured
Core	0.55	0.52	0.03	0.034	0.028	0.023
Inner Blanket[c]	0.047	-	0.007	<0.01	0.016	<0.03
Outer Blanket[c]	0.01	-	0.0006	>0.0004	0.0021	>0.008
Total Radial Blanket[c]	0.057	-	0.0076	<0.011	0.018	<0.044
Structural Gaps	-	-	0.013	0.011	0.026	0.027
Upper + Lower Blanket	0.017	-	0.0074	0.0073	0.015	0.0042

Axial Core Expansion:[d] $\Delta k/k = 0.27\ \Delta L/L$ (predicted) $= 0.28\ \Delta L/L$ (measured).

[a]Effect of change in density.

[b][Table A-1].

[c]Results on blanket substitutions are not well defined because of uncertainty in radial boundary locations in the ZPR-III experiments.

[d]Increase in core height without decrease of density.

It may be concluded that reactivity insertion rates are slightly less than, and shutdown coefficients are essentially unchanged from, those used in analyzing the six accidents. The original analyses [Figs. A-1 to A-22] are essentially unaltered when compared with more recent analyses. The only new conclusion pertaining to the course of these postulated accidents tends to make slightly more time available for either the operator or the circuitry to terminate the excursion. Table F-3 summarizes the six postulated mechanical malfunctions (described earlier - Cases 1 through 6), and their consequences under various conditions.

Table F-3

SUMMARY OF SIX HYPOTHETICAL ACCIDENTS

Case No.[a]	Initial Power, watts	Loss of Administrative Control?[b]	How Terminated	Time, sec[c]	Power Level, watts	Time for Melting,[d] sec
1	8	yes	Period Level	<70 70	- 10^3	120
2	8	yes	Period Level	<25 30	- 10^3	55
3	8	no	Period Level	?[e] ~100	- 10^3	~230[f]
4	6×10^7	no	Period Level	-[g] ~ 5	- 6.9×10^7	20-50[h]
5	8	yes	Period Level	?[i] ?	- $<10^2$	≤ 0.13
6	8	yes	Period Level	<1 4	- 10^3	~6

[a]Case Descriptions (complete description in text):

1. Safety Rod Drive, 2 in./min.
2. Central Core Subassembly Loading Mechanism, 6 in./min.
3. Control Rod Drive, 5 in./min.
4. Control Rod Drive, 5 in./min.
5. Central Core Subassembly Loading Mechanism, gravity induced.
6. Central Core Subassembly Loading Mechanism, 72 in./min.

[b]Is loss of administrative control required to initiate the accident?

[c]After reactivity insertion is initiated.

[d]Time required for melting to occur after reactivity insertion is initiated if both period and level trips are inoperative or not effective.

[e]A 20-second period trip setting may cause a period scram at ~100 sec.

[f]Melting may not occur but fuel alloy-clad eutectic formation temperatures will be exceeded in the fuel alloy.

[g]Period will not be short enough to cause period scram.

[h]To achieve fuel alloy-clad eutectic formation temperature on surface of hottest fuel pin. The clad temperature will be lower. The range is large because the required time depends on (1) control rod position, and (2) the influence of uncertainty factors (Section IV.B.3.).

[i]Both period and level trips will actuate immediately but time may not be available to prevent fuel alloy melting.

The potentially most serious of these accidents, requiring almost immediate response of the automatic trip circuits to prevent serious damage, must be preceded by a gross loss of administrative control during fuel handling (loading the reactor). Normally, the reactor is at least

3% $\Delta k/k$ subcritical while fuel-handling sequences are carried out. To postulate the reactor at delayed critical would require the inadvertent introduction of at least ten enriched inner blanket subassemblies in row 6, in addition to those required for normal operation. The inadvertent introduction of so much reactivity bringing the system to very high multiplications characteristic of an approach to delayed critical certainly would be apparent on subcritical flux-monitoring equipment.

2. Failure of All Primary System Pumps

One type of operational abnormality is represented by the sudden cessation of all primary system pumping power. The objective in this section is to indicate the time-dependent temperature distributions obtaining within the reactor as a result of three assumed modes of losing all pumping power. The following cases are considered:

(1) Loss of all pumping power occurs; reactor scram follows immediately.

(2) Reactor scram occurs; loss of all pumping power occurs soon (seconds) afterward.

(3) Loss of all pumping power occurs; all control rods remain fixed in their initial positions.

Three pumps are provided in the primary system: two large "main" pumps, and one small "auxiliary" pump. Each main pump is supplied with electrical power from the building power supply (which may or may not be interconnected with the EBR-II generator). The auxiliary pump is powered by a rectifier operating on building power, but is backed up by a floating battery power supply. Thus for all primary system pumping power to be lost, either: (1) simultaneous mechanical failure of all three pumps must occur; or (2) both building power supply and auxiliary pump battery supply must be lost simultaneously.

A number of design changes have been made which affect to some degree the analysis presented in ANL-5719 [Pages 213-218]. The two main primary pumps are now of the mechanical, centrifugal type as opposed to the original electromagnetic type; consequently, upon loss of power to these pumps the primary system coolant flow will decay initially at a substantially slower rate (because of the momentum of the impeller, drive shaft, and motor) than originally assumed [Fig. A-23]. The new flow decay curve is shown in Fig. F-1. Control rod acceleration during scram has been revised to 1.5 g; accordingly, the rod displacement vs. time curve [Fig. A-24] is altered to that shown in Fig. 31, and the rate at which reactor power decays subsequent to the start of rod scram [Figs. A-25 and A-28] is lowered slightly. Additional revisions made, which have small effect or

no effect upon this analysis, include: modification of coolant flow distribution; alteration of initial reactor temperature distribution; modification of the reactor outlet piping (to the heat exchanger); increase in expected control rod release time; and reduction of over-all uncertainty factor magnitudes applicable to temperature distribution determination.

The net effect of all of the above changes and improvements in the calculational techniques used in the present analysis is, in most respects, small. Although the shapes of all the original reactor temperature vs. time curves presented [Figs. A-26, A-27, and A-29 through A-34] are altered somewhat (in most cases principally by a shift in the time at which the temperature peaks occur), the temperature maxima exhibited are either increased acceptably or are decreased. The new curves are shown in Figs. F-2 through F-9. As in the earlier report, these curves are based upon the initial reactor temperature distributions actually expected to obtain (without uncertainty factors). If effects of uncertainty factors should alter the initial temperature distributions, the peak maximum core fuel temperatures realized during the transients have been pessimistically estimated to be approximately 100°F higher than those presented. It should be noted that peak maximum core coolant and uranium-clad interface temperatures are expected to approach closely the peak maximum core fuel temperatures.

3. Bowing

The analysis presented in ANL-5719 [Pages 218-226] on bowing of fuel elements and the resultant changes in effective core radius (and reactivity) remains valid except for one change. This change, reduction from 100°F to 50°F of the expected maximum temperature differential (ΔT_M) across the flats of a fifth-row subassembly at full reactor power, is of substantial benefit. While it in no way alters the estimated maximum possible core radius or reactivity change due to bowing, it significantly reduces the magnitude of the maximum possible positive power coefficient of reactivity contemplated, as described in Section IV.I.2.

The above decrease in expected magnitude of ΔT_M has resulted from: increased coolant flow rate through fifth-row subassemblies; improved expected coolant flow distribution (internal) in fifth-row subassemblies, as indicated by water tests conducted on a model subassembly; and reduction in magnitude of the expected gradient in radial power density distribution, as determined by further experimentation and calculation.

Two modifications in design of fuel element subassemblies have been made which also deserve comment here. These are discussed below.

As noted in the discussion on bowing [Page 218], the fuel elements of a subassembly are assumed tightly packed within the containing

(hexagonal) tube. This is a clearly valid assumption in the case of a newly fabricated subassembly, but perhaps should be considered as only a probably valid assumption in the case of a subassembly with a long operating history. The basis for this slight reservation in the latter case stems from a peculiarity of geometry inherent in the use of helically-wound wires about the fuel elements for spacing purposes. It is possible to imagine that, although the top and bottom ends of the fuel element cluster must remain firmly positioned laterally within the subassembly irrespective of operating history, the central portion of the cluster theoretically could, if it were by some process to undergo a major alteration in its geometry, acquire a capacity for independent lateral movement. Conceivably, with prolonged operation, the cluster could sustain a gross distortion such that its original configuration of a right hexagonal cylinder would be transformed into that of a solid helix of hexagonal cross section and 6-inch pitch (the pitch of the spacer wires). In the most extreme case theoretically possible, such a transformation would render the effective "distance across flats" of the cluster 0.049 in. (the thickness of one spacer wire) smaller than that of the original configuration. The 0.049-inch clearance thus created would be available for bowing of the central portion of the cluster within the subassembly container. Despite careful consideration of this theoretical possibility, no reasonably realistic mechanism has been developed which is capable of producing such an extreme, ordered distortion. There does seem to exist some possibility that a limited amount of this type of distortion could be effected as a result of the temperature differential between spacer wire and fuel element jacket incurred during operation; the effect would be for the wire to increase in length by a lesser amount than the jacket and, after absorption of the wire slack, to impose forces tending to warp the jacket helically. Presumably, to whatever extent this might occur on the individual fuel elements, the cluster of elements as a whole would be effected in similar fashion.

The possibility of a significant amount of "loosening up" of the central portion of fuel element clusters as discussed above seems remote. Prolonged testing of a prototype subassembly under sodium temperature and velocity conditions equal to those expected during operation (but without the temperature differential referred to, which cannot be simulated outside the reactor), produced no distortion whatever (see Appendix B). Nevertheless, to reduce somewhat the maximum clearance between cluster and tube which theoretically could be generated, line "dimples" of 0.020 in. height have been added to the inner walls of the tube at elevations approximately half-way between those of the lines of contact between tube and spacer wires. By this means, the theoretical maximum clearance attainable is reduced from 0.049 in. to about 0.029 in. To preclude the possibility of even the latter amount of distortion being realized, subassemblies will be withdrawn periodically from the reactor on a progressive incremental burnup basis and inspected.

The other design change of interest with respect to bowing applies to the control rod subassemblies only. A flow-twisting device has been incorporated in the region between the top of the fuel element cluster and bottom of the upper shielding section of these subassemblies. As described in Section III.A.1.f., the function of this device is to rotate the flow path of the coolant emerging from the fuel section about the longitudinal axis of the subassembly so as to reverse the sign of the temperature differential across the subassembly flats. This action, together with the increased mixing resulting and the higher coolant flow rate now employed, should substantially reduce the magnitude of bowing realized.

4. Fuel Element Failure

There are two important aspects of fuel element failures which can be considered: (1) the cause of failure, and (2) the effect of failure, particularly with respect to the probability of propagation. The failure of a single fuel element does not pose a serious problem since under the worst assumed redistribution of the fuel, the reactivity effect on the reactor is small. Fission products and fuel would be released to the sodium coolant, but this in itself does not represent a hazard, but rather an operational inconvenience. If the failure tends to propagate, involving a larger volume of the reactor, then the consequences can be serious. Both aspects of this problem are considered in this section.

It is difficult to characterize fuel element failure since it may involve: (1) coolant flow blockage by foreign material; (2) coolant flow blockage due to gross swelling or distortion of fuel elements; (3) mild (or slow) failure of the fuel element tube with a small displacement of the fuel alloy into the coolant channel; or (4) rupture of the fuel element with dispersal of the fuel alloy through the subassembly. Of these various possibilities, only the first is relatively amenable to analysis; the remainder involve redistribution of the fissionable material and thus a change in the geometry of the heat source.

The effect of flow blockage of coolant channels was evaluated by assuming five different cases of flow channel blockage caused by foreign material. The following conditions applied to each analysis:

(1) The reactor is at steady-state, full-power operation (62.5 Mw).

(2) The maximum fuel alloy and fuel alloy-clad interface temperatures, 1197°F and 1060°F, respectively, apply prior to the coolant channel blockage. These refer to those fuel elements in a subassembly which normally exhibit the highest temperatures. (It should be noted that these maximum temperatures are slightly lower than those given in Table X and Fig. J-1. Renormalization to those values does not significantly alter the results of these analyses.)

(3) The foreign particle accumulations are assumed to have the thermal conductivity of Type 304 stainless steel (the predominant structural material in the primary system).

(4) Except for Case 4, the foreign particle accumulations are assumed to extend along the entire axial length of the fuel elements.

Case 1 is illustrated in Fig. F-10. The particle accumulation in a single coolant channel triflute increases the maximum fuel alloy temperature from the normal value of 1197°F to about 1213°F. The fuel alloy-clad interface temperature is increased from the normal 1061°F to about 1165°F. In evaluating these and later results it should be noted that the fuel alloy-clad eutectic melting point is 1340°F.

Case 2 is illustrated in Fig. F-11, along with resulting fuel alloy-clad interface temperatures. The thickness of the foreign particle accumulation is equal to the outside diameter of the spacer wire.

Case 3 is illustrated in Fig. F-12. The maximum fuel alloy temperature is increased from the normal 1197°F to about 1261°F. The corresponding maximum fuel alloy-clad interface temperature increases from the normal 1061°F to about 1173°F.

Case 4 assumes particle accumulation to occur in the region of the fuel element grid bars, resulting in restriction of flow to the core section of the subassembly (see left detail on Fig. 7). Figure F-13 shows the resulting temperatures as a function of blocked flow area and resulting reduction in coolant flow. It may be seen that with 50% of the flow area blocked, fuel temperatures increase less than 50°F.

Case 5 is illustrated in Fig. F-14. The particle accumulation is identical to that of Case 1 except that a number of blocked channels are assumed to occur in the same subassembly, but with no fuel element in contact with more than one blocked channel. Maximum fuel alloy and fuel alloy-clad interface temperatures are also shown on Fig. F-14. These increase very slowly as the number of blocked coolant channels increases beyond the first.

The assumptions made in these five cases are believed very pessimistic since it is necessary for the foreign material to assume a very complex geometry and to do so very efficiently. However, it is evident that extensive accumulations of foreign material can be accommodated within the EBR-II core without developing unacceptably high temperatures.

A fuel element containing large voids in the sodium bond could lead to abnormally high fuel alloy temperatures. This problem has been analyzed to establish EBR-II fuel element fabrication requirements.[22] It

was found that the width of a vertical void column in the annular sodium bond region must exceed 60° (out of 360°) to shift the maximum fuel alloy temperature from the interior to the surface of the fuel pin, and that the maximum fuel alloy temperature does not approach 1340°F (the alloy-clad eutectic temperature) until the angular width of the void exceeds 70°. This temperature obtains only so long as the fuel alloy is not in contact with the clad; the clad is cooled by the flowing coolant. The consequences of this sequence are difficult to assess since, undoubtedly, the irradiation damage (swelling) would proceed more rapidly because of the higher alloy temperature. The fuel alloy temperature would be lowered as the pin makes contact with the clad and heat transfer is improved. Theoretically, at the points of contact between the cladding and the fuel alloy, the temperature would be well below the eutectic temperature. Although it cannot be concluded that the eutectic would be formed and the fuel element fail by this mechanism, it is quite probable that some distortion would occur, perhaps more analogous to the cases of flow blockages assumed above. These might tend to combine, i.e., reduced local coolant flow and poor heat transfer from the fuel to the coolant, and in combination cause a fuel element failure. Although the exact mechanism for inducing such a failure is difficult to postulate, such a failure must be considered possible.

If the fuel alloy from one fuel element is significantly redistributed and if some local boiling of sodium occurs simultaneously, a detectable change in power level may occur. In general, the change in power level will be quite small and can lead to either increasing or decreasing values, depending upon the manner of fuel alloy redistribution. A redistribution equivalent to removal of a fuel pin from the reactor would result in a reactivity loss of $<0.02\%\ \Delta k/k$. The equivalent compaction of a fuel pin near the core midplane would increase the reactivity by $<0.005\%\ \Delta k/k$. With less extreme fuel alloy redistribution, an undetectable reactivity change could occur; it is almost certain that a small failure would not be detected by noting a change in power level. Some fission products would be released to the coolant.

From Case 5 above, it can be seen that several such failures can occur independently without serious consequences provided: they are entirely independent; occur at different times; and adjacent coolant passages are not affected. However, it must also be assumed that failure can occur in such a manner as to be self-propagating, i.e., displaced fuel from one fuel element causes blockage of the coolant channel for another fuel element which, in turn, causes failure of that element. If a large number of fuel elements become involved and significant fuel displacement occurs and/or sodium boiling occurs, a change in reactivity should be noted. In addition, a larger release of fission products and fuel to the coolant will occur.

Three different modes (or degrees) of fuel propagation may logically be considered: (1) the central 61 fuel elements (of the 91) in the

subassembly fail; (2) all 91 fuel elements in the subassembly fail; and (3) all 91 fuel elements fail and the failure propagates to adjacent subassemblies. The consequences are as follows.

The peripheral row of 30 fuel elements in the subassembly are overcooled with respect to the remaining 61; the mass coolant flow associated with each peripheral fuel element is 136% of the average coolant flow per element (see Appendix C). The additional capacity (to reach fuel or clad melting) represented by the additional coolant and lower fuel element temperature represents a barrier to propagation of fuel failure. This may halt the failure or at least impose a delay in the propagation.

The subsequent change in reactivity, power level, and rate of change of power level will, in all cases, depend on where and how failure is taking place. An increase in power level of approximately 10% ($\simeq$ 0.025% $\Delta k/k$) can result from fuel alloy compaction (to maximum effectiveness) in as few as 5 to 10 failed fuel elements (five near the center of the core, ten near the core boundary). The simultaneous failure and fuel alloy compaction of 61 of the elements in a subassembly could result in a rapidly damped period of 10 to 65 sec if the failure occurred at the core center or boundary, respectively. The corresponding reactivity losses will be greater if fuel alloy is carried away from the core by the coolant. The gross failure of 61 fuel elements will certainly appear as a power level perturbation. If this leads to an increased power level, the reactor will scram; if the power level decreases, an alarm will occur. It is less probable that such a failure will occur rapidly and cause a period scram.

Even if the failure propagation proceeded through the entire subassembly and all 91 fuel elements failed simultaneously, it is difficult to imagine a fuel rearrangement within a single subassembly large enough to cause a serious reactor incident. The total removal or compaction reactivity worths of all the fuel in a subassembly of maximum worth are approximately 1% $\Delta k/k$ and 0.45% $\Delta k/k$, respectively. The compaction may be postulated to occur in 0.15 sec (Appendix G) under very pessimistic circumstances. If the relatively improbable situation of simultaneous failure of 91 fuel elements occurred, the resulting reactivity insertion rate would not exceed \$5/sec, with the total available reactivity insufficient to reach prompt critical. However, if the failure is not induced by a reactor transient, the time required to compact the fuel alloy will exceed the postulated lower limit of 0.15 sec. The large reactivity changes cited apply to the central core subassembly; similar failures at the core boundary result in lower reactivity changes. Further, the required degrees of coincidence in timing and effectiveness of fuel alloy redistribution make the maximum reactivity insertion rate highly improbable. In fact, it is more probable that if a fuel failure tends to propagate, it will do so slowly and fuel will be carried from the reactor; this will lead to gradual reactivity reduction coupled with power anomalies.

More serious consequences could result from a fuel failure propagating rapidly to adjacent subassemblies. This could involve a large fraction of the reactor and perhaps induce a transient which cannot be accommodated by the control system. Of course, for such a chain of events to occur, the failures must occur almost instantaneously, and this appears quite improbable for the following reasons. In addition to the "propagation barrier" provided by the peripheral fuel elements and coolant, the hexagonal subassembly can also provides a barrier. The can is similarly overcooled, and its heat capacity is available to solidify or to retard the propagation of the fuel alloy. In the event that the can is penetrated, the adjacent subassembly can, as well as the sodium between the cans, is similarly overcooled and a further barrier to propagation is presented. Although fuel propagation into adjacent subassemblies cannot be assumed impossible, it is unlikely that propagation will occur essentially instantaneously. It is quite likely that a failure will be confined within the subassembly, but if it propagates beyond this barrier a time delay will be involved. A serious (prompt critical) reactor incident requires that this occur essentially instantaneously (within ~0.2 sec).

A series of experiments conducted in TREAT tend to confirm the confining characteristics of the subassembly can even though these experiments were conducted under conditions of operation quite different from those anticipated in the EBR-II. Four experiments were performed, each employing a cluster of seven standard EBR-II fuel elements properly spaced, and contained inside a hexagonal stainless steel can with a wall thickness equivalent to the EBR-II subassembly can. The subassemblies, in turn, were contained in sealed capsules with inert gas atmosphere. They were exposed to power excursions designed to cause varying degrees of fuel element failure. These were power transient experiments and, therefore, are difficult to compare with the non-transient conditions postulated for EBR-II.

A semi-qualitative comparison can be made of the rate of temperature rise in the fuel with the assumption that fuel behavior (mode or violence of failure, superheat of fuel alloy upon ejection, etc.) may be related to this variable. The TREAT experiments produced a maximum rate of temperature rise of about 8000°F/sec. If complete coolant flow blockage in an EBR-II subassembly is assumed, and with a power density in the core section of approximately 1 Mw/liter, the rate of temperature rise of the fuel would be about 950°F/sec if heat is transferred to the stagnant sodium (in the core section), and about 2700°F/sec if only the heat capacity of the fuel elements is considered available to absorb the energy. It can be assumed, therefore, that even under the worst conditions, the rate of temperature rise would be slower than existed in the TREAT experiments.

Figure F-15 shows the exterior surface of the four hexagonal test subassemblies after the transients. In all cases, the integrity of the

hexagonal can was maintained. Figure F-16 shows the interior damage resulting from failure of the fuel elements. Samples 1 and 2 contained fuel alloy in all seven fuel elements. Samples 3 and 4 contained fuel alloy in only the central fuel element, with the peripheral elements containing stainless steel. The results show that fuel element failure can propagate under extreme power excursions. All of the transients were designed to achieve fuel element clad temperatures in excess of 1800°F. Sample No. 2 achieved fuel element clad temperatures in excess of 2700°F. Although these results were obtained under conditions quite different from those that will exist in EBR-II, it is believed that the conditions in TREAT were actually more severe. The absence of sodium in the TREAT experiments excludes the heat capacity contribution of the sodium, including that represented by the heat of vaporization (the molten fuel and clad exceed the 1640°F boiling point of sodium).

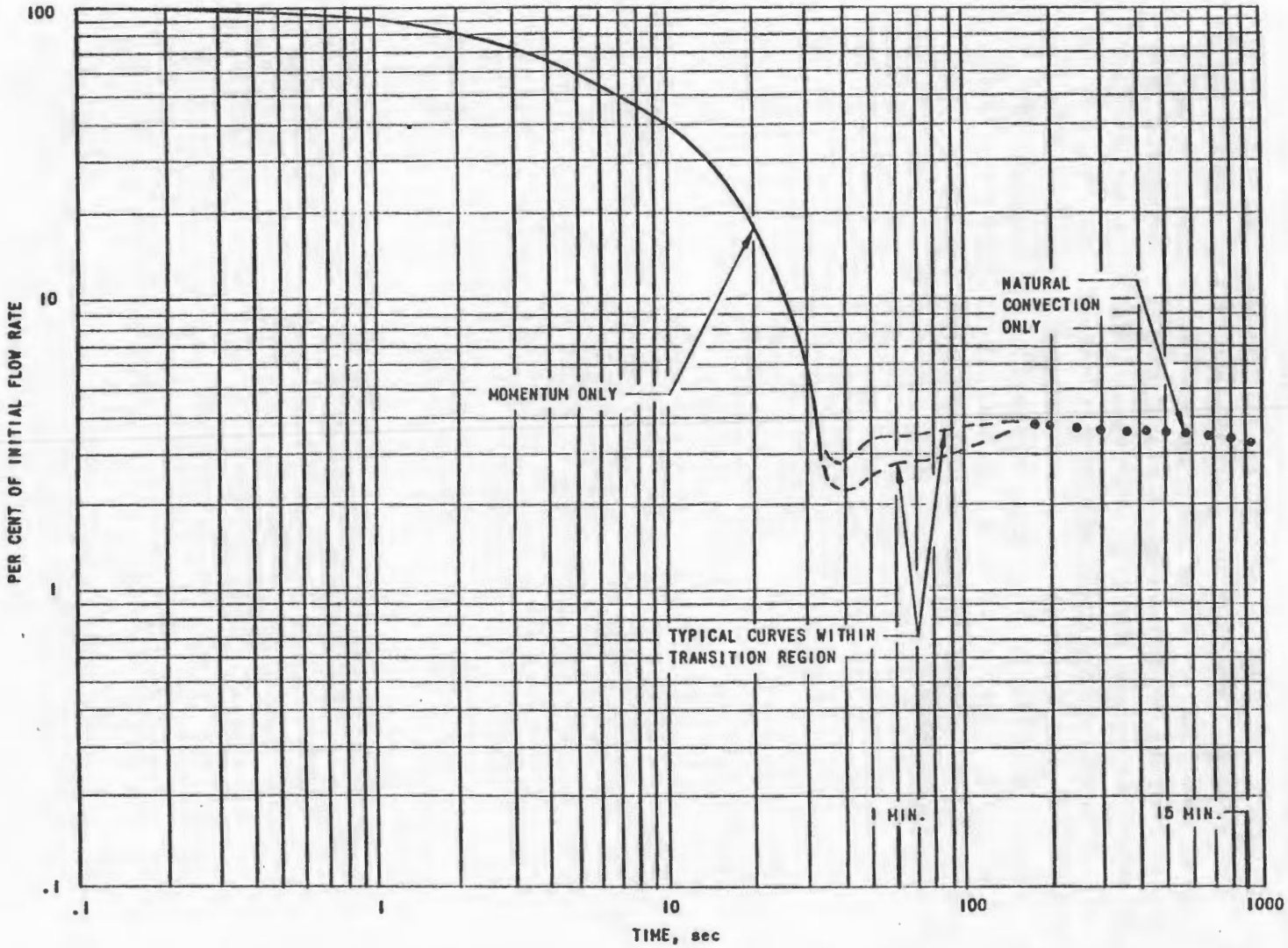

Fig. F-1

Primary System Coolant Flow Rate vs. Time after Cessation of All Pumping Power (Based on 100% Initial Reactor Power and Coolant Flow Rate)

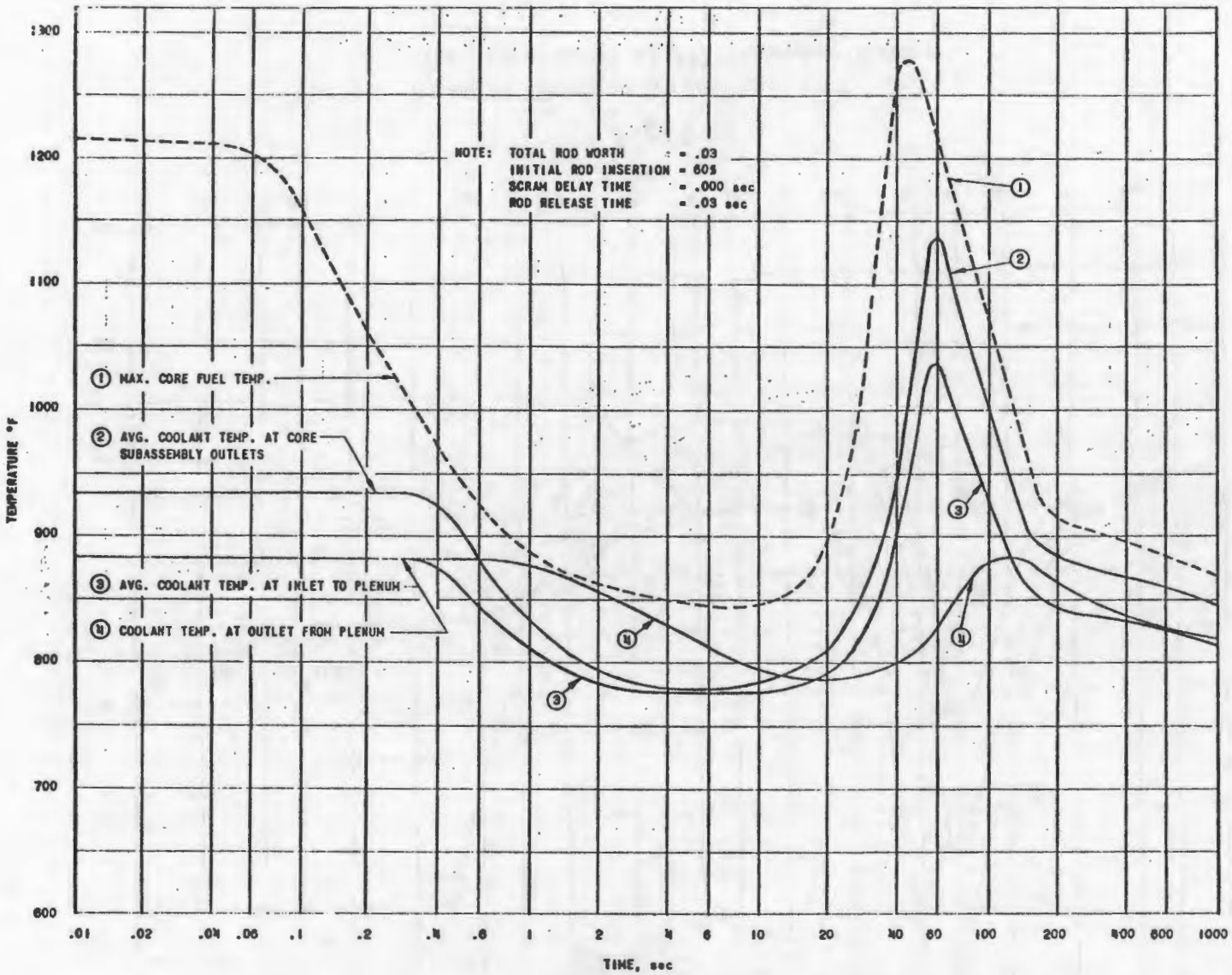

Fig. F-2

Various Reactor Temperatures during Scram vs. Time after Cessation of All Pumping Power

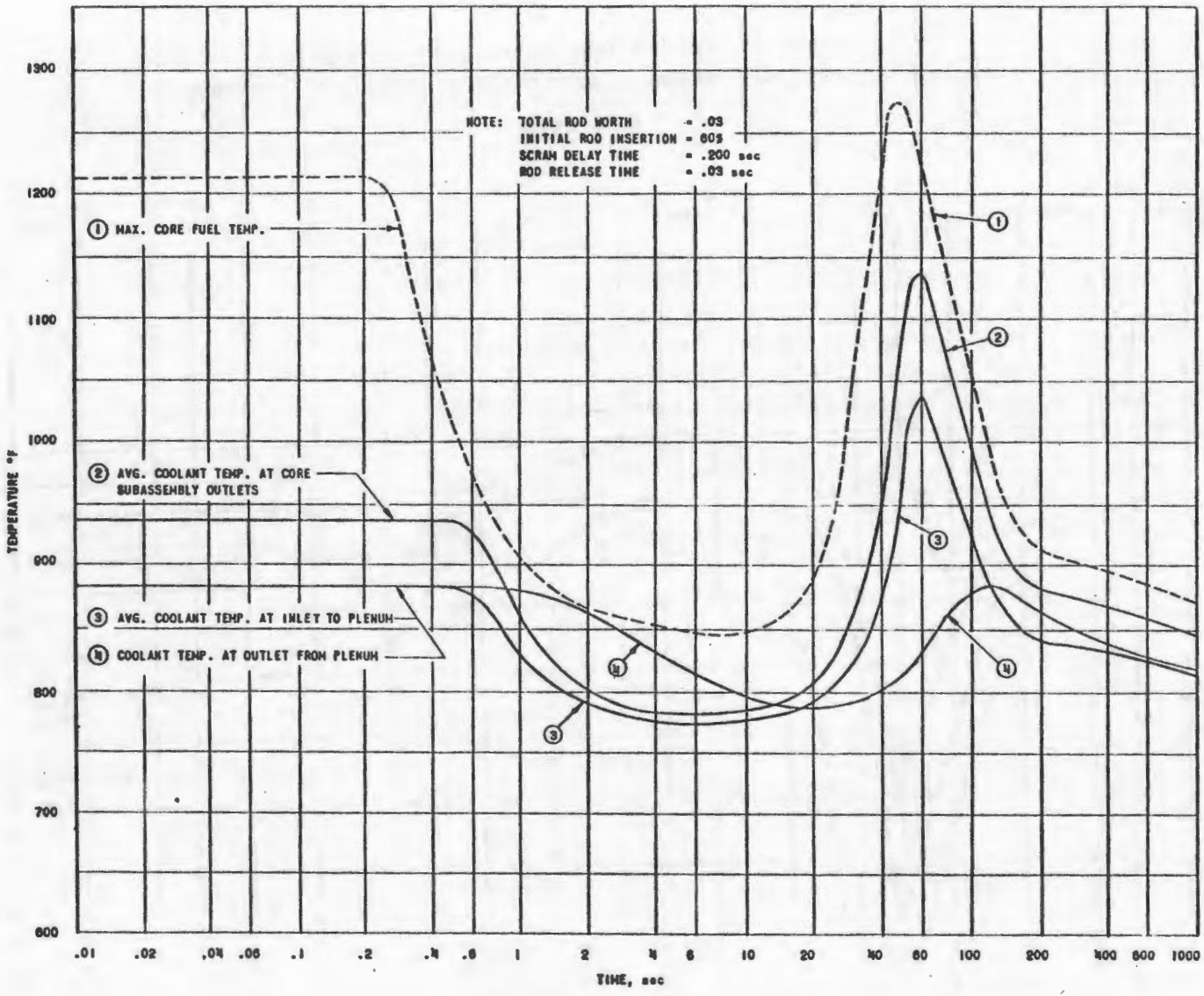

Fig. F-3

Various Reactor Temperatures during Scram vs. Time after Cessation of All Pumping Power

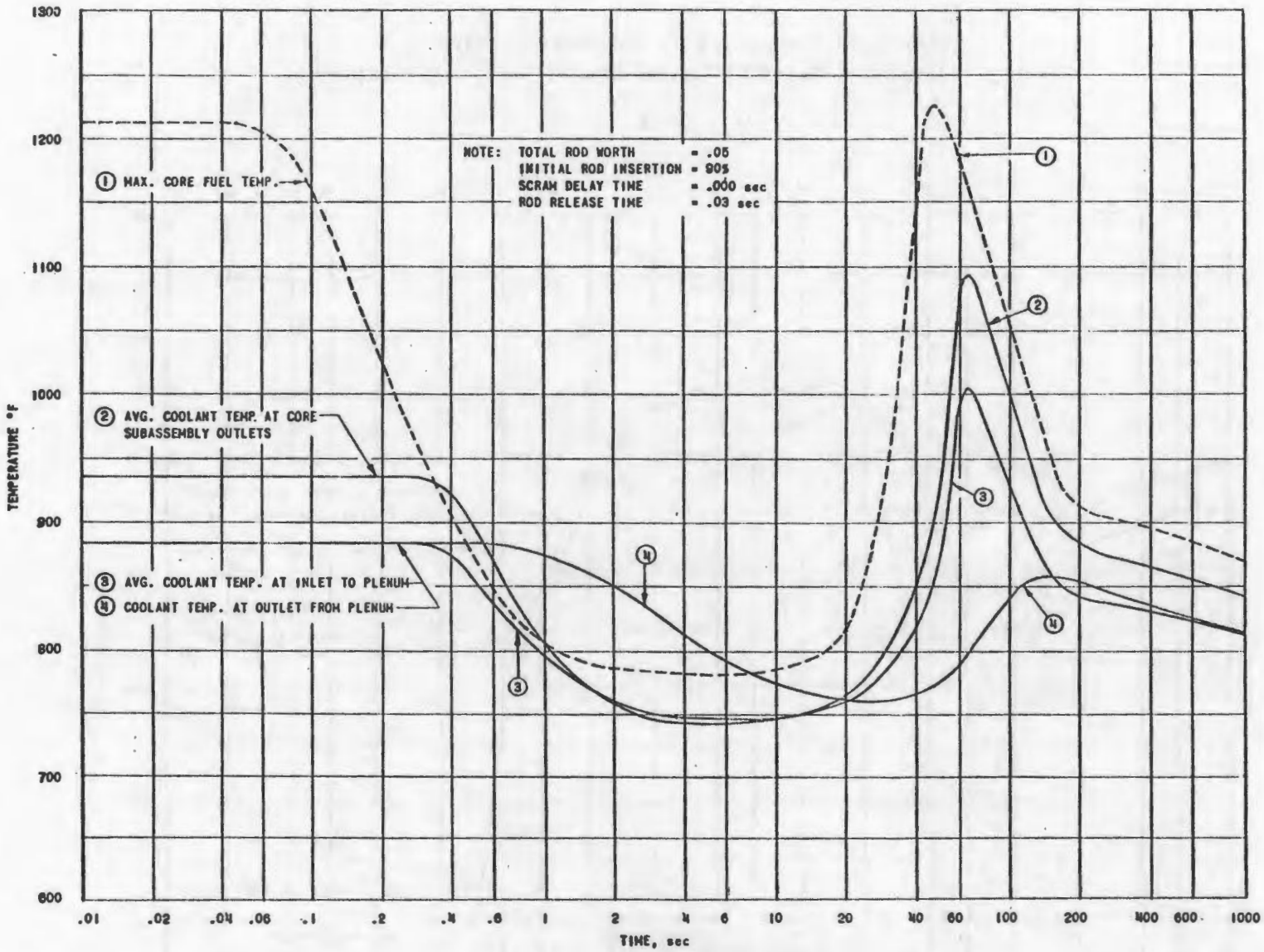

Fig. F-4

Various Reactor Temperatures during Scram vs. Time after Cessation of All Pumping Power

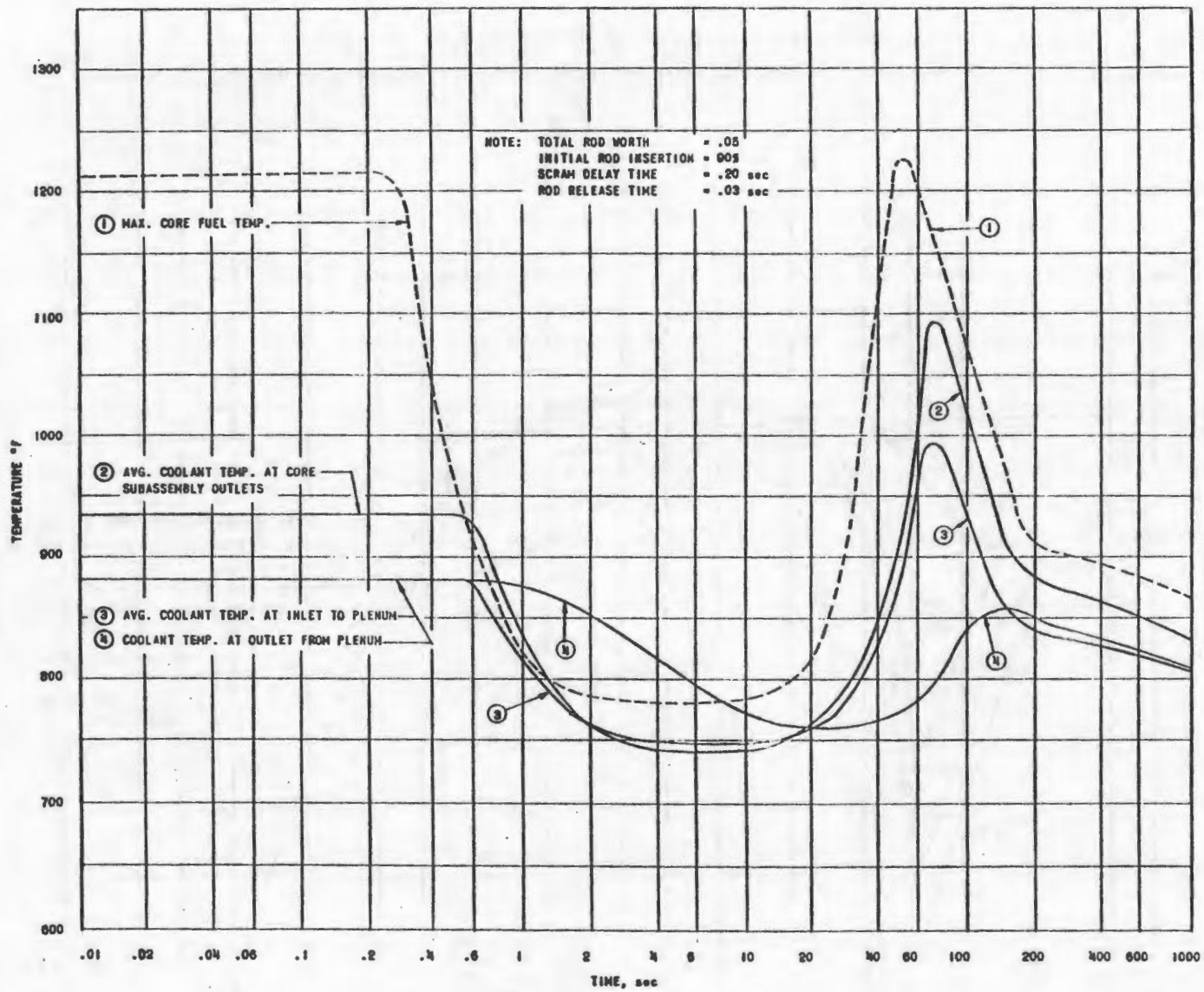

Fig. F-5

Various Reactor Temperatures during Scram vs. Time after Cessation of All Pumping Power

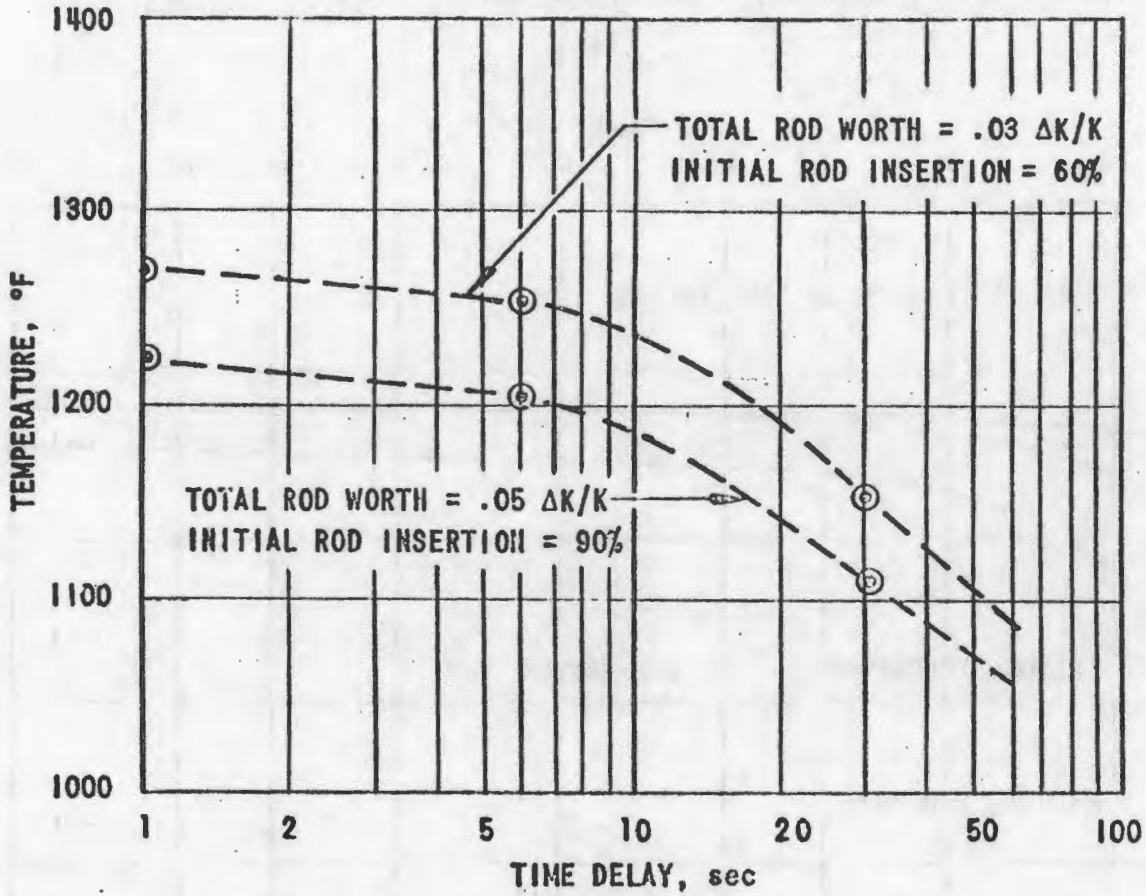

Fig. F-6

Approximate Maximum Core Fuel Temperature Occurring during Transient vs. Time Delay between Start of Scram and Cessation of All Pumping Power

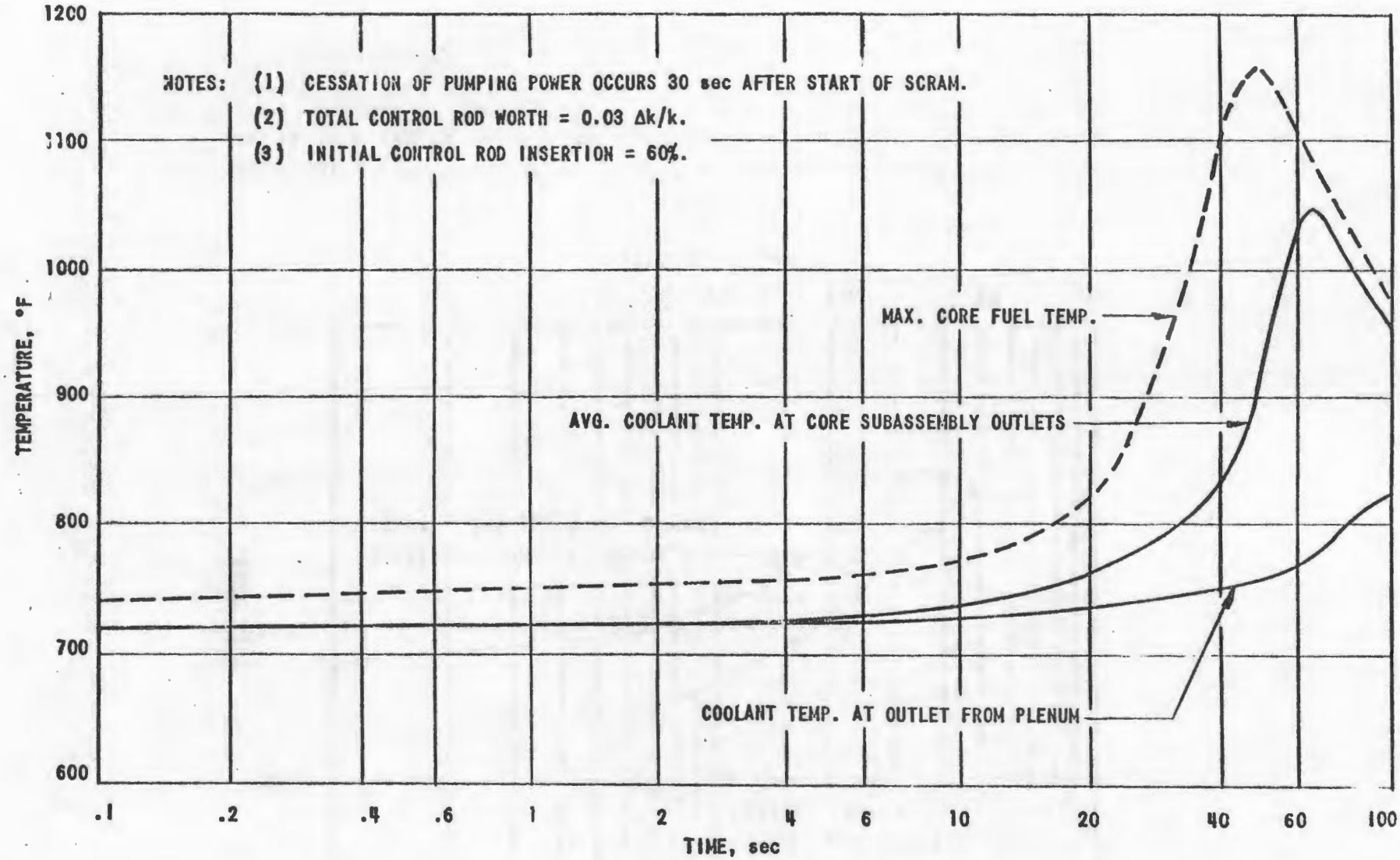

Fig. F-7

Various Reactor Temperatures vs. Time after Cessation of All Pumping Power Subsequent to Scram

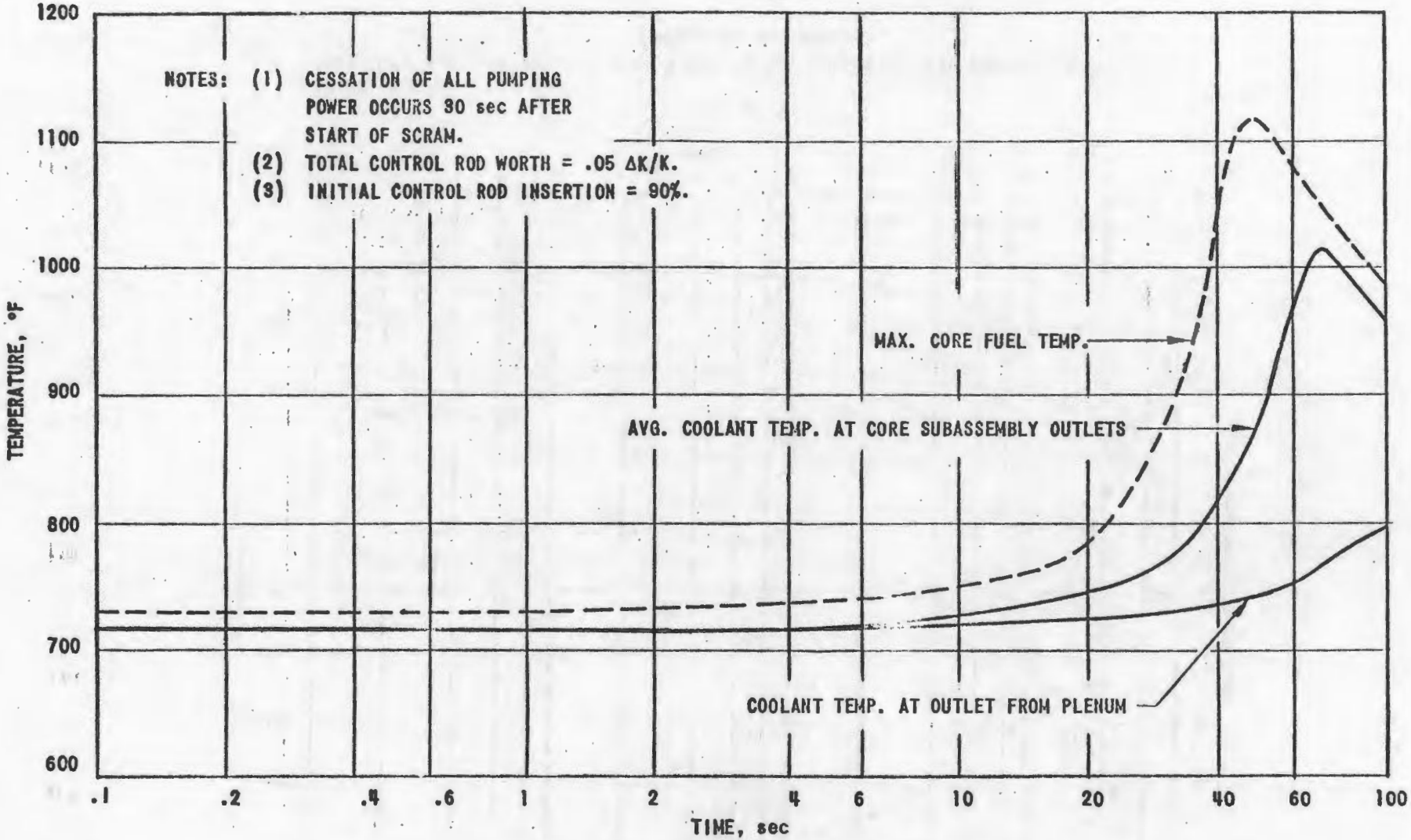

Fig. F-8

Various Reactor Temperatures vs. Time after Cessation of All Pumping Power Subsequent to Scram

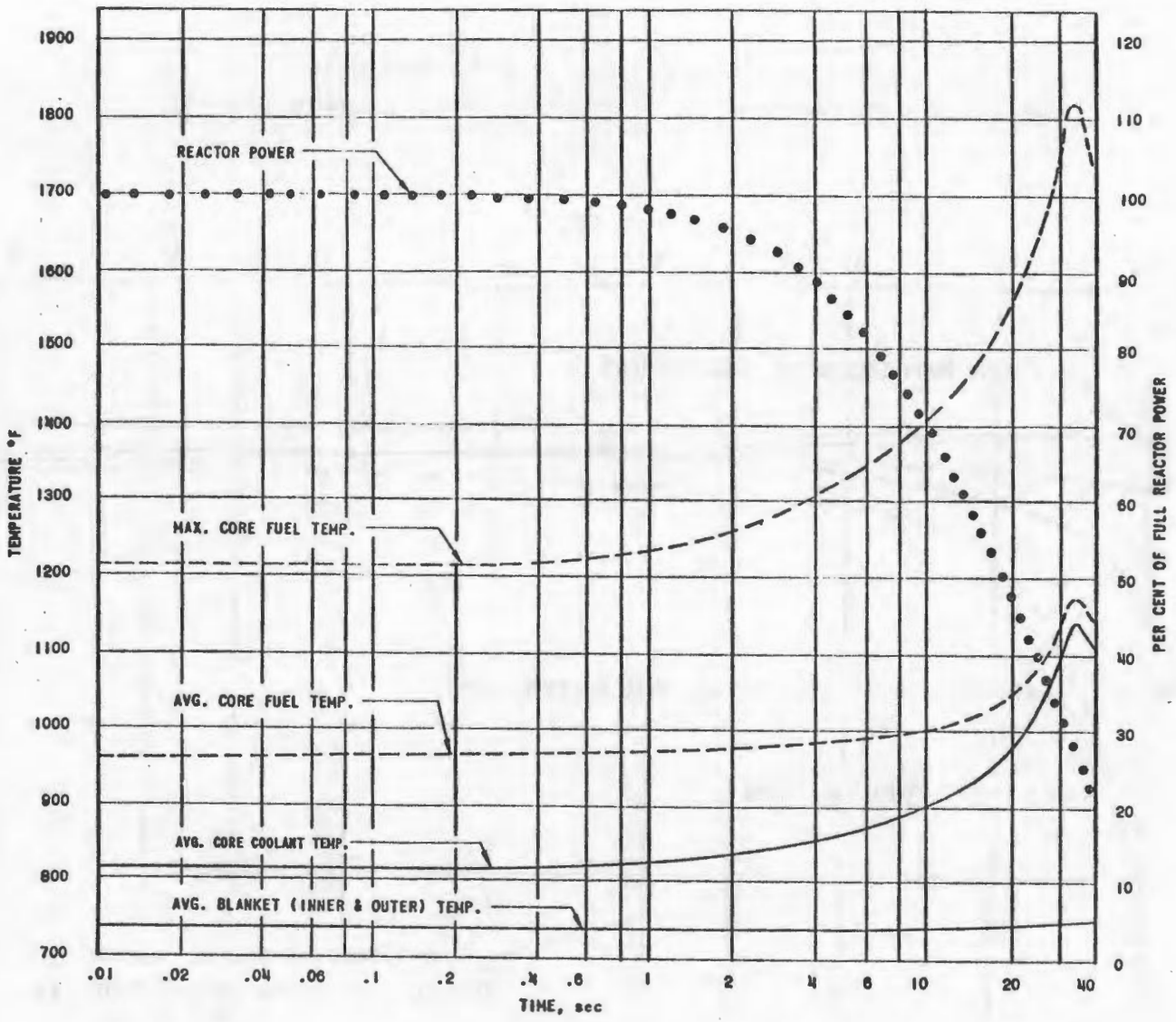

Fig. F-9

Reactor Temperatures vs. Time after Loss of All Pumping Power (Without Scram)

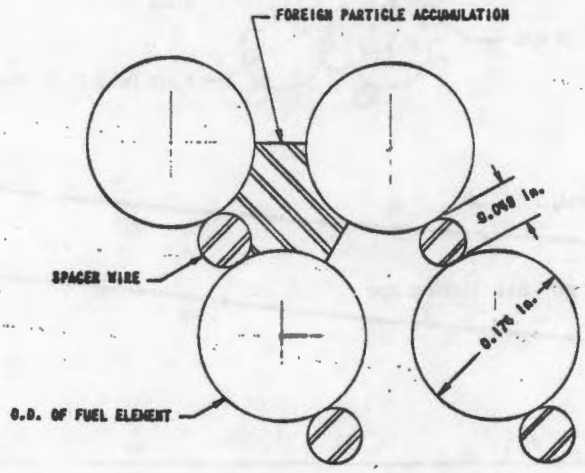

Fig. F-10

Foreign Particle Accumulation (Case 1)

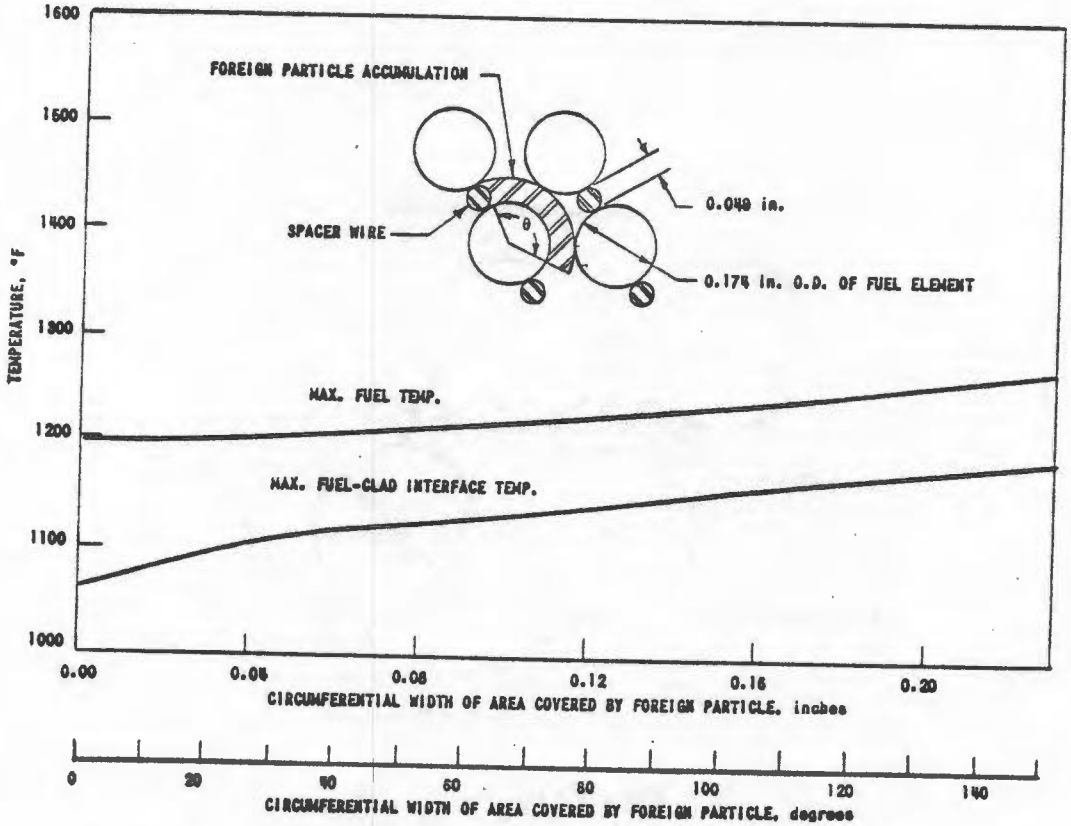

Fig. F-11

Foreign Particle Accumulations (Case 2) and Their Effects on EBR-II Core Temperatures

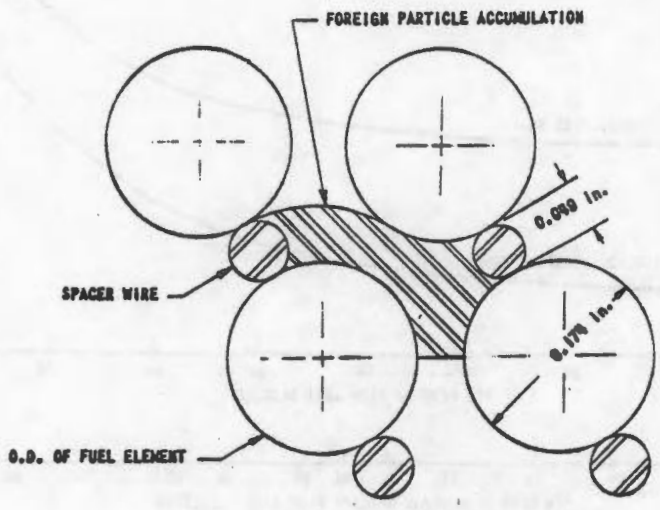

Fig. F-12

Foreign Particle Accumulation (Case 3)

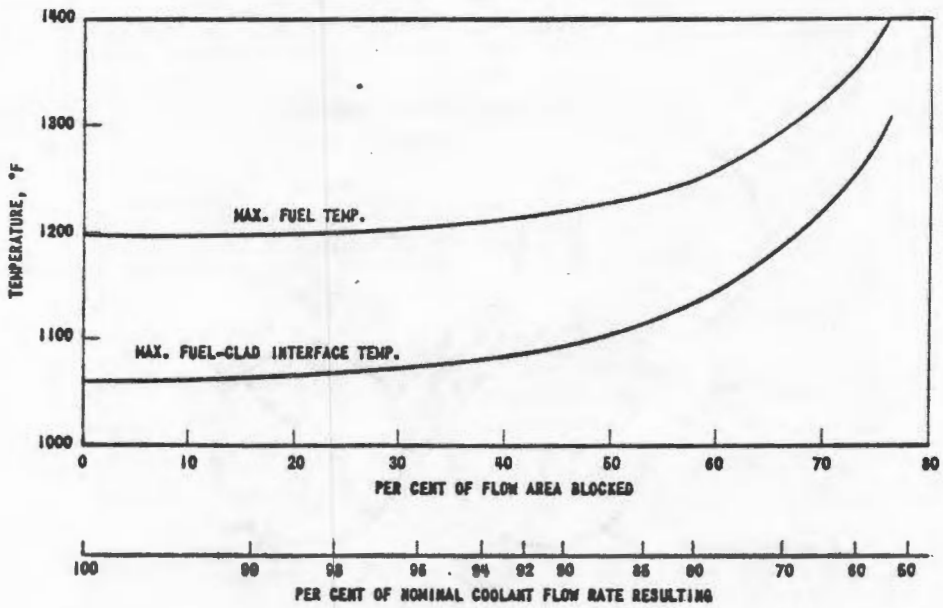

Fig. F-13

Foreign Particle Accumulations (Case 4) and Their Effects on EBR-II Core Temperatures

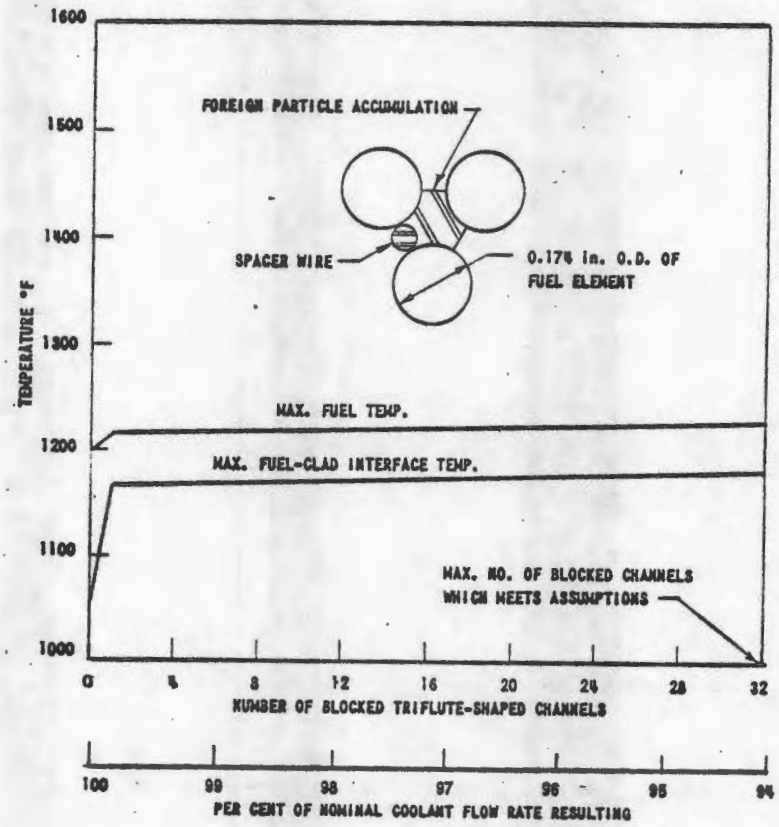

Fig. F-14

Foreign Particle Accumulations (Case 5) and Their Effects on EBR-II Core Temperatures

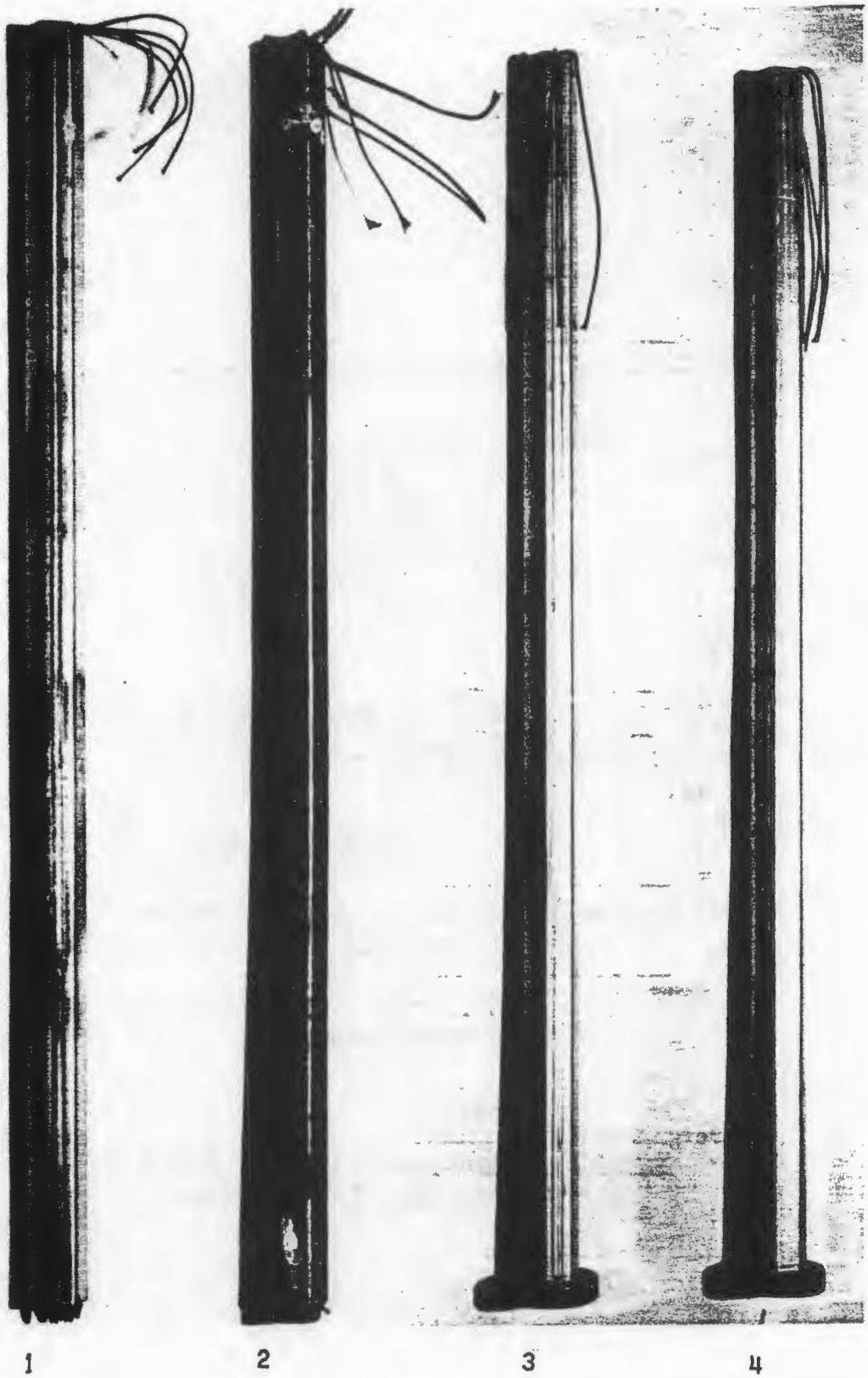

Fig. F-15

Exterior View of Four Test Subassemblies after Extreme Temperature Excursions in TREAT

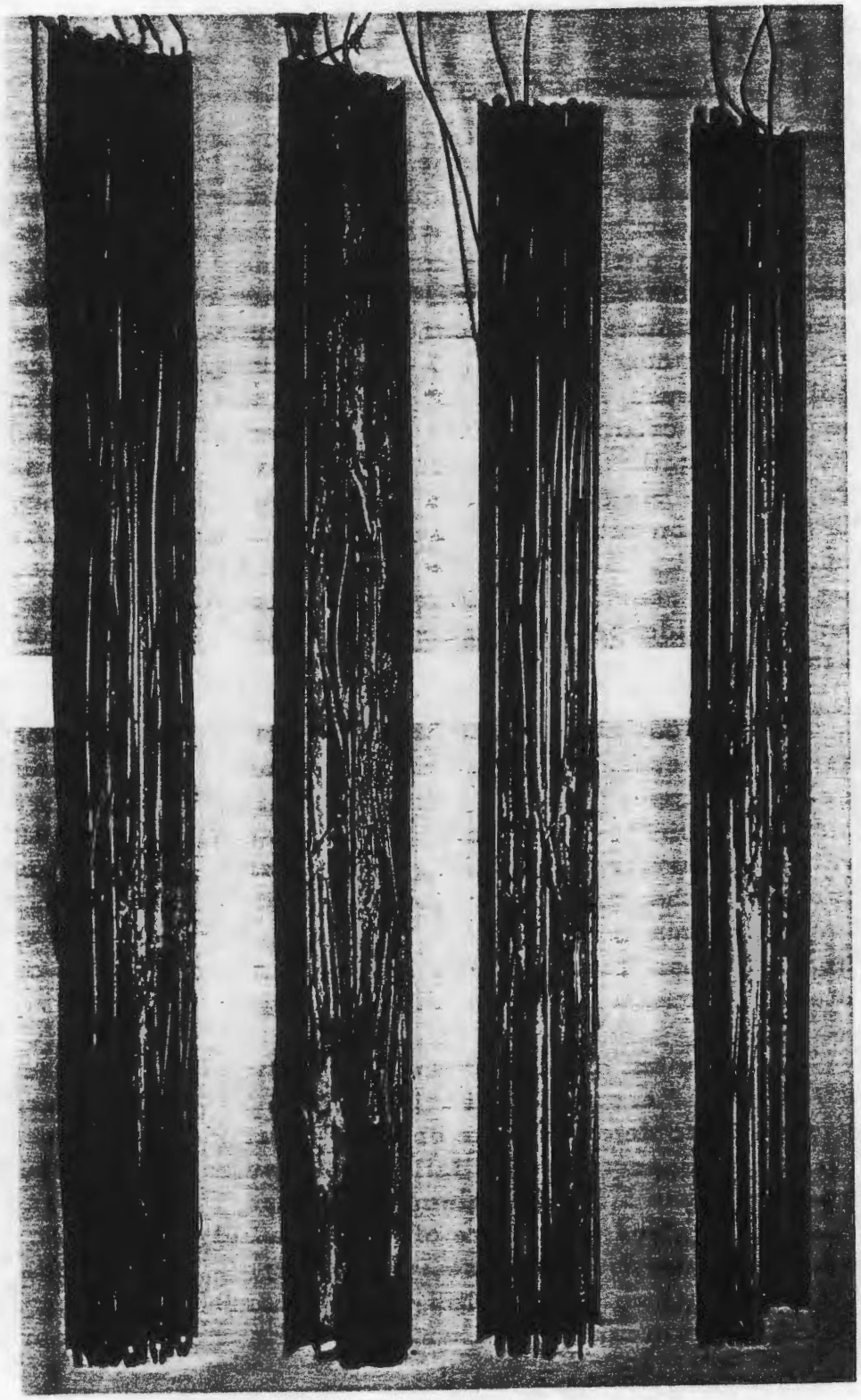

1 2 3 4

Fig. F-16

Interior View of Four Test Subassemblies after Extreme Temperature Excursions in TREAT

APPENDIX G

MAXIMUM CREDIBLE NUCLEAR ACCIDENTS

The reactor core design is such that so long as its integrity and shape are maintained, no serious nuclear accidents are believed possible. Many of the reactor protective circuits are designed specifically to maintain the integrity of the reactor core and blanket under a variety of malfunctions. In most cases, the malfunction must occur coincident with a gross loss of administrative control to precipitate some failure which may lead to a loss of core integrity. Even if the integrity of the core is partially or wholly destroyed, it is still not clear that this will or will not result in a super-prompt critical configuration. Moreover, it is quite difficult to specify realistically the rate at which reactivity is added to achieve super-prompt critical. An estimate was made [Appendix C] of an upper limit of reactivity addition rates caused by a gross meltdown and collapse of the core under gravity. It is believed that this is the potential source of the largest rates of reactivity addition. It is recognized, however, that a large number of coincidences are required to give the cited reactivity insertion rates following a loss of core integrity.

Calculations of reactivity addition, reactivity reduction by core expansion, and resulting nuclear explosions have been extended beyond those cited in [Appendix C].[33] The results of recent and more sophisticated parametric studies[34] are utilized here to re-evaluate the EBR-II. These re-evaluations have resulted in higher explosive yields for given reactivity insertion rates than previously cited [Appendix C]. However, inherent uncertainties in such predictions are large and it is concluded that for all practical purposes, the magnitude and, more important, the order of magnitude of the nuclear explosion is unchanged.

Fuel element meltdown transient heating tests have been conducted in the Transient Reactor Test Facility (TREAT).[35] These experiments have been conducted to determine the behavior of single fuel elements and, at best, can only suggest possible failure mechanisms in the EBR-II (which contains more than 5,500 fuel elements). Also, the majority of the TREAT experiments involved the failure of single fuel elements in an inert gas atmosphere (in the absence of sodium coolant). These results are included and evaluated with respect to EBR-II even though they may not be applicable to an actual in-pile failure mechanism leading to a loss of core integrity.

1. Predicted Consequences of Core Meltdown

Without implying any credence to the accident, the maximum possible nuclear explosion was postulated to be the result of a core collapse under gravity [Section V.E.]. The pessimistic hypotheses to describe the course of the accident were assumed as follows [Pages 109-110]:

"(1) The sodium has boiled away from the center of the reactor.

"(2) The uranium from the middle of the core has trickled down into the lower part of the core and is retained there, producing a region abnormally dense in enriched uranium at the core bottom, with a large gap at the core center.

"(3) At the worse possible moment, the upper portion of the core falls as a single unit, producing a prompt critical configuration at the highest possible insertion rate."

Recent theoretical methods can be used to represent more accurately the physical reactor conditions than in the previous analysis [Appendix C]. The energy density, Q(t), now is accurately determined; previously, its time dependence was assumed exponential to determine the reactivity of the system. The present analysis represents a simultaneous solution of reactivity and energy density, Q(t). In this analysis, the integrated energy continues to increase after the reactivity reaches zero; in the previous analysis, the integrated energy is constant after the reactivity returns to zero.

The magnitude of a possible nuclear explosion is a sensitive function of the maximum reactivity (K_0) attained. This is closely related to the reactivity insertion rate before shutdown mechanisms are operative. For a constant rate of reactivity insertion, the relationship between these quantities is:

$$K_0 = \sqrt{\frac{\dot{K}}{\ell} t_0^2}\ \sqrt{\ell \dot{K}} \approx 7.4\ \sqrt{\ell \dot{K}} \quad ,$$

where

K_0 = Maximum reactivity attained above prompt critical.
$\dot{K}$ = Rate of inserting reactivity.
ℓ = Prompt neutron lifetime.
t_0 = Time required to reach K_0 with reactivity insertion rate, $\dot{K}$.

Jankus[34] has shown that the excess energy density in a nuclear excursion is primarily dependent upon a dimensionless parameter:

$$X = \left[\frac{5}{32} \frac{\Sigma_{tr} \nu \Sigma_f [1 - (6q/5) + (3q^2/7] b^2}{\sqrt{q}\ F} \right] \frac{b^2}{(\gamma - 1) Q^*} \frac{K_0^3}{\ell^2}$$

where for the EBR-II:

$$\Sigma_{tr} \nu \Sigma_f \approx 4.8 \times 10^{-3}\ \text{cm}^{-2}$$

q = core power shape constant ≈ 0.5, where $\phi(r) \sim 1 - qr^2/b^2$
b = core radius ≈ 25 cm
F = importance weighted core fissions

$$= \int_{core} \phi^* \Sigma_f \phi \, dv \int_{reactor} \phi^* \Sigma_f \phi \, dv \approx 1$$

Q^* = threshold energy density; required to fill voids before expansion is initiated $\approx 0.8 \times 10^{10}$ erg/gm U
$\gamma - 1$ = constant relating pressure and energy density ≈ 1
ℓ = prompt neutron lifetime = 8×10^{-8} sec
K_0 = maximum reactivity attained above prompt critical

The relationship between the excess energy density ($Q - Q^*$), the threshold energy density (Q^*), the core power shape constant (q), and X is quite general. This functional relationship may be applied to a specific fast reactor through the numerical evaluation of X and q. For the EBR-II, the interesting reactivity insertion rates range from \$50/sec to \$1000/sec (\$1 $\approx$ 0.73% $\Delta k/k$); the approximate corresponding values of X range from 10^{-2} to 1.0.

The total available energy resulting from a prompt nuclear excursion is obtained by integrating the excess energy density over the reactor core. In the previous analysis, this was obtained by subtracting the energy required to fill voids in the entire core from the total created energy. In the present evaluation, the energy density available to do work is obtained at each point in the reactor. This quantity, $W(r)$, where:

$$W(r) = Q(r) - Q^* = Q(0)\,[1 - (qr^2/b^2)] - Q^*$$

is then integrated, where positive, over the reactor core. The result, W_{max}, is believed to be an overestimate of the available energy, primarily because negative values of $W(r)$ are rejected. This restriction will tend to give higher energy yields for the lower reactivity insertion rates previously cited, while the yields for the higher reactivity insertion rates are increased proportionately less. The latter increase is obtained because of the more accurate evaluation of $Q(t)$.

Table G-1 summarizes the results of the present analysis, based on the work of Jankus.[34] (The results from [Appendix C] and Reference 33 are included for comparison.) These results may be considered upper energy limits for a severe accident because:

(1) The method of averaging the available energy tends to high values.

(2) The adopted value of $q \approx 0.5$ is appropriate to the radial core power distribution. The axial power distribution requires $0.5 < q \leq 0.7$ and an increase in effective q will tend to lower W_{max}.

(3) The mass content of the core has been overestimated. The magnitude of energy released is directly proportional to the mass of the core.

(4) The total available energy is sensitively dependent on the threshold energy Q*. The assumed value is appropriate for the core in the absence of sodium. However, it is difficult realistically to postulate a gross loss of sodium in the EBR-II. In the presence of sodium, the threshold energy, Q*, is reduced; therefore, the energy available to do work is also reduced.

(5) The reactivity insertion rates for specific reactor conditions [Appendix C] are quite pessimistic. The calculated reactivity insertion rates were based on one-dimensional slab geometry with a small radial reflector saving. This is equivalent to a loss of radial reflector effectiveness prior to the initiation of the core meltdown. Two-dimensional (r,z) calculations show conclusively that the reactivity insertion rates cited [Appendix C] may be considered as upper limits.

(6) Finally, the calculated excess energy or maximum available work is an overestimate in terms of actual ability to do work. Certainly some of this energy will be used to heat the core above the threshold temperature.

Table G-1

MAXIMUM REACTIVITY ATTAINED AND MAXIMUM ENERGY DEVELOPED FOR VARIOUS REACTIVITY INSERTION RATES IN THE EBR-II

Analysis (Footnotes)	dK/dt, $/sec	$K_0 \times 10^3$	$\left(\frac{Q}{Q^*} - 1\right)$ at Core Center (r = 0)	$\left(\frac{\epsilon}{Q^*} - 1\right)$[e]	$\left(\frac{W_{max}}{MQ}\right)$[f]	Excess Energy[g]		Upper Limit[h] for Maximum Work, erg x 10^{-15}
						Calculated, erg x 10^{-15}	Upper Limit, erg x 10^{-15}	
a	50	1.42	1.1	0.47	-	1.3	-	-
	200	2.88	1.92	1.05	-	2.9	5.6	-
	600	5.05	4.24	2.67	-	7.5	13.0	-
	1000	6.54	6.83	4.48	-	12.5	20.0	-
b	50	1.26	1.56	0.79	-	-	4.1	-
	200	2.6	3.6	2.22	-	-	11.3	-
	500	4.16	5.9	3.83	-	-	19.0	-
	1000	5.96	10.3	6.91	-	-	35.0	-
c	43	1.33	1.56	0.79	0.79	-	-	3.2
	195	2.86	3.32	2.02	2.03	-	-	8.1
	900	6.15	9.09	6.06	6.06	-	-	24.1
d	54	1.48	1.56	0.79	0.81	-	-	2.5
	245	3.19	3.32	2.02	2.03	-	-	6.3
	1130	6.88	9.09	6.06	6.03	-	-	18.7

[a] From [Appendix C]; core radius = 23 cm; core mass ≈350 kg; $Q^* = 0.8 \times 10^{10}$ erg/gm.

[b] From Ref. 33; core radius = 25 cm; core mass ≈ 500 kg; $Q^* = 1.0 \times 10^{10}$ erg/gm.

[c] Based on Ref. 34; core radius = 25 cm; core mass ≈ 500 kg; $Q^* = 0.8 \times 10^{10}$ erg/gm.

[d] Based on Ref. 34; core radius = 23 cm; core mass ≈ 390 kg; $Q^* = 0.8 \times 10^{10}$ erg/gm.

[e] Average energy density available to do work as defined in [Appendix C].

[f] Upper limit on energy density available to do work based on Ref. 34.

[g] Excess energy is the total energy minus that required to fill voids as defined in [Appendix C].

[h] As defined in text and Ref. 34.

An upper limit on the magnitude of a nuclear explosion is specified by the calculated total excess energy or maximum available work. These are sensitive functions of the core material thermodynamic properties which, along with the initial core void content, determine the threshold energy density (Q^*). Further, the exact core size has a significant bearing on the magnitude of W_{max}. The effect of Q^* may be qualitatively observed by comparing Analyses b and c on Table G-1; a more detailed comparison is given in Reference 33. The effect of core size is demonstrated by comparing Analyses c and d. Another consideration pertains to numerical analyses with the AX-I program described in Reference 34. There it is found that the peak pressures are smaller and total energy yields are larger than in the results given in Table G-1. The reduced peak pressures are certainly due to energy transmission toward the blanket. Therefore, the lower energy yields given by the analyses which provide overestimates of pressure will be used to estimate the explosive severity of the accident.

The energy yields in Table G-1 and corresponding peak pressures must be very cautiously translated to equivalent pounds of TNT. The latter representation is in familiar terms of potential damage. This will not always accurately represent the destructive damage from a severe nuclear accident. In a chemical (TNT) explosion, the energy density is relatively constant at $\sim 4 \times 10^{10}$ erg/gm. In a nuclear explosion, the energy density depends upon the particular reactivity insertion rate. The small nuclear accidents yield energy densities similar to those of the chemical explosion. The large nuclear excursions can have energy densities much higher than a comparable chemical explosion. Similar considerations pertain to a comparison of peak pressures while the energy is created. Finally, the nuclear energy release will probably require less than 100 μ sec, while the equivalent chemical energy release requires more than 100 μ sec.

The above considerations make the transformation of the nuclear energy release to chemical equivalent quite uncertain in terms of potential damage. However, the nuclear analyses were extremely pessimistic, particularly with respect to reactivity insertion rates. Therefore, the equivalence of nuclear and chemical energy release will give overestimates on potential damage. The estimated energy yield from the \$200/sec, \$600/sec, and \$1000/sec accidents described previously [Appendix C] are now increased from 280, 660, and 1,050 lb TNT, respectively, to the equivalent of not more than 370, 850, and 1,240 lb TNT, respectively.

The occurrence of accidents of these magnitudes in the EBR-II is extremely remote. Moreover, the number of required coincidences of timing and disposition of fuel alloy before and during an accident renders the two larger accidents least probable.

2. In-Pile Tests on Single EBR-II Fuel Elements

The TREAT experiments are investigations of fast reactor fuel element behavior under transient power excursions. Fuel element failure and the distribution of resulting meltdown products are studied to determine the important parameters for describing or predicting, where possible, the course of a fast reactor meltdown.

The failure of single, EBR-II-type fuel elements in an inert gas atmosphere has been investigated. Similar experiments with EBR-II fuel elements suspended in stagnant sodium have been initiated and tests in flowing sodium are in preparation.

Some hypothetical accidents can be postulated on the basis of these experimental results. However, such postulates must be qualified because the data may not be at all applicable to fuel element failure in the EBR-II. Also, the TREAT data differed from results of out-of-pile meltdown experiments using electrical heating. The latter investigations were conducted during the EBR-II fuel element development program. Very significantly, both in-pile and out-of-pile experiments showed that unirradiated EBR-II fuel elements can be heated without failure to temperatures appreciably in excess of 725°C (the uranium-stainless steel eutectic temperature) for short periods of time.

TREAT experiments with single EBR-II fuel elements suggest that fuel alloy rearrangements with a gain in reactivity may occur during very large temperature excursions. Pertinent experimental data from TREAT can be separated into roughly three broad categories. These are categorized by the maximum clad temperature registered during an excursion while the fuel element was suspended in an inert gas atmosphere. The temperature ranges are:

950°C to 970°C:	Incipient failure
970°C to 1015°C:	Mild failure
Above 1015°C:	Energetic failure.

A gross malfunction must, of course, take place before such clad temperatures are attained in the EBR-II. (Maximum nominal fuel clad temperatures under normal conditions are between 480°C and 598°C. Sodium boiling is initiated at 892°C.)

The "energetic failures" result in the violent ejection of molten fuel from the stainless steel clad at or near the point of initial failure. The ejection is caused by very high pressure due to vaporized bond sodium. With a nearly constant axial power distribution along the sample, failure is theoretically equally probable everywhere along the length of the fuel element; experiments tend to confirm this effect. Experiments were also

performed with a shaped axial power distribution resembling that in the EBR-II. As anticipated, failures occurred near the synthesized core midplane in the region of highest localized temperature. However, initial experiments in stagnant sodium with an axially shaped power distribution did not indicate any marked tendency for highly localized failure.

If an accident in the EBR-II leads to maximum fuel element temperatures at or near the horizontal midplane of the core, and if the "energetic" type of failure does occur only near the hottest point, it may be possible that fuel alloy will be propelled from the axial extremities of the fuel elements toward the center plane, leading to an increase in reactivity.

Extrapolating this hypothesis directly to EBR-II raises several questions. Does the hot spot always appear near the core center during overheating conditions? Does the position of maximum axial temperature at the time of failure vary considerably as a function of core radius? These two unanswered questions depend very much on the course of the accident. Further, what happens if one or both ends of the fuel pin are not fully melted by the time failure occurs at the hot spot? And, what is the effect of pre-irradiation? Does swelling lead to a different mode of cladding failure? It is not clear that release of fission gases will serve to propel the fuel alloy from its container in the same way sodium vapor does. Out-of-pile experiments indicate a frothing action in the escape of uranium from pre-irradiated EFFBR pins.

The reactivity effects of concentrating fuel at the central core plane have been estimated with 2-group diffusion theory in r,z geometry. It was assumed that fuel originally contained in a single subassembly remained within that subassembly and that fuel was dispersed throughout a central region about 11 cm thick, displacing all sodium and some stainless steel. Table G-2 summarizes these analyses. Included is a calculation which demonstrates the small effect, relative to the total, due to the uncertain coolant disposition during such fuel alloy rearrangement.

The implication of these calculations on reactor safety depends primarily upon the rate of fuel alloy compaction during such an event. These rates can only be inferred from correlating in-pile, high-speed photographs of TREAT sample meltdowns with cladding temperatures. The start of failure can be seen on the photographs. The conclusion of the failure is indicated by large fluctuations in the cladding temperature. The observed duration of this event is usually about 150 ms. Therefore, if 5,500 fuel elements were to fail simultaneously, the resulting reactivity insertion rate would not exceed $140/sec. The duration of failure, including effective fuel compaction must be significantly shorter to achieve the reactivity insertion rates assumed for the gravity-induced accident. It should also be emphasized that not only must the event occur in a shorter time, but that some 5,500 independent events must occur simultaneously and in this shorter time.

Table G-2

TOTAL POSSIBLE REACTIVITY ADDITION BY COMPACTING EBR-II FUEL ALLOY NEAR CORE MIDPLANE

Type of Fuel Alloy Compaction	Reactivity Effect ($\Delta k/k$)			
	Total	Per Core Subassembly	Per Control Subassembly	Per Fuel Element
Seven Central Core Subassemblies	0.03	0.0043	-	0.000044
Twelve Core and Twelve Control Subassemblies (in Row 5)	0.026	0.0013	0.00086	0.000014
Complete 61 Subassembly Core	0.144	-	-	0.000028
Complete 61 Subassembly Core and 50% Core Sodium Removed	0.114	-	-	0.000022

Considering the variation in power density distributions, rates of cooling, etc., it does not appear possible that such precise timing could be achieved. The assumption of non-simultaneous, whole-core failure may be supported by evaluating the consequences of the EBR-I Mark-II meltdown.[36,37] Without suggesting the mechanism of reactor shutdown, the post-mortem analysis shows conclusively that fuel element failure was not simultaneous throughout the whole core, and probably not even simultaneous in the region of the core that did fail.

It is, therefore, concluded that reactivity insertion rates postulated for the gravity-induced meltdown accidents are maximum and can be used to describe the maximum credible accident.

APPENDIX H

CONTAINMENT OF A POSSIBLE ACCIDENT

The containment design of EBR-II has been modified in only minor respects from that originally described [Appendix E]. These modifications are discussed below.

The bottom beam arrangement of the primary tank support structure [Fig. 32], has been improved as described in Section III.A.8. and shown in Fig. 23.

Design of the blast shield surrounding the primary tank [Page 325] has been finalized as described in Section III.A.8. and shown in Fig. 24.

The concrete missile shield lining the containment vessel has been reduced in thickness (above the operating floor) from 14 in. to 12 in. The horizontal concrete missile shield (ceiling) above the building crane [Fig. 5] has been replaced by a 6 in. thick shield of reinforced concrete applied to the inner surface of the building dome (Fig. 5). These new thicknesses are more than adequate to protect the vessel from the high gas temperatures which conceivably could be produced in the event of a significant sodium-air reaction, as well as to protect the vessel from possible missiles.

The nitrogen bleed-in system described on [Page 331] has been eliminated. The intended function of this system was to prevent excessive reduction in building pressure due to consumption of oxygen in the event of a major sodium-air reaction. Final calculations indicated that a reaction resulting in 24-psi initial overpressure (the design pressure of the containment vessel) would not consume more than 20% of the oxygen present and would not effect a final (after cooling) pressure lower than -1.4 psig, including the effect of possible changes in barometric pressure and temperature. Even if 100% of the oxygen were consumed, the final pressure would not be lower than -3.4 psig. Analysis shows that the containment vessel can withstand such pressure differentials without buckling (with no credit taken for the strength of the reinforced concrete missile shield liner which, by itself, should be able to withstand a differential of more than 20 psi), and that a bleed-in system, therefore, is not needed.

All other revisions relate to the penetrations provided in the containment vessel. The penetrations are listed in Tables H-1 and H-2 and are discussed below.

Table H-1

MECHANICAL PENETRATIONS IN CONTAINMENT VESSEL

LARGE PENETRATIONS

Type	Arrangement	Number
Personnel Air Lock	Two doors, interlocked, each with double seal	1
Emergency Air Lock	Two doors, interlocked, each with double seal	1
Equipment Air Lock	Two doors, interlocked, each with double seal	1
Freight "Door"	Two doors, not interlocked, one with double seal	1

SMALL PENETRATIONS

No.	Function	Number of Pipes	Number of Isolation Valves
1	(Spare)	0	0
2	(Spare)	0	0
4	(Spare)	0	0
3	Argon gas supply	1	1
5	RP ventilating air inlet	1	2
6	Building purge air exhaust	1	1
9	RP ventilating air exhaust	1	1
11	Primary system Na fill line	1	0
12	Secondary system vent line	1	0
13L	Freon liquid inlet	2	2
	Freon gas outlet	1	1
13H	Silicone inlet	1	1
	Silicone outlet	1	1
15L	Freon liquid inlet	1	1
	Freon gas outlet	1	1
	Building DP sensing	1	0
15H	Freon liquid inlet	1	1
	Instrument air inlet	1	1
	Plant service air inlet	1	1
16	Shutdown cooler NaK inlet	1	0
17	Shutdown cooler NaK outlet	1	0
18	Shutdown cooler NaK inlet	1	0
19	Shutdown cooler NaK outlet	1	0
20	Freon liquid inlet	1	1
	Freon gas outlet	1	1
21	Freon liquid inlet	1	1
	Freon gas outlet	1	1
22	Secondary system Na outlet	1	0
23	Secondary system Na inlet	1	0
Total: 18 (+3 Spares)		27	19

Note: Penetrations Nos. 7, 8, 10, and 14, do not exist.
RP = Reactor Plant; DP = Differential Pressure

A large number of penetrations through the shell are required for personnel, equipment, freight, electrical conductor, service fluid, and other access. All employ gastight seals, either of the metal-to-metal type or of an organic type, suitably protected from the high temperatures of building gas which could result from an assumed sodium-air reaction. All openings are designed not to detract from the strength of the building shell and to sustain a building pressure equal to the maximum containable by the shell itself.

The personnel air lock incorporates two vertical door openings, each 3 ft wide by 6 ft high. Both doors swing inward toward the Reactor Plant. Each door forms a gastight closure. Door operation is such as to permit personnel access to and from the Reactor Building with maintenance of shell gastightness at all times; positive interlocks are provided to permit only one door to be open at a time. Double seals - one compression, and one inflatable - are employed on each door.

Table H-2

ELECTRICAL PENETRATIONS IN CONTAINMENT VESSEL

No.	Type of Pressure Connector	Number of Pressure Connectors
1	Cannon TBF	7
2	Cannon TBF	7
3	Cannon TBF	7
4	Cannon TBF	7
5	Cannon TBF	7
6	Cannon TBF	7
7	Cannon TBF	7
8	Cannon TBF	7
9	Cannon TBF	7
10	Cannon TBF	7
11	Cannon TBF	7
12	Cannon TBF	7
13	Cannon TBF	7
14	Cannon TBF	7
15	Cannon TBF	7
16	Cannon TBF	7
20	Special MI Seal	6
22	Special MI Seal	6
21	Cannon TBF	1
28	Cannon TBF	1
29	Cannon TBF	1
23	Special MI Seal	6
24 (Spare)	(none)	0
25 (Spare)	(none)	0
26 (Spare)	(none)	0
27 (Spare)	(none)	0
30	Cannon TBF	12
33	Cannon TBF	12
31	Cannon TBF	5
32	Cannon TBF	5
36	Cannon TBF	5
37	Cannon TBF	5
34	Amphenol 100X-(CO-AX)	24
35	Amphenol 100X-(CO-AX)	24
Total: 30(+4 Spares)		225

Note: Penetrations Nos. 17, 18, and 19, do not exist.

A small "emergency" personnel air lock is also incorporated with the same safety features as the large personnel air lock. An equipment air lock is provided principally for transporting subassemblies between the Reactor Plant and the Fuel Cycle Facility. The size and shape of this air lock were determined primarily by the dimensions of the shielded coffin. Two horizontal circular doors (5 ft-8 in. dia.) are used. The same features (door seals, gastightness, operation, and interlocking) as apply to the personnel air locks are incorporated.

A large opening is provided for freight access. This penetration is fitted with double doors that are not interlocked but are required (administratively) to be bolted closed during reactor operation or during fuel-handling operation. The inner door employs double seals, both of the compression type. The outer door utilizes a single, compression-type seal.

Provisions are made to enable periodic leak rate testing of each of the above doors without requiring pressurization of the building. These and all other penetrations through the building shell are protected from possible missiles either by reinforced concrete or heavy steel plate.

All electrical conductors (Table H-2) are brought through leak-tight pressure connectors (pressure rating: 30 psi or higher). Most connectors are A-N-type multiconductor pressure connectors (such as Cannon TBF) which provide solid, leak-tight, through-conductors with terminals at each end. The penetration arrangement and connector details are shown in Figs. H-1 and H-2. A small number of conductors are required to carry large currents, and for each of these the connector consists of a short length of MI cable brazed to a nozzle plate, with the cable insulation sealed at both ends with epoxy resin. This arrangement is shown in Fig. H-3. The electrical penetrations are designed to permit pressure and leak testing without requiring pressurization of the building.

There are 25 service and process fluid pipes of various sizes that penetrate the shell. All but two (the 12-inch secondary system pipes) are seal welded either directly to the shell, or to a blind flange bolted to a thermal sleeve which is welded to the shell. The secondary system pipes are connected to the shell by special flexible seals to accommodate their expected thermal expansion. Eighteen of the 25 pipes are equipped with one or more isolation valves. These valves are normally open, but close automatically in event of a major nuclear incident. The other seven pipes require no isolation valve because the exterior portions of the piping systems involved are capable of withstanding conditions more severe than those anticipated subsequent to a nuclear incident. These include: four NaK pipes for the two shutdown coolers; the two secondary system sodium pipes; and one secondary system vent line.

Two additional pipes provide for sensing building air pressure and for sodium filling of the primary tank; the latter pipe is capped off and welded after filling.

A typical penetration for small pipes is shown in Fig. H-4, for the large air pipes in Fig. H-5, and for the secondary system sodium pipes in Fig. H-6.

A total of 19 isolation valves are employed (including two on the double-branched ventilating air inlet duct). The "building isolation system" includes the isolation valves, nuclear incident detection devices, and system circuitry which controls the position of the valves. All valves are air-to-open, spring-to-close, with electrical (solenoid) pilot valve control. They close automatically upon loss of either air pressure or electrical power. The detectors consist of:

(1) Two radiation detectors to sense radioactivity level inside the building.

(2) One pressure detector to sense building air pressure relative to atmospheric pressure.

(3) Four thermocouples to sense coolant temperature inside the reactor (in upper plenum), at outlets from core subassemblies.

(4) One thermocouple to sense building air temperature.

(5) Two resistance thermometers (long time constant) to sense building air temperature.

The four thermocouples sensing coolant temperature inside the reactor are connected in a two-out-of-four arrangement for trip. The trip is effective only during reactor operation or standby, since fuel-handling operations require the reactor cover (carrying the thermocouples) to be raised to the top of the primary tank.

In the remote event of a significant nuclear incident or primary system sodium fire, trip initiated by one or more of the above detectors will interrupt electrical power to the isolation valves and all valves will immediately close.

As described in [Appendix E], two echelons of containment are incorporated. The first, termed the "primary containment system," surrounds the primary tank in which the reactor is submerged. Its function is to contain the effects of the nuclear energy release without breaching. The second, termed the "building containment system," surrounds the primary containment system and the remainder of the Reactor Plant. The function of this system is to localize within the reactor building the effects of a possible sodium-air reaction energy release.

The analytical evaluation of the building containment system [Pages 331-333] is essentially unchanged. Analysis of the primary containment system has been carried out in greater detail and is reported in Reference 38. Pertinent results are presented below.

An analytical study was made by Armour Research Foundation of the shock wave action, pressure generation, energy dissipation, and certain other phenomena which could be expected to result from a sudden release of nuclear energy within the reactor core equivalent in magnitude to the detonation of 300 lb of TNT. The rate of energy release assumed was that which calculations indicated to be the worst possible from the viewpoint of containment by this particular system (time of energy release equal to about 0.002 sec); a rate either lower or higher than this would be

expected to produce less violent conditions. Major results of the study are:

(1) The presence of the very large volume of sodium which immediately surrounds the reactor is of considerable advantage. Because of the rapid absorption of shock wave energy within this bulk sodium by the waste heat process, the fraction of total energy released available for loading or destruction of the containment system is greatly minimized. About 10% of the total energy is unabsorbed upon arrival of the shock wave at the primary tank sodium boundaries; quantitatively, this amount is equivalent to an average of 5 cal/cm^2 of surface area.

(2) The presence of the free surface of the primary tank bulk sodium is also of great advantage. Because of the acoustic impedance mismatch presented at this free surface, the maximum pressure exerted on the bottom of the vessel top closure or primary tank cover (or rotating plugs) is reduced by more than two orders of magnitude.

(3) The peak argon gas pressure exerted on the bottom of the vessel top closure (or the rotating plugs) is not more than about 1.4 atm. abs., or 6 psig, and this pressure is effective for about 0.002 sec.

(4) The peak pressure exerted on the bottom of the top closure (or the rotating plugs) by impingement of sodium is not more than about 3.53 atm. abs., or 37 psig, and this pressure is effective for less than 0.002 sec.

(5) The total thrust and energy imparted to the rotating plugs by the argon gas pressure and sodium impingement pressure (3 and 4 above), and the reactions of attached mechanisms which extend downward into the bulk sodium, are sufficiently small as to permit use of uncomplicated plug-to-structure locking arrangements for prevention of plug ejection. (All plugs other than the rotating plugs are bolted to their respective nozzles. The holddown arrangement for the two rotating plugs is shown in Fig. H-7.)

(6) The total energy transferred to the top closure by mechanisms or components fastened to the closure and extending through the primary tank argon gas blanket into the bulk sodium is insufficient to appreciably strain the top structure.

(7) Small void spaces provided around the 12-inch sodium pipes of the heat exchanger are adequate to assure pressure relief entirely within the primary tank or the heat exchanger plug, without rupture of the pipes external to the pressure vessel.

(8) The peak sodium pressure exhibited at the primary tank walls is approximately 700 bars. Because of the action of the surrounding gas space and the blast shield, however, the magnitudes of both the peak pressure and the energy transmitted to the pressure vessel wall, or the biological shield, are reduced to negligible values.

(9) Components wholly submerged in the primary tank bulk sodium such as the reactor vessel cover, blanket subassemblies, and miscellaneous steel fragments are not potential missiles. The velocities acquired by these components are a function of component shape and other factors, but are in all cases negligibly low. For example, the 14-ton reactor vessel cover, which is located initially close to the center of explosion, could attain a maximum possible velocity of about 35 fps and a final velocity of about 6 fps upon striking the primary tank cover (or rotating plugs), after being decelerated by vertical transit through 9.5 ft of sodium. As hypothetical examples, solid steel spheres of size ranging from one to five inches in diameter and initially located within a few feet of the explosion center could acquire maximum possible velocities of about 80 fps and striking velocities (velocities at emergence from the bulk sodium) of considerably less magnitude. Such striking velocities are negligible in view of the obvious stopping power of the primary containment system structure wall, and top and bottom closures.

(10) Because all sodium and argon pipes make a right angle turn to a horizontal run inside the top closure, it seems evident that no pipe which conceivably might be torn loose from its plug could be ejected through the top of the closure as an effective missile.

(11) It is highly improbable that any of the control rod, safety rod, or fuel handling mechanisms (drive shafts) could be ejected through the top closure as a missile. They are of very long, slender configuration and would require essentially perfect axial alignment of thrust to preclude bending. As shown in [Fig. 7], they pass through several feet of top closure and primary tank cover with only small clearances; a relatively small amount of bending would probably produce binding during any attempted ejection. The control rod and fuel-loading mechanism drive shafts also pass through more than 2.5 ft of reactor tank cover, so that significant tipping of this cover also would tend to bind these particular mechanisms.

(12) Ejection of a control or fuel-handling mechanism through the top closure is considered to be the most pessimistic assumption which may be made with respect to determination of appropriate missile protection. The maximum possible velocity of such a missile is not more than 70 fps. Such velocity is probably insufficient to enable the missile to travel far enough even to make contact with the reactor building

enclosure, and therefore indicates that only minimal, if any, missile shielding need be provided. The minimum shield thickness provided (6 in.) is more than adequate.

The above results, while differing in detail from those reported earlier [Pages 326-327], serve to confirm the original conclusions as to the adequacy of the primary containment system for an assumed energy release of 300 lb TNT equivalent [Page 328] or greater [Page 329].

Two series of pressure tests and leakage tests have been conducted on the EBR-II building containment system. The first series was run upon completion of construction of the shell proper, with the air locks and freight door installed, but with no other penetrations. At that time, the shell was bare - without paint, bitumastic, insulation, etc., - and was supported by temporary steel columns, so that the entire shell surface was accessible for inspection. A preliminary leak test was effected with 10-psig internal air pressure by soap-suds testing the full length of every weld on the shell, all air locks, and the freight door. A pressure (strength) test then was conducted at 30-psig internal pressure. Finally, a leak rate test was performed at 24 psig over a period of more than 72 hr. The results showed a total leak rate from the system of less than 560 ft^3/day (32°F, 36.2 psia), well under the 1000 ft^3/day considered acceptable [Page 331].

The second series of tests was run upon completion of construction of the Reactor Plant except for installation of certain mechanisms and equipment inside the building. All penetrations had been incorporated, the shell had been set on its permanent foundation, and all painting, insulating, backfilling etc., had been completed. These tests were conducted, in essence, on the "integral" containment system. Three of the total number of penetrations were temporarily sealed off: the two penetrations for the secondary system pipes, because their flexible seals were not yet available; and one electrical penetration, because a connector was known to leak and required replacement. (The two secondary piping penetrations will be leak tested after installation of the flexible seals has been completed. The faulty electrical connector has been replaced and the penetration successfully tested.) A pressure test was first conducted at 30 psig. Then a final leak rate test was performed at 24 psig over a period of more than 72 hr. The results of this test, more accurate than those of the earlier test, showed a total leak rate from the system of less than 100 ft^3/day (32°F, 36.2 psia). This is equivalent to less than 0.03% of the building air volume, at the same conditions, per day.

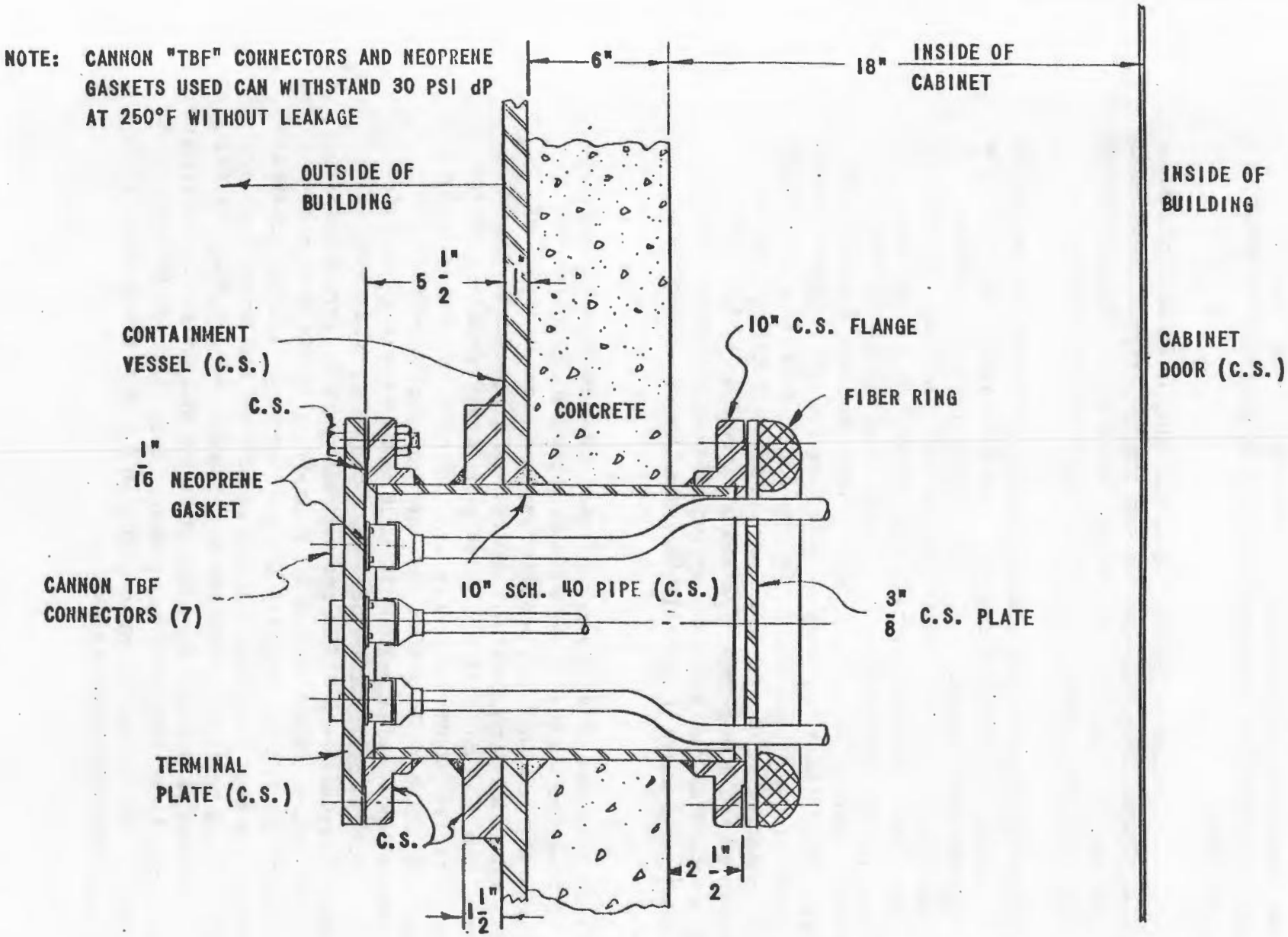

Fig. H-1

Electrical Penetration Nos. 1 through 16

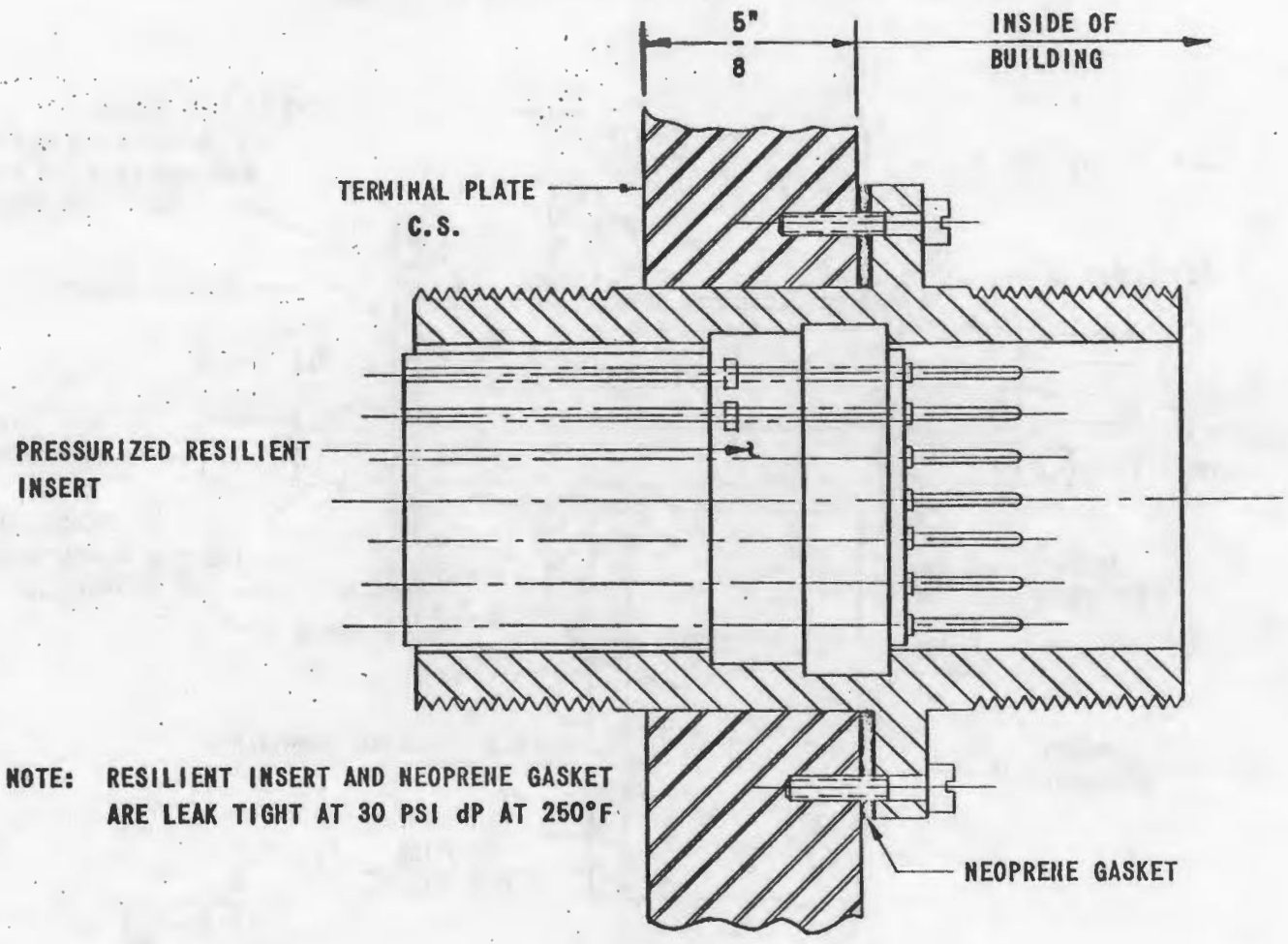

Fig. H-2

Cannon Type "TBF" Connector

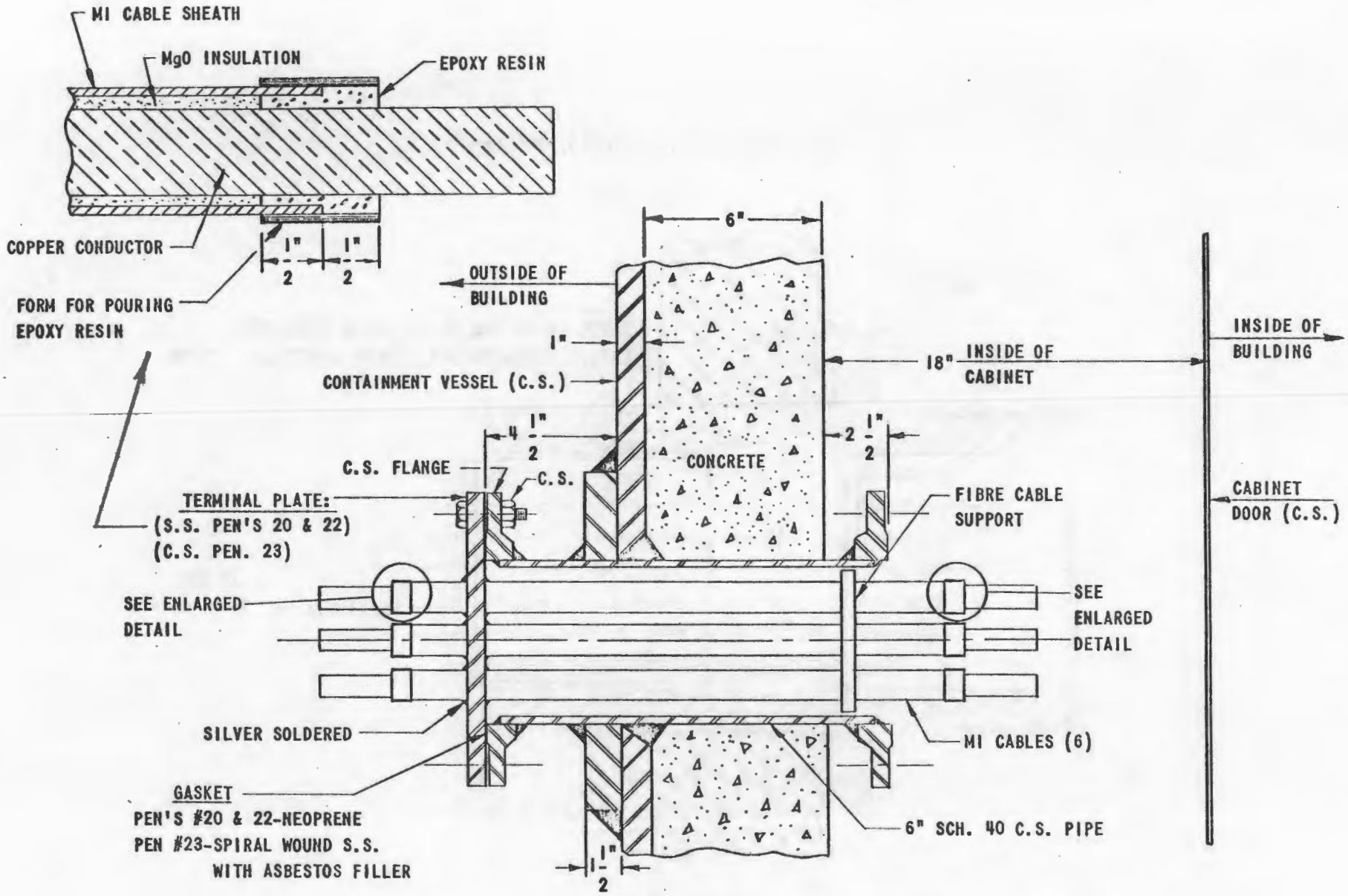

Fig. H-3

Electrical Penetration Nos. 20, 22, and 23

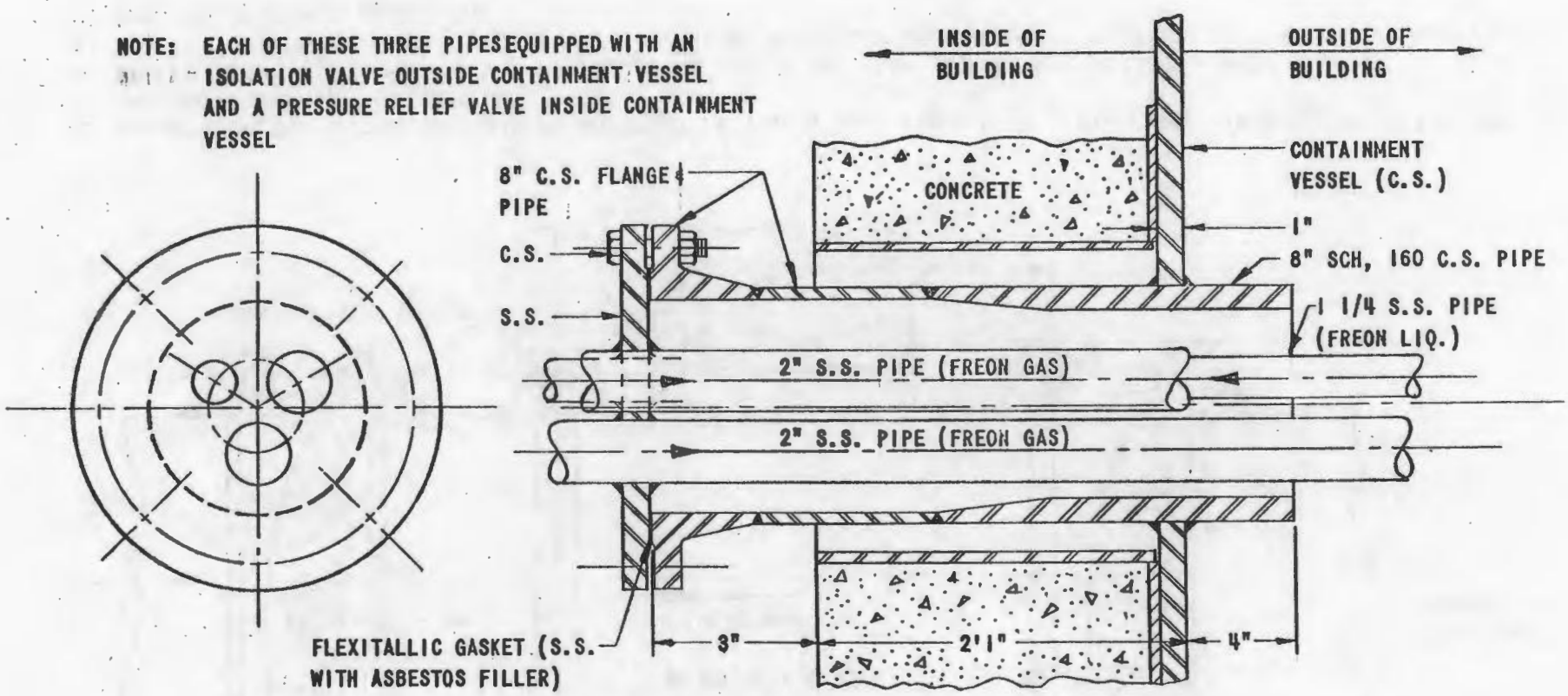

Fig. H-4

Mechanical Penetration No. 13L

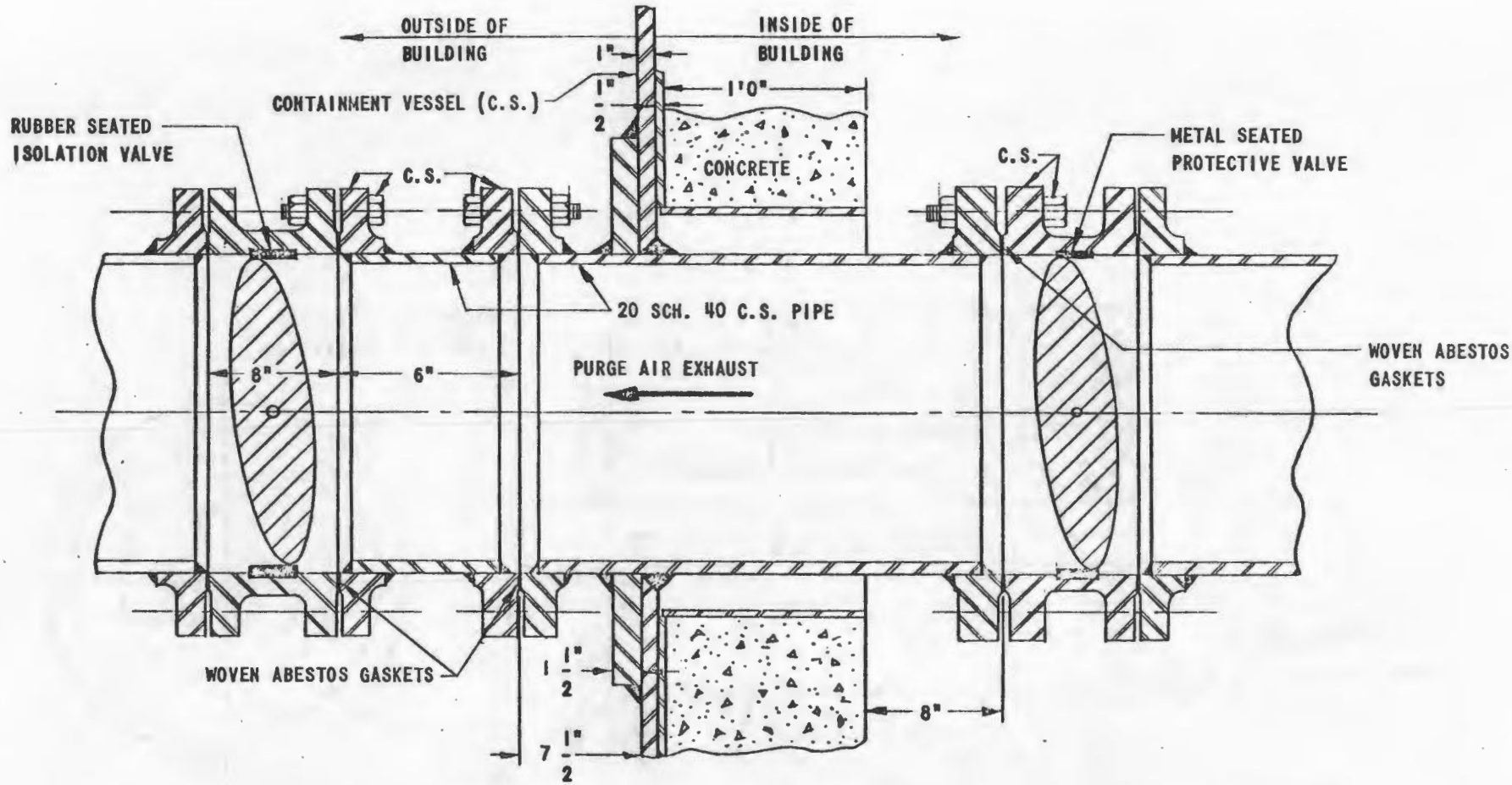

NOTE: 1. THIS PIPE EMPLOYED ONLY TO PURGE BUILDING ATMOSPHERE IN EVENT OF SMALL SODIUM FIRES OR OTHER MINOR AIR-CONTAMINATION ACCIDENTS NOT INVOLVING SIGNIFICANT RADIOACTIVITY.

2. BOTH VALVES NORMALLY CLOSED. IF OPEN TEMPORARILY FOR PURGING, BOTH CLOSE AUTOMATICALLY IN EVENT OF MAJOR INCIDENT.

3. METAL SEATED VALVE NOT GASTIGHT; ITS PURPOSE IS TO PREVENT SIGNIFICANT COMMUNICATION OF BUILDING ATMOSPHERE WITH RUBBER SEATED ISOLATION VALVE WHICH IS GASTIGHT.

Fig. H-5

Mechanical Penetration No. 6

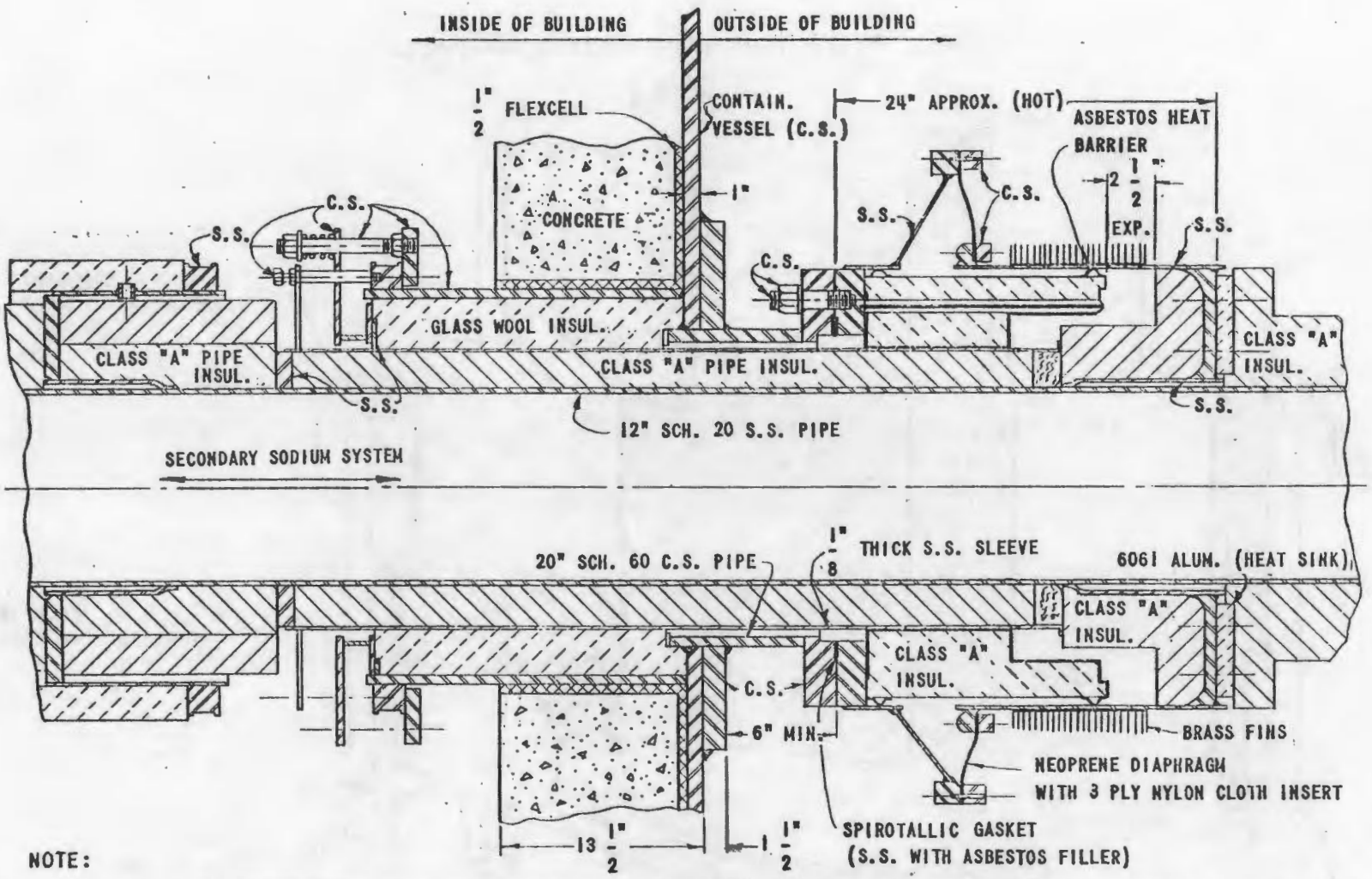

NOTE:

1. THIS PIPE CARRIES SECONDARY SYSTEM SODIUM BETWEEN MAIN HEAT EXCHANGER AND STEAM GENERATOR. THE FLEXIBLE SEAL ARRANGEMENT SHOWN IS NECESSARY TO ACCOMMODATE PIPE THERMAL EXPANSION (IT BEING IMPRACTICAL TO PROVIDE AN EXPANSION LOOP INSIDE THE REACTOR BUILDING).
2. OPERATING TEMPERATURE RANGE OF THE Na, 500°F - 900°F

Fig. H-6

Mechanical Penetration Nos. 22 and 23

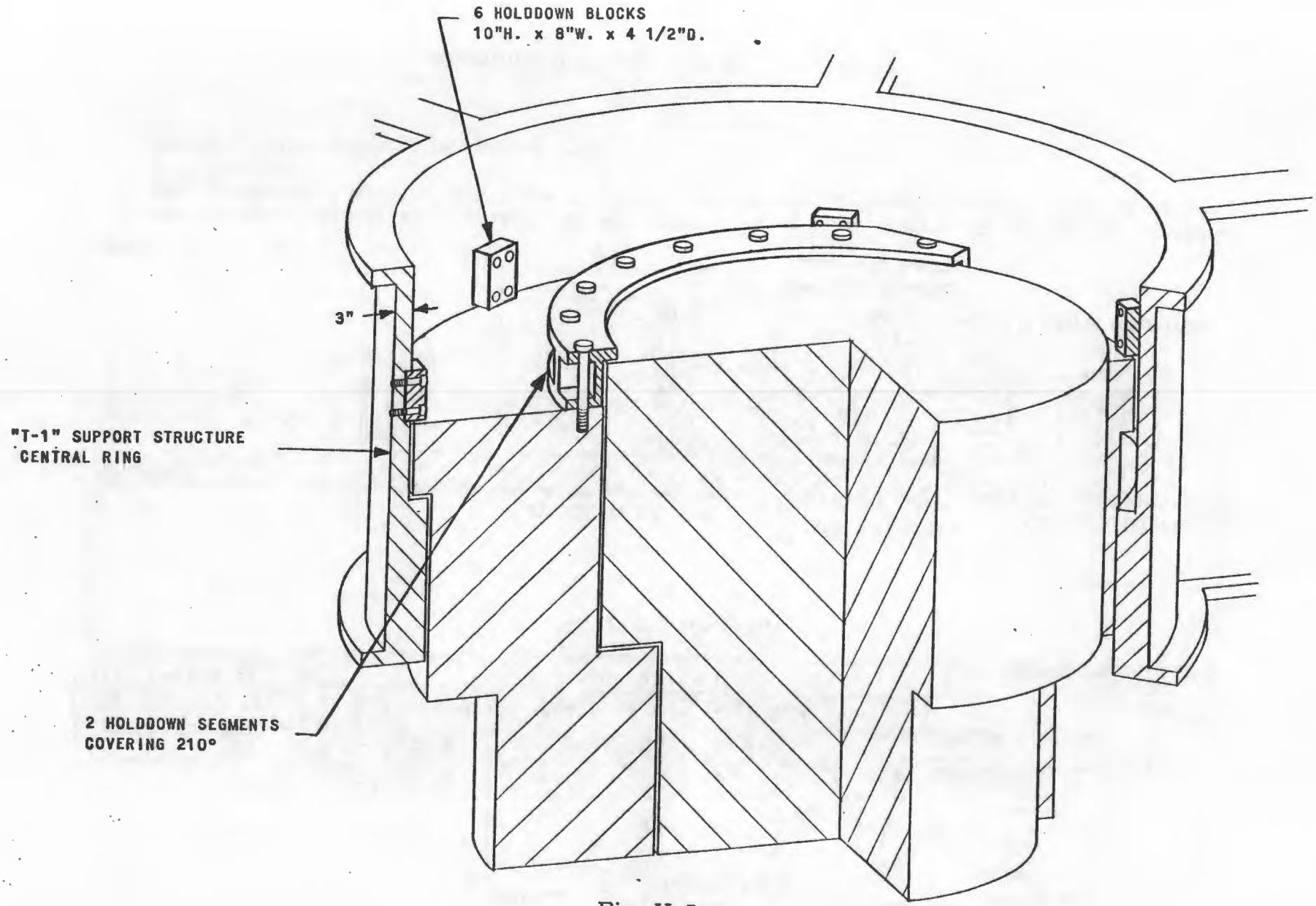

Fig. H-7

Holddown Arrangement for Rotating Plugs

APPENDIX I

EXPERIMENTAL EQUIPMENT

1. Reactivity Generator

The reactivity generator (Fig. I-1) is a specially designed device to sinusoidally perturb the critical reactor system. Such reactivity perturbation, when correlated with the resulting sinusoidal flux perturbation, can be used to extract the reactor transfer function under a variety of reactor conditions. The complete reactivity generator assembly consists of three separate units: (1) the oscillator rod; (2) the mechanical actuator; and (3) the drive mechanism.

The oscillator rod has been designed to replace one of the reactor control rods. The reference oscillator rod contains ~100 gm $B_4^{10}C$, which can be moved vertically in a control rod thimble.

The mechanical actuator provides the link between the oscillator rod and the drive mechanism. It consists of a suitably supported, long extension rod and a "Scotch Yoke" which translates rotary motion into vertical oscillatory motion.

The drive mechanism is comprised of an electrical gear motor and position-indicating equipment required for correlating reactivity perturbation with the resulting flux perturbation.

The design of the reactivity generator permits a maximum stroke of 8 in. for frequencies less than 1 cps, or a shorter stroke of 4 in. for all frequencies up to 2 cps.

2. Fuel Element Failure Detector

The detection of fuel element failure (or incipient failure) in a sodium-cooled reactor is desirable but difficult. In the EBR-II, the remote-controlled handling of fuel and blanket subassemblies precludes direct temperature measurements which might indicate most types of incipient failure. There are a total of 26 coolant outlet thermocouple locations which may give qualitative warning of incipient and/or accomplished failure at various reactor locations if such failure is caused by, or results in, unusual sodium coolant exit temperature from the subassembly. However, these thermocouples are intended for measurement of coolant outlet temperature distribution and are not expected to provide reliable fuel element failure detection.

There are a number of methods which can, in principle, be used to detect fuel element failure by detecting fission products released from the fuel elements. These include:

(1) Detection of delayed neutrons from fission products released to the primary sodium coolant.

(2) Detection of fission products released to the primary sodium coolant by sampling and analysis.

(3) Detection of fission product Xe and Kr in the argon blanket gas.

The first of these methods is independent of fuel alloy burnup while the other two would be most sensitive with high burnup fuel.

In principle, the detection of delayed neutrons is a method whereby indication is as rapid as coolant circuits permit. In fact, because of the short half-life of the fission products emitting delayed neutrons, this system must have a rapid response. On the other hand, it may be a relatively insensitive system because of: (1) a possible low rate of release of fuel and fission products to the sodium coolant for a given extent of fuel element damage; (2) dilution of the fission products in the sodium coolant; (3) the high gamma background from the coolant in which the low-level neutron flux must be measured, and (4) the possible delayed neutron background due to uranium contamination in the sodium above which a change must be measured to indicate a fuel element failure.

A device of this type has not been tested in an operating reactor system; however, provisions have been made in the EBR-II for the investigation, evaluation, and development of a fuel element failure detector. An experimental loop has been provided which will circulate primary sodium from the heat exchanger outlet to a point external to the primary tank where experimental facilities can be accommodated. At full power and full flow, the transit time for sodium from the center of the reactor to the heat exchanger outlet is approximately 11 sec. At maximum flow in the experimental loop, the transit time for sodium from the heat exchanger to the experimental section is approximately 6.5 sec. The loop includes a d-c electromagnetic pump of 100 gpm capacity, and the flow rate can be varied from 10 to 100 gpm (a transit time of 6.5 to 65 sec). The arrangement of the reactor, primary system, and experimental loop are shown schematically in Fig. I-2. Development work is in progress on experimental delayed neutron detector systems for investigation in conjunction with this experimental facility.

The routine sampling procedures to be employed for sodium analysis will provide samples for spectrochemical analysis of metallic impurities and radio-chemical analysis of neutron activation products and fission products. This method suffers from the time lag between possible failure and detection since the samples will be removed from the primary coolant system periodically and the analyses cannot be performed until Na^{24} activity has decayed. In addition, samples will be removed more frequently for gross gamma activity and spectrometric gamma analysis after allowing

for decay of Na^{24} activity. These data will indicate any change in fission product concentration, and will be useful for the determination of gradual change in general fission product contamination of the primary sodium system. (It may be possible to correlate these data with neutron background data from the delayed neutron detector.)

Taps have been provided to facilitate experimental methods of continuous or intermittent monitoring of the argon blanket gas system for fission product gases (Xe and Kr). It will be possible to install a gas chromatograph as the first experimental method of detection. This method of detection also suffers from rate of response, and possibly sensitivity, since the gases are released to the sodium, must escape to the gas blanket where they are diluted, and then be transported to the detector. There is some evidence to indicate that the solubility of these gases in sodium is low, and adequate sensitivity may be achieved. It appears that this system may be more reliable (but significantly slower) than the delayed neutron detector, but with much more rapid response than the sampling procedure.

The EBR-II reactor system will be instrumented experimentally to detect failure of fuel and/or blanket elements to the extent that these experimental systems are effective. A continuing development program will utilize the EBR-II as an experimental facility to evaluate systems as they are developed. It is believed that the sampling techniques will be most reliable for initial periods of operation, with the promise of more effective systems from the development program.

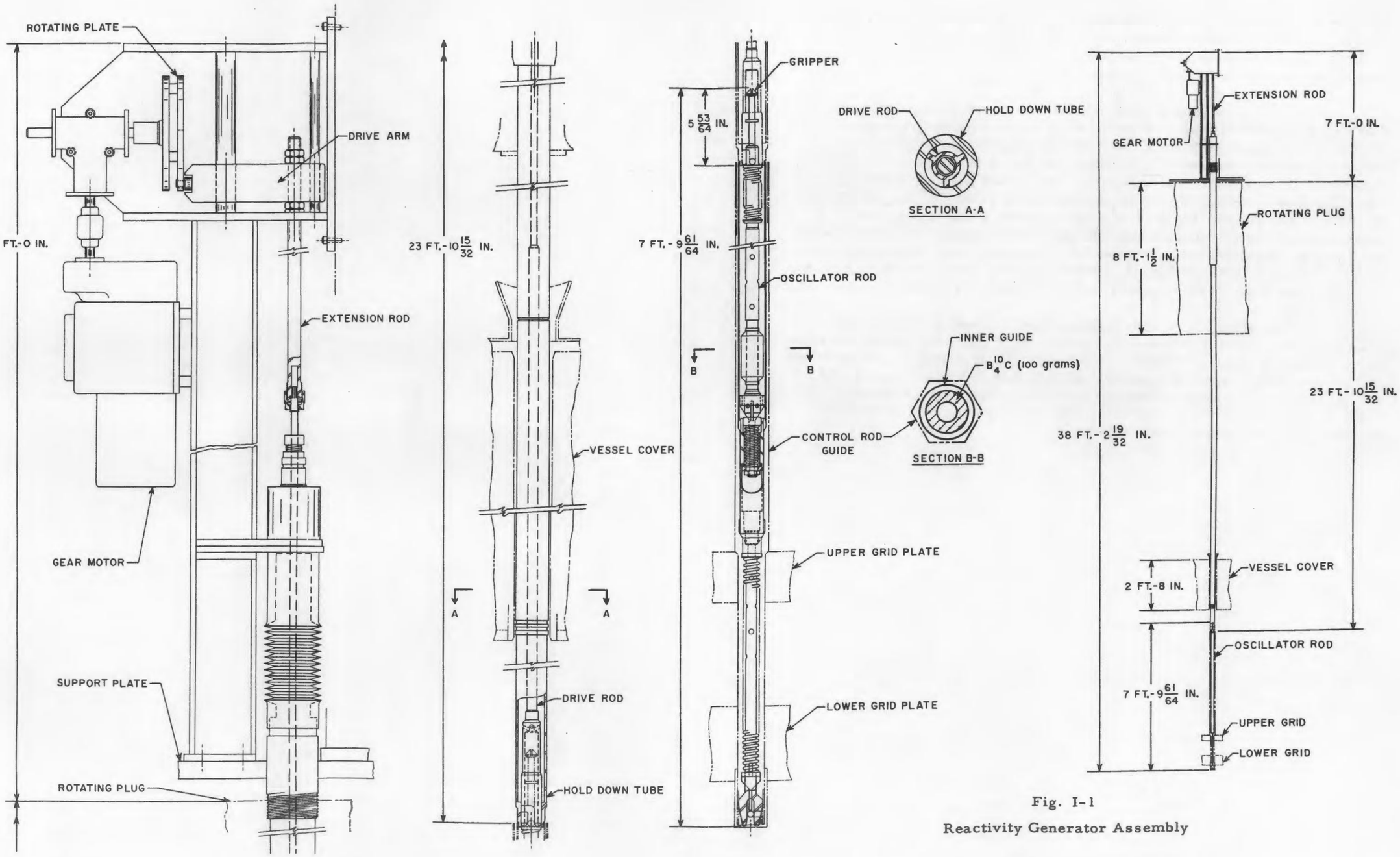

Fig. I-1

Reactivity Generator Assembly

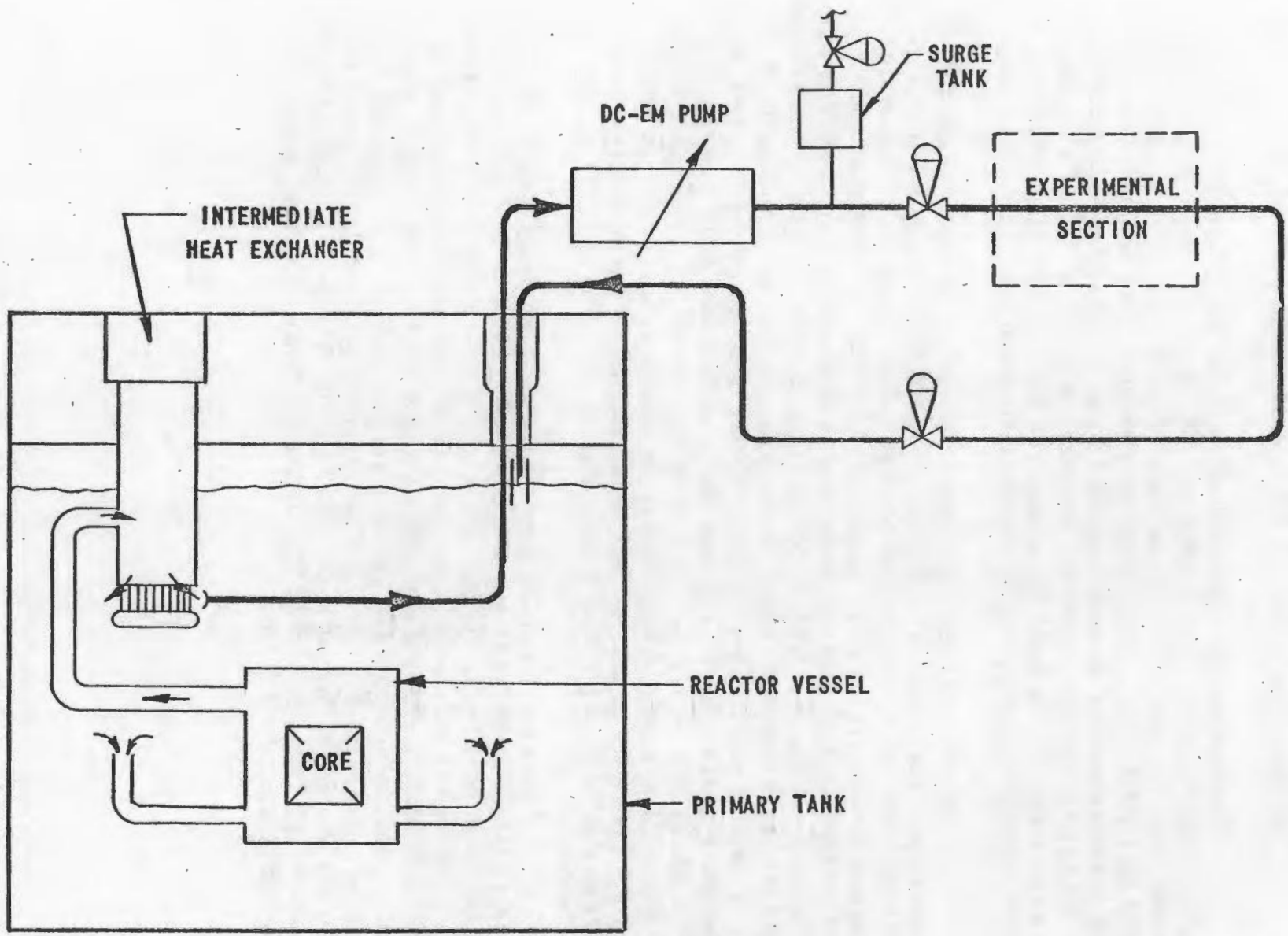

Fig. I-2

Schematic of Experimental Loop Arrangement

APPENDIX J

OPERATION WITH 61- TO 73-SUBASSEMBLY CORE

Normal steady-state operation at full power and at "three-fourths" power is described in Section IV.B. and C. for the reactor with a nominal core loading. The nominal core is comprised of 67 subassemblies, including 2 safety and 12 control subassemblies. This is considered the most probable number of subassemblies to be required for initial criticality. The actual number, however, may vary from 61 to 73. It is of importance, therefore, to examine the changes in reactor conditions resulting from operation with core configurations throughout this entire size range.

The "hottest channel" temperatures are of greatest interest. As the core is made larger by adding subassemblies (beginning with 61), power densities at core and upper blanket hottest channels continuously decrease; similarly, the peak temperatures within the core and upper blanket continuously decrease (reduction in flow rate per subassembly being more than compensated for by reduction in power density). The effects within the inner and outer blankets, however, do not follow this pattern. In these zones, as each core-type subassembly is added (in the 6th row), subassemblies adjacent to or very near the added subassembly experience an abrupt increase in power density. At the same time, other subassemblies of the same zones may undergo either no change or a decrease in power density. The result is that neither zone exhibits a smooth progression of increasing or decreasing peak temperatures with increasing core size.

Figures J-1 and J-2 present the reactor temperatures of chief interest calculated for core sizes of 61, 62, 67, 68, and 73 subassemblies. (Interpolation is permissible for core sizes of 63-66 and 69-72 subassemblies.) Shown are maximum temperatures of uranium, uranium-clad interface, and coolant occurring with rows 1 and 4 (core), rows 6 and 7 (inner blanket), and row 8 (outer blanket), for each core size, both with and without uncertainty factors. For the 67-subassembly core only, the same temperatures are shown for all rows 1 through 10. Figure J-1 pertains to the full power (62.5 Mw) case, and Fig. J-2 to the "three-fourths" power (45.0 Mw) case.

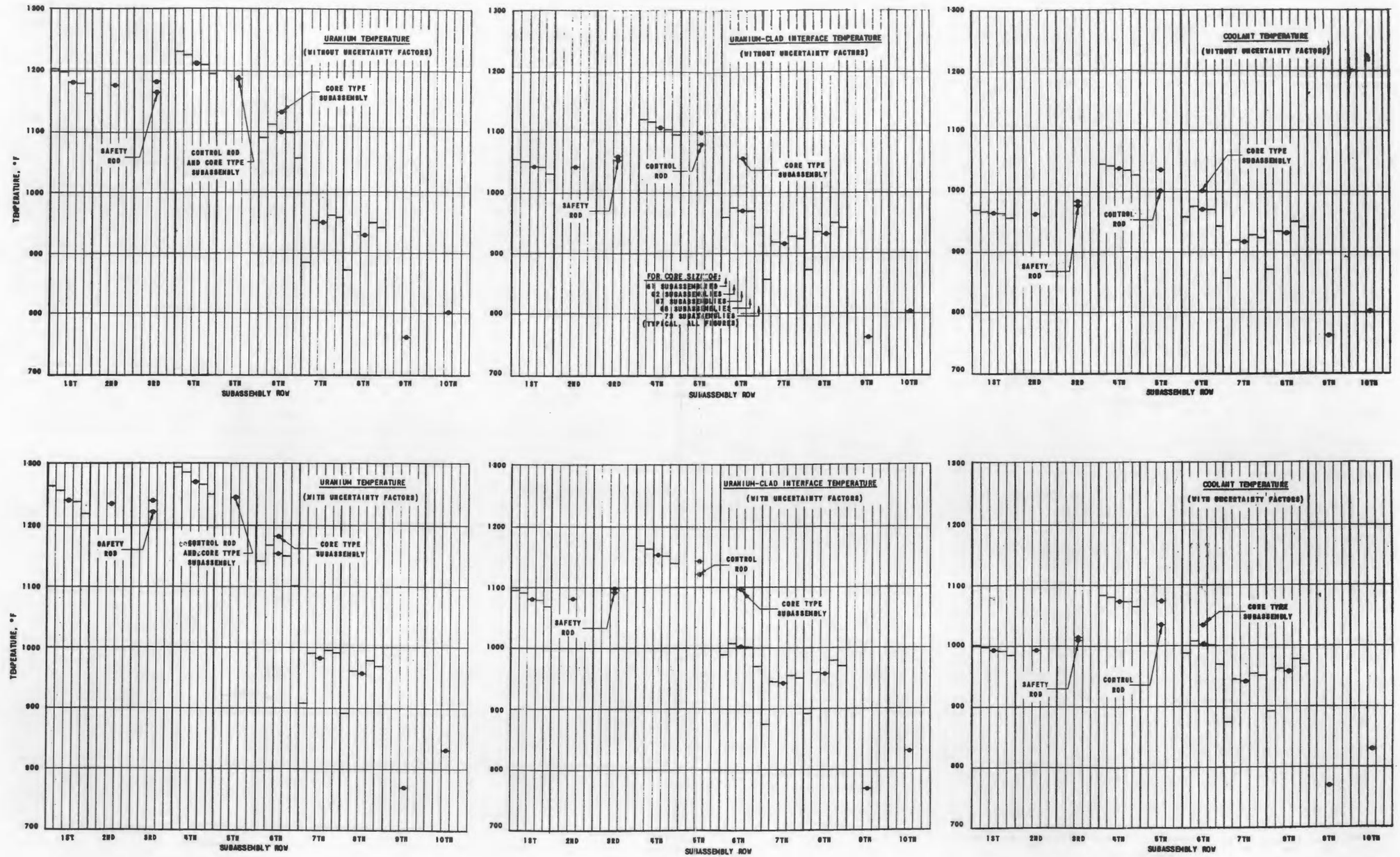

Fig. J-1

Maximum Temperatures in Each Subassembly Row and the Effect of Core Size upon Certain of Them (For Reactor Power of 62.5 Mw)

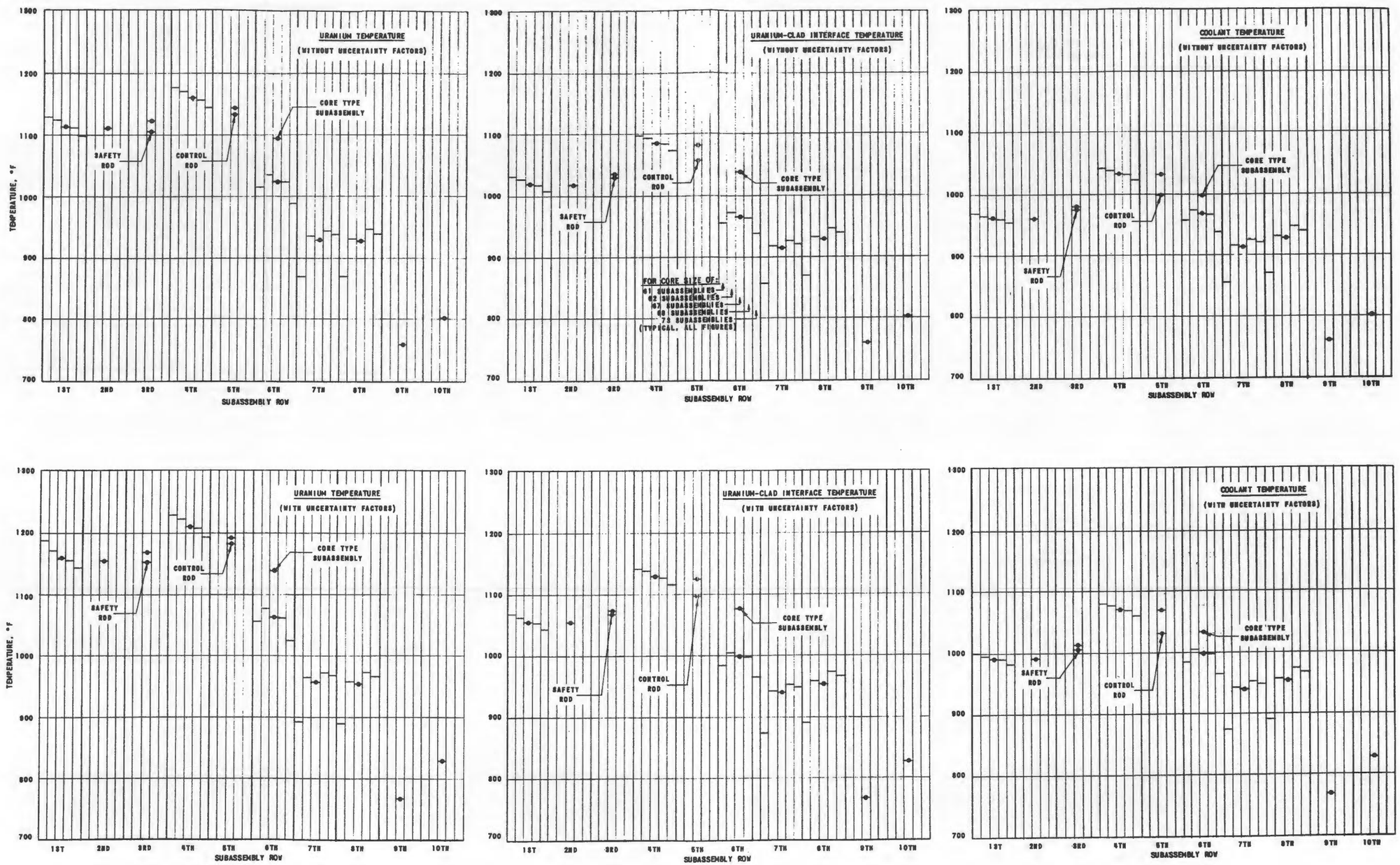

Fig. J-2

Maximum Temperatures in Each Subassembly Row
and the Effect of Core Size upon Certain of Them
(For Reactor Power of 45.0 Mw)

APPENDIX K

SYSTEM ABNORMALITIES CAUSING ALARM

Table K-1 is a comprehensive list of the system abnormalities that will cause alarm only ("alarm" meaning both indication and annunciation). All such abnormalities, including those unassociated with reactor plant operation or with little or no relevance to safety, are incorporated for completeness. The abnormalities which cause scram during reactor operation or fuel handling are listed in Table III of Section IV.A.1. This listing (Table K-1) is far more detailed than that given in the original report [Table VII] and for this reason, no attempt is made here to correlate the two.

Table K-1

SYSTEM ABNORMALITIES CAUSING ALARM

Primary System

1. Reactor Inlet Coolant (high pressure) No. 1 Flow High
2. Reactor Inlet Coolant (high pressure) No. 1 Pressure High
3. Reactor Inlet Coolant (high pressure) No. 2 Flow High
4. Reactor Inlet Coolant (high pressure) No. 2 Pressure High
5. Reactor Inlet (high pressure) Plenum Pressure High
6. Reactor Outlet Coolant Flow High
7. Reactor Coolant Differential Temperature (Inlet "high pressure" Plenum vs. Outlet Plenum) High
8. Primary Pump No. 1: Motor Blower Air Flow Low
9. Primary Pump No. 1: MG Clutch Temperature High
10. Primary Pump No. 1: MG Brake Temperature High
11. Primary Pump No. 1: Any One of Ten "General" Temperatures (on Pump and MG Set) High
12. Primary Pump No. 2: Motor Blower Air Flow Low
13. Primary Pump No. 2: MG Clutch Temperature High
14. Primary Pump No. 2: MG Brake Temperature High
15. Primary Pump No. 2: Any One of Ten "General" Temperatures (on Pump and MG Set) High
16. Primary Heat Exchanger: Differential Temperature (Heat Exchanger Outlet vs. Bulk Sodium) High

Table K-1

SYSTEM ABNORMALITIES CAUSING ALARM

Primary System (Cont'd.)

17. Bulk Sodium Temperature Low
18. Primary Tank Argon Blanket Gas Pressure Low
19. Argon-Silicone Heat Exchanger: Argon Outlet Temperature High
20. Argon Retention Tank Pressure High
21. Argon Floating Head Tank Pressure High
22. Argon Floating Head Tank Pressure Low
23. Argon Floating Head Tank Float Level High
24. Argon Floating Head Tank Float Level Low
25. Argon Receiver Tank Pressure High
26. Argon Blower Power "OFF"
27. Sodium Purification System: Surge Tank Level High
28. Sodium Purification System: Surge Tank Level Low
29. Sodium Purification System: Crystallizer Tank Heater Power "OFF"
30. Sodium Purification System: Sodium out of Crystallizer Tank Temperature High
31. Sodium Purification System: d-c, EM Pump Power "OFF"
32. Sodium Purification System: a-c, EM Pump Power "OFF"
33. Sodium Purification System: Piping Meltdown Heaters Power "OFF"
34. Sodium Purification System: Piping Clam Shell Heaters Power "OFF"
35. Primary Sodium to Sodium Purification System Flow Low
36. Primary Sodium from Sodium Purification System Flow Low
37. Sodium Purification Cell Exhaust Fan: Exhaust Air Pressure Low
38. Sodium Leak in Sodium Purification Cell
39. Silicone-Water Heat Exchanger: Silicone Outlet Temperature High
40. Silicone Pump No. 1 Power "OFF"
41. Silicone Pump No. 2 Power "OFF"
42. NaK to Shutdown Cooler No. 1 Flow Low

Table K-1

SYSTEM ABNORMALITIES CAUSING ALARM

Primary System (Cont'd.)

43. NaK to Shutdown Cooler No. 2 Flow Low
44. Shutdown Cooler Surge Tank No. 1 Level High
45. Shutdown Cooler Surge Tank No. 2 Level High
46. Rotating Plug Upper Seal Temperature High
47. Rotating Plug Lower Seal Temperature Low
48. Rotating Plug Seal Heater Power "OFF"
49. Sodium Leak into Primary Tank Annulus
50. Reactor Plant Pressure Low
51. Reactor Plant Operating Floor Smoke
52. Reactor Plant Basement Smoke
53. Reactor Plant Sub-Basement Smoke
54. Control Rods Shock Absorber Oil Level Low

Secondary System

55. Sodium to Superheater Temperature High
56. Sodium from Superheater Temperature High
57. Sodium to Superheater Pressure High
58. Sodium from Superheater Pressure High
59. Sodium from Superheater Pressure Low
60. Sodium to Primary System Heat Exchanger Temperature High
61. Sodium from Primary System Heat Exchanger Temperature High
62. Differential Pressure across Primary System Heat Exchanger High
63. Sodium to Primary System Heat Exchanger Flow Low
64. Sodium Relief 1st Rupture Disk Open
65. Sodium Relief 2nd Rupture Disk Open
66. Sodium Relief System Flow
67. Sodium from Evaporator Header No. 1 Temperature High
68. Sodium from Evaporator Pressure Low

Table K-1

SYSTEM ABNORMALITIES CAUSING ALARM

Secondary System (Cont'd.)

69. Sodium to Evaporator Pressure Low
70. Sodium Purification System: Sodium to Cold Trap Economizer Temperature High
71. Sodium Purification System: Sodium from Cold Trap Economizer Temperature High
72. Sodium Purification System: Differential Pressure across Cold Trap Economizer High
73. Sodium Purification System: Sodium to Cold Trap Crystallization Chamber Temperature High
74. Sodium Purification System: Sodium from Cold Trap Crystallization Chamber Temperature High
75. Sodium Purification System: Differential Pressure across Cold Trap Crystallization Chamber High
76. Sodium Differential Pressure across Main a-c, EM Pump High
77. Sodium to Main a-c, EM Pump Pressure Low
78. Sodium from Main a-c, EM Pump Pressure Low
79. Sodium from Recirculating Pump Pressure Low
80. Sodium from Recirculating Pump Flow Low
81. Sodium Surge Tank Level Low
82. Sodium Storage Tank Level High
83. Sodium Storage Tank Level Low
84. Sodium Storage Tank Recirculation Section Level Low
85. Sodium System Piping Temperature High
86. Sodium System Piping Temperature Low
87. Sodium Boiler Plant West Wing Main Floor Smoke
88. Sodium Boiler Plant West Wing Basement Smoke
89. Sodium Boiler Plant East Wing Smoke

Steam System

90. Steam Drum Water Level High
91. Steam Drum Water Level Low

Table K-1

SYSTEM ABNORMALITIES CAUSING ALARM

Steam System (Cont'd.)

92. Feed Water to Steam Drum Pressure Low
93. Feed Water to Steam Drum Temperature High
94. Feed Water to Steam Drum Temperature Low
95. Steam Drum Pressure High
96. Steam Drum Pressure Low
97. Steam Drum Safety Valve Open
98. Superheater Outlet Steam Pressure Low
99. 1250-lb Steam Header Pressure High
100. 1250-lb Steam Header Pressure Low
101. 1250-lb Steam Header Temperature High
102. 1250-lb Steam Header Temperature Low
103. 1250-lb Steam Header Safety Valve Open
104. 1250-lb Steam Bypass Flow Low
105. Bypass Steam to Condenser-Steam Temperature High
106. Turbine Steam Flow Minimum
107. Turbine Exhaust Steam Temperature High
108. Turbine Turning Gear Power "OFF"
109. Turbine Gland Exhauster Power "OFF"
110. Turbine Hydrogen System Abnormal
111. Turbine Thrust Bearing Excessive Wear
112. Turbine Lube Oil Temperature High
113. Turbine Lube Oil Pressure Low
114. Turbine Hydraulic System Pressure Low
115. Turbine Oil Tank Oil Level High
116. Turbine Oil Tank Oil Level Low
117. Condenser Vacuum Low
118. Condenser Hotwell Water Level High
119. Condenser Hotwell Water Level Low

Table K-1

SYSTEM ABNORMALITIES CAUSING ALARM

Steam System (Cont'd.)

120. Condenser Cooling Water Flow Low
121. Condenser Cooling Water Inlet Temperature High
122. Condenser Cooling Water Outlet Temperature High
123. Condenser Cooling Water Pump No. 1 Power "OFF"
124. Condenser Cooling Water Pump No. 2 Power "OFF"
125. Cooling Tower Water Level Low
126. Condensate Storage Tank Water Level High
127. Condensate Pump "Motor Driven" Discharge Pressure Low
128. Condensate Pump "Motor Driven" Power "OFF"
129. Condensate Pump "Turbine Driven" Discharge Pressure Low
130. Feed-water Pump "Turbine Driven" Discharge Pressure Low
131. Feed-water Pump "Turbine Driven" Auxiliary Oil Pump Power "ON"
132. Feed-water Pump "Turbine Driven" Oil Pressure Low
133. Feed-water Pump "Motor Driven" Discharge Pressure Low
134. Feed-water Pump "Motor Driven" Auxiliary Oil Pump Power "ON"
135. Feed-water Pump "Motor Driven" Oil Pressure Low
136. Feed-water Pump "Motor Driven" Power "OFF"
137. Feed-water Specific Electrical Conductivity High
138. Feed-water Heater No. 1 Water Level High
139. Feed-water Heater No. 2 Water Level High
140. Feed-water Heater No. 2 Water Level Low
141. Feed-water Heater No. 3 Water Level High
142. Feed-water Heater No. 4 Water Level High
143. Flash Tank High-Pressure Water Level High
144. Flash Tank Low-Pressure Water Level High
145. Air Ejector Inlet Steam Pressure Low
146. Vapor Extractor Power "OFF"

Table K-1

SYSTEM ABNORMALITIES CAUSING ALARM

Steam System (Cont'd.)

147. Blowdown Specific Electrical Conductivity High
148. Make-up Water Specific Electrical Conductivity High
149. Startup Feed-water Pump Discharge Pressure Low

Electrical System

150. 138-kv Tie Breaker Trip
151. Transformer No. 1: 13.8-kv Secondary Breaker Trip
152. Transformer No. 2: 13.8-kv Secondary Breaker Trip
153. 13.8-kv TREAT Feeder Breaker Trip
154. Transformer No. 3: 13.8-kv Primary Breaker Trip
155. Transformer No. 3: 2400-volt Secondary Breaker Trip
156. Transformer No. 3: Oil Temperature High
157. Transformer No. 4: 13.8-kv Primary Breaker Trip
158. Transformer No. 4: 2400-volt Secondary Breaker Trip
159. Transformer No. 4: Oil Temperature High
160. Transformer No. 5: 13.8-kv Primary Breaker Trip
161. Transformer No. 5: 480-volt Secondary Breaker Trip
162. Transformer No. 5: Oil Temperature High
163. Transformer No. 6: 13.8-kv Primary Breaker Trip
164. Transformer No. 6: 480-volt Secondary Breaker Trip
165. Transformer No. 6: Oil Temperature High
166. Generator 13.8-kv Circuit Breaker Trip
167. Generator Differential Lockout Trip
168. 13.8-kv Bus Tie Breaker Trip
169. 13.8-kv Bus Section No. 1 Lockout Trip
170. 13.8-kv Bus Section No. 2 Lockout Trip
171. 13.8-kv Bus Section No. 1 Undervoltage
172. 13.8-kv Bus Section No. 2 Undervoltage

Table K-1

SYSTEM ABNORMALITIES CAUSING ALARM

Electrical System (Cont'd.)

173. 13.8-kv Bus Section No. 1 Ground
174. 13.8-kv Bus Section No. 2 Ground
175. 2400-volt Secondary Sodium Pump Feeder Breaker Trip
176. 2400-volt Pump House No. 1 Feeder Breaker Trip
177. 2400-volt Pump House No. 2 Feeder Breaker Trip
178. 2400-volt Bus Undervoltage
179. 2400-volt Bus Ground
180. 480-volt Emergency Switchgear E-1 Feeder Breaker Trip
181. 480-volt Power Plant MCC-P2A Feeder Breaker Trip
182. 480-volt Reactor Plant MCC-R1A Feeder Breaker Trip
183. 480-volt Laboratory and Service Building Feeder Breaker Trip
184. 480-volt Lighting Distribution Center E-2 Feeder Breaker Trip
185. 480-volt Power Plant MCC-P2B Feeder Breaker Trip
186. 480-volt Primary Tank Immersion Heater Feeder Breaker Trip
187. 480-volt Fuel Handling and Sodium Purification MCC-R3 Feeder Breaker Trip
188. 480-volt Fuel Cycle Process Feeder Breaker Trip
189. 480-volt Power Plant MCC-P1 Feeder Trip
190. 480-volt Sodium Boiler Plant Feeder Breaker Trip
191. 480-volt Fuel Cycle MCC-F1A Feeder Breaker Trip
192. 480-volt Control Rod Power "OFF"
193. 480-volt Emergency Bus MCC-R2A Undervoltage
194. 480-volt Emergency Bus E-1 Undervoltage
195. 400-kw Diesel Generator Fail to Start
196. 400-kw Diesel Generator 480-volt Breaker Closed
197. 400-kw Diesel Generator Cooling Water Temperature High
198. 400-kw Diesel Generator Lube Oil Pressure Low
199. 400-kw Diesel Generator Overspeed

Table K-1

SYSTEM ABNORMALITIES CAUSING ALARM

Electrical System (Cont'd.)

200. 100-kw Diesel Generator Fail to Start

201. 100-kw Diesel Generator 480-volt Breaker Closed

202. 100-kw Diesel Generator Cooling Water Temperature High

203. 100-kw Diesel Generator Lube Oil Pressure Low

204. 100-kw Diesel Generator Overspeed

205. 125-volt, d-c Battery Bus Ground

Radiation Monitoring

206. Reactor Plant: Personnel Air Lock Door

207. Reactor Plant: Primary Tank Top

208. Reactor Plant: Secondary Sodium Line

209. Reactor Plant: Operating Floor, N. E. Wall

210. Reactor Plant: Thimble Cooling Exhaust

211. Reactor Plant: Argon Purification Cell

212. Reactor Plant: Argon Receiver Tank

213. Reactor Plant: Sodium Purification Cell Exhaust Fan

214. Reactor Plant: Shield Cooling Filters

215. Reactor Plant: Air Exhaust

216. Reactor Plant: Operating Floor Air

217. Reactor Plant: Sub-Basement Air

218. Fuel Cycle Facility: Air Exhaust Plenum

219. Fuel Cycle Facility Off-Gas System: Hold-Up Tank Discharge to Stack

220. Laboratory and Service Building

221. Sanitary and Industrial Waste Pump House: Liquid Waste Monitor

222. Main Suspect Stack Air Exhaust

Table K-1

SYSTEM ABNORMALITIES CAUSING ALARM

Auxiliary System

223. Process Instrumentation Continuous Power System Abnormal

   a. Low d-c Supply to MG Set
   b. Regulated a-c Output Voltage High
   c. Regulated a-c Output Voltage Low
   d. Regulated a-c Output Voltage Frequency High
   e. Regulated a-c Output Voltage Frequency Low

224. Nuclear Instrumentation Continuous Power System Abnormal

   a. Low d-c Supply to MG Set
   b. Regulated a-c Output Voltage High
   c. Regulated a-c Output Voltage Low
   d. Regulated a-c Output Voltage Frequency High
   e. Regulated a-c Output Voltage Frequency Low

225. Shield Cooling System: Exhaust Flow Low

226. Shield Cooling System: Recirculating Air Flow Low

227. Shield Cooling System: Normal Refrig. 40-ton Compressor Power "OFF"

228. Shield Cooling System: Standby Refrig. Compressors No. 1 and No. 2 Power "OFF"

229. Shield Cooling System: Normal Refrig. 40-ton Compressor Suction Pressure Low

230. Shield Cooling System: Normal Refrig. 40-ton Compressor Discharge Pressure High

231. Shield Cooling System: Normal Refrig. 40-ton Compressor Suction Pressure High

232. Shield Cooling System: Normal Refrig. 40-ton Compressor Lube Oil Pressure Low

233. Shield Cooling System: Recirculating Air Fan No. 1 Power "OFF"

234. Shield Cooling System: Recirculating Air Fan No. 2 Power "OFF"

235. Shield Cooling System: Recirculating Air Temperature High

236. Shield Cooling System: Recirculating Air High Temperature Switchover

237. Shield Cooling System: Exhaust Fan No. 1 Power "OFF"

238. Shield Cooling System: Exhaust Fan No. 2 Power "OFF"

Table K-1

SYSTEM ABNORMALITIES CAUSING ALARM

Auxiliary System (Cont'd.)

239. Thimble Cooling Air Temperature High

240. Thimble Cooling System: Exhaust Air Turbo-Compressor No. 1 Power "OFF"

241. Thimble Cooling System: Exhaust Air Turbo-Compressor No. 2 Power "OFF"

242. Thimble Cooling System: Branch A Air Exhaust Temperature High

243. Thimble Cooling System: Branch B Air Exhaust Temperature High

244. Thimble Cooling System: Branch A Air Exhaust Flow Low

245. Thimble Cooling System: Branch B Air Exhaust Flow Low

246. Reactor Plant Auxiliary Water Pump (for outside heat exchangers) Power "OFF"

247. Reactor Plant Purge Fan Power "ON"

248. Reactor Plant Operating Floor East Air-Handling Unit: Refrig. Compressor Power "OFF"

249. Reactor Plant Operating Floor North Air-Handling Unit: Refrig. Compressor Power "OFF"

250. Reactor Plant Outside Air Supply Fan Power "OFF"

251. Reactor Plant Operating Floor East Air-Handling Unit: Cond. Fans Power "OFF"

252. Reactor Plant Operating Floor North Air-Handling Unit: Cond. Fans Power "OFF"

253. Reactor Plant Outside Air-Condensing Unit Power "OFF"

254. Reactor Plant Operating Floor, East Air-Handling Unit: Fan Power "OFF"

255. Reactor Plant Operating Floor, North Air-Handling Unit: Fan Power "OFF"

256. Reactor Plant Air-Handling Units: Outlet Air Temperature Low

257. Reactor Plant Basement Air Cooling Fan Power "OFF"

258. Reactor Plant Sub-Basement Air Cooling Fan Power "OFF"

259. Power Plant High Bay Area Air Washer Pump: Discharge Pressure Low

Table K-1

SYSTEM ABNORMALITIES CAUSING ALARM

Auxiliary System (Cont'd.)

260. Suspect Stack Exhaust Fan Power "OFF"
261. Instrument Air Pressure Low
262. Plant Air Pressure Low
263. Emergency between Personnel Air Lock Doors
264. Personnel Air Lock Outside Door Open
265. Personnel Air Lock Inside Door Open
266. Emergency Air Lock Inside or Outside Door Open
267. Equipment Air Lock Inside or Outside Door Open
268. Space-Heating Boiler No. 1 Power "OFF"
269. Space-Heating Boiler No. 2 Power "OFF"
270. Space-Heating Boilers: Feed-water Pressure Low
271. Space-Heating Boilers: Light Oil Tank Level Low
272. Space-Heating Boilers: Fuel Oil Tank Level High
273. Space-Heating Boilers: Fuel Oil to Boilers Pressure Low
274. Space-Heating Boilers: Demineralized Water Pressure Low
275. Space-Heating Boilers: Steam Pressure Low
276. Space-Heating Boilers: Emergency Fuel Oil Storage Tank Level Low
277. Space-Heating Boilers: Feed-water Storage Tank Level Low
278. Potable Water Tank Level Low
279. Potable Water Tank Level High
280. Potable Water Main Pressure Low
281. Water Treatment Chlorine Cylinder Weight Low
282. Plant Cooling Water Pressure Low
283. Sewage Pit Level High
284. Industrial Waste Pit Level High

APPENDIX L

THE DRY CRITICAL EXPERIMENTS

The Dry Critical Experiments[1,2] were zero power experiments (<500 w) that were performed in the EBR-II Reactor prior to filling the primary system with sodium coolant. The experiments were initiated on September 18, 1961. The reactor achieved initial criticality on September 30, 1961, and the experimental program was completed on November 1, 1961.

The Dry Critical Experiments provided a final pre-operational "Proof Test" for the neutronic calculations and extrapolations pertaining to the EBR-II. The experiments also provided a means of measuring some parameters (localized spatial variations in power density, etc.) which could not be measured on the EBR-II mock-up on ZPR-III.

The Dry Critical Experiments confirmed that the neutronics of the EBR-II are well understood. The agreement between predicted and measured quantities surpassed expectations.

The reduction of uncertainties, through the performance of these experiments, served to eliminate various development problems. For example, the control rods were measured to be slightly more effective than had been expected. This observation obviates the need for "special" control rods with poison followers. Similarly, observations demonstrate that in-core instrumentation will not be necessary for the Wet Critical Experiments. Adequate unmultiplied source flux counting rates can be obtained in the normal shield instrument thimbles.

The experimental program included four distinct types of investigations:

(1) Neutron source strength and related subcritical instrument response.

(2) The approach to critical and the Dry Critical configuration.

(3) The neutron flux and power distributions.

(4) Reactivity measurements.

Detailed experimental results are given in Reference 2. The results are briefly reviewed.

1. Neutron Source and Instrument Response

Three Sb-Be neutron sources were available for the experiments. Two "strong" sources were provided to produce adequate subcritical counting rates. One "weak" source was provided to permit low-power level operation without source effects after the critical size was achieved.

Nine channels of low-power instrumentation were provided for monitoring neutron flux. Seven of these were operative at all times. Five of these seven were connected to the reactor shutdown circuit. All five were set to trip on reactor periods shorter than 15 sec. Three of the five were set to trip on power level greater than 1000 w. Table L-1 summarizes the "unmultiplied" source response of the low power channels.

Table L-1

LOW-POWER INSTRUMENT RESPONSE

Channel	Counter Type	Location[a]	Approximate Unmultiplied Counts/Minute[b]
1	Fission	J-1	260
2	Fission	J-1	250
3	Fission	J-2	220
A	H. T. Fission[c]	6-B-1	5450
B	H. T. Fission[c]	7-C-1	3180
C	Abs. Fission[d]	6-B-1	0
D	Abs. Fission[d]	7-C-1	0
E	BF_3	11-A-8	700
F	BF_3	13-B-8	280

[a]See Fig. 54.

[b]Reactor loaded with depleted uranium and dummy steel subassemblies. (Central fuel subassembly loaded and control rods "down.") Count rates corrected to a neutron source having 190 curies of Sb activity.

[c]High-Temperature Fission Counter.

[d]Absolute Fission Counter.

In addition, the three intermediate-power level (Channels 4, 5, and 6) and the linear-flux level (Channel 7) instruments became operative at about 5 w. The intermediate-power level channels were set to trip on a 15-second period; the linear-flux channel was set to trip at ~80% of each manually adjustable range.

The three high-power level safety channels showed significant response only in excess of 100-watt reactor operation. The power-level trip on these channels was set at ~40 kw.

The unmultiplied source flux investigation suggested several simplifications for the Wet Critical Experiments:

(1) In-core instrumentation will not be required if a startup source having at least 500 curies of Sb activity is provided.

(2) It will not be necessary to provide clad ZrH in the instrument thimbles for reactor startup.

(3) Elimination of ZrH permits the use of two high-sensitivity BF_3 counters in the J-2 and J-3 thimbles for low multiplication flux monitoring.

(4) The Dry Critical operating experience demonstrates that the strong startup source may be disassembled by remote controlled methods (the antimony rod removed) and replaced by a weaker neutron source after the critical loading has been achieved.

(5) The antimony rod may be stored in a suitable thimble in the Outer Blanket, thus minimizing high-activity handling on the operating floor.

Prior to unloading the fuel, two of the six channels (A and B) of incore instrumentation were transferred to normal instrument thimbles (with high-sensitivity BF_3 counters) in the neutron shield (Channels G and H). This procedure provided counters in the contemplated positions for the Wet Critical Experiments. Counting rates observed while fuel was being unloaded closely represent what will be observed during the Wet Critical Experiments. Table L-2 summarizes the counting rates obtained with the reactor ~6% $\Delta k/k$ subcritical (control and safety rods down). The neutron source strength was ~70 curies at the time of measurement.

Table L-2 illustrates the overlap in startup counting rates with the BF_3 and fission counters.

It is to be noted that the instrument thimble response experiments in the dry reactor are essentially consistent with similar experiments on the EBR-II Mock-up on ZPR-III[19] for an "aluminum-cooled" reactor.

Table L-2

COUNTING RATES WITH INSTRUMENTS
DISPOSED AS FOR WET CRITICAL EXPERIMENTS

(Reactor ~6% $\Delta k/k$ Subcritical)

Channel	Counter Type	Location*	Approximate Counts/Minute**
1	Fission	J-1	1300
2	Fission	J-1	1200
3	Fission	J-2	1160
G	BF_3	J-3	9240
H	BF_3	J-2	8210

*See Fig. 54.

**Neutron source had ~70 curies of Sb activity.

2. The Critical Approach and the Dry Critical Configuration

The reactor was loaded as described in Sections V.B. and V.C. of Reference 1. The only deviation from this procedure was the use of some smaller loading increments than given in Reference 1. In addition, a subcritical count was obtained before and after each subassembly was loaded.

During the loading to critical, all of the pertinent reactor and instrument components had to function simultaneously. The very small amount of "down time" (~12 hr) during this two-week period attests to the high degree of reliability built into the mechanical and electrical components of the system.

The critical approach was governed by the nine channels of low-power instrumentation. Subcritical count rates were obtained; inverse count rates were plotted as a function of the total number of fuel subassemblies loaded into the reactor. No multiplication anomalies appeared during the loading and all monitoring channels predicted essentially the same critical reactor size. At no time did any of the channels predict a larger critical size than was finally observed. (More complete data are given in Reference 2.)

The reactor became critical with 87 fuel subassemblies, including control and safety subassemblies (a total loading of 232.18 kg U^{235}). Criticality was achieved with ten of the twelve control rods fully raised and the eleventh about 80% inserted. The reactor diverged on a period of approximately 100 sec. The dry critical mass was 227.9 kg U^{235} (see Reference 2).

The dry critical mass is in substantial agreement with the predicted core size of 85 plus 7 or minus 5 subassemblies.[1,17] This is very encouraging because the dry critical reactor had not been mocked up on ZPR-III. The information pertaining to the dry reactor was inferred from substitution experiments on the "aluminum-cooled" EBR-II mock-up on ZPR-III with a critical mass of ~165 kg U^{235}.

3. Neutron Flux and Power Distributions

Neutron flux measurements provided data relevant to the power distribution and plutonium production in the radial reflector. The effectiveness of the dry reactor neutron shield was investigated by measuring the shield leakage flux.

Highly enriched and depleted uranium foils were irradiated in three Outer Blanket locations. At each location, an axial distribution of U^{235} and U^{238} fissions as well as of U^{238} captures was obtained. The foils were irradiated at positions 8-D-4, 11-D-6, and 15-D-8 (see Fig. 54). These experiments suggest that the neutron flux and thus the power production in the very outermost rows of the Outer Blanket is about 15% higher than had been predicted.

Special foil-bearing subassemblies were used to investigate the details of the power distribution in the Inner Blanket. The investigation was oriented toward the determination of the spatial variation of the power density within a single Inner Blanket subassembly. The foils were located on the "corner," "flat," and in the center of the hexagonal subassembly. In each case an axial distribution of U^{235} and U^{238} fissions, and U^{238} captures was obtained. Four arrangements of fuel and blanket subassemblies around the foil-bearing blanket subassembly were studied in detail:

a. Foil Subassembly in 7-C-4

This arrangement afforded the measurement of the power distribution in a blanket subassembly facing the core. Row 6 was loaded with fuel subassemblies. Rows 7 and 8 were loaded with blanket subassemblies. The "corner" of the foil subassembly had two "flats" facing fuel subassemblies. The significant result is the ratio of "corner" to central power density, at the core midplane. The measured ratio of 1.56 agrees well with the predicted value.

b. Foil Subassembly in 7-D-1

This arrangement, when compared with the previous measurement, provided quantitative information on the variation of neutron flux along a hexagonal row of the core. Here, only one "flat" of the foil

subassembly was facing a fuel subassembly in 6-D-1. The core midplane ratio of the fission power in 7-C-4, to that in 7-D-1, was measured to vary between 1.7 and 1.9, depending on the specific locations within the foil subassembly.

c. Foil Subassembly in 7-F-5

A fuel subassembly was placed adjacent to the foil subassembly in Row 7 (Position 7-F-4). With Row 6 containing fuel subassemblies, three "flats" of the foil subassembly faced fuel. The core midplane ratio of "corner" to central power density did not exceed 1.56; however, the "corner" to "flat" ratio of 1.3 measured here may be compared with 1.56 in subsection a above. In this experiment, the "flat" of the foil subassembly faced the fuel subassembly in Row 7.

d. Foil Subassembly in 6-C-4

Here, a fuel subassembly was located on both sides of the foil subassembly in Row 6. Thus four flats of the foil subassembly were facing a fuel subassembly. The measured "corner" to "flat," and "corner" to center power densities were 1.25 and 1.43, respectively.

The effectiveness of both the axial and radial graphite neutron shield was determined by measuring BF_3 counter response with and without a cadmium sleeve. Three measurements were made at the core midplane outside the radial neutron shield, while three other measurements pertained to the axial shield in the reactor cover. In general, it was found that the emerging neutron spectrum was softer than predicted. This result suggests that predictions of secondary system sodium activation may be high.

4. Reactivity Effects

Table L-3 summarizes reactivity measurements pertaining to fuel subassemblies, and control and safety rods. The agreement between prediction and measurement is adequate. The two major implications of these results are: (1) reactivity held by the control rods is adequate for power operation; and (2) "special" control rods are not required for power operation.

The dry isothermal temperature coefficient was measured by cooling the reactor to 58°F and then heating to 99°F. The temperature difference of 41°F resulted in a 1.86-inch shift in control rod setting for the critical reactor at fixed power. The measured dry isothermal temperature coefficient is -2.6×10^{-5} $(\Delta k/k)/°C$. This may be compared to a predicted value[17] of -1.8×10^{-5} $(\Delta k/k)/°C$.

Table L-3

REACTIVITY WORTH OF CONTROL AND SAFETY RODS AND FUEL SUBASSEMBLIES

Effect	Location[a]	Reactivity Effect, % Δk/k	
		Measured	Predicted[b]
Twelve Control Rods	-	4.33	3.84
Eleven Control Rods plus one "Special" Control Rod	5-A-1[c]	4.54	<4.1
One Control Rod	5-B-3	0.37	0.32 (Average)
One Control Rod	5-D-1	0.33	
One Control Rod	5-F-3	0.39	
One Control Rod	5-B-1	0.32	
One Control Rod[d]	5-D-3	0.36	
Special Control Rod	5-A-1	0.58	<0.6
Two Safety Rods	3-A-1 3-D-1	0.94	1.1
Depleted → Enriched Subassembly	6-F-1	0.28	0.3 (Average)
Depleted → Enriched Subassembly	6-D-3	0.39	

[a]See Fig. 54.

[b]Reference 1.

[c]Special Control Rod with $B_4^{10}C$ Follower.

[d]Reactor was reloaded by replacing fuel with blanket subassemblies in positions 6-D-3 and 6-D-4.

A prototype, vertical-motion oscillator rod was statically calibrated with 71 gm and with 129 gm $B_4^{10}C$. The experiments show that the reactivity worth is linear as a function of axial displacement for at least 3 in. of stroke (1.5 in. amplitude) over certain ranges of rod insertion. Such an oscillator rod will provide sinusoidal reactivity amplitudes of not less than 2.5×10^{-4}% Δk/k per gram of $B_4^{10}C$ in the rod.

BIBLIOGRAPHY

1. L. J. Koch, et al., "EBR-II Dry Critical Experiments - Experimental Program, Experimental Procedures, and Safety Considerations," ANL-6299 (February, 1961).

2. R. L. McVean, et al., "EBR-II Dry Critical Experiments - Experimental Results," ANL-6462 (February, 1962).

3. B. W. LeTourneau and R. E. Grimble, "Engineering Hot Channel Factors for Nuclear Reactor Design," Nuclear Sci. Eng., 1, No. 5, 359-369. (October, 1956).

4. C. F. Bonilla (ed.), "Nuclear Engineering," (New York: McGraw-Hill Book Co., 1957), pp. 442-446.

5. A. Hitchcock, "Statistical Methods for the Estimation of Maximum Fuel Element Temperature," (UKAEA) IGR-TN/R-760 (January, 1958).

6. Kaiser Engineers Div., Henry J. Kaiser Co., and Atomic Energy Div., Allis Chalmers Mfg. Co., "Experimental Gas-Cooled Reactor: Preliminary Hazards Summary Report," ORO-196 (May, 1959).

7. "Gas-Cooled Reactor Project Quarterly Progress Report for Period Ending June 30, 1960," ORNL-2964 (August, 1960).

8. J. R. Parrette, "Frequency Functions for Products of Engineering Hot Channel Factors," Trans. Am. Nuclear Soc., 2, No. 1, 94 (1959).

9. P. A. Rude and A. C. Nelson, Jr., "Statistical Analysis of Hot Channel Factors," Nuclear Sci. Eng., 7, 156-161 (1960).

10. J. R. Dietrich and W. H. Zinn, "Solid Fuel Reactors," (Reading, Mass.: Addison-Wesley Publishing Co., Inc., 1958), pp. 262-266.

11. F. H. Tingey, "Error Propagation in Hot Channel - Hot Spot Analysis," IDO-16558 (October, 1959).

12. "Army Gas-Cooled Reactor Systems Program Semiannual Progress Report for July 1 through December 31, 1959," IDO-28549 (February 1960).

13. S. T. Zegler and M. V. Nevitt, "Structures and Properties of Uranium-Fissium Alloys," ANL-6116 (July, 1961).

14. "Metals Handbook," (Cleveland: American Society for Metals, 1948).

BIBLIOGRAPHY

15. C. B. Jackson (ed.), "Liquid Metals Handbook - Sodium-NaK Supplement," TID-5277 (July, 1955).

16. H. O. Monson, "Comments on Liquid Metals as Coolants in High Power Density Power Reactors," Paper presented at the Technical Briefing Session, Idaho Falls, Idaho, November 1-2, 1955, TID-7506, Part I (July, 1956), p. 109.

17. W. B. Loewenstein, "The Physics Design of the EBR-II," ANL-6383 (July, 1961).

18. H. H. Hummel and L. T. Bryant, "Stability Analysis of EBR-II." ANL-6484 (January, 1962).

19. W. P. Keeney and J. K. Long, "Zero-Power Reactor-III (ZPR-III)," Idaho Division Summary Report, July-September, 1960, ANL-6301, p. 45.

20. J. H. Monaweck and E. S. Sowa, "Summary Report on Irradiation of Protype EBR-II Fuel Elements," ANL-6010 (September, 1960).

21. H. F. Jelinek, N. J. Carson and A. B. Shuck, "Manufacture of EBR-II Core Fuel," ANL-6274 (November, 1961).

22. N. J. Carson, et al., "Fabrication of EBR-II Core-I Fuel Elements," ANL-6276 (November, 1961).

23. A. B. Shuck, et al., "Development of Methods and Equipment for Production of EBR-II Fuel Rods," ANL-6272 (December, 1961).

24. J. E. Ayer and A. B. Shuck, "The Design and Construction of the EBR-II Initial Fuel Loading Facility," ANL-6092 (June, 1961).

25. D. C. Hampson, "Preparation of Alloy for the First Core Loading of EBR-II", ANL-6290 (August, 1961).

26. O. S. Seim and R. A. Jaross, "Characteristics and Performance of 5000-gpm AC Linear Induction and Mechanical Centrifugal Sodium Pumps," Proc., 1958 Geneva Conference, 7, Paper No. 2158, p.88.

27. D. T. Rymsa and G. P. Wachtell, "Flow Model Study of the EBR-II," The Franklin Institute, FA-2201 (January, 1962).

BIBLIOGRAPHY

28. T. R. Bump and H. O. Monson, "Flow Characteristics of the EBR-II Subassembly," ANL-6549 (1962).

29. R. R. Smith, et al., "Instability Studies with EBR-I, Mark-III," ANL-6266 (December, 1960).

30. R. R. Smith, et al., "A Mechanism Explaining the Instability of EBR-I, Mark-III," ANL-6354 (September, 1961).

31. J. K. Long, et al., "Fast Neutron Power Reactor Studies with ZPR-III," Proc., 1958 Geneva Conference, 12, Paper No. 598, p. 119.

32. W. B. Loewenstein and D. Okrent, "The Physics of Fast Power Reactors; Status Report," Proc., 1958 Geneva Conference, 12, Paper No. 637, p. 16.

33. W. J. McCarthy, et al., "Studies of Nuclear Accidents in Fast Power Reactors," Proc., 1958 Geneva Conference, 12, Paper No. 2165, p. 207.

34. V. Z. Jankus, "A Theoretical Study of Destructive Nuclear Bursts in Fast Power Reactors," ANL-6512 (February, 1962).

35. C. E. Dickerman, et al., "Studies of Fast Reactor Fuel Element Behavior Under Transient Heating to Failure - I. Initial Experiments on Metallic Samples in the Absence of Coolant," ANL-6334 (1961).

36. R. O. Brittan, "Analysis of the EBR-I Core Meltdown," Proc., 1958 Geneva Conference, 12, Paper No. 2156, p. 267.

37. J. H. Kittel, et al., "The EBR-I Meltdown-Physical and Metallurgical Changes in the Core," ANL-5731 (November, 1957).

38. H. O. Monson and M. M. Sluyter, "Containment of the EBR-II," Proc., 1958 Geneva Conference, 11, Paper No. 1892, p. 124.